

THE MUISNE, ECUADOR EARTHQUAKE OF 16 APRIL 2016

A FIELD REPORT BY EEFIT



THE M_w7.8 MUISNE ECUADOR EARTHQUAKE OF 16 APRIL 2016

Guillermo Franco, Ph.D., *Guy Carpenter*
Harriette Stone, *University College London*
Bayes Ahmed, Ph.D., *University College London*
Siau Chen Chang, Ph.D., *National University of Singapore*
Fiona Hughes, *University of Cambridge*
Nina Jirouskova, *Imperial College*
Sebastian Kaminski, *Arup*
Jorge Lopez, *Arup*
Nicolas van Drunen, *INBAR*
Carlos Molina Hutt, *University College London*
Manuel Querembás, *Director of the School of Military Engineering (Ecuador)*

Report reviewed by:
Carlos Molina Hutt

September 2018

Executive Summary

On 16 April 2016 an M_w 7.8 earthquake with an epicentre 29km south-southeast of Muisne in the northern Ecuadorian province of Manabí caused an estimated 668 fatalities, 6,300 severe injuries and widespread damage. The coastal towns – particularly Pedernales, Canoa, Bahía de Caráquez, Manta, and Portoviejo, all centres of tourism and major hubs of activity in the region – suffered extensive damage after the main shock, with associated Modified Mercalli Intensities (MMI) of VI-VIII (USGS, 2016). The resulting peak ground accelerations (PGA) recorded at seismometer stations by the *Instituto Geofísico* (IG) ranged from 0.51g in Portoviejo to 1.55g in Pedernales in the most affected regions (IG, 2016).

Between 24 May and 7 June an Earthquake Engineering Field Investigation Team (EEFIT) was deployed with the objective of surveying and recording observations and measurements that would help the scientific and professional communities understand the event and its consequences. For logistical reasons, the field mission focused on the Manabí region, primarily in the coastal area, although a day was spent investigating some major damage inland. The team surveyed structural damage to buildings and infrastructure, took micro-tremor measurements, obtained aerial photography with drones, validated satellite-derived landslide data, and interviewed the vulnerable communities at the temporary shelters. The most salient observations and findings, discussed in detail in this report, are summarised below.

Geological and Geotechnical Observations:

- The event was related to the Nazca plate subduction activity, most likely additionally influenced by the presence of the local geodynamics of the Carnegie Ridge. Vast geophysical imagery efforts are yet to identify the geophysical asperities that may explain the pervasive seismicity pattern of the offshore historic seismicity epicentres. The seismic waves associated with the mainshock on the 16 April 2016 seem to have preferentially propagated along the Manabí coastal cordillera and basin in a southwestern direction from the inferred northern-most extent of the Carnegie Ridge. Conflicting studies exist, but the event seems to have mobilised an area last ruptured in 1906.
- Few geological and local active faulting studies were found, including the absence of site condition reports for IG seismometer stations. It is crucial that future efforts focus on understanding regional site effects, particularly due to the complex geomorphology and high potential of liquefaction of the coastal and alluvial deposits.
- TROMINO® microtremor tests were carried out throughout the affected region, with the aim of building on experiences from the EEFIT mission to Nepal in 2015 (Tallet-Williams *et al.*, 2016), and collecting some site amplification effects data. The analyses showed that site amplification was unlikely to have been the sole contributor to the response magnitude, with topographic and other geomorphological effects also likely to have contributed.
- Liquefaction and landslides also contributed heavily to the extent of the damage observed throughout the region, impacting on the initial emergency response. Liquefaction-induced damage was observed on structural foundations (*e.g.* tilting and seismic isolator damage due to large displacements). Landslides caused heavy damage to buildings located adjacent to slopes, and disrupted key road infrastructure.
- In general, it was observed that appropriate mitigation measures were not taken against liquefaction, lateral spreading of river banks, and major man-made or natural slope failures, resulting in vast amounts of damage. Efforts to map all earthquake-induced hazards are required to provide the basis of a more resilient disaster management plan for the region.
- The current seismic design code was published in 2015. It is mostly considered to be robust. However the zonation used to designate the seismic hazard factor for simplified

design approaches (i.e. when site-specific site response analysis is not carried out) seems oversimplified, and for the Manabí region may be unconservative.

Structural Observations:

- The two predominant building typologies observed during the mission in the affected region were (i) reinforced concrete (RC) frame with masonry infill walls and (ii) timber/bamboo frames with/without masonry infill (including vernacular buildings of quincha/bahareque). Other typologies (steel frame, unreinforced masonry, etc.) were seen in very small quantities.
- Typically, the RC frames with masonry infill walls were formed of either: (i) non-engineered, typically low-rise (<6 storeys), or (ii) engineered, typically high-rise (≥ 6 storeys).
- Very high levels of structural damage were seen in the non-engineered low-rise types of the RC frame with masonry infill walls buildings. The engineered high-rise buildings generally experienced low levels of structural damage and low to moderate levels of non-structural issues. The most salient types of damage observed in the building typology RC frame with masonry infill were:
 - Inadequate design and detailing of RC moment frames;
 - Inadequate masonry infill design and construction;
 - Inadequate shear design and detailing;
 - Weak and soft storeys;
 - Inadequate laps in steel reinforcement;
 - Short columns;
 - Insufficient cover to steel reinforcement;
 - Pounding;
 - Inadequate detailing in plastic hinge region;
 - Inadequate securing of non-structural elements; and
 - Poor quality concrete.
- The most salient types of damage observed in buildings using bamboo or timber were:
 - Rot and damage due to insects;
 - Inadequate connections between primary structural elements; and
 - Debris impact from adjacent buildings.
- The team collected damage data from over 1,200 buildings using rapid surveys in Manta, Portoviejo, Jama, and Pedernales. The use of this data needs to bear in mind the number of limitations outlined in this report.
- The team made a number of observations on the method of the immediate structural safety inspections carried out. It was observed that the 'traffic light' tagging system used in the affected areas varied in interpretation in the different cities and towns.

Social Observations:

The social survey team conducted structured questionnaire surveying in the earthquake refuge shelters from 28 May to 5 June 2016. The case study shelters were located in Portoviejo, Canoa, and Pedernales. A total of 120 families living in the temporary shelters were surveyed using a random sampling method. Questions were asked on demographic information, economic status, change of occupation, damaged house (year of construction, material type, ownership pattern), losses due to earthquakes, household preparedness, problems faced in the shelters, and future housing and livelihood recovery plans. The questionnaire was piloted in Manta shelters. Necessary ethical clearance was ensured before conducting the anonymous questionnaire surveying and only non-vulnerable adults were surveyed after taking oral consent.

The results from the questionnaire survey suggest most people were: adult working-class (18-65 years old) without higher educational background (mostly completing primary level); low-earning households (US \$75-300/month); involved in retail business, fishing, construction work, and day-labour jobs. In general, they became unemployed after the disaster and their first priority was to restart providing a decent livelihood for their families. The affected people were predominantly one-storey house owners made of reinforced concrete (RC)-timber/bamboo. Most of the affected buildings were constructed in the 1990s and 2010s, and were one and two storeys. The families were happy with the facilities and services provided in the temporary shelters. None of the respondents were prepared for the earthquake disaster. The victims now want to continue their livelihood in urban areas. Primarily the victims from multi-storey buildings made of RC or RC-timber/bamboo want to relocate into single-storey buildings made of timber and bamboo.

Disaster Management Observations:

The key findings on disaster management are summarised as follows with the caveat that the mission did not involve a detailed assessment of the disaster response or management process. These findings are based on impressions obtained during the team's visit without the ability to corroborate broadly neither in time nor space. These observations are summarised as follows:

- The initial emergency response was seen a relative success. It was rapidly executed, combining support from the international community as well as the local community led primarily by military agencies.
- The disaster response seems to have been fairly inconsistent between cities and provinces, and between urban and rural areas.
- Relocation of the population encountered many issues, aggravated by a sense of the lack of a clear longer-term recovery plan.

Acknowledgements

The EEFIT team received enormous and generous support from many local experts. Without them, the mission would not have been as successful as it was: Ing. Marcelo Romo (Escuela Politécnica del Ejército), Dr. Davide Besenon Venegas (ESPOL), Archs. Jean Paul Demera and Nguyen Ernesto Baca (Historical Preservation), Milton Cedeño (ULEAM), Guillaume Roux-Fouillet (IFRC, ShelterCluster), Leanne Marshall (IFRC, ShelterCluster), Anna Pont (IFRC, ShelterCluster), Paulina Soria (INBAR), Christian Riofrio (AIMA), Gen. Mosquera, Crnl. de E.M.C. William Aragon, Col. Ramos, Col. Negrete, Col. Parra, Lt. Col. Iturralde, Maj. de E. Henry Cordova (Secretaria de Gestión de Riesgos), Maj. Fabricio Godoy (ISSFA). During the mission, we received support from our London-based colleagues, EEFIT coordinators Berenice Chan, Sean Wilkinson, and Tristan Lloyd.

During the mission, two individuals joined the team additionally: Nicolas van Drunen, originally from Delft University and on a placement helping the local efforts of INBAR; and Everth Luis Mera, student at the School of Civil Engineering of Portoviejo. The EEFIT team is very grateful for their precious help.

Prior, during and after the field mission, we received briefings and support from Anna Pavan, Francisco Pavia, Matthew Free (Arup), Antonios Pomonis (Cambridge Architectural Research & World Bank), Tom Dijkstra, Helen Reeves and Colm Jordan (British Geological Survey), James Daniell (Kahlsruhe Institute of Technology & World Bank Group), Oscar Ishizawa and Rashmin Gunasekera (World Bank Group), Emilio Franco (Gestió de Infraestructures SA, retired), Thomas Ferre (MicroVest Capital Management, LLC), Marjorie Greene and Forrest Lanning (EERI), Eduardo Miranda (Stanford University), Enrique Morales (University of Buffalo), Mario Calixto Ruiz Romero, Alexandra Alvarado and Pedro Espín (Instituto Geofísico), Lizzie Blaisdell (Build Change), Kevin Hagen (EWB-USA), Diego Paredes (UK Embassy in Ecuador), Carla Muirragui (Cámara de Industrias y Producción), Sandra Silva, Jenny Nino, Carolina Gallegos Anda, Natividad Garcia Troncoso (Imperial College), Alby Del Pilar Aguilar Pesantes (ESPOL), Michael Davis, Luz Gutiérrez, and Santiago del Hierro.

The Engineering and Physical Sciences Research Council (EPSRC) provided funding for team members Ahmed, Hughes, and Jirouskova. Bayes Ahmed was a Commonwealth Scholar funded by the UK govt. Ahmed's work was partially supported by the UCL Institute for Risk and Disaster Reduction (UCL IRDR). Old Centralian Trust and the Imperial College Faculty of Engineering Dean's Fund provided further support for Jirouskova. The School of Technology at the University of Cambridge and Queens' College Cambridge provided further support for Hughes. The Centre for Urban Sustainability and Resilience at University College London (UCL) provided funds for Stone. Arup supported members Kaminski and Lopez and also provided funding for vehicles. Guy Carpenter supported team lead Franco. The Ecuador Army provided additional land and sea transportation to the team. This financial support made the mission possible.

Finally, the EEFIT Corporate Sponsors are thanked for their support over the years. They are: AECOM, AIR Worldwide Ltd, Arup, Atkins, Guy Carpenter & Co. Ltd, Risk Management Solutions, Sellafield Ltd and Willis Towers Watson.

Table of Contents

Executive Summary	ii
Acknowledgements	v
1. Introduction	1
1.1. Mission Objectives and Organisation.....	1
1.2. Report Structure.....	2
2. Seismotectonic Setting	4
2.1. Tectonic Setting	4
2.2. Local Faulting and Active Faulting.....	7
2.3. The 2016 Sequence of Events	12
3. Site Effects and Microtremor Tests	18
3.1. Geological Setting.....	18
3.2. Microtremor Tests	24
3.3. Field Equipment	26
3.4. Filtering/Processing.....	26
3.5. Analysis of the Results and Stratigraphy Interpretation.....	27
3.6. Site Effects Interpretation	37
4. Observations of Geotechnical Failures	44
4.1. Overall Survey Scope.....	44
4.2. Liquefaction.....	45
4.3. Landslides.....	52
5. Perspective on Seismic Hazard Considerations in Local Building Code	65
5.1. Seismic Code History in Ecuador	65
5.2. Current Seismic Design Code Hazard Provisions (NEC-15)	66
5.3. Seismic Hazard Code Provision Performance in the 2016 Muisne event	70
6. Building Performance Observations	73
6.1. Introduction	73
6.2. Survey Methodology	73
6.3. Observed Building Stock	74
6.4. Overview of Observed Building Damage.....	78
6.5. Damage Data from Rapid Surveys	87
6.6. Jama	93
6.7. Pedernales.....	93
6.8. Case Study Observations.....	94
6.9. Observations on the Immediate Structural Inspection of Buildings.....	99
7. Infrastructure Performance Observations	105
7.1. Roads	105
7.2. Bridges.....	107
7.3. Other Infrastructure	115
8. Socio-Economic and Community Vulnerability	117
8.1. Background.....	117
8.2. Location of the Earthquake Shelters.....	117
8.3. Getting Accommodation in the Shelters.....	117
8.4. Facilities in the Shelters	119
8.5. Norms and Regulations.....	121
8.6. Findings from the Questionnaire Surveying	122
8.7. Summary of the Social Survey Findings	133
References	134
Appendix A: External geotechnical investigation data available	141
Appendix B: Microtremor test readings	156
Appendix C: BGS Rapid satellite-based landslide assessment maps ground-proofing	162
Appendix D: Examples of activities and services provided in the temporary earthquake refugee shelters in Ecuador	179

Appendix E: Questionnaire for assessing community vulnerability to earthquake disasters in the refugee shelters: the Ecuador 16 April 2016 earthquake.....	182
Appendix F: Contingency tables from the questionnaire.....	185

Table of Figures

Figure 2-1 Tectonic plates speed distribution (Map from UNAVCO Plate Motion Calculator: http://sps.unavco.org/crustal_motion/dxdt/model/).....	4
Figure 2-2 Major regional tectonic features and plate boundaries (after Trenkamp <i>et al.</i> , 2002 and Bourgeois <i>et al.</i> , 2013). BB' and AA' shown in Figure 2-3. Acronyms: CNSC-Cocos-Nazca Spreading Center; DGM-Dolores-Guayaquil Megashear; GGTB-Gulf of Guayaquil-Tumbes Basin; MAT-Middle America Trench; NAB- North Andean Block; PCT-Peru Chile Trench.	5
Figure 2-3 Subduction fault models for Section A-A' (above) and B-B' (below) shown in Figure 2-2 respectively from Parra <i>et al.</i> (2016) and Trenkamp <i>et al.</i> (2002).	6
Figure 2-4 3-D view of the two-tear model for the Carnegie Ridge collision featuring: a steep ESE-dipping slab beneath central Colombia; a steep NE-dipping slab from 1°S to 2°S; the Peru flat slab segment south of 2°S; a northern tear along the prolongation of the Malpelo fossil spreading centre; a southern tear along the Grijalva FZ; a proposed Carnegie flat slab segment (C.F.S.) supported by the prolongation of Carnegie Ridge (after Gutscher <i>et al.</i> , 1999). Sections A-A' and B-B' mentioned in Figure 2-2 and 2-3 are also approximately shown indicatively.....	6
Figure 2-5 (a) Inferred extension of the Carnegie Ridge under the North Andean block, also showing earthquake fault plane solutions from the Harvard CMT (centroid moment-tensor) catalogue (after Gutscher <i>et al.</i> , 1999). The 16 of April 2016 mainshock epicentre location is shown as a red star, and the area of most concentrated damage highlighted in blue; (b) Tectonic detailing of spreading centre between the Carnegie ridge and Cocos Ridge (Gutscher <i>et al.</i> , 1999).	7
Figure 2-6 Geomorphological reconstitution of the Ecuadorian Coastal Cordillera – Most recent evolution (Pleistocene sup. To now) (after Reyes, 2008). The green area shows the potential Carnegie Ridge extension, based on Gutscher <i>et al.</i> , 1999 (Figure 2-5) and the geomorphological lineaments identified in Reyes (2008), assuming that the lineaments are indeed directly linked to the dynamics of the Carnegie Ridge underneath. The blue and violet thick lines in the Mache-Rioverde and Jama blocks may be considered for further analysis in understanding the barriers to the 2016 rupture propagation (see Section 4.2).	8
Figure 2-7 Active fault map (from Eguez <i>et al.</i> , 2003).....	9
Figure 2-8 South American subduction seismicity for events $M_w > 6$ (USGS, 2014).	10
Figure 2-9 Subduction earthquake types showing interface and intra-slab events. NB: at surface, the concentric red shape illustrates the epicentre and wave propagation corresponding here to an interface event.	11
Figure 2-10 Historic subduction seismicity analysis and identification of seismic gap (after Chlieh <i>et al.</i> , 2014). The red star shows the approximate location of the epicentre of the 2016 main shock.	11
Figure 2-11 Earthquake catalogue and seismic hazard zoning in Parra (2016) (a). $M_w > 6$ events from catalogue and associated tectonic seismogenic type (b) (NB: interface and in-slab are two type of subduction earthquakes – c.f. Figure 2-9).	12
Figure 2-12 The 16 April 2016 event mainshock characterisation (left) and PAGER Intensity map (right) (USGS, 2016).....	13
Figure 2-13 Rate of aftershocks with elapsed days based on modified Omori's law (left). Number of aftershocks with earthquake magnitude based on Gutenberg-Richter relationship (right).	13
Figure 2-14 (a) Aftershocks of the 2016 16 April main shock (IG, 2016 - http://www.igepn.edu.ec/mapas/mapa-evento-20160416.html – data extracted on the 17/11/2016) (b) Historic seismicity map and cross-sections in the vicinity of the interplate seismogenic zone: results from the 3-D approach and P-wave arrivals (Font <i>et al.</i> , 2013). The yellow dotted lines illustrate the axes of greater concentration of aftershocks. The green area bounds the aftershocks' greatest concentration area.	14
Figure 2-15 (a) Epicentres of the main event (red star) and location of aftershocks (circles sized according to magnitudes) over 35 days following the mainshock from the Geophysical Institute of the National Polytechnic School at Ecuador (http://www.igepn.edu.ec/portal/ultimo-sismo/informe-ultimo-sismo.html) superimposed on the slip model (Ye <i>et al.</i> , 2016). The green area illustrates the greatest aftershocks concentration area. The coloured segments shown correspond to the subduction rupture lengths associated to the past big events as interpreted by Chlieh <i>et al.</i> (2014).	15

Figure 2-16 Comparison of P waves at E–W component of the 1942 (purple) and 2016 (blue) events at station DBN with Galitzin instrumental response (pendulum/galvanometer periods ~25 s and gain factor of 310). The waveform for 1942 is from Swenson and Beck (1996) with peak-to-peak amplitude confirmed by Bernad Dost from the DBN station bulletin. The waveform for the 2016 event is the convolution of displacement (after removal of the broadband instrumental response) with the Galitzin instrumental response. They are aligned at the beginning (left) and at the peak (right). (Ye *et al.*, 2016).16

Figure 2-17 Seismometer locations and IDs, with associated acceleration recordings of the main shock (after IG, 2016).17

Figure 2-18 Main shock Shakemap and recorded PGAs at seismometer stations (from GEER, 2016 based on Shakemap and IG, 2016 data).17

Figure 3-1 Main geomorphological units of Ecuador (Reyes, 2008).19

Figure 3-2 Paleogene stratigraphy of the Jipijapa Zone in Manabi (from Luzieux *et al.*, 2006).20

Figure 3-3 Localisation of the geological Neogene Basins of the Coast of Ecuador (Reyes, 2008).20

Figure 3-4 Neogene stratigraphy of the Manabi Basin (modified from Reyes, 2008 after Deniaud, 1999).21

Figure 3-5 Geological map of the study area (from Reyes & Michaud, 2012). Q: Quaternary; Pl: Pliocene; M: Miocene; O: Oligocene; E: Eocene; P: Paleocene; K: Cretaceous (for details, see reference).22

Figure 3-6 Example of seismic bedrock at different depths which generate H/V peaks at different frequencies. Case 1: bedrock at 300 m depth, case 2: bedrock at 20 m depth, case 3: bedrock at 4 m depth (Micromed, 2012).25

Figure 3-7 Microtremor test set up in Tarqui, Manta.25

Figure 3-8 APO1 (T9) amplitude spectrum of the recorded surface waves and H/V spectral ratio.26

Figure 3-9 Example of amplitude spectra showing "eyes" for stratigraphic interpretation.27

Figure 3-10 Location and ID of the microtremor tests carried out during the mission.28

Figure 3-11 Comparison of the H/V T2 in-situ measurement and its fit to V_s profile model at the Shelter location, Manta.29

Figure 3-12 Comparison of the H/V T13 in-situ measurement and its fit to V_s profile model at Tarqui, Manta.29

Figure 3-13 V_s profile models for Manta30

Figure 3-14 H/V T8 reading and corresponding spectrum for V_s simplified model derived for the Botanical Garden sites (T6-T9).31

Figure 3-15 H/V T4 reading and corresponding spectrum for the first option of interpretation of the V_s simplified model derived for the Z0 sites (T3 & T4).31

Figure 3-16 H/V T4 reading and corresponding spectrum for the second option of interpretation of the V_s simplified model derived for the Z0 sites (T3 & T4).32

Figure 3-17 H/V reading and corresponding spectrum for the first option of interpretation of the V_s simplified model derived for the Portoviejo river bank at T5.32

Figure 3-18 H/V reading and corresponding spectrum for the second option of interpretation of the V_s simplified model derived for the Portoviejo river bank at T5.32

Figure 3-19 Interpreted V_s measurements and models for Portoviejo. The Tamarindos and APO1 MASW and MAM V_s measurements come from GEER (2016). The CAC V_s profiles are derived from SPT-N measurements (Hidroplan, 2016) (see Appendix A).33

Figure 3-20 H/V reading and corresponding spectrum for the first option of interpretation of the V_s simplified model derived for the Bahía Hospital site T10.34

Figure 3-21 H/V reading and corresponding spectrum for the second option of interpretation of the V_s simplified model derived for the Bahía Hospital site T10.34

Figure 3-22 H/V reading and corresponding spectrum for the V_s simplified model derived for the NW embankment of the Los Caras Bridge, site T12.35

Figure 3-23 V_s profiles for Bahía. The PMB profiles are derived based on SPT-N values from LUP (2016), and the Los Caras Bridge best estimate V_s profile is based on a SPT-N simplified profile provided to GEER (2016) by the Ecuador’s Army Corps of Engineers (see Appendix A).35

Figure 3-24 Comparison of the APED microtremor test reading H/V ratio to that of the corresponding simplified V_s profile derived.36

Figure 3-25 V_s profile derived for APED, Pedernales.36

Figure 3-26 Preliminary rapid assessment damage map (IGM, 2016).38

Figure 3-27 Rapid damage assessment map for Portoviejo (a - UNOSAT, 2016; b- IGM, 2016).40

Figure 3-28 Rapid damage assessment map for Bahía de Caraquez and San Vicente, across the Chone Estuary (IGM, 2016).	41
Figure 3-29 Rapid damage assessment map for Pedernales (IGM, 2016).....	42
Figure 3-30 Jama and Canoa SPT-based V_s profiles (based on LUP (2016) measurements).....	43
Figure 4-1 (a) Primary causes of damage to buildings (left) and the second main cause of damage (right) in 50 earthquakes that occurred between 1989 and 2003; (b) Primary causes of damage to transportation systems (left) and utilities (right) in earthquakes between 1989 and 2003 in which there was significant damage to these two categories of exposure (Bommer <i>et al.</i> , 2006).	44
Figure 4-2 Location and type of geotechnical surveys carried out by EEFIT.	45
Figure 4-3 Lateral spreading in Portoviejo (a) liquefaction of fill below VelBoni carpark (b) tension cracking due to liquefaction of a lower layer.....	46
Figure 4-4 Structural damage due to lateral spreading along Rio Portoviejo consisting in the rotation and settlement of structures at sports pitch.	47
Figure 4-5 Collapse of structures along Rio Portoviejo due to liquefaction induced lateral spreading.....	47
Figure 4-6 Damage to south-west of Mejía Bridge (a) lateral spreading of embankment, (b) sliding and rotation of gabions.	48
Figure 4-7 Liquefaction induced damage to shrimp farm dykes in Chone River estuary.	49
Figure 4-8 Lateral spreading of mangrove swamps in Chone River Estuary.	49
Figure 4-9 Protrusion of manholes in Manta (a) and Pedernales (b).	50
Figure 4-10 Relative uplift of structure with underground storage tanks in Pedernales, showing locations of measured relative settlement.	50
Figure 4-11 Collapse of structures on timber piles in Chamanga.	51
Figure 4-12 Settlement of building in Chamanga (a) increased settlement from left to right of structure (b) settlement relative to road and step.	51
Figure 4-13 Damage due to differential settlement of building in Chamanga (a) concrete cracking due to differential settlement, (b) detail of structural damage to building.....	52
Figure 4-14 Location of region where landslides were observed and surveyed circled in red.....	53
Figure 4-15 Examples of landslides observed. Coastal landslides observed from Highway 15 between San Vicente and Canoa, a) shallow seated, b) deep seated. Landslides in low-lying hills near San Isidro, c) shallow seated, d) deep seated.	53
Figure 4-16 Graphs to show the accuracy of the preliminary co-seismic landslide inventory maps for the sites surveyed around Bahía de Caraquez and in Portoviejo; (a) location, (b) failure type.....	55
Figure 4-17 Localisation of the landslide sites surveyed close to San Isidro, and the town of San Isidro on the right on which one of many co-seismic landslides is visible.	57
Figure 4-18 Panoramic view of the ground failure at Site A (yellow lines indicate primary scars, and blue ones the secondary ones; the blue arrows show the movement of the soil).....	57
Figure 4-19 Isidro site A taken from a drone, looking along the ridge at location (A) on figure above.....	57
Figure 4-20 San Isidro site A, rotation and translation of surficial blocks of soil close to the head of the slope. Photo taken of ground along the path defined as (B) on panoramic picture above.	58
Figure 4-21 Face of scar at location C shown on panoramic picture of Site A above.....	58
Figure 4-22 San Isidro site B, taken from a drone. A river runs through the trees at the bottom of the slope, to the right of the figure (the yellow circle shows the intact house next to the slope that failed).	59
Figure 4-23 El Relleno San Isidro Site B Landslide analysis by Echeverria (2016).	59
Figure 4-24 Site A and B relatively to the main surrounding cities and the potential active Canaveral fault segments mapped by Egeuz (2003) shown as red lines.....	60
Figure 4-25 Example of a landslides on the coastal road between San Vicente and Canoa (Echeverria, 2016).	61
Figure 4-26 Road Rehabilitation Works carried out on the coastal road between San Vicente and Canoa.....	61
Figure 4-27 Informal settlement damage South of Pedernales due to slope failure (drone image of the head of the slope on the right).	62
Figure 4-28 Slope instability damage North of Pedernales.....	62
Figure 4-29 Major landslide observed on the road from Canoa to San Isidro	63
Figure 4-30 Map of landslide sightings in the San Isidro area (courtesy of Echeverria and Sevilla, 2016).	63
Figure 4-31 Unsafe practice clearing landslide debris (Chone Estuary).....	64
Figure 5-1 Ecuador seismic hazard zonation from NEC-SE-DS (NEC-15).	68

Figure 5-2 Ecuador seismic code’s elastic response spectrum for 5% damping, from NEC-SE-DS (NEC-15). NB: dashed line for periods $T < T_0$ is only allowed for modes of vibration other than the fundamental mode of vibration when performing modal response spectrum analysis.	69
Figure 5-3 Comparison of recorded motions at the seismometer locations listed and the NEC15 design spectra for $Z=0.5$ and site conditions ranging from Class B to E. Ground motion records locations: AES2 – Esmeraldas record; APED – Pedernales record; ACHN - Chone Estuary record; AMNT – Manta record; APO1 – Portoviejo record; AGYE: Guayaquil record.....	71
Figure 5-4 Comparison of the recorded motions to the adapted NEC-15 for Manta, Portoviejo and Pedernales with appropriate Site Conditions from V_s measured by (GEER, 2016) and back calculated $Z=PGA_{bed}$ from recorded ground motion.	72
Figure 6-1 Reinforced concrete frame with masonry infill walls – non-engineered low-rise.	75
Figure 6-2 Reinforced concrete frame with masonry infill walls – engineered high-rise.....	75
Figure 6-3 Quincha structure.	76
Figure 6-4 Timber frame with masonry infill.	77
Figure 6-5 Informal rural housing.....	77
Figure 6-6 Collapsed building, showing failure of façade and frame.	78
Figure 6-7 Inadequate masonry infill wall design and construction.....	79
Figure 6-8 Inadequate design and detailing for shear – insufficient link spacing, poor link detailing and plain links used.	80
Figure 6-9 Weak and soft storey failures.....	81
Figure 6-10 Exposed reinforcement with possible inadequate lap lengths for future construction, and an upper storey soft/weak storey failure.	81
Figure 6-11 Short columns at a school in Pedernales.	82
Figure 6-12 Short columns at a shop front – note the local crushing of the masonry lining up with an imaginary compression strut and local shear failure of the column.....	82
Figure 6-13 Insufficient cover to rebar – note 100% section loss to some of the links.	83
Figure 6-14 Pounding of a column head by a slab of an adjacent building.	83
Figure 6-15 Inadequate design of plastic hinges.....	84
Figure 6-16 Inadequate securing of non-structural elements – the image on the right depicts a hospital corridor.	84
Figure 6-17 Poor quality concrete.	85
Figure 6-18 Examples of rot and insect damage.....	86
Figure 6-19 Lack of positive connection between frame and masonry upstand, leading to sliding of column laterally.	87
Figure 6-20 Possible damage due to debris from adjacent buildings.....	87
Figure 6-21 Survey routes (blue lines) in the restricted zone (yellow shaded area) in Tarqui, Manta. Centre of image: (-0.9535, -80.7149).....	89
Figure 6-22 Survey routes (purple lines) near Manta seismometer station. Centre of image: (-0.9415, -80.7332).	90
Figure 6-23 Overview of Portviejo with key locations (blue dots), video survey routes (purple lines), ground zero (yellow shaded area), ground zero survey routes (red lines), and survey routes near the seismometer station (light blue lines). Centre of image: (-1.0432, -80.4569).	91
Figure 6-24 Survey routes (light blue lines) near Portoviejo seismometer station. Centre of image: (-1.0373, -80.4622).	91
Figure 6-25 Map of survey routes (purple lines) in Jama. Centre of image: (-0.2017, -80.2639).	93
Figure 6-26 Map of Pedernales showing key sites (blue dots), and survey routes (purple lines). Centre of photo: (0.0721, -80.0520).	94
Figure 6-27 Shear cracking due to short column effect.	95
Figure 6-28 Complete out-of-plane failure of masonry perimeter infill walls.	95
Figure 6-29 In-plane shear cracking of masonry infill walls.	95
Figure 6-30 Pounding at movement joint.....	95
Figure 6-31 Movement joint filled with rubble (prior to event).....	96
Figure 6-32 Permanent lateral drift of buildings relative to one another of approximately 50mm (follow movement joint below “DE”).	96
Figure 6-33 Steel plate retrofit to reinforced concrete column.	97

Figure 6-34 Site welded steel plate.	97
Figure 6-35 Hospital Miguel Hilario Alcivar De Bahía De Caraque.	97
Figure 6-36 In-plane shear cracks.	97
Figure 6-37 Significant damage to false ceiling and fittings.	98
Figure 6-38 Damage at interface between coupled column and shear wall.	98
Figure 6-39 Pedernales Cathedral, with damage to the roof and masonry façade.	98
Figure 6-40 Internal damage to ceiling tiles and masonry walls.	98
Figure 6-41 Main municipality building in Pedernales.	99
Figure 6-42 Local damage to head of RC column.	99
Figure 6-43 Moderate damage to RC staircase.	99
Figure 6-44 Heavy non-structural damage to internal and external masonry wall panels.	99
Figure 6-45 Coordination meeting at the OSOCC upon arrival in Portoviejo.	100
Figure 6-46 Map of Portoviejo illustrating the extents of Zone Zero (delimited by faded red dashed line). .	101
Figure 6-47 The tagging system.	102
Figure 6-48 Placard for demolition.	102
Figure 7-1 Landslide damage to roads (a) on the Highway 15, near Canoa (b) on rural road near San Isidro.	105
Figure 7-2 Examples of cracking on roads near San Isidro.	106
Figure 7-3 Damage to roads due to liquefaction induced lateral spreading (a) Chone river estuary near San Vicente, (b) Portoviejo, close to the Rio Portoviejo.	106
Figure 7-4 Road damage in Pedernales due to settlement of trench fill (a) and settlement of sand underneath (b).	107
Figure 7-5 Mejía bridge – Highway 39A Portoviejo – Rocafuerte (-0.9899N; -80.4697E). Gabion walls provided on this side of the bridge only. Left – from EEFIT mission; Right - from EERI (2016), posted on twitter just after the main shock (http://www.eqclearinghouse.org/).	108
Figure 7-6 Mejía bridge, differential settlement between the two separate sections as seen from the bridge’s approach.	108
Figure 7-7 Mejía bridge, embankment (left) and gabion wall (right) failure.	108
Figure 7-8 Mejía bridge, damage in abutment.	109
Figure 7-9 Los Caras bridge (-0.6094N; -80.4162E), viewed from Bahía de Caraquez. The piles can be seen at low tide.	109
Figure 7-10 Los Caras bridge, 45m-long decks supported by 4-column piers (left) and deck’s prestressed concrete beams showing also seismic isolators (right).	110
Figure 7-11 Los Caras bridge, continuous connection between main spans (left) and movement joint between main spans (right).	110
Figure 7-12 Los Caras bridge, location of seismic isolators (left) and close-up view of seismic isolator (right).	111
Figure 7-13 Los Caras Bridge liquefaction susceptibility analysis.	112
Figure 7-14 Collapsed footbridge in Canoa.	113
Figure 7-15 Footbridge in Canoa, right end anchorage block (left) and suspension cable end that failed at anchorage (right).	113
Figure 7-16 Footbridge in Canoa, left end anchor points experienced uplift.	114
Figure 7-17 Structural damage due to lateral spreading along Rio Portoviejo observed on the rotation and lateral displacement of foundations of the Puente Chile in Pedernales.	114
Figure 7-18 Movement of soil from around the Velasco Ibarra bridge foundations.	115
Figure 7-19 Bridge collapse in Guyaquil after the 2016 Ecuador Main Shock (http://abcnews.go.com/International/drone-video-captures-deadly-earthquake-aftermath-ecuador/story?id=38473672).	115
Figure 7-20 Manta Port damage (left: aerial photograph showing extent of liquefaction damage at surface; right: port wall damage, showing for scale K. Rollins, at GPS 0o56'29.6"N, 80o43'27.4"E – from GEER, 2016).	116
Figure 7-21 Airport control tower collapse.	116
Figure 8-1 The earthquake refugee shelters in (a) Portoviejo, (b) Canoa, and in (c) Pedernales, Ecuador. Source: Bayes Ahmed, field visit, May-June 2016.	118

Figure 8-2 The location of the shelters in Aeropuerto Reales Tamarindos, Portoviejo (1°2'45" South 80°28'5" West), Ecuador. Image (a) was acquired on 17 April 2016 and image (b) was captured on 24 April 2016. It depicts the increase of shelters in the airport. Source: The Google Earth Images..... 119

Figure 8-3 The location of the earthquake shelters in Canoa, Ecuador. (a) It was a football field back in 2013, and (b) later was converted to temporary shelters. Source: The Google Earth Images. 120

Figure 8-4 Information board of the Aeropuerto Reales Tamarindos camp in Portoviejo [30 May 2016]. 121

Figure 8-5 The survey team members conducting questionnaire interview in the shelters in Ecuador. 122

Figure 8-6 Relationship ($\chi^2 = 0.000$) between building material and number of floors (before scenario)..... 128

Figure 8-7 Relationship ($\chi^2 = 0.002$) between year of construction and number of floors (before scenario).
..... 129

Figure 8-8 Relationship ($\chi^2 = 0.028$) between year of construction and destruction pattern (before scenario).
..... 130

Figure 8-9 Relationship ($\chi^2 = 0.254$) between building material and destruction pattern (before scenario). 130

Figure 8-10 Relationship ($\chi^2 = 0.167$) between year of construction and building materials (before scenario).
..... 131

Table of Tables

Table 2-1 Caribbean system tectonic plates dynamics.	4
Table 2-2 Description of the couple most damaging aftershock events following the 16 April 2016 event	14
Table 2-3 Seismometer stations in Manabi and Esmeraldas closest to sites visited. Ground motion record data and seismometer properties from IG-EPN (2016). $V_{s,30}$ from Vera-Grunauer (2014) in Guayaquil, and Geostudios (2016) for the other locations where available.	16
Table 3-1 List of ground investigation data analysed.	23
Table 3-2 Use of Equipment associated to microtremor tests.	26
Table 3-3 TROMINO® tests coordinates.	28
Table 3-4 Number of V_s profiles derived compared to number of TROMINO® tests per city surveyed.	28
Table 3-5 NEHRP Site Categorisation (BSSC, 2004).	37
Table 3-6 SPT- V_s correlation recommendations from Wair <i>et al.</i> (2012).	37
Table 3-7 Summary of site frequency and categorization based on available geotechnical information for Manta.....	39
Table 3-8 Summary of site frequency and categorization based on available geotechnical information for Portoviejo.....	40
Table 3-9 Summary of site frequency and categorization based on available geotechnical information for Bahía de Caraquez and the mouth of the Chone Estuary.	42
Table 3-10 Summary of site frequency and categorization based on available geotechnical information for Pedernales.	43
Table 5-1 Summary of seismic code history in Ecuador.	65
Table 5-2 Seismic zone factor Z from NEC-SE-DS (NEC-15).	66
Table 5-3 Soil type for seismic design from NEC-SE-DS (NEC-15).	67
Table 5-4 F_a , F_d , and F_s factors for construction of elastic response spectrum S_a (see Figure 5-2), from NEC-SE-DS (NEC-15).	69
Table 5-5 Building importance classification and importance factor I, from NEC-SE-DS (NEC-15).	69
Table 5-6 Strength reduction factor R for ductile and limited ductility structural systems, from NEC-SE-DS (NEC-15).	70
Table 5-7 Comparison between Seismic Hazard PGA Level Recommendations from literature review and recorded PGAs for Manta, Portoviejo and Pedernales.....	72
Table 6-1 Rapid visual survey data collected.....	73
Table 6-2 Damage data from Tarqui, Manta.	89
Table 6-3 Damage data from Manta seismometer station survey.....	90
Table 6-4 Damage data for ground zero, Portoviejo.....	92
Table 6-5 Damage data from surveys near to the Portoviejo seismometer station.	92
Table 6-6 Damage data from the Portoviejo video survey.	92
Table 6-7 Damage data from Jama.....	93
Table 6-8 Damage data for Pedernales.	94
Table 6-9 Number of assessed buildings for rapid and detailed assessment in Portoviejo.	103
Table 6-10 Number of assessed buildings for safe route access and demolition verification in Portoviejo...	103
Table 6-11 Number of assessed buildings in Pedernales.	103
Table 7-1 Los Caras liquefaction susceptibility analysis. N60 values provided by Morales 2016. Water table 8 m above ground surface (river bed).....	112
Table 8-1 Age group distribution.....	122
Table 8-2 Gender distribution.	123
Table 8-3 Educational background.	123
Table 8-4 Current monthly household income.	123
Table 8-5 Changes in occupation pattern.....	124
Table 8-6 Construction year of the damaged buildings.	124
Table 8-7 Number of floors in the building (before earthquake scenario).....	125
Table 8-8 Building materials (before scenario).....	125
Table 8-9 Ownership of the house.	125
Table 8-10 Settlement location (before scenario).	125
Table 8-11 Household destruction pattern.....	125

Table 8-12 Earthquake preparedness.....	126
Table 8-13 Problems living in the shelters (first priority).....	126
Table 8-14 Problems living in the shelters (second priority).....	126
Table 8-15 Recovery plan from the disaster (first priority).....	127
Table 8-16 Recovery plan from the disaster (second priority).....	127
Table 8-17 Number of floors in the building (after scenario).....	127
Table 8-18 Building materials (after scenario).....	127
Table 8-19 Settlement location (after scenario).....	127
Table 8-20 Building material before and after scenario.	131
Table 8-21 Floor height before and after scenario.	131
Table 8-22 Results from the linear regression modelling.	132

1. Introduction

1.1. Mission Objectives and Organisation

The Earthquake Engineering Field Investigation Team (EEFIT) was deployed to Ecuador on 24 May 2016 and remained on site for approximately two weeks until 7 June. The objective of the team was to carry out a general assessment of structural damage to building stock, to bridges and to other facilities; to document and observe soil failures, landslides, liquefaction and faulting; to obtain measurements and acquire data whenever possible; to develop a view of the performance in response to the event, and; to investigate the socioeconomic context through interviews. Several disciplines were represented by the team members including structural engineering, architecture, social sciences, disaster risk management, catastrophe insurance, and geotechnical engineering. Included with the team's equipment were a microtremor instrument (TROMINO®) and an unmanned aerial vehicle (UAV) or quadcopter drone. These instruments allowed the group to collect data useful in understanding the event.

Prior to departure, the deployed team included seven official members: Guillermo Franco (lead), Harriette Stone (co-lead and structural engineering), Sebastian Kaminski (structural engineering), Jorge Lopez (structural engineering), Nina Jirouskova (geotechnical engineering and resilience civil engineering), Fiona Hughes (geotechnical engineering), and Bayes Ahmed (disaster recovery & social sciences). Additionally, Darren Chian (geotechnical engineering) supported the team remotely from his home location in Singapore.

As we gathered local support, the team expanded to include co-author Major Manuel Querembás, director of the School of Military Engineering of the Ecuadorian Army. The access we enjoyed to restricted sites, remote rural areas, bridges, etc. was facilitated by Major Querembás and his superiors who made sure all doors were open to the team and safety was ensured throughout the mission. We also had access to military vehicles including ground transportation and a boat to assess damages to the Los Caras Bridge. As anyone who has done this kind of work in the field knows, this was a luxury that allowed the team to maximise its efficiency on the ground. In addition, Major Querembás provided treasured insights into the event as he had been involved in the response and assessment since the outset.

Further support included the addition of Nicolas van Drunen, a student of architecture at Delft university in Holland, originally from Ecuador. Nicolas is part of INBAR (International Network for Bamboo and Rattan) and was assisting the Ecuadorian efforts to assess bamboo construction as an alternative to reinforced concrete. He joined the mission from the beginning assisting Bayes Ahmed with translation and in the preparation of the family surveys as well as providing insight into the bamboo reconstruction endeavours. Everth Luis Mera, student at the School of Civil Engineering of Portoviejo, also helped in the day to day activities of the mission.

Authors of this report also include Carlos Molina Hutt who participated in reconnaissance of the event through the European Union's Civil Protection unit prior to the EEFIT's activities, and whose experience benefitted the posterior visit tremendously. Carlos also contributed to large portions of section 6.9.1 regarding the structural observations immediately after the event. These observations were important as many anomalies were detected in the tagging and demolition of certain areas.

All in all, the team grew from the original eight official EEFIT mission members to the eleven authors of this report as the mission was ongoing. We could not have been luckier to assemble this great group of individuals and are deeply grateful for everyone's contributions. In addition, we received great support from many individuals and organizations listed in the acknowledgement section.

The preparation of the mission was ongoing for about three weeks prior to deployment and included numerous activities securing transportation, instrumentation, local contacts, security, coordinating travel, etc. The mission itself extended over approximately two weeks and there was an intense period of data collection and writing directly after the return spanning another four weeks. This culminated with the preparation of an article for the World Conference on Earthquake Engineering, which was presented in Santiago de Chile in January 2017 (Franco *et al.*, 2017).

During the period of September 2016 until January 2017, the team concentrated on the analysis and summary of the datasets compiled resulting in a series of drafts that would comprise this report. These sections were compiled into a uniform draft report during the period of February to April 2017. This draft underwent several reviews culminating in its publication in late 2017.

1.2. Report Structure

The main report is divided into eight sections. The content of the following sections is summarised below:

- **Section 2** presents the seismotectonic setting in the region and collects information acquired from literature regarding the relevant context of the Muisne event. This section also presents the main characteristics of the mainshock as well as of the rest of the sequence observed during April 2016. This section was compiled by Chian, Jirouskova, and Hughes.
- **Section 3** focuses on the site effects interpretation, including an analysis of the role of site effects in the response observed in buildings. Site effects considered include soil amplification, topographic effect and basin effect. The interpretation of the microtremor tests conducted on site was done through the calibration of the measurements on other local geotechnical and geological data gathered post-mission through extensive work. This section was compiled by Chian, Jirouskova, and Hughes.
- **Section 4** describes the larger geotechnical failures observed on the terrain, including the investigation of earthquake-induced landslides, liquefaction and fault ruptures. This section presents the landslides investigation which was coordinated with the British Geological Survey (BGS) as part of a validation effort of their landslide identification system which employs satellite imagery. This section was compiled by Chian, Jirouskova, and Hughes.
- **Section 5** provides a link between the hazard-related sections and the damage discussions by reviewing historical building code provisions in Ecuador. This effort helps to understand the context for building performance in this event. It also provides some basis to the critical analysis of the adequacy of the current building code in Ecuador and how it might have performed under the level and type of hazards undergone. This section was compiled by Lopez and Jirouskova.
- **Section 6** summarises the work carried out during the many structural surveys that the team undertook during our mission. In this part of the report, we identify the different types of buildings observed as well as their most salient damage patterns, their detailing, and other features relevant to the effects of the earthquake. As in the geotechnical section, much of the effort on site consisted of capturing valuable and perishable data that then had to be compiled and analysed. These datasets involved the structural assessment of over a thousand buildings through quick inspection surveys. This section was compiled by Stone, Kaminski, and Lopez, with contributions from Molina Hutt.
- **Section 7** presents the observations from the surveys of key infrastructure assets, focusing mainly on roads and bridges, including critical facilities such as schools, and

EEFIT

commentaries on the performance of the electricity and power network, as well as the waste management systems. This section was compiled by Lopez, Hughes, and Jirouskova.

- **Section 8** describes the socio-economic aspects of the affected population. This primarily derives from household-based questionnaire interviews carried out at shelter sites distributed across the Manabí region. This section was compiled by Ahmed and van Drunen.

2. Seismotectonic Setting

2.1. Tectonic Setting

Ecuador is situated in a complex and very active tectonic setting, at a crossing between the Nazca, Cocos, Caribbean and South American Plates. These plates are dominantly oceanic and contain a diversity of interesting tectonic features. All three typical types of plate boundaries (convergent, divergent, transform) can be found in this region, including other features such as multiple triple junctions, hotspots, and subduction.

Although the formation of most of the plates in the Caribbean region can be traced back to events in the Cenozoic (Cediel & Shaw, 2003), most of the present-day plates are fragments of their respective precursors. The Nazca plate, for example, is a remnant of the former Farallon plate which split during inter-plate spreading ~23 Ma (Lonsdale, 2005). The North Andean plate contains sedimentary rocks spanning from ~199 to ~23 Ma (Ramos, 1999), indicating the lengthy development of the rigid body that makes up the plate.

Today, the plate motions of the Caribbean tectonic region are one of the most active in the world (Figure 2-1). Notably, the Nazca plate exhibits one of the world's fastest rate of convergence along its eastern boundary with South America and the world's fastest rate of divergence to its western boundary. Speeds, direction and rotation of the main regional tectonic plates are described in more details in Table 2-1.

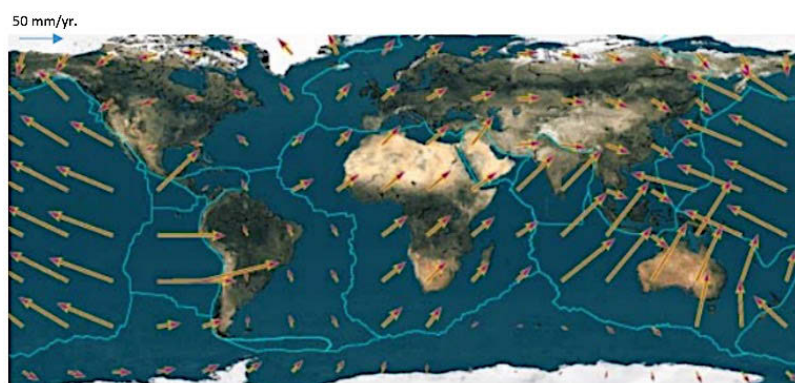


Figure 2-1 Tectonic plates speed distribution (Map from UNAVCO Plate Motion Calculator: http://sps.unavco.org/crustal_motion/dxdt/model/).

Table 2-1 Caribbean system tectonic plates dynamics.

Plate	Speed (mm/yr)	Direction (deg)*	Rotation (deg/my)	Model/Reference
Nazca	77	46.8	0.695	NNR-MORVEL (Argus & De Mets, 2011; Bird, 2003)
Caribbean	32	35.2	0.286	
North Andes	11	20.8	0.116	
Panama	33	33.7	0.317	

* directions are degrees from North clockwise.

The Manabi region is part of the North Andean Microplate belonging to the Caribbean Plate system with the Galapagos, Panama and Caribbean microplates. The North Andes microplate is delimited from the South-American Plate by the East Andean Fault System to the East and the subduction boundary with the Nazca Plate to the West (see Figure 2-2).

The geomorphology, tectonics and geological hazards of the Manabi region are largely governed by the plate movement of the Nazca subduction at an approximate rate of 60-80mm/year. As shown in Figure 2-3, the Nazca plate dips progressively with increasing angles underneath the North Andean/ South American Plate with angles from 6° to 35°.

Another key feature of the local geodynamics is the Carnegie Ridge, linked to the Galapagos Islands. The Carnegie Ridge is 1,350km long and up to 300km wide. It faces the Manabi basin perpendicularly to the subduction axis and subducts along with the Nazca plate, under the Andean block (c.f. Figure 2-4 and Figure 2-5). Its specific geological and geodynamic properties render the local tectonics and geomorphology more complex to understand. There remains much scope for research to better understand the influence and interaction of this feature in the regional tectonic and seismogenic context. It is worthwhile noting however that the seismic waves associated to the mainshock on the 16 of April 2016 seem to have preferentially propagated along the Manabi coastal cordillera and basin in the South-West direction from the inferred North-most extent of the Carnegie Ridge (Figure 2-5).

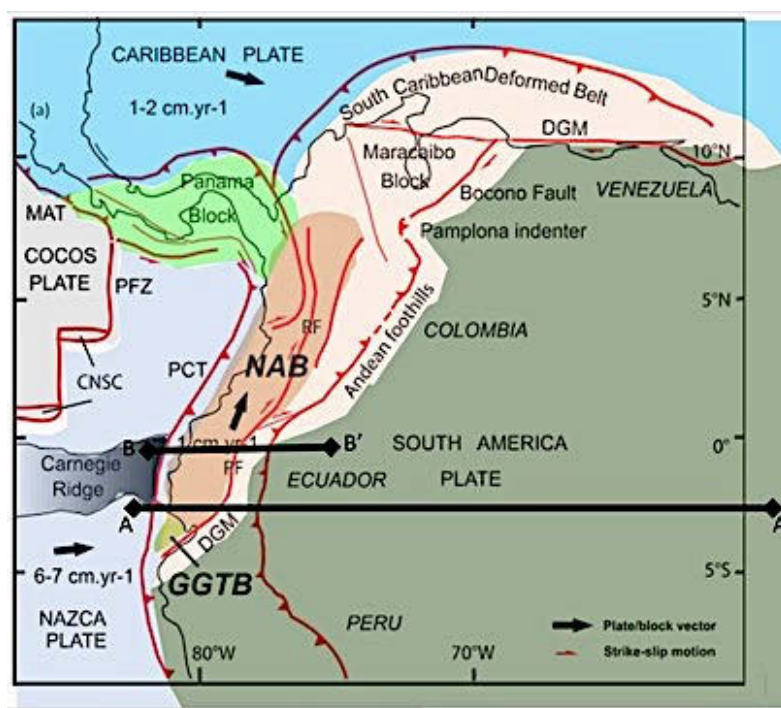


Figure 2-2 Major regional tectonic features and plate boundaries (after Trenkamp *et al.*, 2002 and Bourgeois *et al.*, 2013). BB' and AA' shown in Figure 2-3. Acronyms: CNSC-Cocos-Nazca Spreading Center; DGM-Dolores-Guayaquil Megashear; GGTB-Gulf of Guayaquil-Tumbes Basin; MAT-Middle America Trench; NAB- North Andean Block; PCT-Peru Chile Trench.

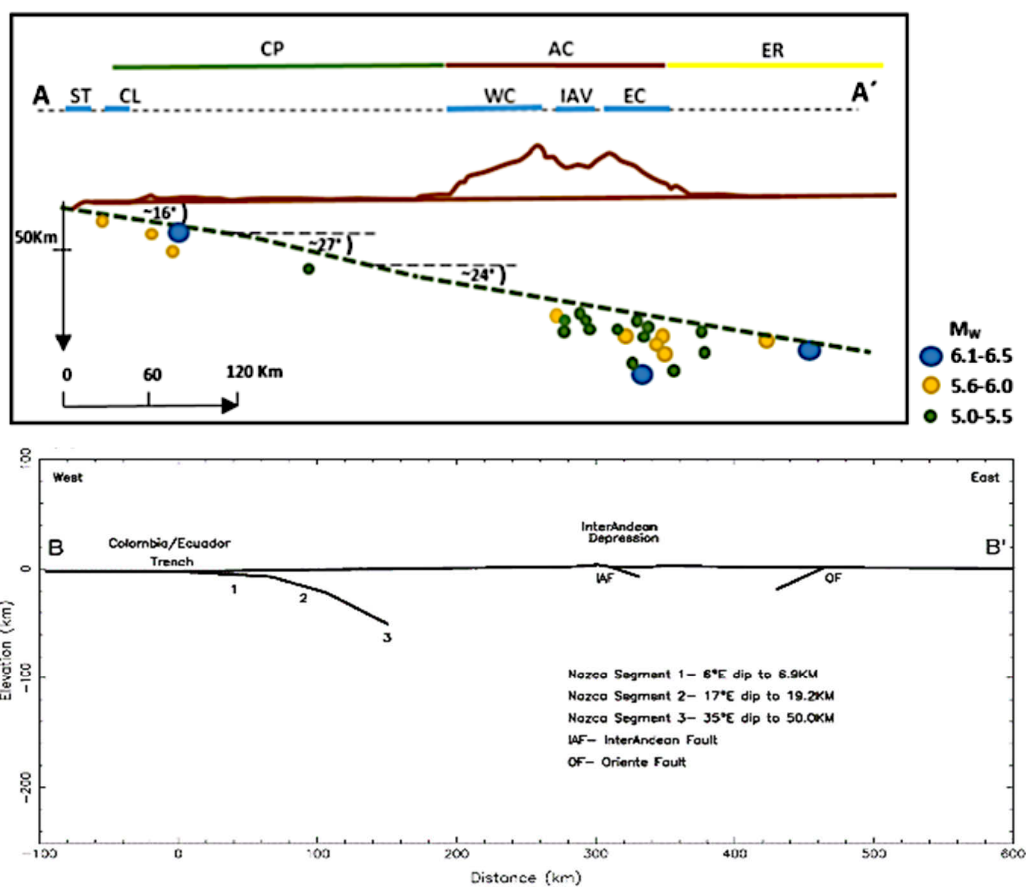


Figure 2-3 Subduction fault models for Section A-A' (above) and B-B' (below) shown in Figure 2-2 respectively from Parra *et al.* (2016) and Trenkamp *et al.* (2002).

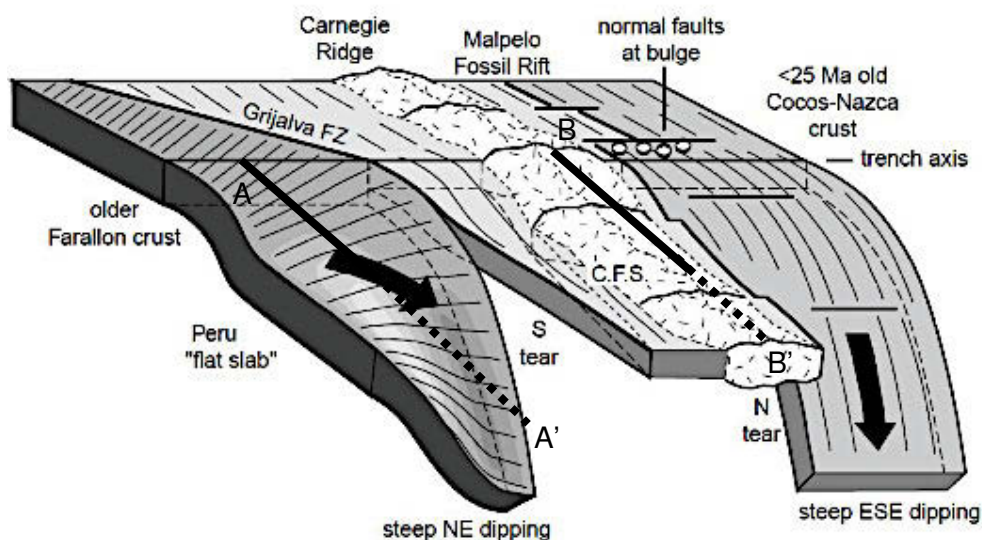


Figure 2-4 3-D view of the two-tear model for the Carnegie Ridge collision featuring: a steep ESE-dipping slab beneath central Colombia; a steep NE-dipping slab from 1°S to 2°S; the Peru flat slab segment south of 2°S; a northern tear along the prolongation of the Malpelo fossil spreading centre; a southern tear along the Grijalva FZ; a proposed Carnegie flat slab segment (C.F.S.) supported by the prolongation of Carnegie Ridge (after Gutscher *et al.*, 1999). Sections A-A' and B-B' mentioned in Figure 2-2 and 2-3 are also approximately shown indicatively.

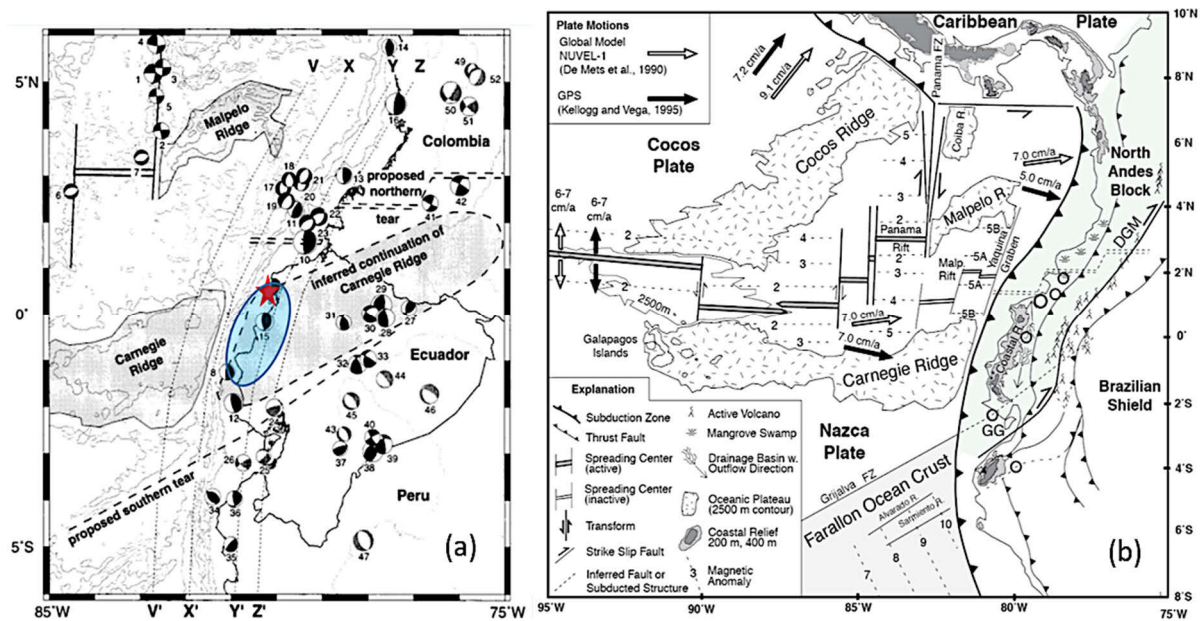


Figure 2-5 (a) Inferred extension of the Carnegie Ridge under the North Andean block, also showing earthquake fault plane solutions from the Harvard CMT (centroid moment-tensor) catalogue (after Gutscher *et al.*, 1999). The 16 of April 2016 mainshock epicentre location is shown as a red star, and the area of most concentrated damage highlighted in blue; (b) Tectonic detailing of spreading centre between the Carnegie ridge and Cocos Ridge (Gutscher *et al.*, 1999).

2.2. Local Faulting and Active Faulting

The regional tectonics and geodynamics have progressively shaped the geology and geomorphology of the study area. Possibly associated to the dynamics of the Carnegie ridge and the convergence of the North Andes and Nazca plates, local features have surfaced over geological times. Few studies have investigated these developments, and a lot remains to be done to fully understand the geological formation of this area and its associated tectonic features.

According to one of the latest studies, *i.e.* Reyes (2008), two fault systems have broadly guided the evolution of the coastal cordillera: the Jipijapa system and the Jama system that is prolonged in the East of Río Esmeraldas (Figure 2-6). Each fault system consists of many smaller faults, formed by similar geodynamics. These faults therefore have properties in common, such as their general direction. The Jama and Jipijapa fault systems have been interpreted by Reyes (2008) as being separated by a feature newly identified in that study: The Rocafuerte-Flavio Alfaro Fault. The most active blocks, according to Reyes (2008), are Mache-Rioverde block, the Jipijapa, the Bahía-Jama and the Manta blocks, in decreasing order of total uplift.

A study led by the USGS (Eguez *et al.*, 2003) mapped the potentially active faults over the north-western region of Ecuador (Figure 2-7). This remains one of the most recent and comprehensive study of the region to date, although the newly proposed Rocafuerte-Flavio Alfaro Fault in Reyes (2008) has yet to be added. It is important that more work is carried out to consolidate the understanding of local fault activity and assess their impact on the seismic hazard in the region in the near future.

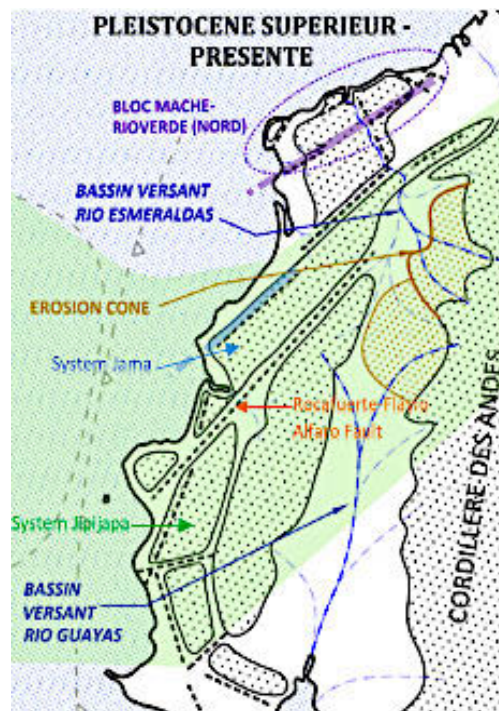


Figure 2-6 Geomorphological reconstitution of the Ecuadorean Coastal Cordillera – Most recent evolution (Pleistocene sup. To now) (after Reyes, 2008). The green area shows the potential Carnegie Ridge extension, based on Gutscher *et al.*, 1999 (Figure 2-5) and the geomorphological lineaments identified in Reyes (2008), assuming that the lineaments are indeed directly linked to the dynamics of the Carnegie Ridge underneath. The blue and violet thick lines in the Mache-Rioverde and Jama blocks may be considered for further analysis in understanding the barriers to the 2016 rupture propagation (see Section 4.2).

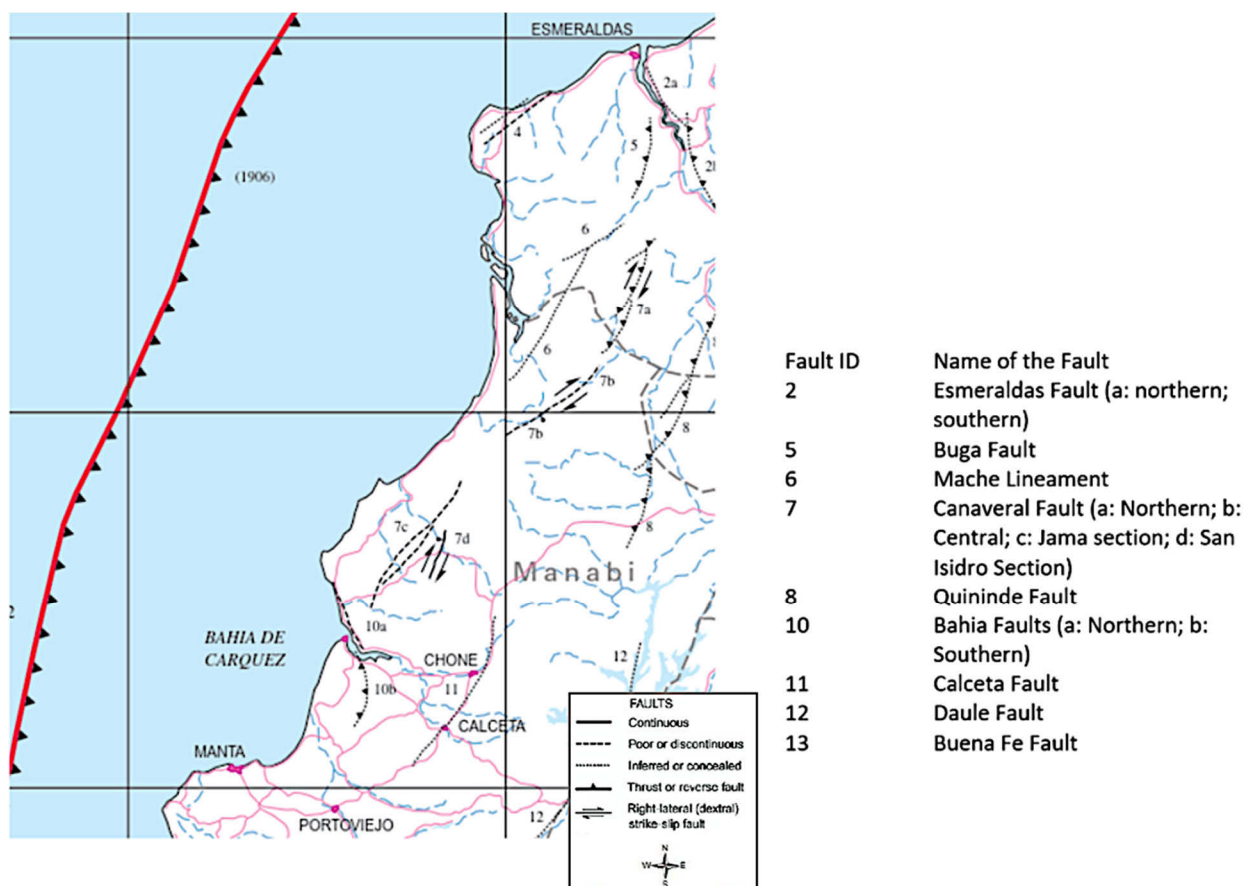


Figure 2-7 Active fault map (from Egeuz *et al.*, 2003).

The regional and local tectonic activity results in an exceptional concentration of geological hazards, such as volcanoes, tsunamis and earthquakes. The subduction of the Nazca Plate underneath the South American Plate triggered the largest recorded earthquake in the world (c.f. Figure 2-8), which occurred on 22 May 1960, in Chile, with a magnitude $M_w 9.5$ (USGS, 2016). On 31 January 1906, the 7th largest earthquake occurred along the coast of Ecuador, north from the 2016 mainshock event, with a magnitude $M_w 8.8$ (USGS, 2016). Most of these large earthquakes correspond to subduction interface events, whilst a few correspond to deeper intraslab events, with epicentres much further inland. These two types of subduction events are illustrated in Figure 2-9. In addition to these events, the Manabi and Esmeraldas regions have had a history of large seismic events exceeding $M_w 7$. The epicentre of the 2016 earthquake was located at the southern end of the 400-500km long rupture area of the 1906 $M_w 8.8$ event which generated a tsunami that resulted in hundreds of casualties (USGS, 2016). Closer to the 2016 epicentre, a $M_w 7.8$ earthquake occurred in 1942, 43km south of the recent April event, and a $M_w 7.2$ event in 1998 close to Bahía de Caráquez. As pointed out by Chlieh *et al.* (2014) and shown on Figure 2-10, this left a seismic gap which may have led to the 2016 mainshock rupture.

These earthquakes, including the 2016 sequence of events, relate to the interface seismicity of the northern central section of the Ecuadorian subduction which is characterised by greater dip angles and larger recorded magnitudes associated to shallower interface events than the southern section of the subduction which dips at an angle of about 10° and is governed mostly by in-slab events (Parra *et al.*, 2016; Font *et al.*, 2013; Hayes *et al.*, 2012; Guiller *et al.*, 2001). The recorded seismicity of Ecuador until the end of 2015 is shown in Figure 2-11. The seismogenic source zonation from the most recent national hazard study carried out by Parra

EEFIT

(2016) is also shown in the above-mentioned figure. Due to the variability in subduction angles and seismic events distribution, the subduction interface seismicity was modelled as three distinct zones, one in the North, one in the Centre, and the last one in the South. The presence of the Carnegie Ridge may partly explain this variation in subduction behaviour from North to South (Michaud *et al.*, 2009; Trenkamp *et al.*, 2002). More clarity on the tectonics and geodynamics associating the coupled effects of the subduction of the Nazca Plate and the Carnegie Ridge under the North Andean plate would provide a better representation of the zonation for probabilistic seismic hazard assessment of the country.

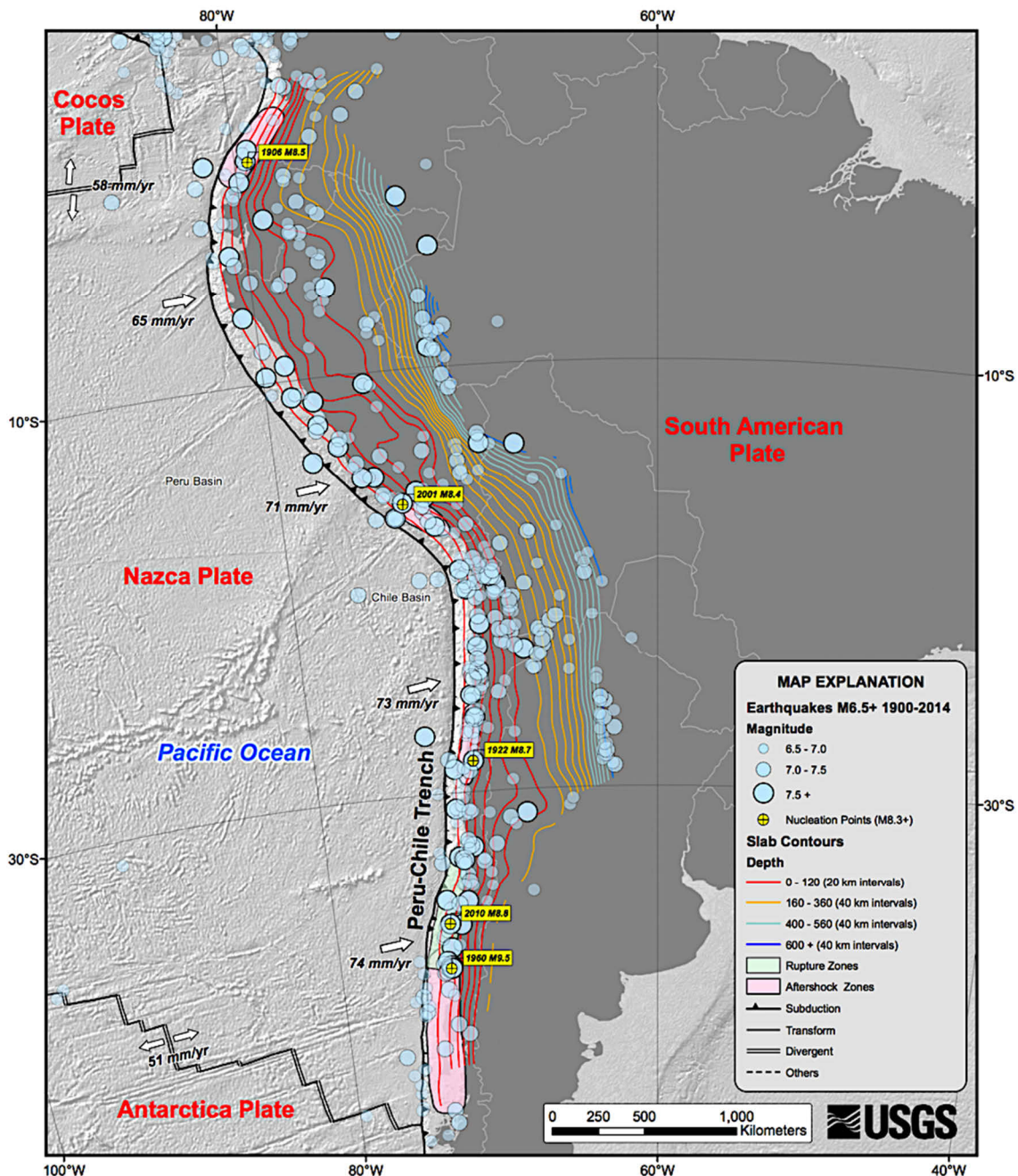


Figure 2-8 South American subduction seismicity for events $M_w > 6$ (USGS, 2014).

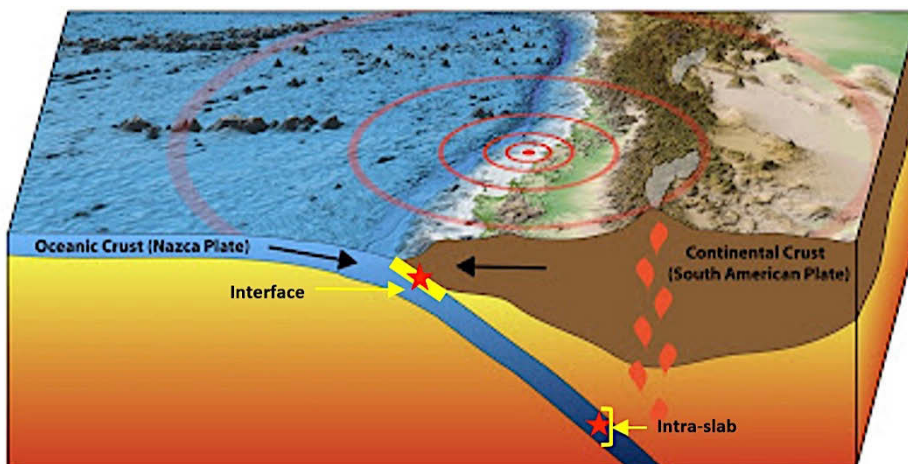


Figure 2-9 Subduction earthquake types showing interface and intra-slab events. NB: at surface, the concentric red shape illustrates the epicentre and wave propagation corresponding here to an interface event.

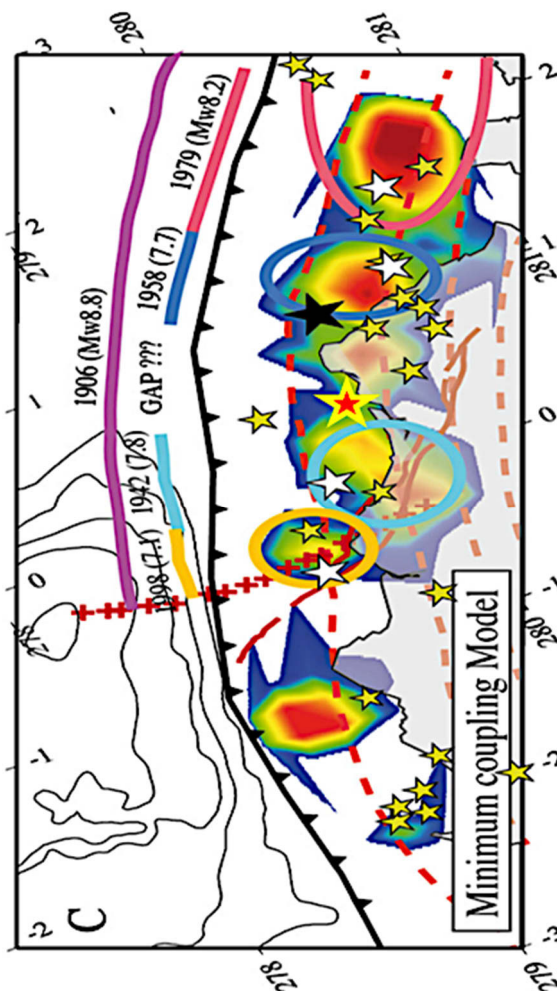


Figure 2-10 Historic subduction seismicity analysis and identification of seismic gap (after Chlieh *et al.*, 2014). The red star shows the approximate location of the epicentre of the 2016 main shock.

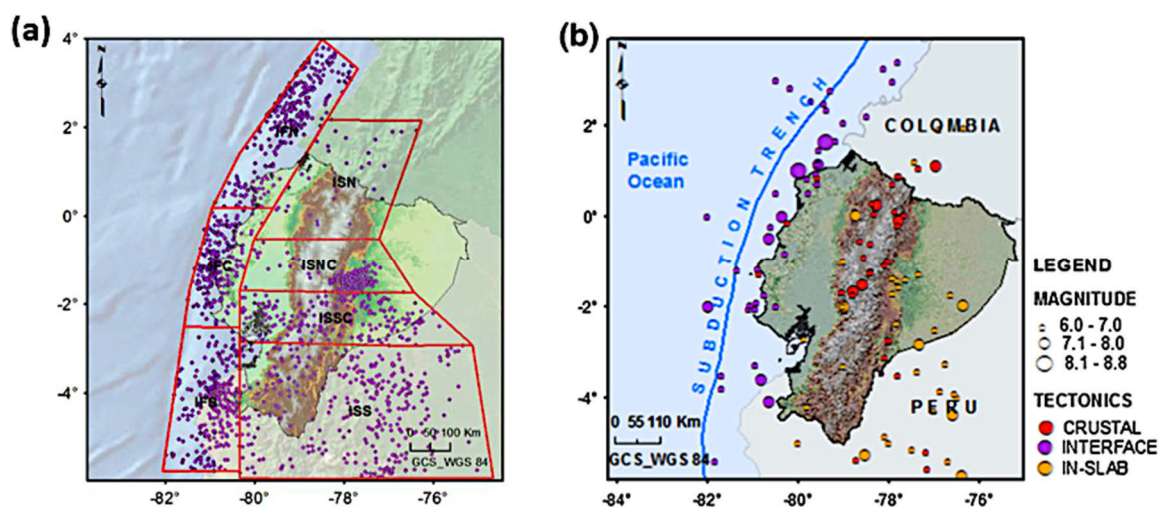


Figure 2-11 Earthquake catalogue and seismic hazard zoning in Parra (2016) (a). $M_w > 6$ events from catalogue and associated tectonic seismicogenic type (b) (NB: interface and in-slab are two type of subduction earthquakes – c.f. Figure 2-9).

2.3. The 2016 Sequence of Events

2.3.1. The Mainshock

The M_w 7.8 megathrust earthquake shook Ecuador on the evening of 16 April 2016 at 18:58 local time (23:58 UTC). The hypocentre of the earthquake was located approximately 29km SSE of Muisne, and 168km from the country's capital Quito at 0.371°N , 79.94°W and at a depth of about 19.2km (USGS, 2016). This 2016 mainshock earthquake event (see Figure 2-12) is henceforth referred to as the 'Muisne event' in this report.

Much of the observed damage due to the event extends south from the hypocentre in the Manabí region, following the direction of the fault rupture propagation. The coastal towns – particularly Pedernales, Canoa, Bahía de Caráquez, Manta and Portoviejo – suffered extensive damage after the main shock, with associated intensities of VI-VIII on the Modified Mercalli Intensity (MMI) (USGS, 2016 – see Figure 2-12). The resulting peak ground accelerations (PGA) recorded at seismometer stations by the Instituto Geofísico ranged from 0.51g in Portoviejo to 1.55g in Pedernales (IG, 2016). More information on the recorded ground motions at different locations in the region is provided in Section 2.3.4.

2.3.2. 2016 Aftershock Sequence

Aftershocks followed the 16 of April 2016 mainshock, including nine above M_w 6 (IG, 2016). The sequence of aftershock and rate of occurrence with elapsed days from the main shock seem to validate well both the modified Omori's and Gutenberg-Richter empirical relationships (Figure 2-13).

The likelihood of a significant aftershock occurring whilst on a post-earthquake reconnaissance mission is significantly lower, as an EEFIT mission usually take place at least a month after the main event. However, significant aftershocks can still occur later on (see Table 2-2). Therefore, appropriate risk management measures were taken during the mission in case such low probability but potentially high consequence events would occur. Fortunately, no significant aftershocks occurred whilst on site. However, the week before the mission, on 18 May 2016, one person was killed and a dozen injured by one of the most significant

aftershocks of the sequence, also causing loss of power in the region and numerous landslides on the coastline.

Aftershocks also raise the issue of distinguishing observations associated with the main shock or the aftershocks. Talking to the people on site or comparing observations to satellite or other imagery from after the main shock are a couple of solutions to overcome this problem.

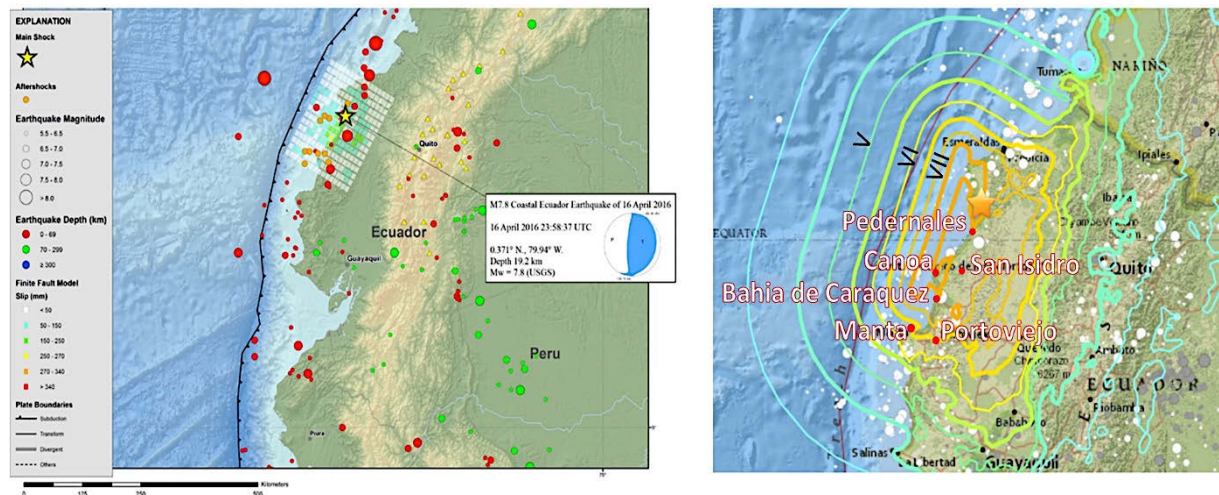


Figure 2-12 The 16 April 2016 event mainshock characterisation (left) and PAGER Intensity map (right) (USGS, 2016).

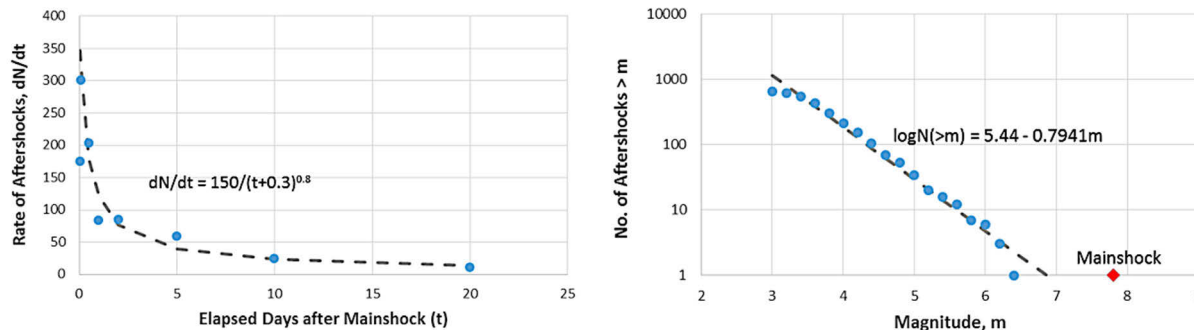


Figure 2-13 Rate of aftershocks with elapsed days based on modified Omori's law (left). Number of aftershocks with earthquake magnitude based on Gutenberg-Richter relationship (right).

Figure 2-14 shows the location of the aftershocks following the April 2016 main shock. Axes of greater concentration of the aftershocks are highlighted as yellow dotted lines on the figure. Similar trends can also be identified in historic seismicity distribution patterns (see Figure 2-14b). Although vast research efforts have gone into seismic imaging of the structure of the central Ecuador convergent margin associated to the SISTEUR cruise project (Sanclemente, 2014; Gailler *et al.*, 2007; Font *et al.*, 2013; Collot *et al.*, 2002, 2008), geophysical asperities that may explain the pervasive seismicity pattern of the epicentres offshore have yet to be identified, although they are likely to be associated to the Carnegie Ridge (Chlieh *et al.*, 2014).

It is interesting to note that the sequence of events should not only consider aftershocks but also foreshocks. No information was found on this aspect however. Investigating it could potentially provide an interesting additional input to the understanding of the sequence and the seismic hazard in the region.

Table 2-2 Description of the couple most damaging aftershock events following the 16 April 2016 event

Aftershock Date	Magnitude (M_w)	Area primarily Impacted	Damage
18 May 2 events (just before the mission)	6.7 & 6.8	Manabi	Loss of power; 1 killed; Dozen injured; Landslides
10 July 2 events (about a month after the mission)	5.9 & 6.4	Esmeraldas	Loss of power and phone service; Damage to Bailey bridge; 80 people displaced

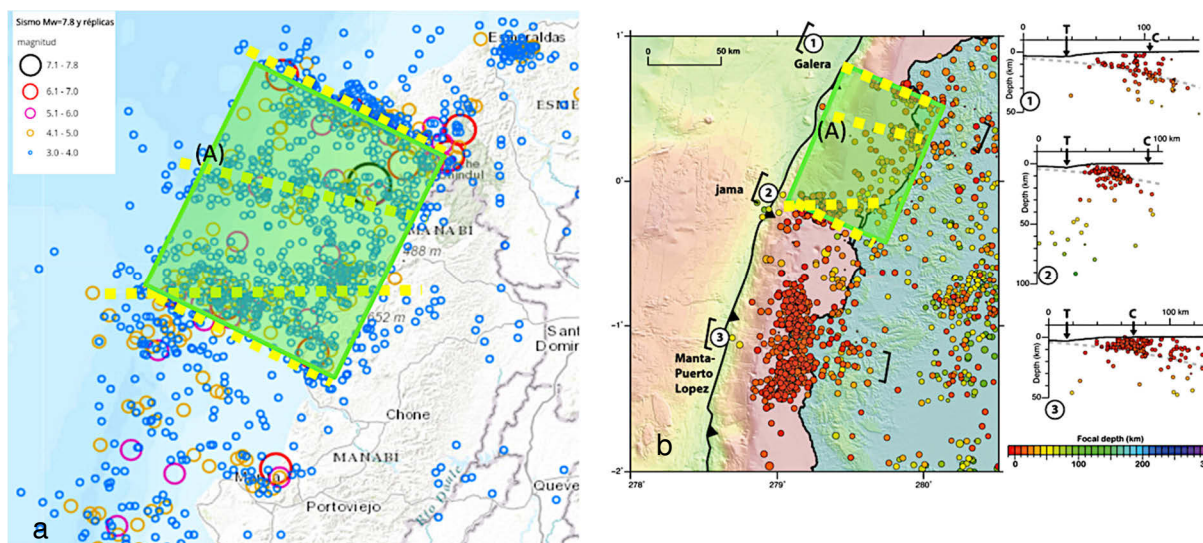


Figure 2-14 (a) Aftershocks of the 2016 16 April main shock (IG, 2016 - <http://www.igepn.edu.ec/mapas/mapa-evento-20160416.html> – data extracted on the 17/11/2016) (b) Historic seismicity map and cross-sections in the vicinity of the interplate seismogenic zone: results from the 3-D approach and P-wave arrivals (Font *et al.*, 2013). The yellow dotted lines illustrate the axes of greater concentration of aftershocks. The green area bounds the aftershocks' greatest concentration area.

2.3.3. Seismic Rupture Interpretation

Many researchers and experts are currently looking to better understand the 2016 sequence of events and the associated seismogenic rupture. Looking at the aftershocks distribution, studying the slip distribution (see Figure 2-15), and accelerograms of the two events (see Figure 2-16), Ye *et al.* (2016) suggests that the ~120km long area of highest aftershock concentration (green area in figures) may be the same as the one mobilised in the 1942 sequence. However, this seems to be conflicting with the findings from Chlieh *et al.* (2014) resulting from a vast research program in the area associated to the SISTEUR cruise geophysical measurements project. According to the latter study, the 1942 sequence of events were associated with a smaller rupture area, and the 2016 sequence of events may have mobilised part of a seismic gap identified in the study (Figure 2-15). The geophysical asperity which may explain the northern boundary of the 1942 sequence according to Chlieh *et al.* (2014) may be evidenced by the slightly less pronounced pervasive seismicity distribution pattern identified as (A) in Figure 2-14 and Figure 2-15.

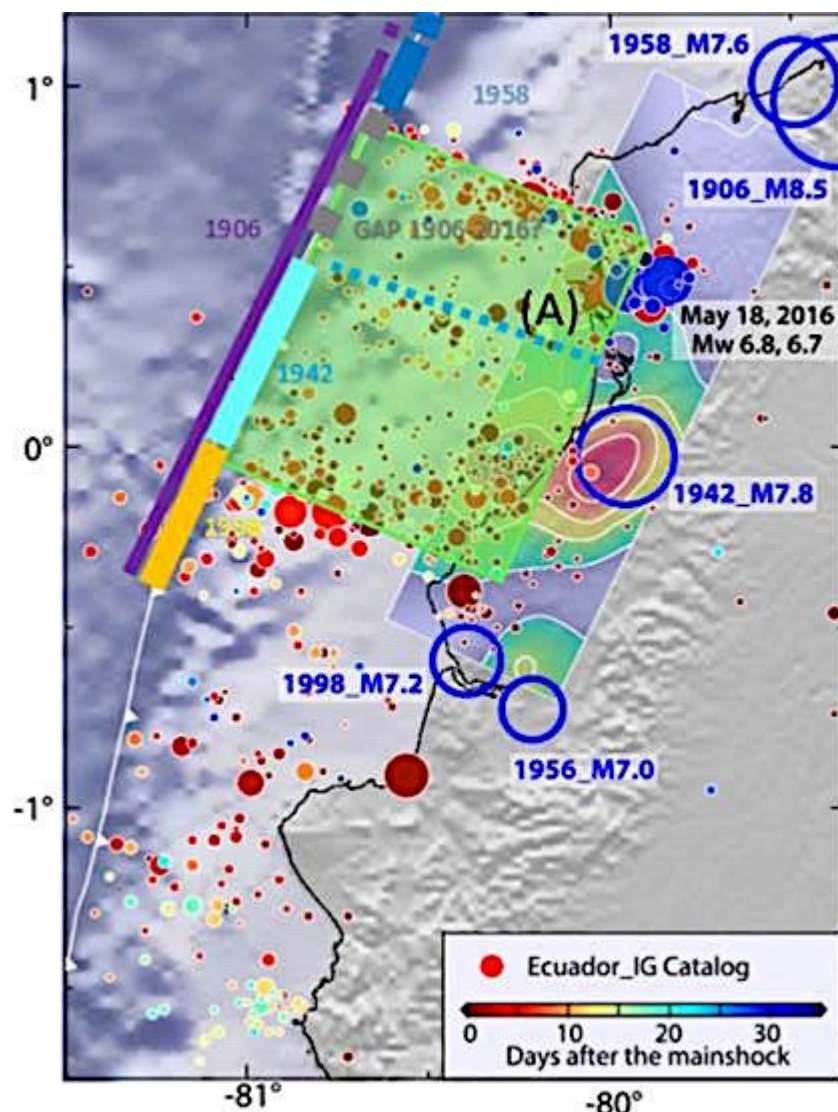


Figure 2-15 (a) Epicentres of the main event (red star) and location of aftershocks (circles sized according to magnitudes) over 35 days following the mainshock from the Geophysical Institute of the National Polytechnic School at Ecuador (<http://www.igepn.edu.ec/portal/ultimo-sismo/informe-ultimo-sismo.html>) superimposed on the slip model (Ye et al., 2016). The green area illustrates the greatest aftershocks concentration area. The coloured segments shown correspond to the subduction rupture lengths associated to the past big events as interpreted by Chlieh et al. (2014).

2.3.4. Seismometer Network and Recorded Ground Motions

The National Accelerometer Network RENAC (Red Nacional de Acelerógrafos) in Ecuador is managed by IG-EPN. Two types of instruments were used, either from Guralp or Reftek (IG, 2016). As reported by GEER (2016), some of the instruments were adversely affected by the events either by power outages or building collapse. Additionally, the OCP (oil pipeline network) and LMI (a collaborative project between IG-EPN and the Institute of Research for Development (IRD, France) had more seismograph data (according to GEER, 2016). Data from these sources had not been accessed at the time of the mission. A vast network of seismographs was installed following the main shock to record aftershocks, an effort supported by the International Federation of Digital Seismograph Network. This data was not available at the time of writing. Therefore, this report will only make use of the RENAC data.

The RENAC seismometer stations in the Manabi and Esmeraldas regions that recorded the highest accelerations in the 2016 sequence of events are shown in Figure 2-16. These recorded PGAs correspond well to the Shakemap contours as shown in Figure 2-18. Higher accelerations have been recorded in the direction of the propagation of the rupture, *i.e.* south. The highest PGA was recorded in the EW direction in Pedernales, also associated to the highest azimuthal difference between EW and NS components. It also recorded by far the highest vertical motion, with 0.742g compared to a range between 0.01 and 0.17g for records in other cities. The higher PGA recorded in Guayaquil (green dots in Figure 2-18) compared to the neighbouring measurements are attributed to alluvial soft deposits seismic wave amplification. This cannot be seen in the AGYE recording since the station is situated on hard rock ($V_{s,30}=1800\text{m/s}$) but can be at AGY1 and AGY2. These shear-wave velocities and soft sites effects in Guayaquil were measured and analysed by Vera-Grunauer (2014).

This illustrates the importance of site effects and the need to record the $V_{s,30}$ information for each ground motion recording location. The IG-RENAC website does not currently provide information on the site conditions at the seismometer locations, hence hindering the interpretation of the data provided. During the GEER-ATC mission (2016), Geostudios (2016) measured $V_{s,30}$ at a number of seismometer locations, as reported in Table 2-3. It is important that $V_{s,30}$ measurements are made at all remaining seismometer sites of the RENAC network and communicated with the seismometers' data on the IG website to inform the seismicity records analyses. GEER also contributed to the processing and analysis of the time history data from ten seismometer stations in the region, including those mentioned in Table 2-3. The results are available for download from the GEER website at www.geerassociation.org.

Table 2-3 Seismometer stations in Manabi and Esmeraldas closest to sites visited. Ground motion record data and seismometer properties from IG-EPN (2016). $V_{s,30}$ from Vera-Grunauer (2014) in Guayaquil, and Geostudios (2016) for the other locations where available.

Seismometer ID	City	Geographic location			Instrument	R_{rup} (km)	$V_{s,30}$ (m/s)	PGA (g)		
		Coordinates		El (m)				EW	NS	VER
AES2	Esmeraldas	0° 59' 27.6" N	79° 38' 45.6" W		4 Reftek	51	-	0.154	0.111	0.044
PDNS	Pedernales	0° 6' 39.6" N	79° 59' 27.6" W		442 Kephren	21	-	1.034	0.942	0.573
APED	Pedernales	0° 4' 4.8" N	80° 3' 25.2" W		15 Reftek	20	342	1.408	0.83	0.742
ACHN	Chone	0° 41' 52.8" S	80° 5' 2.4" W		18 Reftek	34	200	0.328	0.371	0.173
APO1	Portoviejo	1° 2' 16.8" S	80° 27' 36" W		47 Reftek	73	224	0.317	0.381	0.105
AMNT	Manta	0° 56' 27.6" S	80° 44' 6" W		38 Guralp	76	496	0.404	0.525	0.162
AGYE	Guayaquil	2° 3' 14.4" S	79° 57' 7.2" W		30 Guralp	155	1800	0.019	0.024	0.015
AGY1	Guayaquil	2° 15' 3.6" S	79° 54' 36" W		7 Reftek	175	178	0.059	0.065	0.02
AGY2	Guayaquil	-2° 11' 56.4" S	79° 53' 56.4" W		11 Reftek	170	101	0.094	0.098	0.038

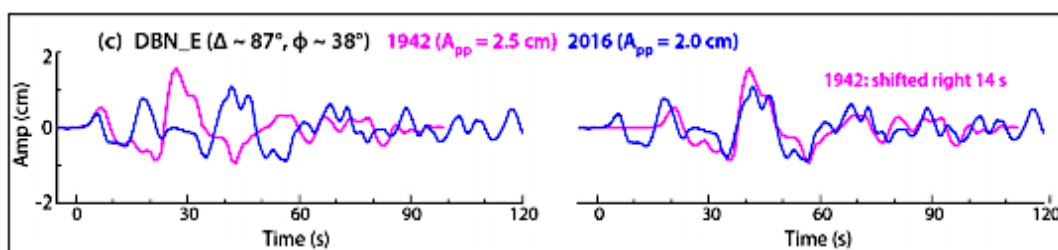


Figure 2-16 Comparison of P waves at E-W component of the 1942 (purple) and 2016 (blue) events at station DBN with Galitzin instrumental response (pendulum/galvanometer periods ~ 25 s and gain factor of 310). The waveform for 1942 is from Swenson and Beck (1996) with peak-to-peak amplitude confirmed by Bernad Dost from the DBN station bulletin. The waveform for the 2016 event is the convolution of displacement (after removal of the broadband instrumental response) with the Galitzin instrumental response. They are aligned at the beginning (left) and at the peak (right). (Ye *et al.*, 2016).

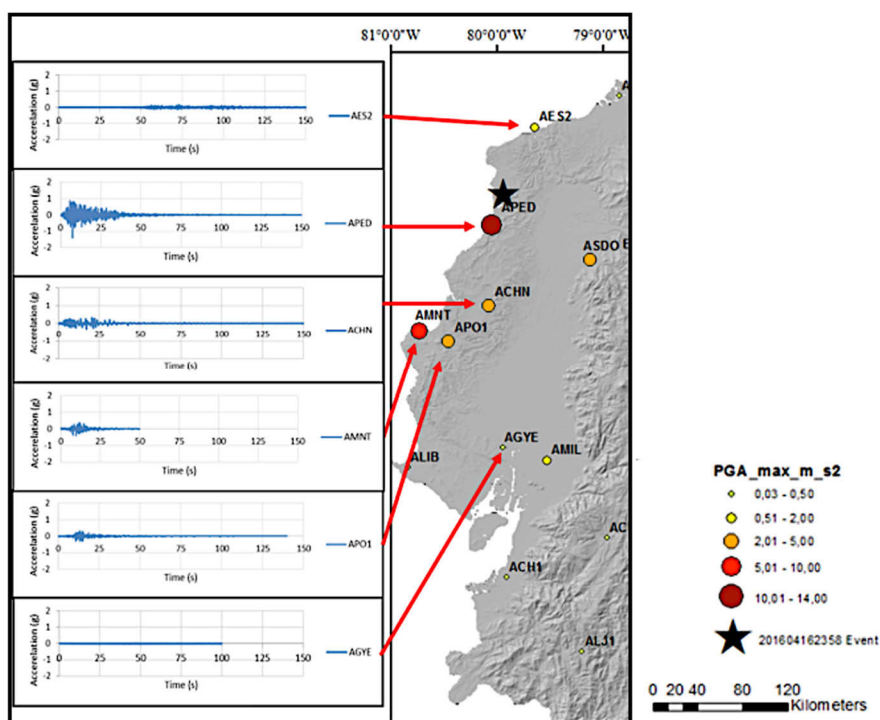


Figure 2-17 Seismometer locations and IDs, with associated acceleration recordings of the main shock (after IG, 2016).

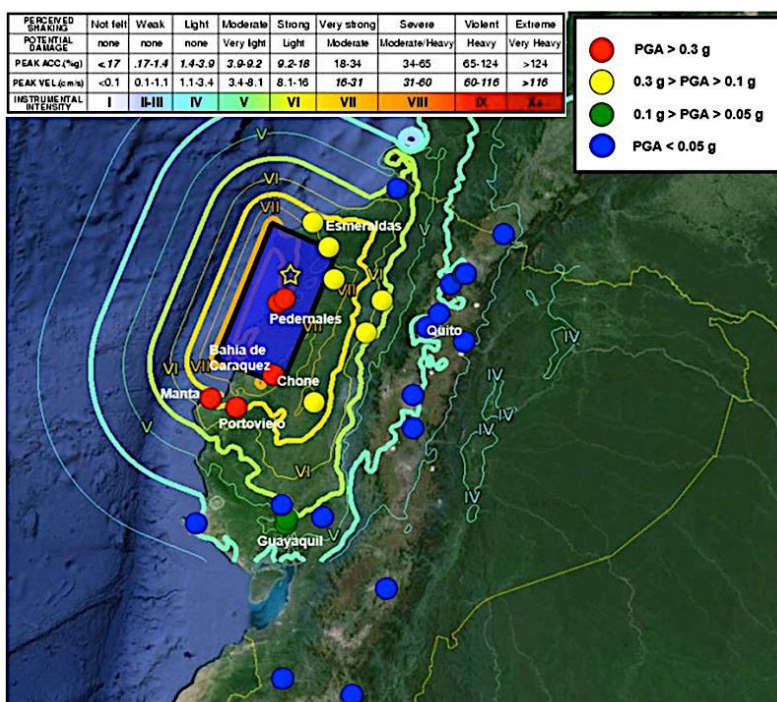


Figure 2-18 Main shock Shakemap and recorded PGAs at seismometer stations (from GEER, 2016 based on Shakemap and IG, 2016 data).

3. Site Effects and Microtremor Tests

This section presents the analysis and interpretation of potential site effects that may have contributed to the amplification or attenuation of the ground motion at the surface. This is carried out with the available external ground investigation information as well as the results of the microtremor tests carried out during the mission at several locations. By deriving simplified shear wave velocity profiles based on this data, a categorisation of the sites based on the NEHRP classification is proposed. This may be used to ascertain how safe and adequate the design parameters for the nearby structures are.

3.1. Geological Setting

3.1.1. Regional and Local Geology

The north-western border of South America is characterised by an overlay of allochthonous and indigenous oceanic and continental land. As shown in Figure 3-1, Ecuador's geomorphology can be modelled as four main units from West to East: The Coastal Cordillera (most impacted by the 2016 earthquake sequence), the Western Cordillera, the Cordillera real, and the "Oriente" Basin. The oldest geological formations ranging from Palaeozoic to Mesozoic are preserved in the eastern Cordillera or "Real" and were accreted during the Cretaceous era to the South American Craton (Litherland *et al.*, 1994). The Eastern Sedimentary Basin "Oriente" is located on the Precambrian Guyanese craton which formed in the Jurassic era (Tschopp, 1953; Litherland *et al.*, 1994). Meanwhile, the underlying rocks of the Western Cordillera and the coastal plain formed towards the beginning of the Upper Cretaceous and accreted to the South American Plate during the same geological era (Hughes and Pilatasig, 2002). The sediments covering the coastal cordillera (Benítez, 1995) and the Oriente basin (Tschopp, 1953) were deposited during Cenozoic. Figure 3-2 shows a representative stratigraphic log of the Paleogene geology in the Coastal Cordillera.

The Ecuadorian fore-arc region, known as the "Coastal Region", was characterised during Neogene times by the development of four sedimentary basins extending from North to South: the Borbon basin, the Manabi basin, the Progreso basin and the Guayaquil basin (Figure 3-2). All these basins are related to dextral shear affecting the coastal region in response to the oblique subduction at the Ecuadorian trench. Extensive hydrocarbon exploration and cartography have been carried out in the region early on and therefore, numerous data have been collected regarding its deep geology, especially associated to its Neogene stratigraphy (among others Faucher and Savoyat, 1973 ; Baldock, 1982 ; Evans and Whittaker, 1982).

As described in Deniaud *et al.* (1999), the Neogene stratigraphy of the Ecuadorian fore-arc sedimentary basins may be divided in 4 mega-sequences, namely M1 to M4, separated by unconformity and possible hiatus (see Figure 3-4). The M1 sequence is only known in the Progreso Basin however, and will therefore not be further described in this report which will focus on the Manabi region. The M2 sequence is a rich clayey marine transgressive sequence that reaches 1000m in the Manabi basin (Tosagua formation). The M2 age ranges from the Lower Miocene to the Middle Miocene. It corresponds to a generalised extension in the Coastal region. The M3 sequence is a thick sandy, silty and clayey sequence ranging in age from the Middle Miocene to the Upper Miocene. In the Manabi Basin, M3 is a regressive sequence that starts with the sandy shore deposits of the Angostura Formation, is followed by the silty deposits of the Lower Onzole Formation, and ends with the 50m thick regressive sandy and conglomeratic Choconcha Member (Benitez, 1995). Finally, in the Manabi basin, the M4 sequence corresponds to a regressive sequence which age ranges respectively from the Upper Miocene to the Lower Pleistocene. It is formed by the Upper Onzole and Borbon formations, respectively corresponding to tuffaceous silty and clayey soil, and sandstone. A

1:500000 geological map of the region was developed by Reyes and Michaud (2012) recently (Figure 3-5). Additional information is needed on the shallow stratigraphy to assess amplification effects of the seismic waves, usually modelled through the average shear wave velocity in the first 30m depth deposits.

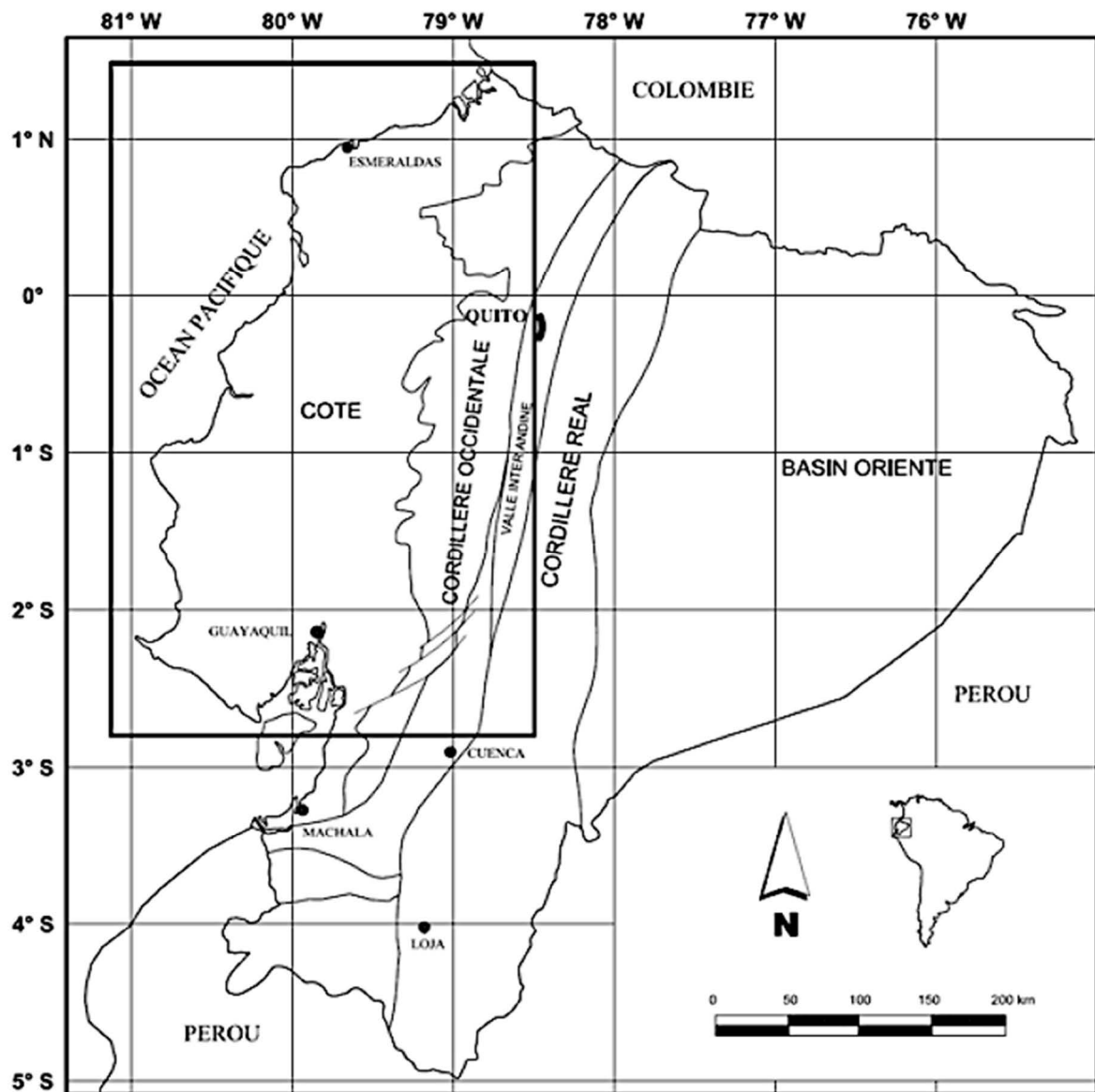


Figure 3-1 Main geomorphological units of Ecuador (Reyes, 2008).

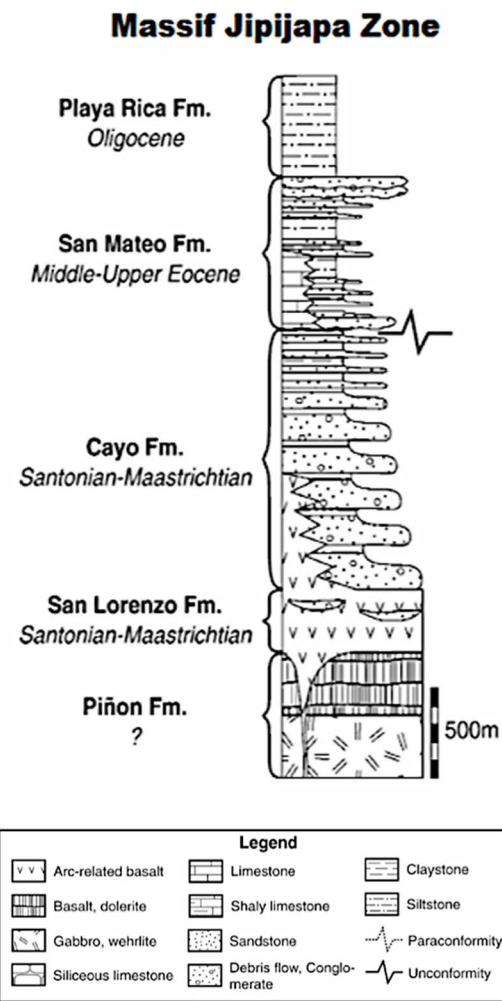


Figure 3-2 Paleogene stratigraphy of the Jipijapa Zone in Manabi (from Luzieux *et al.*, 2006).

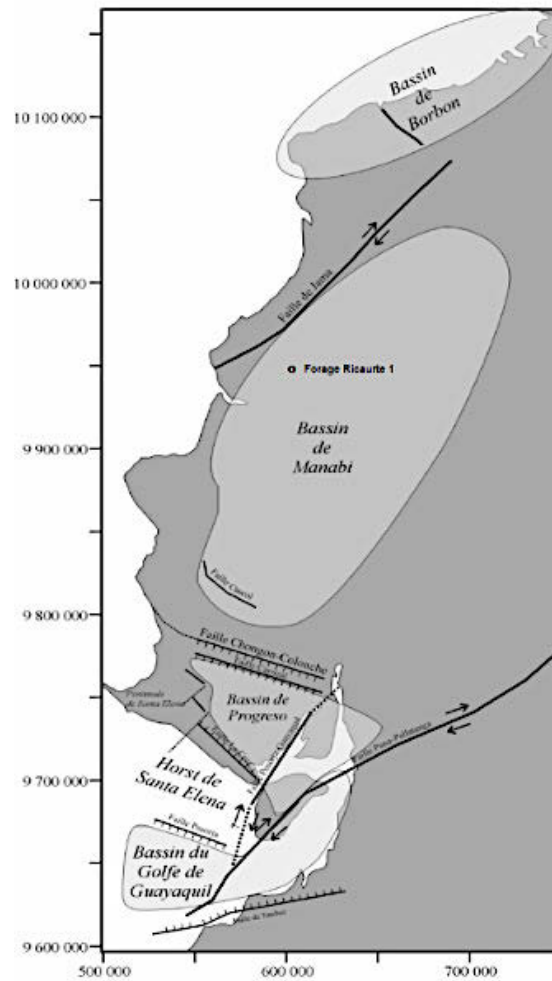


Figure 3-3 Localisation of the geological Neogene Basins of the Coast of Ecuador (Reyes, 2008).

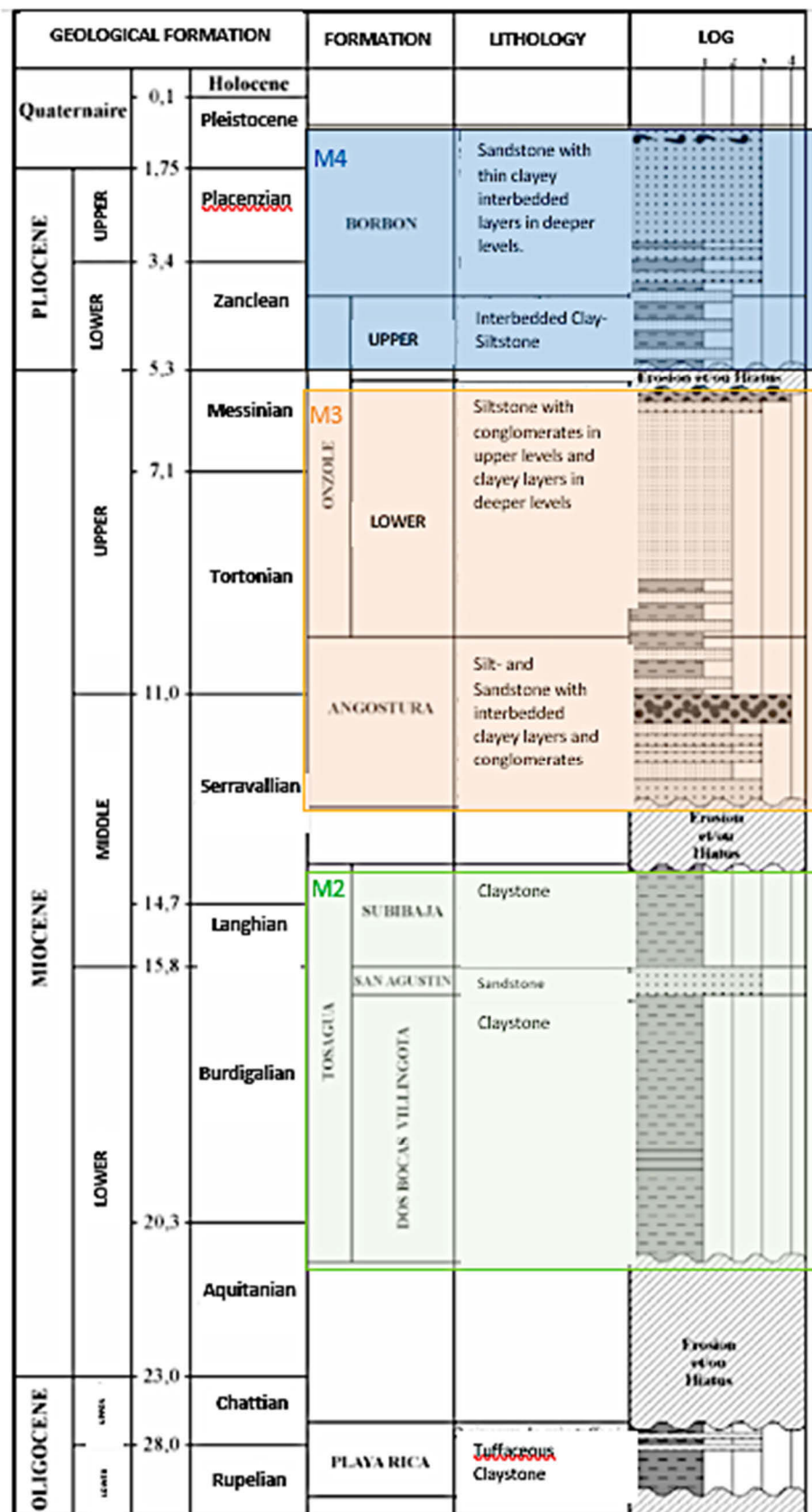


Figure 3-4 Neogene stratigraphy of the Manabi Basin (modified from Reyes, 2008 after Deniaud, 1999).

3.1.2. Available Geotechnical Investigation Data

With the support of ESPOL and in particular Dr. Davide Besenon Venegas, some local ground investigation data were gathered for different locations surveyed during the mission. Information gathered through the GEER mission in April 2016 was also utilised (GEER, 2016). The data gathered are listed in Table 3-1 for each location surveyed, alongside with their source, depth of investigation and type of information accessed. More detailed information on the available data for each site surveyed is provided in Appendix A.

SPT-N, shear wave velocity in-situ measurements and TROMINO® tests were utilised to analyse potential site amplification effects, and Atterberg limits, granulometry and soil description were also useful in assessing liquefaction. It is worthwhile noting that groundwater depth was rarely recorded and/or communicated, which is essential especially for liquefaction risk. Reduced level of the ground was also rarely indicated, whilst this is critical in building robust geological models for a better understanding of the local geology.

Obtaining ground investigation data has been very challenging, and remain fairly limited. In order to better inform seismic risk mapping and management in Ecuador in the future, it is highly recommended that efforts are made to facilitate population and access to existing geological investigation data. The need for intrusive and non-invasive ground investigation, such as in-situ shear wave velocity measurements complemented by microtremor tests, to better understand potential soil amplification effects on the ground shaking at the surface should also be emphasised.

Table 3-1 List of ground investigation data analysed.

Location	GI ID	Source	Depth of Investigation (m)	Information Accessed							
				GL	GW depth	Log	G	AL	SPT-N	V _s	HVSR
Manta	HV1 to HV7	GEER (2016)	-	x	x	x	-	-	-	-	x
	BH Mobil		5	?	x	x	-	-	-	-	-
	VS_AMNT		60	-	-	-	-	-	-	x	x
	VS_MPWD		23	-	-	-	-	-	-	x	-
	VS_MPPA		60	-	-	-	-	-	-	x	x
	VS_IESS		60	-	-	-	-	-	-	x	x
	B116; B123; B138	Ripalda (2007)	45-60	-	-	x	-	-	-	x	-
T1; T2; T13	THIS MISSION	-	x	-	-	-	-	-	-	x	
Portoviejo	APO1	GEER (2016)	40	x	x	-	-	-	x	x	-
	Los Tamarindos		40	-	-	-	-	-	x	x	-
	P1-P10	Hidroplan (2016)	15	x	x	x	x	x	x	-	-
	T3-T9	THIS MISSION	-	x	-	-	-	-	-	-	x
Bahía	GI_Bridge	GEER (2016)	70	-	-	x	-	-	x	-	-
	B01-B09	LUP (2016)	16	x	x	-	-	-	x	-	-
	T10; T12	THIS MISSION	-	x	-	-	-	-	-	-	x
Canoa	C1-C3	LUP (2016)	16	-	-	x	x	x	x	-	-
Jama	J1-J3	LUP (2016)	16	-	x	x	x	x	x	-	-
Pedernales	APED	GEER (2016)	80	x	-	-	-	-	-	x	-
	T11	THIS MISSION	-	x	-	-	-	-	-	-	x

GL: Ground Level
GW: Ground Water
Log: Geological Log (Soil description)
G: Granulometry
AL: Atterberg Limit
SPT-N: SPT test
 V_s : Shear-wave velocity measurement
HVSR: Horizontal/Vertical Spectral Ratio Microtremor Tests

3.2. Microtremor Tests

3.2.1. Why Microtremor Tests?

During this reconnaissance mission in Ecuador, microtremor test equipment was used to obtain in-situ measurements of site effects for the following reasons:

- Site effects were suspected to be a significant contributing factor in observed damage in the region; and
- A lack of understanding of site effects and geological/geotechnical data was acknowledged.

The mission needed a fast and cheap technique for site effect assessment. The test also had to be portable and deployable by a small crew (two geotechnical engineers were involved in the fieldwork, Fiona Hughes and Nina Jirouskova). The results needed to be reliable enough to grossly assess site effects on seismic wave amplification, complementarily with other ground investigation data, and help identify the need for further ground investigation efforts. The microtremor tests met all these criteria.

EEFIT successfully used the TROMINO® equipment in its mission following the earthquake in Nepal in 2015 (Tallet-Williams *et al.*, 2016), and Nina Jirouskova had also had the chance to work with microtremor test results on a seismic microzonation study for the North-West New Territories of Hong Kong. This latter study, comparing SASW, MASW, DH and PS logging shear wave velocity in-situ measurements to TROMINO® tests showed a very good agreement in site characterisation (Pappin *et al.*, 2012). Tallet-Williams *et al.* (2015) also showed the value in using this technique and its agreement, within 10%, of the estimated $V_{s,30}$ with other non-invasive geophysical methods such as SCPT and MASW. According to the manufacturer Micromed, the TROMINO® is expected to provide V_s estimates within 20% accuracy, which is considered to be good enough for the purpose of site characterisation, and in line with the accuracy of most non-invasive geophysical V_s measurement methods.

3.2.2. Underlying Principle

Seismic tremor, commonly called seismic “noise”, exists everywhere on the Earth’s surface. It mainly consists of surface waves, which are the elastic waves produced by the constructive interference of the P and S waves in the layers near the surface. Seismic noise is mostly produced by wind and sea waves. Also, industries and vehicle traffic locally generate tremor, although essentially at higher frequencies, which are quickly attenuated.

Background seismic noise acts as an excitation function for the local resonance of subsoil. For example, if the subsoil has natural frequencies of 0.8 and 20 Hz, the background seismic noise will excite these frequencies, making them clearly visible in the tremor spectrum measured. The microtremor instrument typically has three orthogonal accelerometers and velocimeters to pick up the resonance of the soil in the ambient noise at surface (Micromed, 2012). The Nakamura (1989) H/V technique can then be used to identify significant stratigraphic interfaces in the subsoil. Strong velocity contrasts in the subsurface indeed result

in peaks appearing in the frequency H/V spectral ratio domain (see Figure 3-6). The highest amplitude peak corresponds to the maximum fundamental site period (Bard, 1999).

To solve the inversion problem and derive the corresponding simplified V_s profile, the analyses need to be constrained by the depth to the first impedance contrast. This requires microtremor tests to be interpreted in light of intrusive ground investigation results. However, in the context of this mission, only microtremor tests were carried out. The results were hence analysed complementarily with other sources' in-situ V_s measurements where data close to the TROMINO® test locations existed. The results of the tests can then be re-interpreted when new V_s or geological log data become available.

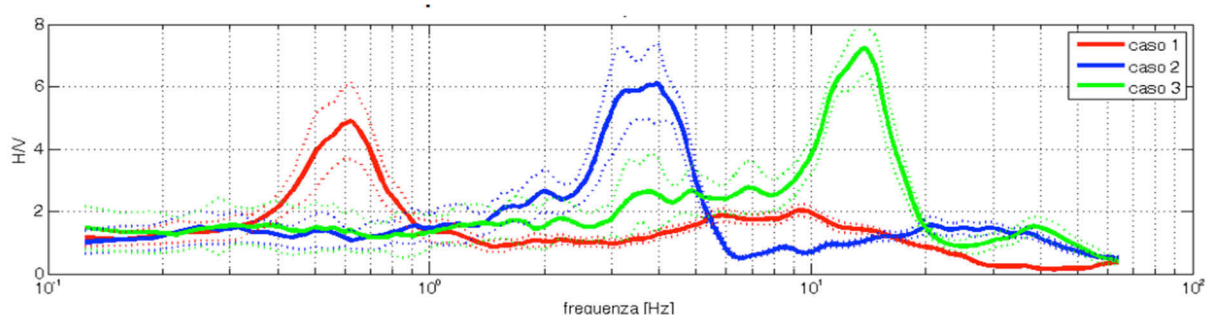


Figure 3-6 Example of seismic bedrock at different depths which generate H/V peaks at different frequencies. Case 1: bedrock at 300 m depth, case 2: bedrock at 20 m depth, case 3: bedrock at 4 m depth (Micromed, 2012).

3.2.3. Methodology

The microtremor tests were carried out with the Micromed TROMINO® equipment shown in Figure 3-7. The methodology for setting up the tests on site and processing and analysing the results are explained thereafter.



Figure 3-7 Microtremor test set up in Tarqui, Manta.

3.3. Field Equipment

The equipment consisted of the TROMINO® box, a bubble level meter, a compass, a small spade, a timer, a GPS, and a notebook for the purposes indicated in Table 3-2.

Table 3-2 Use of Equipment associated to microtremor tests.

Piece of Equipment	Use
TROMINO® box + metallic feet	Record surface waves
GPS	Record location of the test (and elevation)
Compass	Head the instrument North
Spade	Reach “natural” ground for measurement when possible and dig the dried superficial “crust” that may exist. Dig out any obstructions and flatten the surface.
Bubble Level Meter	Ensure the level of which the box is laid out is horizontal.
Timer	Duration of the measurement: 15min. Also to use in conjunction with notebook to record perturbations.
Notebook	Record any noise, rain, any perturbation that may influence the reading.

TROMINO® is designed to minimise the influence on measurements of external noise (wind, electronic noise, noise induced by external cables and so on). However, the device should be placed during the recording far from noise sources, especially from electromagnetic sources such as mobile phones -cellular and cordless-, PCs, displays, and monitors). These can emit strong pulsed electromagnetic fields which appear as background noise on the trace. The strongest perturbation observed during the field measurement was hence close to the APO1 seismometer station, located within a meteorological station area. This can be seen in the “wobbly” end of the spectra in Figure 3-8.

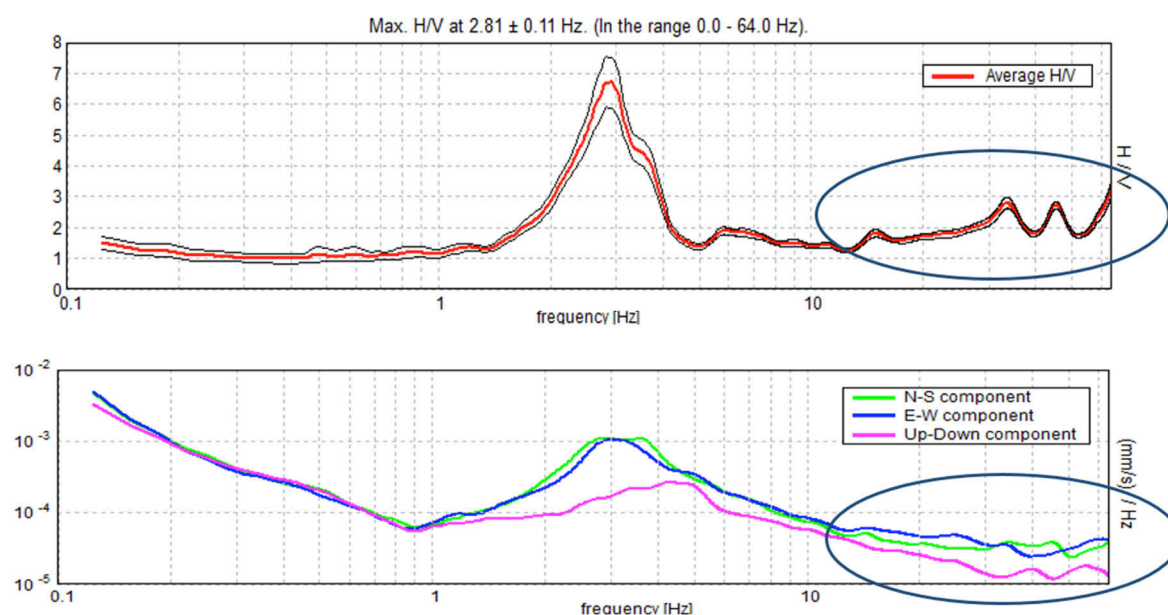


Figure 3-8 APO1 (T9) amplitude spectrum of the recorded surface waves and H/V spectral ratio.

3.4. Filtering/Processing

During the processing phase, if any noise was noted during the recording, attention would be paid to filter out the noise if necessary. The need to clean the reading would show, especially in the instability diagram, the large dispersion in the H/V spectrum and potentially the “wobbly” end of the frequency spectra.

Fortunately, favourable locations for the tests were available where noise were sufficiently low and very little filtering was necessary. In the case of the APO1 seismometer station measurement, an alignment of three other measurements were carried out to evaluate the variation in stratigraphy, but the difference in the readings was minimum, showing little lateral variation in stratigraphy along that axis. Therefore, site effect interpretation exercise was carried out based on one of the clean readings further away from the meteorological station.

3.5. Analysis of the Results and Stratigraphy Interpretation

The analysis of the TROMINO® readings is conducted with the support of the analysis of the amplitude spectrum, in which the “eyes” show layer interfaces (see Figure 3-9). In the presence of a stratigraphy made of many successive thin layers, the “eye” would not “close”. These “eyes” should correspond to peaks in the H/V spectral ratio. The main peak is identified on the spectral ratio figure with its associated frequency corresponding to the minimum natural frequency of the site (f_0).

If the depth of the first stratum is known, the following equation can be constrained to find the average shear wave velocity V_s over the depth down to the main stratigraphic interface (H: thickness of the layer):

$$f_0 = V_s / (4H)$$

In cases where a single peak is observed, the shear wave velocity of the underlying soil layer is set such that the amplitude of the peak (*i.e.* impedance in velocity) is accurate by a best fit approach.

When there are multiple major peaks (*i.e.* n peaks) in the spectrum, n+1 layers need to be modelled. In that case, the embedded synthetic model in the GRILLA software associated to TROMINO® was used. This model is constrained by the thickness of the shallowest layer (*i.e.* highest frequencies) to which a peak corresponding to the interface with the layer underneath can be identified on the spectrum.

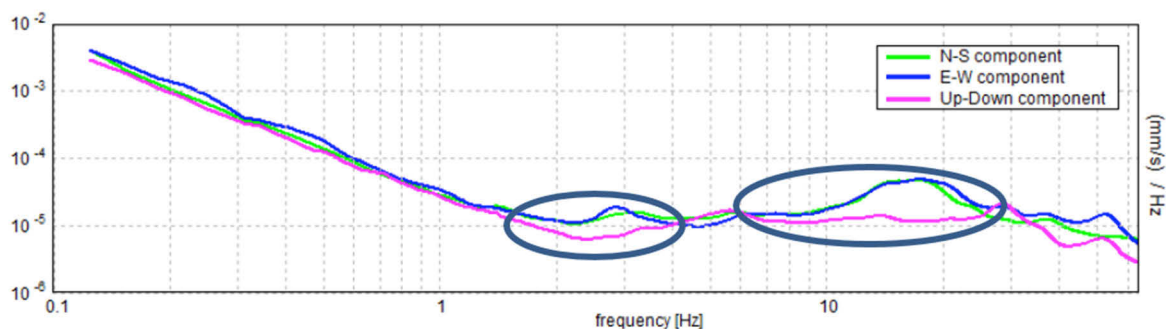


Figure 3-9 Example of amplitude spectra showing "eyes" for stratigraphic interpretation.

3.5.1. Test Locations

Microtremor testing was carried out in a number of locations to establish the role of ground conditions on building and infrastructure damage (see Figure 3-10 and Table 3-3).

Tests were undertaken within the areas most severely affected by the earthquake and those which experienced comparatively less damage to compare the potential changes in ground conditions between these sites. Tests were also undertaken close to the locations of seismometers installed by the Instituto Geofísico in Pedernales and Portoviejo.



Test ID	Lat	Long	EI (m)
T1	0°57'26.45"S	80°41'43.14"W	19
T2	0°57'25.79"S	80°41'39.83"W	17
T3	1° 3'17.70"S	80°27'10.20"W	45
T4	1° 3'25.02"S	80°27'6.24"W	45
T5	1° 3'43.36"S	80°27'3.16"W	36
T6	1° 2'13.75"S	80°27'36.04"W	42
T7	1° 2'13.93"S	80°27'35.94"W	42
T8	1° 2'14.10"S	80°27'35.81"W	43
T9	1° 2'15.42"S	80°27'34.34"W	44
T10	0°37'19.00"S	80°25'39.50"W	19
T11	0° 4'4.36"N	80° 3'25.95"W	15
T12	0°36'26.19"S	80°24'27.73"W	0
T13	0°57'5.28"S	80°42'51.95"W	10

Figure 3-10 Location and ID of the microtremor tests carried out during the mission. Table 3-3 TROMINO® tests coordinates.

3.5.2. H/V Interpretation

The interpretation of the microtremor consists of identifying the major peaks of the H/V spectrum, of which the greater peak corresponds to the minimum site frequency of the site and in deriving a corresponding V_s profile model. The V_s inversion problem was informed by the understanding of the regional geological setting and by the other ground investigation information available from other sources summarised in Appendix A.

The results of this interpretation are presented hereafter per city where TROMINO® tests were carried out. When several tests were carried out in one city, the readings were compared, and grouped together if found similar for a common interpretation. Table 3-4 shows the number of V_s profile models derived for each city location. This provides a sense of the variability in soil conditions captured through these tests.

Table 3-4 Number of V_s profiles derived compared to number of TROMINO® tests per city surveyed.

City	No. of TROMINO® tests	No. of V_s Models
Manta	3	2
Portoviejo	6	3
Bahía	2	2
Pedernales	1	1

a) Manta

The T1 recording could not be used due to excessive noise although the general reading is in good agreement with record at T2. As shown in Figure 3-11 and Figure 3-12, the H/V spectra obtained at T2 and T13 locations have similarities but also some differences that justify deriving two distinct V_s profiles. They are sited at the Manta Shelter location and just outside of the most damaged area of Tarqui, respectively.

Although the frequencies of the set of four main peaks at each location are not vastly different, they seem slightly shifted to lower frequencies for the Tarqui reading compared to the Shelter

site. The impedance at 1.8Hz is also much more pronounced in T13 than in T2, where the minimum natural site frequency is identified to be around 8Hz instead. A second peak is very close in amplitude in the latter trace, at 0.5Hz instead.

This is in agreement with the GEER (2016) HVSR measurements that seem to indicate higher maximum natural periods of the sites going East to West towards the river (see Appendix A), which could be consistent with alluvial deposit basin along the river.

The V_s profiles derived through an inversion constrained by a first peak corresponding to a shallow stratigraphic transition at 2-3m depth are shown in Figure 3-13.

It should be noted that the shorter the reading, the less reliable the deeper layer interfaces (lower frequency peaks) are in the interpretation of the microtremor test. For a 15min reading, it is unlikely that any interface below 100m can be accurately defined. Therefore, the V_s profiles derived hereby, although matching fairly well down to frequencies as low as 0.4Hz, should only be considered as indicative below 100m.

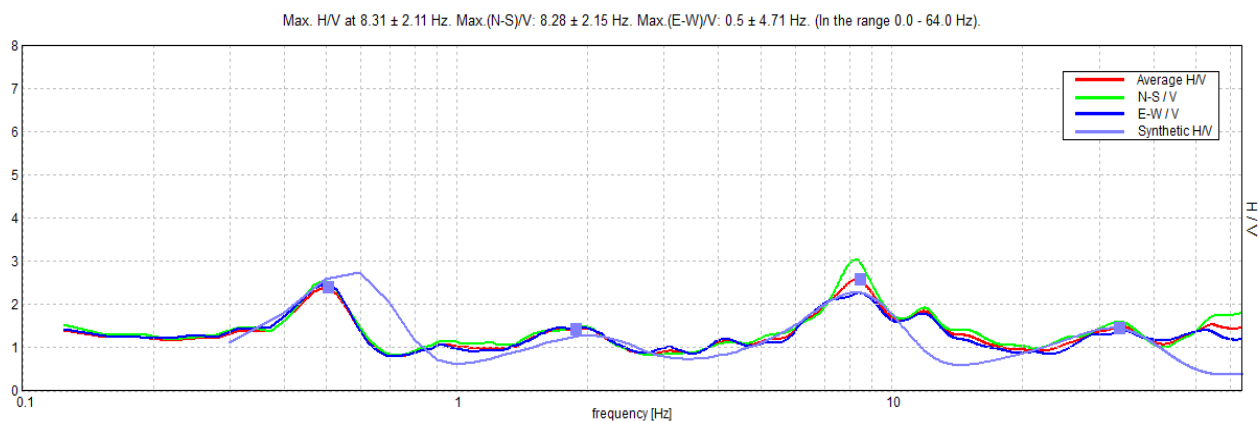


Figure 3-11 Comparison of the H/V T2 in-situ measurement and its fit to V_s profile model at the Shelter location, Manta.

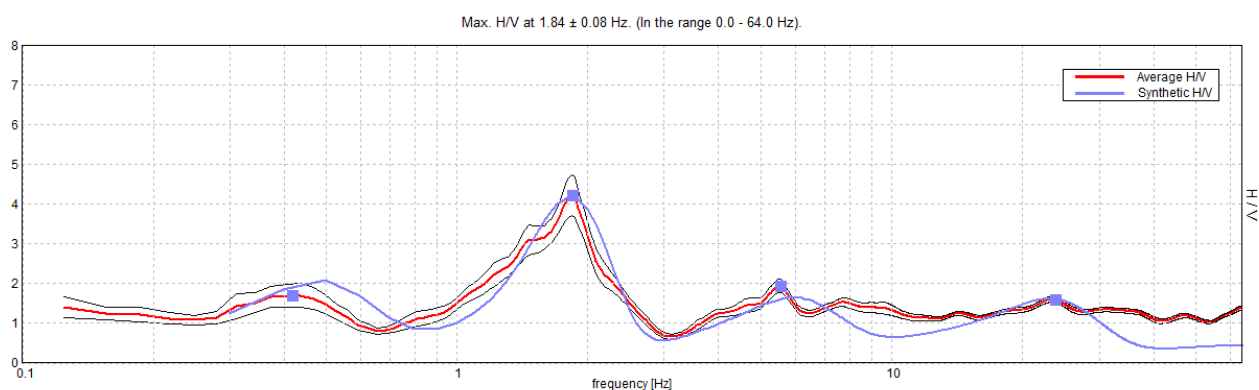


Figure 3-12 Comparison of the H/V T13 in-situ measurement and its fit to V_s profile model at Tarqui, Manta.

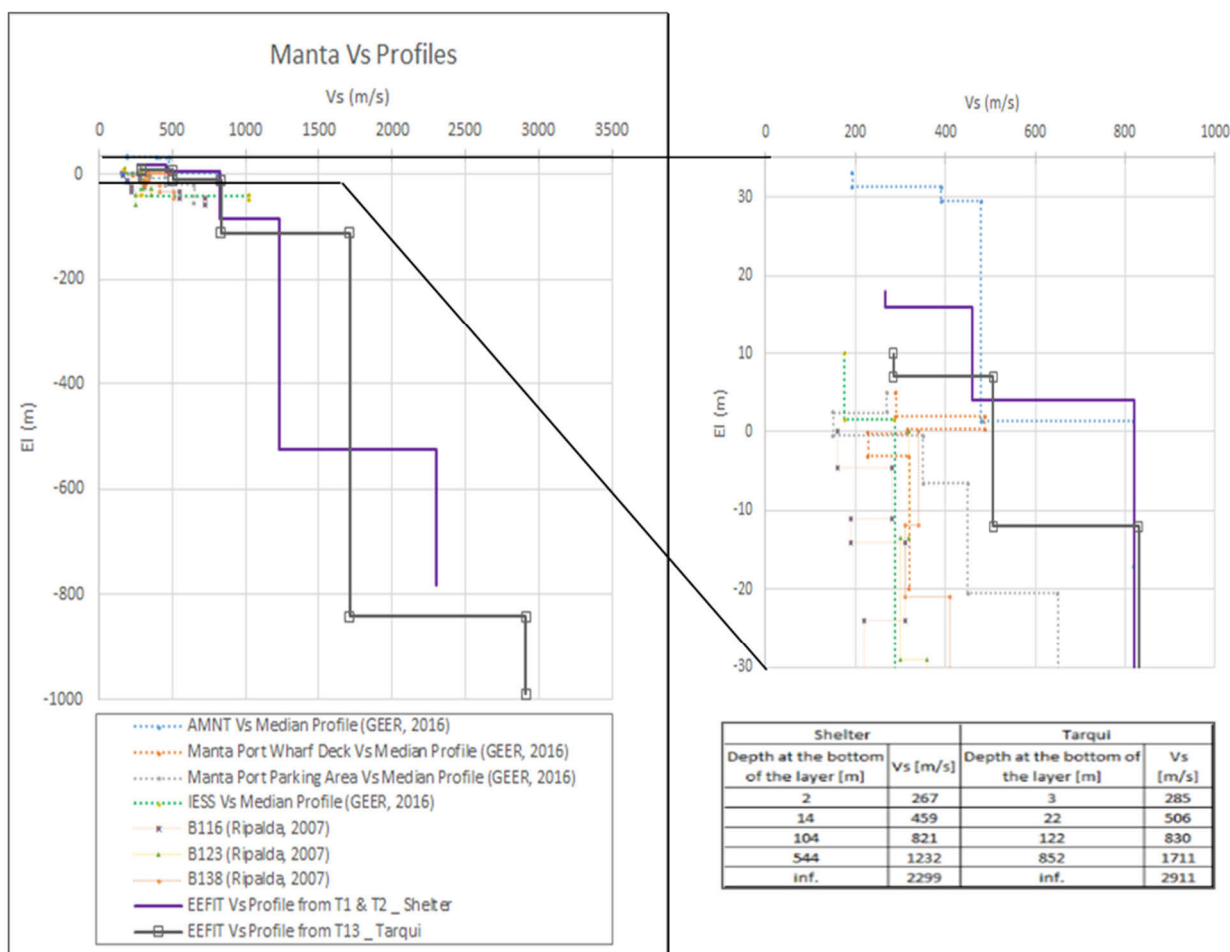


Figure 3-13 Vs profile models for Manta.

b) Portoviejo

Seven microtremor tests were carried out in Portoviejo: four of them in the Botanical Garden close to the APO1 seismometer station; two in the Z0 area at the time of the survey (restricted access area with very heavily damaged structures); and one on the banks of the river, where slope instability induced damage was observed.

The readings at T6 to T9 close to APO1 were very consistent with each other, proving very little lateral variation in stratigraphy along the alignment of the measurements. Figure 3-14 shows the reading at T8 and the H/V spectral ratio corresponding to the simplified Vs model derived for the botanical garden sites (T6 to T9). Figure 3-19 shows that the simplified Vs model is in good agreement with the APO1 in-situ Vs measurement carried out by GEER (2006).

The measurements in Z0 (T3 and T4) are very similar and therefore interpreted together for a common Vs simplified model (Figure 3-19). The reading at T5 is also fairly similar to those at T3 and T4, although it has a distinct single peak whilst in Z0, the main peak is bi-headed, indicating the presence of two main stratigraphic interfaces close together.

For both Z0 area measurements and T5 on the river banks, two options of Vs model interpretation were proposed. In Option 1, the constraint is given as the depth to bedrock (~30m depth) in order for it to be consistent with the APO1 profile. This would however imply

that the average shear wave velocity of the upper layers would be lower than at the APO1 site (from 360m/s to about 140m/s). In Option 2, the constraint is set at the average shear wave velocity of the upper stratum to be similar to that in the APO1 model (*i.e.* 360m/s). That would however entail that the depth to bedrock is much greater (from about 30 to about 80m depth). The Option 2 analysis seems to be, in both cases, the best fit for the H/V spectral ratio in terms of amplitude of the main peak. This may be consistent with a sedimentary basin along the river and fits well other sources' ground investigation data.

APO1 (T6 to T9)

H = 32m; $V_s = 360$ m/s; $V_{s,l} = 780$ m/s

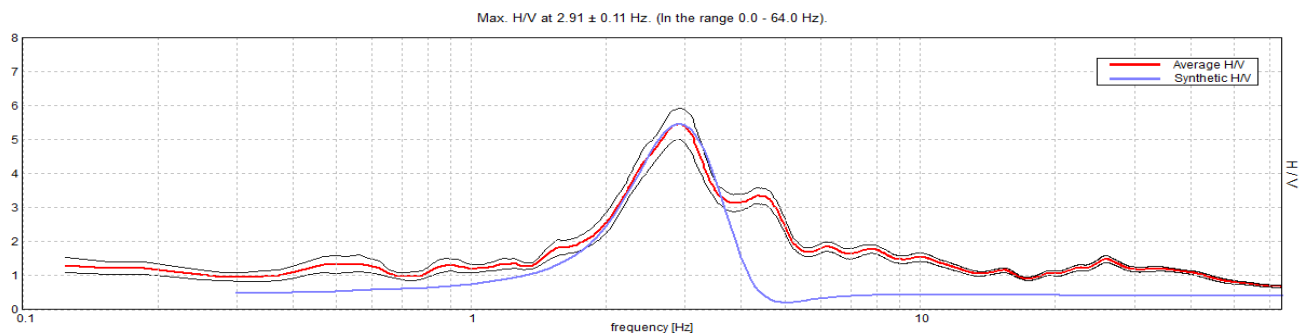


Figure 3-14 H/V T8 reading and corresponding spectrum for V_s simplified model derived for the Botanical Garden sites (T6-T9).

Z0 (T3 & T4)

Option 1: H = 32m; $V_s = 144$ m/s; $V_{s,l} = 800$ m/s

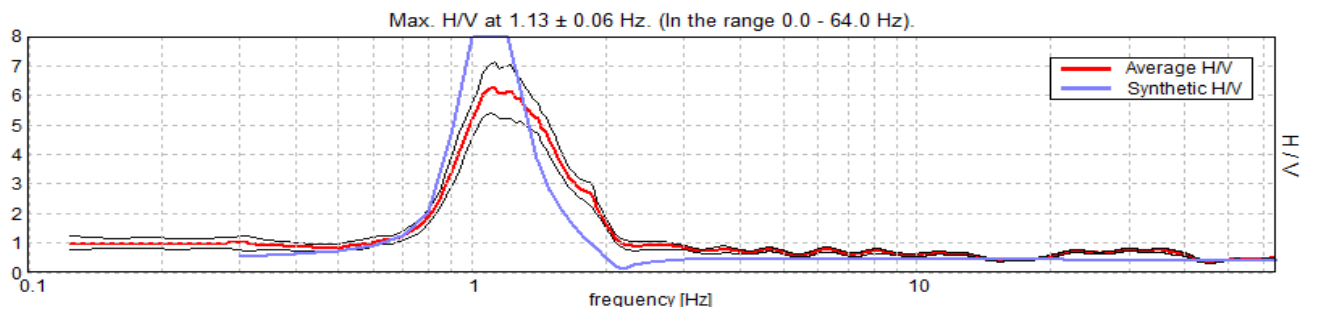


Figure 3-15 H/V T4 reading and corresponding spectrum for the first option of interpretation of the V_s simplified model derived for the Z0 sites (T3 & T4).

Option 2: H = 80m; $V_s = 360$ m/s; $V_{s,l} = 800$ m/s

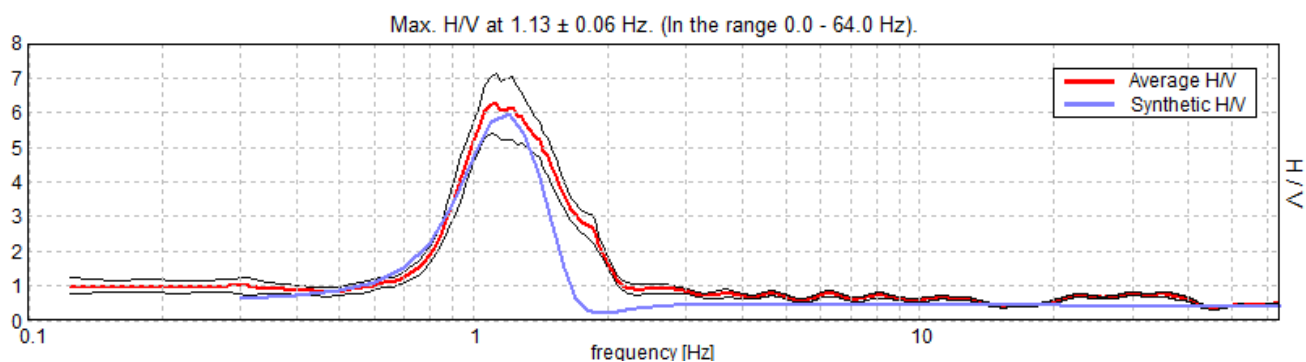


Figure 3-16 H/V T4 reading and corresponding spectrum for the second option of interpretation of the V_s simplified model derived for the Z0 sites (T3 & T4).

River Bank (T5)

Option 1: $H=28\text{m}$; $V_s = 140 \text{ m/s}$; $V_{s,i}=1000\text{m/s}$

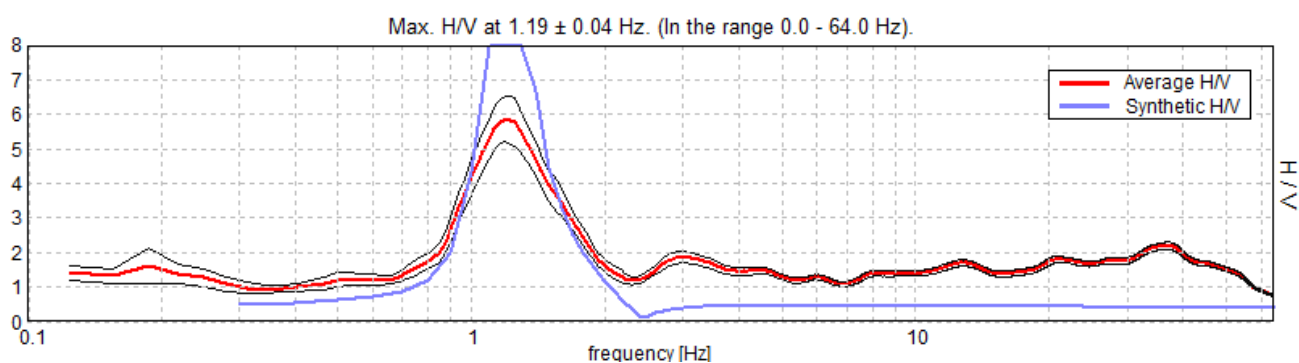


Figure 3-17 H/V reading and corresponding spectrum for the first option of interpretation of the V_s simplified model derived for the Portoviejo river bank at T5.

Option 2: $H=76 \text{ m}$; $V_s=340\text{m/s}$; $V_{s,i}=800\text{m/s}$

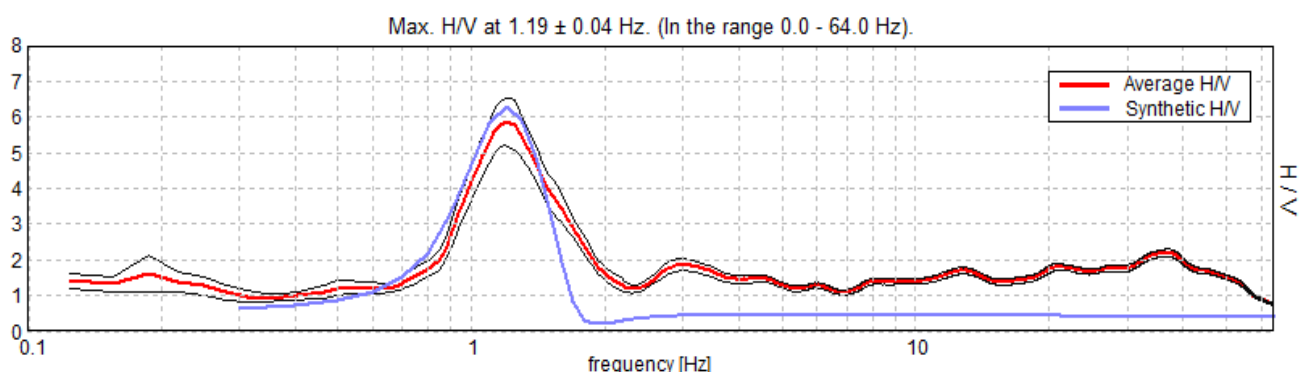


Figure 3-18 H/V reading and corresponding spectrum for the second option of interpretation of the V_s simplified model derived for the Portoviejo river bank at T5.

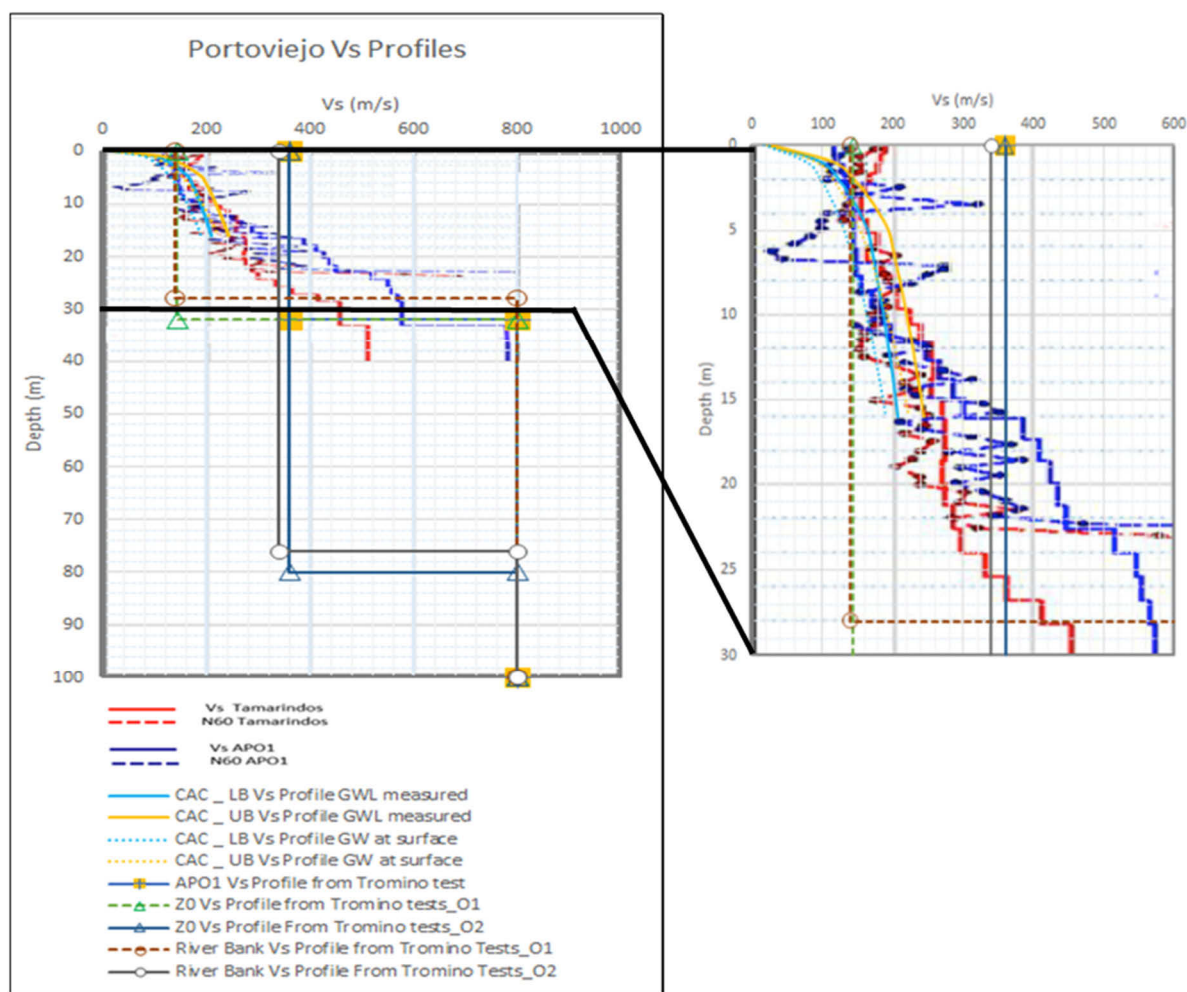


Figure 3-19 Interpreted V_s measurements and models for Portoviejo. The Tamarindos and APO1 MASW and MAM V_s measurements come from GEER (2016). The CAC V_s profiles are derived from SPT-N measurements (Hidroplan, 2016) (see Appendix A).

c) Bahía de Caraquez and Surroundings

Two microtremor tests were carried out in the vicinity of Bahía de Caraquez: one on the site of the Hospital Miguel A. Alcivar (T10) which was very badly damaged during the 2016 main shock; and one (T12) on the north-west bank of the iconic Los Caras bridge where liquefaction-induced damage was observed.

Both readings are very clear and show distinct dominant peak, at 0.68Hz and 1.53Hz for T12 and T10 respectively. Two options for the interpretation of T10 in terms of V_s profile are proposed (see Figure 3-20 and Figure 3-21).

The first one is constrained by the average V_s derived from the SPT measurements at the closest available ground investigation site PMB, *i.e.* 400m/s (see Figure 3-23). The second one is constrained on the other hand by the depth to bedrock to be close to that of the NW bridge measurements. The two options provide a very good and very similar match to the recorded H/V spectral ratios. However, as seen in Figure 3-5, the geology differs on the North and South side of the Chone river at the mouth of the estuary, and therefore Option 1 of the V_s interpretation of the T10 recording is likely to be closer to the field condition.

The T12 V_s interpretation matches well the SPT-based V_s simplified profile for the Los Caras bridge (GEER, 2016), courtesy of the Ecuador's army Corps of Engineers, on the basis of which it was constrained, *i.e.* the depth to bedrock of about 70m (see Figure 3-23). It also provides a good fit in terms of H/V spectral ratio to the record (Figure 3-22).

Bahía Alcivar Hospital (T10)

Option 1: $H=72$; $V_s = 400$; $V_{s,l} = 1000\text{m/s}$

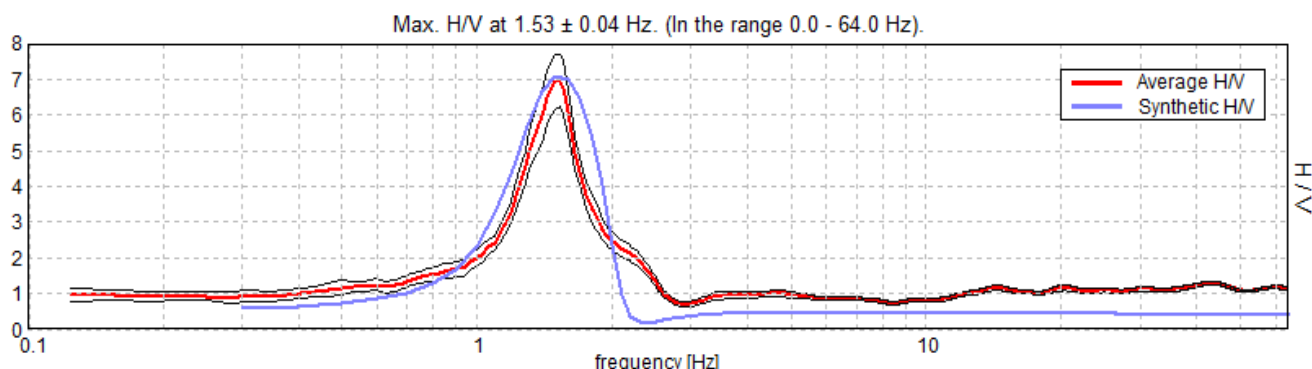


Figure 3-20 H/V reading and corresponding spectrum for the first option of interpretation of the V_s simplified model derived for the Bahía Hospital site T10.

Option 2: $H = 100$; $V_s = 560$ m/s; $V_{s,l} = 1400\text{m/s}$

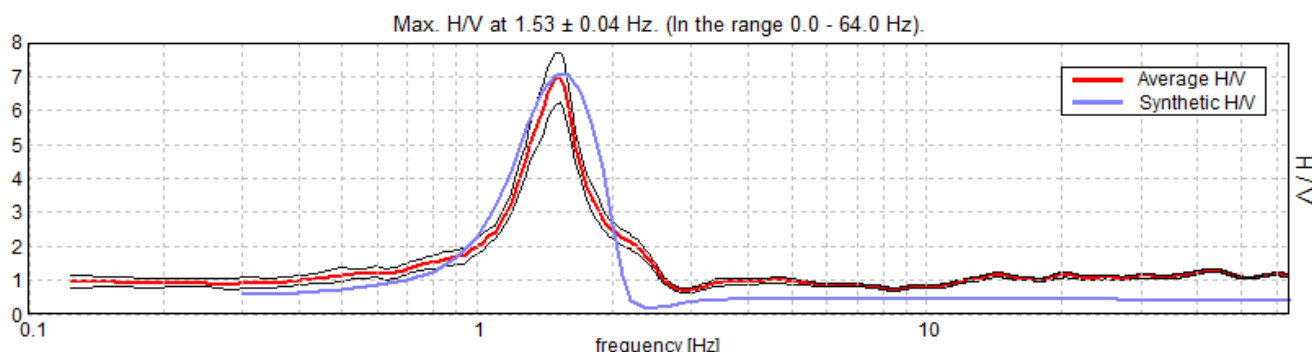


Figure 3-21 H/V reading and corresponding spectrum for the second option of interpretation of the V_s simplified model derived for the Bahía Hospital site T10.

NW embankment of the Los Caras Bridge (T12)

$H= 75\text{m}$; $V_s = 200\text{m/s}$; $V_{s,l} = 489\text{m/s}$

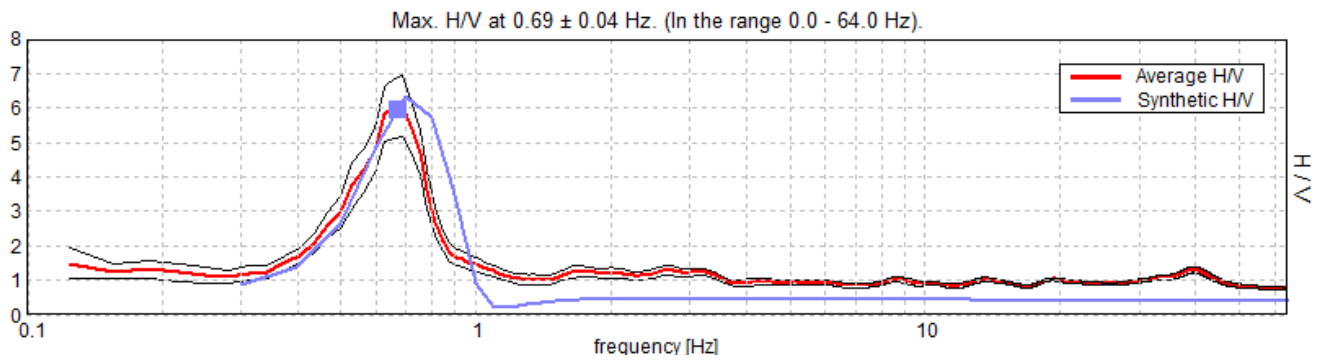


Figure 3-22 H/V reading and corresponding spectrum for the V_s simplified model derived for the NW embankment of the Los Caras Bridge, site T12.

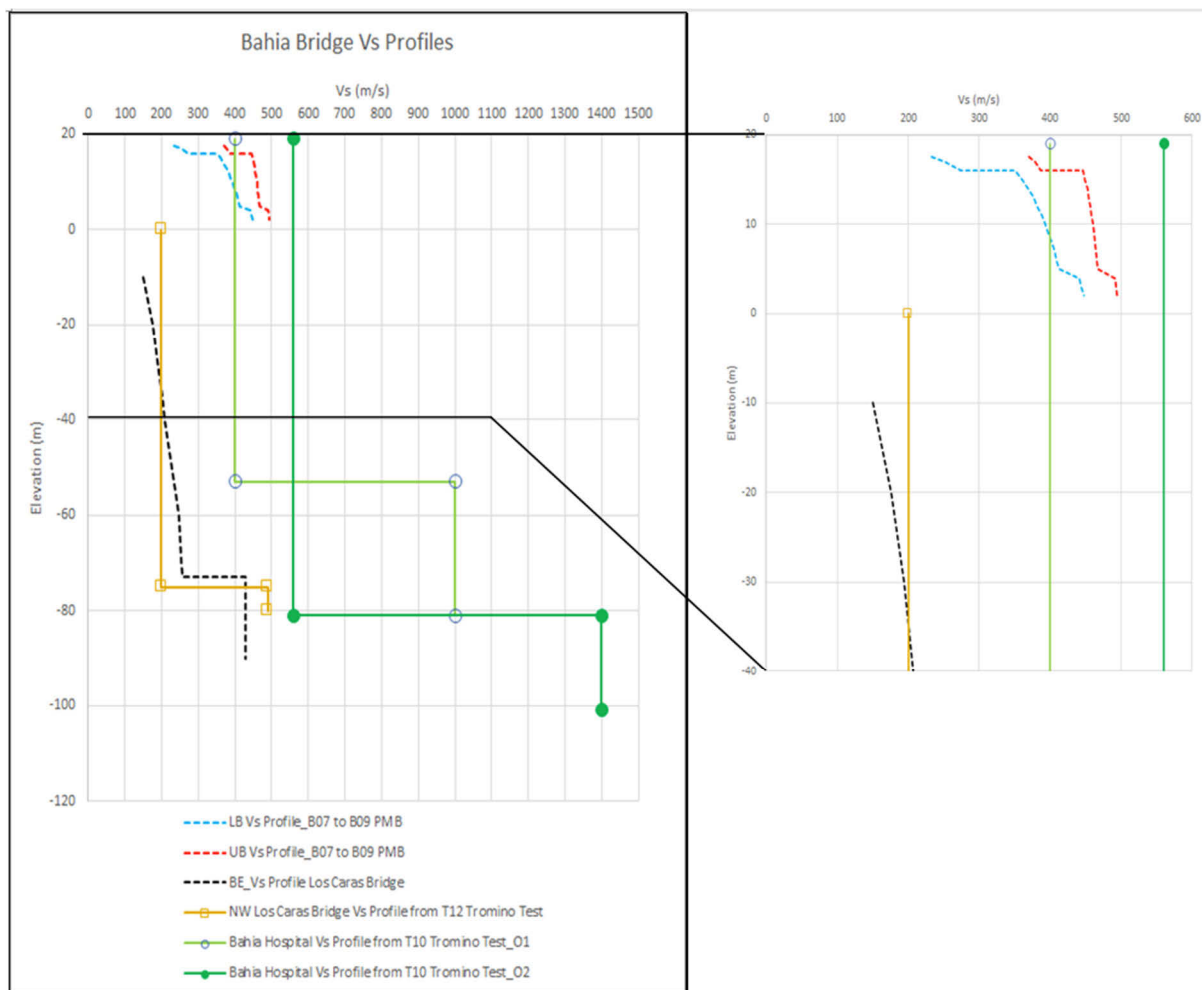


Figure 3-23 V_s profiles for Bahía. The PMB profiles are derived based on SPT-N values from LUP (2016), and the Los Caras Bridge best estimate V_s profile is based on a SPT-N simplified profile provided to GEER (2016) by the Ecuador's Army Corps of Engineers (see Appendix A).

d) Pedernales

One microtremor test was carried out at the APED seismometer station location in Pedernales. It is located within a private development and access was granted by the owners. The house

was only very slightly damaged, with a crack observed on the ceiling and no more significant damage reported by the owner. The seismometer was located in the garden. Quite a lot of noise of heavy traffic and machinery was noted during the tests, but they do not seem to have had a significant impact on the reading, which remains clear (Figure 3-24). A simplified V_s profile was derived which corresponds well with the GEER (2016) in-situ measurement (Figure 3-25).

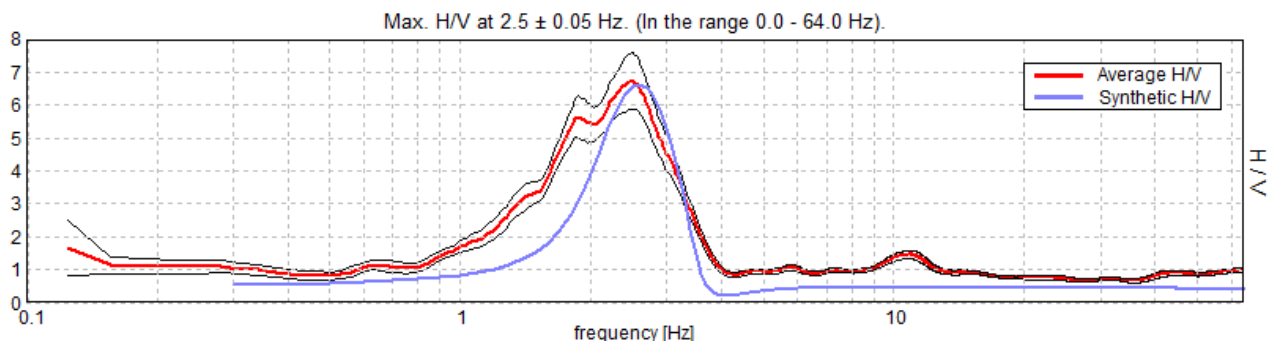


Figure 3-24 Comparison of the APED microtremor test reading H/V ratio to that of the corresponding simplified V_s profile derived.

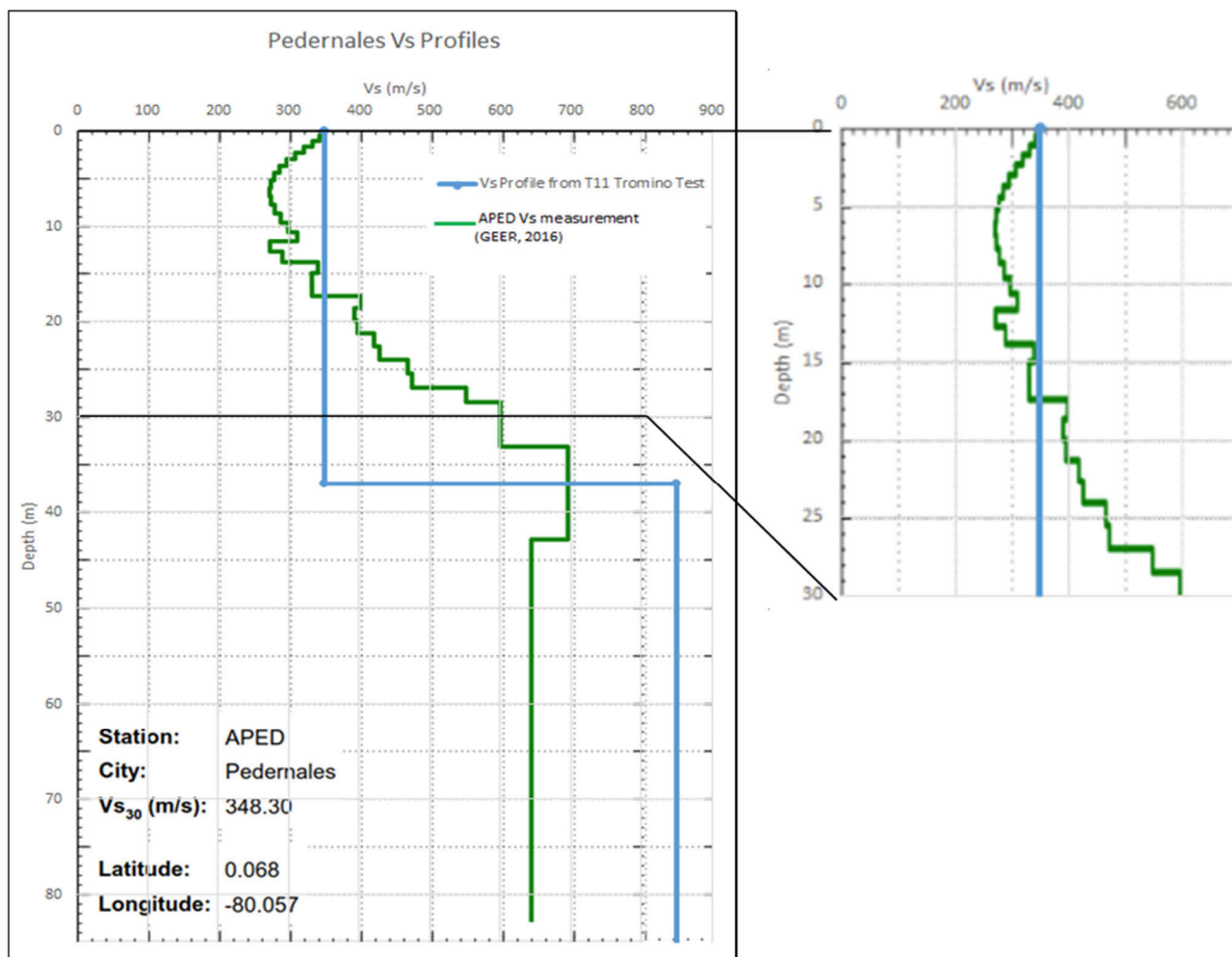


Figure 3-25 V_s profile derived for APED, Pedernales.

3.6. Site Effects Interpretation

Based on the analysis of the microtremor tests and the available geological and geotechnical information, a view on the potential contributing site effects to the observed damage is proposed for the different locations surveyed during the mission. In particular, a categorization of the sites based on average shear wave velocity analysis of the first 30m depth is proposed using the NEHRP classification system (BSSC, 2004), as reproduced below in Table 3-5.

It should be noted that whenever shear wave velocity had to be derived based on SPT measurements, the PEER Wair *et al.* (2012) guidance for SPT- V_s correlations was used (Table 3-6).

Information on all external ground investigation information used for site categorisation interpretation complementarily to the EEFIT in-situ tests are presented in more detail in Appendix A.

Table 3-5 NEHRP Site Categorisation (BSSC, 2004).

Site Class	Soil Profile Name	V_{S30}	SPT N-Value	Undrained Shear Strength
A	Hard Rock	> 5,000 ft/s >1,500 m/s	---	---
B	Rock	2,500 to 5,000 ft/s 760 to 1,500 m/s	---	---
C	Very Dense Soil and Soft Rock	1,200 to 2,500 ft/s 360 to 760 m/s	> 50 bpf	> 2,000 psf > 100 kPa
D	Stiff Soil	600 to 1,200 ft/s 180 to 360 m/s	15 to 50 bpf	1,000 to 2,000 psf 50 to 100 kPa
E	Soft Soil ¹	< 600 ft/s < 180 m/s	< 15 bpf	< 1,000 psf < 50 kPa
F	Soils Requiring Site-Specific Evaluation ²	---	---	---

¹Site Class E also includes any profile with more than 10 ft (3 m) of soft clay, defined as soil with Plasticity Index > 20, water content > 40%, and undrained shear strength < 500 psf (25 kPa).

²Site Class F includes: (1) Soils vulnerable to failure or collapse under seismic loading (i.e., liquefiable soils, quick and highly sensitive clays, and collapsible weakly-cemented soils). (2) Peat and/or highly organic clay layers more than 10 ft (3 m) thick. (3) Very high plasticity clay (PI > 75) layers more than 25 ft (8 m) thick. (4) Soft to medium clay layers more than 120 ft (36 m) thick.

Table 3-6 SPT- V_s correlation recommendations from Wair *et al.* (2012).

Soil Type	Shear Wave Velocity for Quaternary Soils (m/s)			Age Scaling Factors	
			(Eq #)	Holocene	Pleistocene
All Soils	30	$N_{60}^{0.215} \sigma_v^{0.275}$	(4.17)	0.87	1.13
Clays & Silts	26	$N_{60}^{0.17} \sigma_v^{0.32}$	(4.40)	0.88	1.12
Sands	30	$N_{60}^{0.23} \sigma_v^{0.23}$	(4.77)	0.90	1.17
Gravels - Holocene	53	$N_{60}^{0.19} \sigma_v^{0.18}$	(4.98)	---	---
Gravels - Pleistocene	115	$N_{60}^{0.17} \sigma_v^{0.12}$	(4.102)	---	---

σ_v measured in kPa

3.6.1. Manta

As shown in Appendix A, ground investigation information is mostly available in the vicinity of the most damaged area of Tarqui (see Figure 3-26) and in the Port area. The results may support the evidence of a basin perpendicular to the river channel.

The profile derived at the site of the shelter, further away from the centre, hence best matches the profile at the seismometer station AMNT, which is located furthest on the other side of the river estuary (see Figure 3-13). In Tarqui and in the port area, closer to the river, sites are softer. The EEFIT microtremor test in Tarqui corresponds fairly well to the GEER (2016) HVSR tests results. Their minimum site frequencies varied from about 0.6 to 2.7Hz, with increasing values towards the river (Appendix A and Figure 3-7).

The simplified V_s profile derived from the EEFIT T13 measurement corresponds to a $V_{s,30}=570\text{m/s}$, which is much stiffer than the trends indicated by the ground investigations West of the river, characterised by a range of $V_{s,30}$ between 240m/s and 360m/s. As shown in Appendix A, Reyes & Michaud (2012) indicated a potential active fault line in the alignment of the river's axis close to the estuary. This may potentially explain this difference of site conditions west and east of the river axis. Further investigation should be carried out to provide evidence of the existence of this fault and its characteristics.

It would also be necessary to gather more information in a North-South direction to better describe the variability in soil conditions of Manta and its potential correlation to damage distribution. More ground investigation (GI) is therefore needed to fully understand the site effect contribution to the relatively high concentration of damage in northern Tarqui observed compared to its surroundings (see Figure 3-26).

Site categorisation can however be carried out based on the simplified V_s . All sites for which ground investigation is available were classified as either Site Class C or D (Table 3-7).

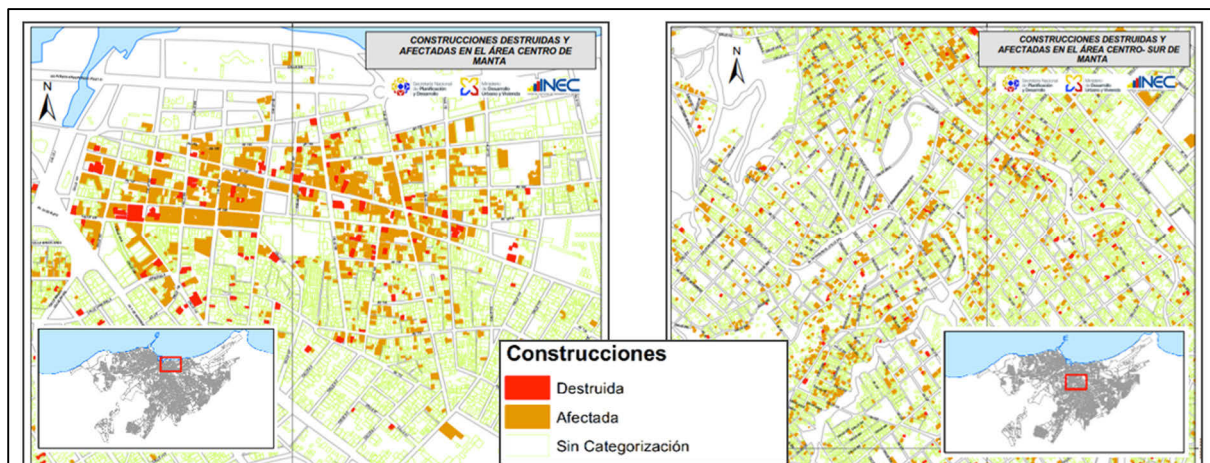


Figure 3-26 Preliminary rapid assessment damage map (IGM, 2016).

Table 3-7 Summary of site frequency and categorization based on available geotechnical information for Manta.

Source	GI ID	EI (m)	Min.site frequency (Hz)	No. of peaks	Associated frequencies for each peak (Hz)	v_0 (Hz)	$V_{s,30}$ (m/s)	Site Class
GEER (2016)	HV1	?	1.8	3	0.5; 1.8; 5.5			
	HV2	?	0.6?	3	0.6;2;8			
	HV3	?	0.8?	4	0.8;1.5;2;7			
	HV4	?	1.8	3	0.6;1.8;7.5			
	HV5	?	2.4	4	0.5;2.4;4.5;15			
	HV6	?	1.2	3	1.2;1.8;5			
	HV7	?	2.7	3	1.5;2.7;7			
	VS_AMNT	33				3.47	440	C
	VS_MPWD	5				-	-	-
	VS_MPPA	5				5	360	C-D
VS_IESS	10				1.28	240	D	
Ripalda (2007)	B116	0					250	D
	B123	0					310	D
	B138	0					350	D
THIS MISSION	T1	19	8.31 +/- 2.11 (i.e. P3)	4 (P1 to P4)	P1 (0.5); P2 (1.8); P3 (8.5); P4 (32)		640	C
	T2	17						
	T13	10	1.84 +/- 0.08 (i.e. P2)	4 (P1 to P4)	P1 (0.45); P2 (1.8); P3 (5.5); P4 (25)		570	C

3.6.2. Portoviejo

Figure 3-27 shows the rapid damage assessment carried out based on satellite imagery by UNOSAT for Portoviejo as well as the one carried out by IGM. Both maps are in fairly good agreement in terms of identification of the most damaged area. It corresponds to quite a localised area in the city centre. The seven microtremor tests carried out by EEFIT in the city and the other ground investigation data presented in Appendix A were analysed to understand the potential site effect contribution to the damage intensity distribution.

Table 3-8 and Figure 3-19 show that the V_s profiles at the different ground investigation locations are fairly consistent in terms of superficial alluvial deposits. The main difference is the depth to bedrock, which is interpreted, as expected, to be deeper in the sites closer to the river (T3 to T5). These sites also correspond to the locations of high levels of damage observed (zone 0 and bank of the river). However, the damage intensity distribution cannot be solely explained by this basin effect, since this trend was not observed along the river symmetrically. It may be hypothesised that the seismic wave amplification may have been increased by the topography. The shortest distance to higher bedrock levels (hills) from the sites on deeper alluvial deposits indeed corresponds to where most of the damage was concentrated (see arrows in Figure 3-27).

Sites were mainly categorised as Class D throughout, with the most conservative interpretation as Class E at the deepest alluvial deposits sites closest to the river. The stiffer profiles closer to the hills (close to the APO1 seismometer site) were classified as Site Class C to D.

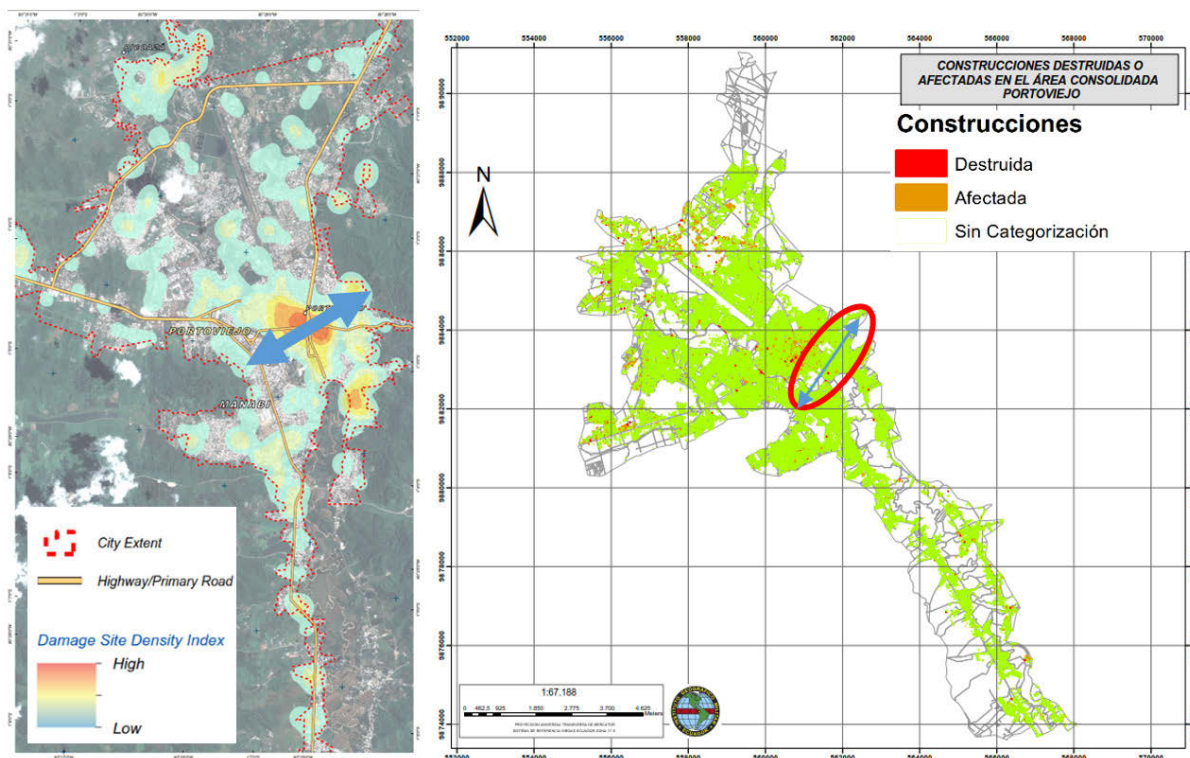


Figure 3-27 Rapid damage assessment map for Portoviejo (a - UNOSAT, 2016; b- IGM, 2016).

Table 3-8 Summary of site frequency and categorization based on available geotechnical information for Portoviejo.

Source	GI ID	El (m)	min.site frequency (Hz)	No. of peaks	associated frequencies (Hz)	vo (Hz)	Vs,30 (m/s)	Site Class			
GEER (2016)	APO1	41				2.6	240	D			
	Los Tamarindos	-				1.9	~250	D			
Hidroplan (2016)	P1	45									measurements to depth investigated (15m) match well overall trend of the APO1 and Los Tamarindos GEER in-situ measurements
	P2	45									
	P3	45									
	P4	45									
	P5	45									
	P6	45									
	P7	45									
	P8	45									
	P9	45									
	P10	45									
EEFIT (2016)	T3	45	1.03	1*	1.03		140-360	D-E			
	T4	45	1.13	1*	1.13		D-E				
	T5	36	1.19	1*	1.19		140-340	D-E			
	T6	42	2.91	1 to 2*	2.91; 4.5		360	C-D			
	T7	42	2.81	1 to 2*	2.81; 4.5						
	T8	43	2.91	1 to 2*	2.91; 4.5						
	T9	44	2.81	1 to 2*	2.81; 3.5						

* and many small peaks at larger frequencies

3.6.3. Bahía de Caraquez and Surroundings

The two microtremor tests carried out on each side of the mouth of the Chone Estuary in Bahía de Caraquez (T12) and San Vicente (T10) are in good agreement with the nearby ground investigation results from other sources: *i.e.* the LUP (2016) data and the Los Caras bridge GI data taken from GEER (2016) respectively (Table 3-9). The ground investigations carried out close to the North embankment of the Los Caras bridge on the San Vicente side indicate a softer profile, categorised as Class D, compared to the sites categorised as Class C on the Bahía de Caraquez side (Figure 3-23).

As shown in Appendix A, this difference may be associated to a difference in geology, whereby the north bank is associated to the Borbon formation, whilst the southern side is characterised by the presence of the older Onzole formation. The topography is also steeper on the Bahía side than in San Vicente where thicker estuarine deposits may be present. Finally, the concentration of higher damage levels in the circled area in Figure 3-28 may potentially partly be due to some degree of topographic effect, since it corresponds to some of the higher grounds. The topographic differential was of about 30m between the end of the peninsula and the furthest inland part of the area circled in red. However, a significant number of structures remained not categorised in the peninsula at the time Figure 3-28 was issued. On site, some significant damage was observed there as well (see Section F).

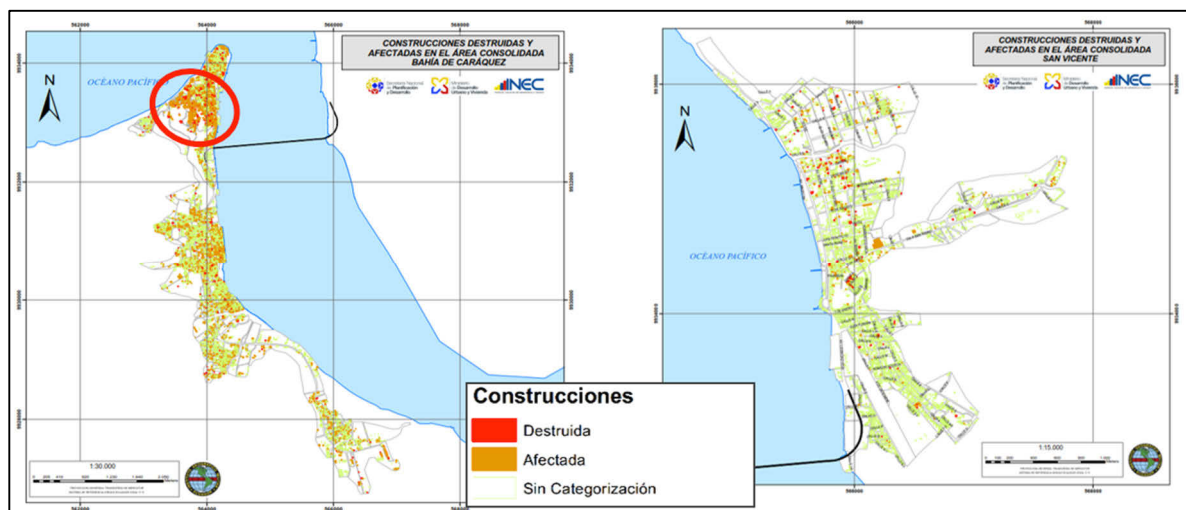


Figure 3-28 Rapid damage assessment map for Bahía de Caraquez and San Vicente, across the Chone Estuary (IGM, 2016).

3.6.4. Pedernales

Limited ground investigation is available for Pedernales. However, the V_s profile inversion from the microtremor test carried out during the mission close to the seismometer station APED matches well with the in-situ V_s measurement results from GEER (2016) (see Figure 3-25). Over the first 30m depth, the average shear wave velocity is assessed to be around 350m/s, hence corresponding to a relatively stiff Site Class D site.

3.6.5. Perspectives on Jama, Canoa

Although geotechnical surveys were not carried out in Canoa and Jama by the EEFIT team, structural surveys were carried out there. Some external ground investigation information (LUP, 2016) was gathered to understand the potential site effect contribution to the damage

observed at these locations. The V_s profiles derived from the SPT measurements carried out down to 16m depth using the PEER (Wair *et al.*, 2012) SPT- V_s correlation recommendations are shown in Figure 3-30. The profiles are very similar at both locations and if the trend continues for the following 15m depth, the site can be expected to be categorised as Site Class D. This would of course need to be confirmed and evidenced by further ground investigation.

Table 3-9 Summary of site frequency and categorization based on available geotechnical information for Bahía de Caraquez and the mouth of the Chone Estuary.

Source	GI ID	El (m)	min.site frequency (Hz)	No. of peaks	associated frequencies (Hz)	$V_{s,30}$ (m/s)	Site Class
GEER (2016) **	GI_Bridge	~ -5m				~200	D
LUP (2016)	B01	10				-	-
	B02	10				-	-
	B02	10				-	-
	B04	10				-	-
	B05	10				-	-
	B06	10				-	-
	B07	17				-	-
	B08	17				-	-
	B09	17				-	-
EEFIT (2016)	T10	19	1.53	2*	1.53; 2.3	200	D
	T12	0	0.69	1*	0.69	400-560	C

* and many lower amplitude peaks at greater frequencies
 ** Courtesy of the Ecuador's Army Corps of Engineers, Alfredo Caicedo

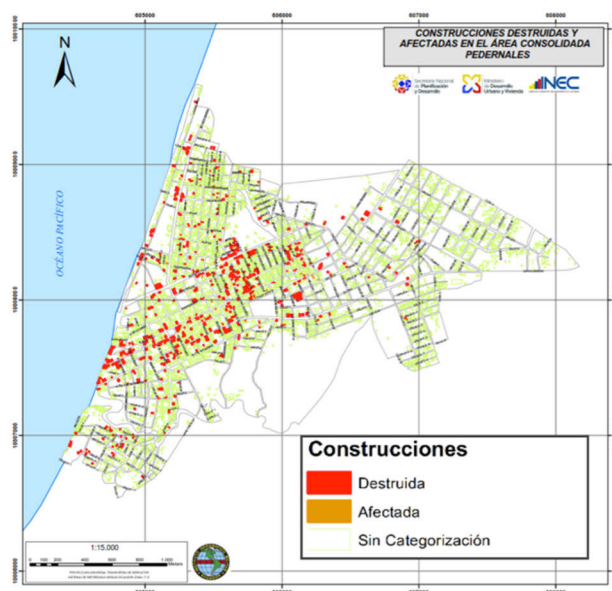


Figure 3-29 Rapid damage assessment map for Pedernales (IGM, 2016).

Table 3-10 Summary of site frequency and categorization based on available geotechnical information for Pedernales.

Source	GI ID	EI (m)	Min.site frequency (Hz)	No. of peaks	Associated frequencies (Hz)	$V_{s,30}$ (m/s)	Site Class
GEER (2016)	APED	15		-		350	D (close to C)
THIS MISSION	T11	15	2.5	3	1.8; 2.5; 12	350	D (close to C)

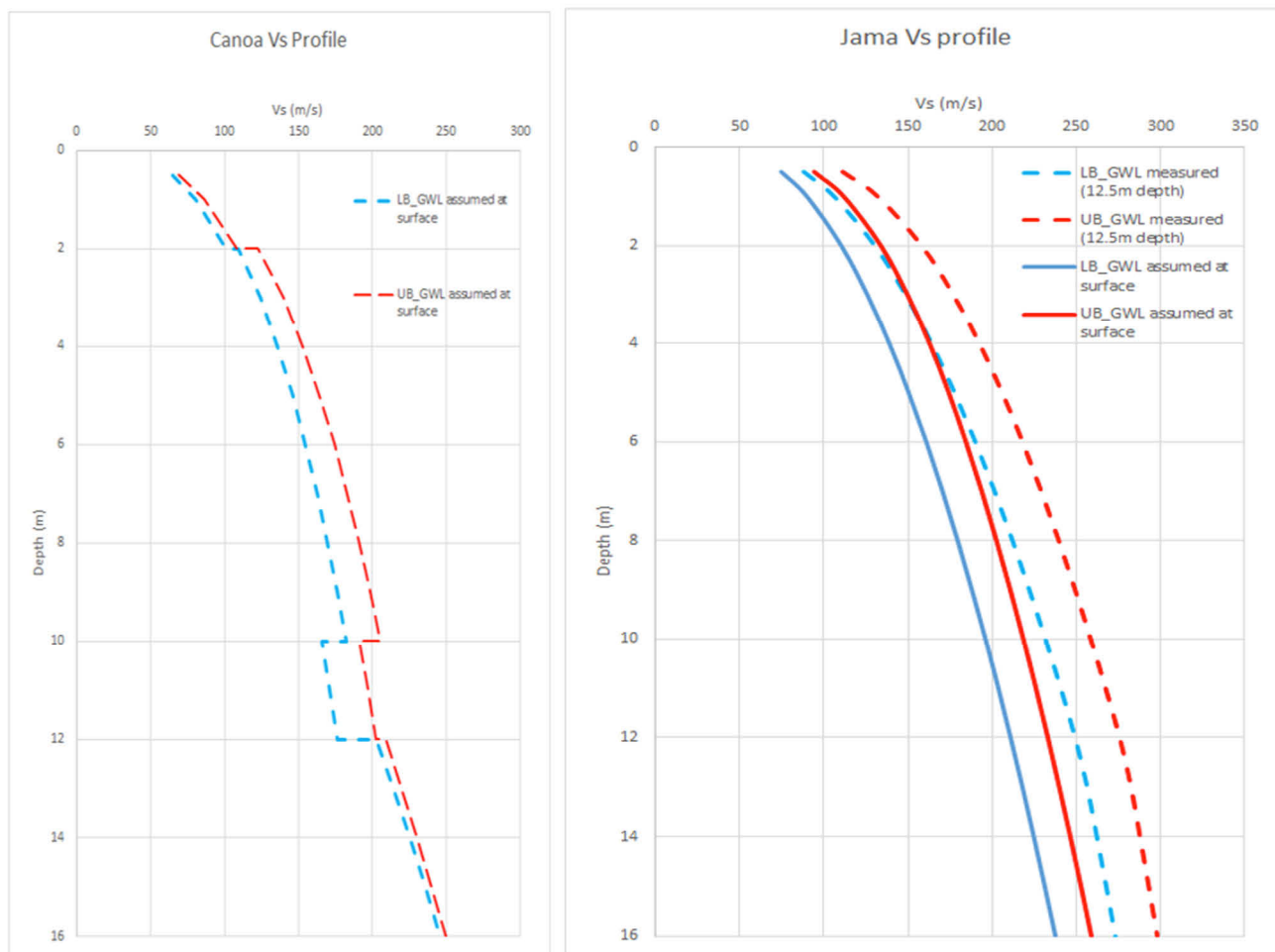


Figure 3-30 Jama and Canoa SPT-based V_s profiles (based on LUP (2016) measurements).

4. Observations of Geotechnical Failures

Damage to structures and infrastructure are generally attributed to the direct effect of ground shaking in the event of a major earthquake. Other geotechnical failures such as landslides, liquefaction or fault rupture can significantly contribute to it as well (Figure 4-1). The EEFIT geotechnical team sought to assess the extent in the case of the 2016 Ecuador sequence of events.

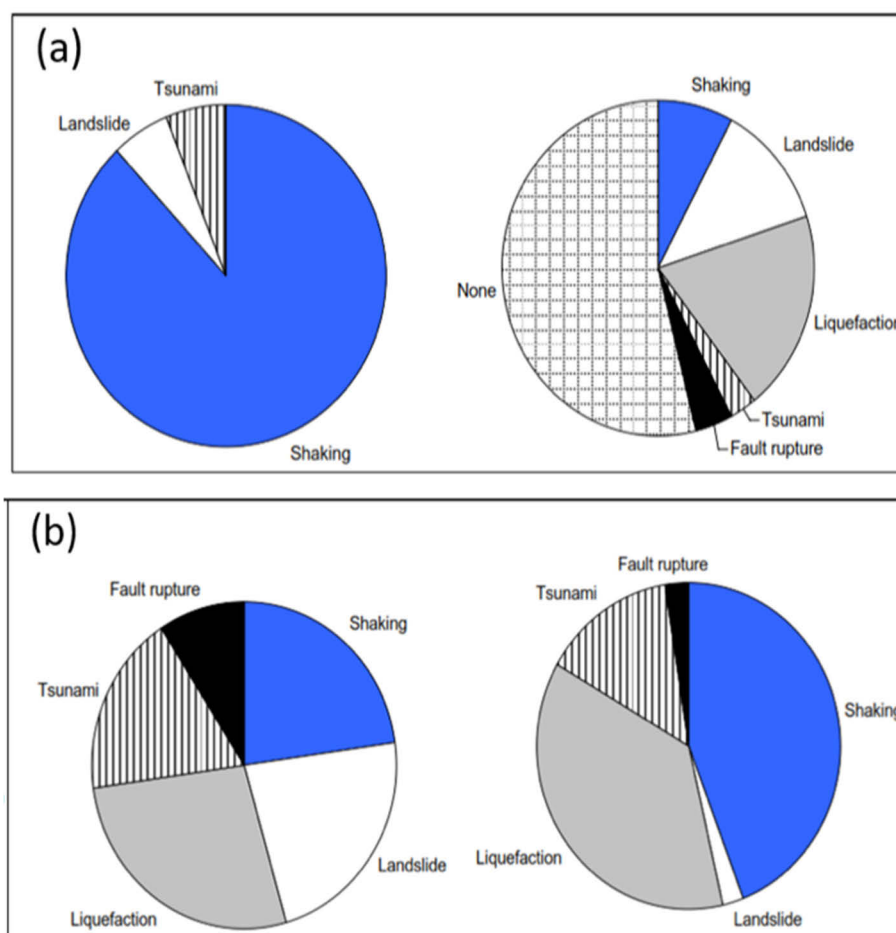


Figure 4-1 (a) Primary causes of damage to buildings (left) and the second main cause of damage (right) in 50 earthquakes that occurred between 1989 and 2003; (b) Primary causes of damage to transportation systems (left) and utilities (right) in earthquakes between 1989 and 2003 in which there was significant damage to these two categories of exposure (Bommer *et al.*, 2006).

4.1. Overall Survey Scope

Prior to the mission, a desktop study was undertaken to acquire an initial understanding of the extent of geotechnical damage. This included discussions with collaborators both on site and who had returned from other missions, and a review of other information available online. Liquefaction issues were noted in Manta, Portoviejo, Pedernales and Chamanga mainly, whilst landslides along the coast around Bahía de Caraquez and an impressive landslide in the rural area of San Isidro further inland were pinpointed as areas of interest for the survey. In addition, a collaboration with the British Geological Survey (BGS) was set up to ground-truth their rapid satellite-imagery-based landslide assessment maps. Out of several areas covered by the BGS, those with the most damage identified were selected for the ground-truthing exercise, in the Chone Estuary and Portoviejo.

The focus of the geotechnical failure survey was hence mainly on landslides and liquefaction at the locations shown in Figure 4-2 . Evidence of potential fault rupture was also looked for where the Reyes & Michaud (2012) and Eguez *et al.* (2003) maps showed potentially active faults in the region, *i.e.* close to Bahía and San Isidro. However, no evidence of fault rupture could be observed, apart from the landslide in San Isidro which might have been associated to the rupture of the San Isidro section of the Canaveral Fault (see Section 4.4.3.).

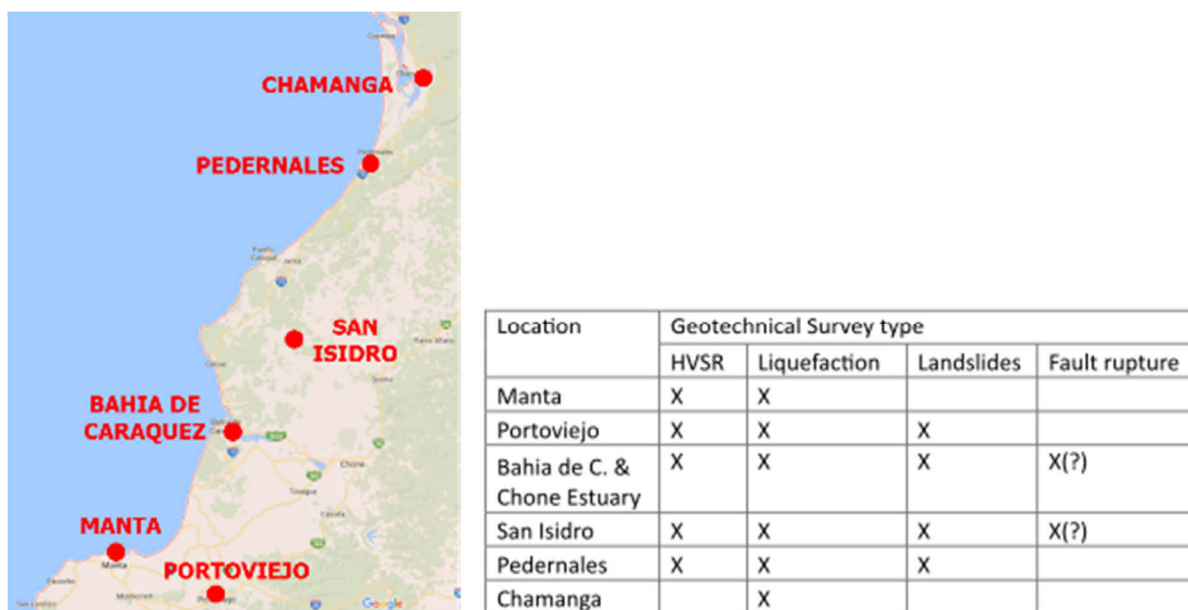


Figure 4-2 Location and type of geotechnical surveys carried out by EEFIT.

4.2. Liquefaction

Liquefaction is defined as the loss of strength and stiffness of loose, saturated soils due to an increase in excess pore pressure and reduction in effective stress caused by cyclic loading, such as earthquakes. Liquefied soils behave as viscous fluids rather than as a solid. Sediments most susceptible to liquefaction include (Youd *et al.*, 2001; Krinitzsky and Hynes, 2002):

- Holocene to late Pleistocene ages deposits;
- River channel and flood plain alluvium;
- Aeolian deposits; and
- Poorly compacted fills.

The 16 April earthquake occurred towards the end of the annual rainy season (December to May), which had possibly been intensified by the 2015-2016 El Niño. In the week preceding the earthquake, news articles show that flooding occurred in numerous locations within the Manabí province, including some of the locations most severely affected by the earthquake. Locals feared that bridges in Portoviejo were about to be breached. As a consequence, the river levels and ground water table were abnormally high at the time of the mainshock. Higher ground water table is detrimental to the stability and shear strength of the soil due to the presence of higher pore water pressure. This, in combination with young and soft quaternary sediment deposited along rivers, estuaries and the coast (Reyes and Michaud, 2012), resulted in large volumes of ground being highly susceptible to liquefaction.

Evidence of liquefaction induced damage was reported in a large number of locations in Manabi province following the Ecuador 2016 sequence of events. However, given that the EEFIT mission to Ecuador took place six weeks after the mainshock, a significant amount of demolition and reconstruction had taken place prior to the mission. In addition, rainfall had also occurred which might have added to the removal of such evidences of liquefaction by the time of the mission, particularly minor scale superficial features like sand boils.

The different liquefaction-induced damage types observed are discussed in the following sections.

4.2.1. Lateral Spreading

The significant reduction in stiffness of soil due to liquefaction can cause flow failure or lateral spreading of sloping ground (Ishihara, 1993). This can in turn cause significant damage to structures built on or near sloping ground. No flow failures were observed in the locations visited by the EEFIT team. Lateral spreading was observed on numerous occasions in a range of locations.

In Portoviejo, lateral spreading was observed at numerous locations along the banks of the Rio Portoviejo, the river which runs through the centre of the city. The course of this section of the Rio Portoviejo has been significantly altered by human activity. The river was reportedly redirected to force it to take a straighter course through the city. Annually, the river is dredged and a 30° angle slope is restored to the river banks by redistributing sediments in the river channel. This is likely to have increased the volume of loose soil on the river banks. In addition, a number of locations have used fill material to build outwards into the river.

The recently constructed VelBoni shopping centre car park in Portoviejo displaced laterally towards the river. In this case the failed slope was manmade, and appeared to consist predominantly of fill material. The rotation and translation of surficial blocks of soil can be clearly seen in Figure 4-3a. In other locations, tension cracks parallel to the river indicate that liquefaction of subsurface layers of soil may have occurred (Madabhushi et al., 2013), causing the upper non-liquefied layers to move laterally towards the river (see Figure 4-3b).



Figure 4-3 Lateral spreading in Portoviejo (a) liquefaction of fill below VelBoni carpark (b) tension cracking due to liquefaction of a lower layer.

Liquefaction induced lateral spreading caused damage to a significant number of structures in Portoviejo. The example of the induced settlement and rotation of two structures adjacent to a sport pitch beside the Rio Portoviejo are shown in Figure 4-4. The damage to the pitch surface was also extremely detrimental to the owners of the land and operators of the pitch, with whom the team met and talked. Concern on the loss of revenue from pitch rental business interruption was great, as was the cost to remodel the damaged surface to make it operable again. Section 7.2.3. also mentions the damage induced to a footbridge close by.



Figure 4-4 Structural damage due to lateral spreading along Rio Portoviejo consisting in the rotation and settlement of structures at sports pitch.

A number of structures suffered catastrophic collapse due to lateral spreading. At the site shown in Figure 4-5, seven structures, including a vehicle mechanic's garage, collapsed and four people were killed. At the time of the EEFIT mission, these structures had been demolished. Figure 4-5 is a photograph of the official post-earthquake structural survey documents given to the owner of the garage by the Portoviejo municipality.



Figure 4-5 Collapse of structures along Rio Portoviejo due to liquefaction induced lateral spreading.

Borehole data obtained from a site away from the river in Portoviejo (-1.07244 °N -80.4471 °E) show layers of inorganic clay and clayey silts. These layers have a plasticity index greater

than seven, indicating a clay-like behaviour, and therefore are not susceptible to liquefaction (Boulanger and Idriss, 2006). Liquefaction in Portoviejo was therefore limited to the alluvial soils surrounding the Rio Portoviejo.

To the north of Portoviejo, on the 39A towards Rocafuerte, lateral spreading caused significant damage to the embankments and bridge approaches to the Mejía Bridge, particularly to the south-west of the bridge. Post-earthquake CPTu tests conducted to the south-west of the bridge show the soil to be mostly clay and silty clay, but with some sand layers between a depth of 10 and 14m (GEER 2016). These sand layers have SPT-N values between 7 and 10 blows/30cm, and a factor of safety against liquefaction of greater than one (GEER 2016). Vertical settlements of up to 1.6m and lateral spreading of up to 3m of the south-west embankment were observed (Figure 4-6a). Sizeable lateral and vertical displacement and rotation of the gabions positioned adjacent to the south-west abutment of the bridge occurred (Figure 4-6b). On the north-west side of the bridge the gabions appeared to be unaffected by the earthquake. Significant reconstruction works had been undertaken prior to the EEFIT team visiting the bridge to enable the bridge to be passable. Therefore, the earthquake damage to the carriageway was not observed, but has been documented by a number of other organisations, including PEER and GEER (GEER, 2016).



Figure 4-6 Damage to south-west of Mejía Bridge (a) lateral spreading of embankment, (b) sliding and rotation of gabions.

Lateral spreading was observed in the Chone River estuary, to the east of San Vicente. Numerous shrimp farms were located along the northern banks of the Chone River Estuary, close to San Vicente. The design of the dykes across this area, both separating the shrimp pools from each other and from the river, appeared to be very similar. The dykes were constructed to be approximately 2m wide and had steep sides, with no slope reinforcement. Dyke settlements of 800mm and lateral spreading of 600mm were common across the shrimp farms in this area (Figure 4-7). Large cracks were observed running parallel to the dykes, often 500mm wide. Dykes running in the north-south direction appeared to be more heavily damaged than those running in the east-west direction. One dyke bordering the River Chone failed and the shrimp pool contents spilled into the River Chone. Shrimp farming is one of the major sources of income for this area. The liquefaction induced damage to the shrimp farms has had a considerable impact on productivity.

In addition to the lateral spreading of shrimp farm dykes, lateral spreading of mangrove swamps in the River Chone Estuary (Figure 4-8) was observed. These mangrove swamps fall within a nature reserve, Refugio de Vida Silvestre – Islas Corazon y Fragatas. Some of these areas were identified as having been affected by liquefaction during the satellite image analysis conducted by the British Geological Survey (BGS). Significant rotation of mangrove

trees was observed along the northern bank of the River Chone. From discussions with locals, it was understood that lateral movements of trees along the river bank of up to 15m occurred. Given the density of this vegetation and the natural environment, these significant movements would not have been noticeable to a first time visitor to the area. It is understood, from discussions with locals, mangrove swamps in the centre and south of the river were affected in a similar manner and to a similar extent. However, this was not verified by the EEFIT mission.



Figure 4-7 Liquefaction induced damage to shrimp farm dykes in Chone River estuary.



Figure 4-8 Lateral spreading of mangrove swamps in Chone River Estuary.

4.2.2. Uplift of Underground Structures

Liquefaction of soil can cause underground structures which have a unit weight less than that of the liquefied soil adjacent to them to float due to buoyancy (Koseki *et al.*, 1997; Chian *et al.*, 2014). This type of damage can be particularly problematic for subsurface distribution systems for water, gas and waste products, which are commonly placed in trenches backfilled with fill material which is susceptible to liquefaction.

Liquefaction induced uplift of a pipe by 20mm and a manhole by 40mm in Manta were observed (Figure 4-9a). Two potential sand boils were observed close by. In Pedernales, manholes protruding by 30mm were observed (Figure 4-9b). The limited uplift of these structures is likely to have been due to the conditions of the soil surrounding the backfilled trenches, which will have had a notable effect on the drainage conditions (Yasuada and Kiku, 2006).

On the seafront in Pedernales, a shrimp farm showed evidence of the effect of liquefaction induced buoyancy on underground structures. The shrimp farm consists of multiple structures adjacent to one another. One of the structures contained concrete underground storage tanks which extended approximately 3m below the ground surface. These tanks were used in the shrimp farming process, and were empty at the time of the earthquake. The other adjacent structures housed above ground storage tanks and a sizeable amount of machinery. They did not have any underground storage tanks. The absolute settlements of the structures were not known since the surrounding ground has settled. However, the differential settlement was measured and showed a relative uplift of 210mm between the structure housing the underground storage tanks and the structure behind it (Figure 4-10a) and 120mm higher than the white structure to its right (Figure 4-10b).



Figure 4-9 Protrusion of manholes in Manta (a) and Pedernales (b).



Figure 4-10 Relative uplift of structure with underground storage tanks in Pedernales, showing locations of measured relative settlement.

4.2.3. Foundation Failure

Part of the rural community of Chamanga is built on what used to be a mangrove swamp on the edge of the estuary, similar to those observed in the Chone River estuary. No tell-tale signs of liquefaction were observed (sand boils or lateral spreading of slopes), however given the loose, saturated river deposits below many of the damaged structures and the damage in the Chone River estuary, it is believed that liquefaction played a role in the damage observed.

In Chamanga, a large number of residential buildings were constructed on timber piles. Piers to launch fishing boats were also constructed in this fashion. The piles were reportedly

embedded 1.5m into the riverbed. A sizable number of these residential buildings and piers collapsed due to the earthquake (Figure 4-11). This is likely to be due to the piles having insufficient lateral and vertical capacity when the soil liquefied. This is despite the structures built on them being relatively lightweight which demonstrates the possibility of soil liquefaction occurrence.



Figure 4-11 Collapse of structures on timber piles in Chamanga.



Figure 4-12 Settlement of building in Chamanga (a) increased settlement from left to right of structure (b) settlement relative to road and step.

A number of buildings located on flat ground adjacent to the estuary settled (Figure 4-12 and Figure 4-13). These buildings are believed to be on shallow foundations. Differential settlements across the buildings have resulted in substantial cracking of concrete components. For the building shown in Figure 4-12, a maximum differential settlement compared to the road was measured to be 290mm and the differential settlement between the corners of the building was 120mm.

Evidence of building foundation failure in larger, more developed cities was minimal. This is believed to be largely due to other factors playing the dominant role in the performance of the buildings – such as steel reinforcement detailing and construction practices, which will be discussed in detail in Section 6.

4.2.4. Mitigation Methods

Liquefaction induced damage was observed across the Manabi province. Liquefaction susceptibility maps do not appear to exist for the region. Therefore, a detailed and systematic study to identify susceptible areas would be beneficial to a large number of parties to enable them to assess the risks to their land and properties.

Given the extent of liquefaction induced damage across the Manabi province, it is evident that there is a lack of understanding and/or utilisation of methods to mitigate potential liquefaction hazards. These mitigation methods include:

- Removal and replacement of liquefiable soils;
- Ground densification;
- In situ stabilisation, using grouting;
- Dewatering to lower the water table;
- Improved drainage;
- Slope support – buttressing with piles or in-ground retaining walls; and
- Utilisation of appropriate foundations, for example piled foundations to extend below liquefiable layers.



Figure 4-13 Damage due to differential settlement of building in Chamanga (a) concrete cracking due to differential settlement, (b) detail of structural damage to building.

4.3. Landslides

Many co-seismic landslides were observed across the Manabí region (Figure 4-14). This included deep and shallow seated landslides in both coastal cliffs and in low-lying mountainous regions to the south of the epicentre.

A few of these were natural slope failures, but most of them were failures of man-made slopes. These are likely to have been due partly to the ground motion of the earthquake and partly due to other possible comingling effects such as:

- Saturated soil from the heavy rainfalls preceding the earthquake;
- Liquefaction of soft alluvial and marine soil layers;
- Fault ruptures (*e.g.*, Bahía de Caráquez or San Isidro);
- Lack of stabilisation in man-made slopes;
- River bank management measures which increased stream velocities and erosion of embankments;
- Flood plains next to vulnerable man-made slopes (*e.g.*, in Portoviejo).

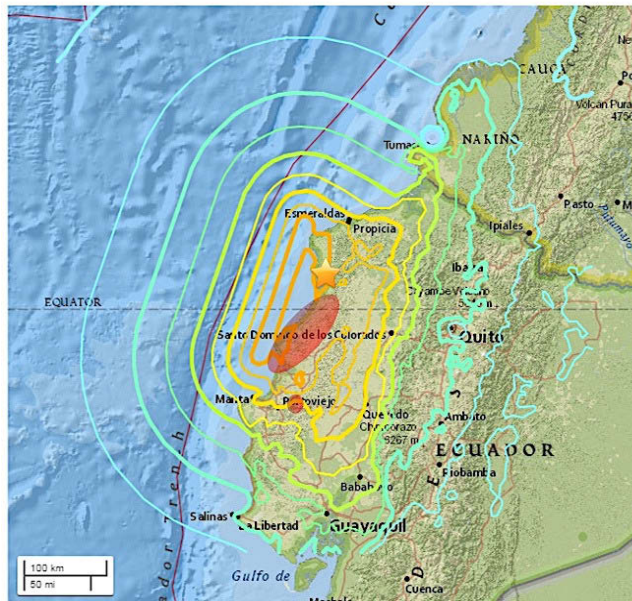


Figure 4-14 Location of region where landslides were observed and surveyed circled in red.



(a)



(b)



(c)



(d)

Figure 4-15 Examples of landslides observed. Coastal landslides observed from Highway 15 between San Vicente and Canoa, a) shallow seated, b) deep seated. Landslides in low-lying hills near San Isidro, c) shallow seated, d) deep seated.

4.3.1. Overall Scope and Methodology of the Survey

The scope of the landslide survey was set out to:

1. Spot-check the rapid assessment landslide maps derived by the BGS (2016) based on satellite imagery at locations chosen to be particularly representative of significant landslides, which were also accessible;
2. Observe and try to better understand the underlying mechanisms that led to the spectacular landslides in San Isidro highlighted in news reports and hence identified ahead of the mission as a priority. These landslides have the specificity of being quite far inland in the rural and mountainous area of the coastal Cordillera, which provides the opportunity of diversifying the field of observation;
3. Understand how the landslides are likely to have impacted on the transportation network (roads *etc.*).

A GPS was used to localise the slope instabilities. The surveys of the landslides were then carried out by taking photographs from different angles and heights when possible in order to get a 3D appreciation of the slope failures. Complementarily to the photographs, drone imagery was captured at sites in San Vicente, San Isidro and Pedernales where the landslides were larger. Additionally, talking to local residents was instrumental to better understand when exactly the landslides observed occurred. This was particularly important to first determine whether they were indeed co-seismic or the result of heavy rain during the rainy season, and secondly to know whether they were triggered by the main shock or subsequent events.

4.3.2. BGS Ground-truthing Exercise

The team collaborated with the BGS to provide field validation for their preliminary landslide assessment, which was initiated by a request from the UK Department for International Development (DfID) and based on satellite imagery from UNITAR/UNOSAT. Photographic and drone imagery were taken on site and interviews were conducted at locations of identified landslides. 12 sites were surveyed in Portoviejo and 21 in the vicinity of Bahía de Caráquez as part of this exercise. Guided by the BGS satellite images, the team visited these locations and provided observations which are detailed in Appendix C.

The following section will compare the location and dominant failure type of the sites surveyed during this ground-truthing exercise. A size comparison has not been undertaken to date, so will not be discussed here.

Portoviejo

The PGA measured in Portoviejo was 0.38g. All the landslides identified in this region were along the banks of the Rio Portoviejo which runs through the city. This area had been severely flooded in the days preceding the earthquake, which is anticipated to have resulted in the water table being abnormally high at the time of the main shock. 12 sites were surveyed in Portoviejo (see Appendix C for further details). Figure 4-16 shows the accuracy of the identification of the location and dominant type of the sites surveyed compared to that mapped by BGS using satellite imagery.

The dominant landslide type for every site mapped in this area by BGS was rotational. From the field observations it is believed that the dominant failure type for each of these sites was liquefaction induced lateral spreading. The movement of land at some of these sites did have notable rotational components.

The most significant co-seismic slope failure to occur in Portoviejo was not identified on the BGS landslide map. On the satellite image used, a cloud was positioned directly over this site. This highlights a major limitation of this technique. A number of additional sites of liquefaction

induced lateral spreading along the river were also observed in the field but not identified in the satellite mapping. These sites can be characterised as having smaller lateral movements of ground towards the river.

The site incorrectly identified as being the site of a landslide was flooded at the time of the earthquake. It is believed that a number of the sites that were missed by the satellite image identification were also flooded at the time of the main shock.

Chone Estuary

The closest seismometer station to Bahía de Caráquez was 35km to the south-southeast in Chone, where the measured PGA was 0.37g. Landslides of steep man made slopes above highway 383A were common and resulted in considerable debris across the road. Liquefaction induced damage severely affected productivity of the many shrimp farms within the river estuary, and also caused significant lateral movement of mangrove swamps within the Isla Corazon nature reserve (see Section 4.2.1).

21 sites were surveyed in the area covered by the BGS preliminary co-seismic landslide inventory map for Bahía de Caráquez (see Appendix C for further details). Figure 4-16 shows the accuracy of the identification of the location and dominant type of the sites surveyed compared to that mapped by BGS using satellite imagery.

Landslides situated on steep sided slopes were mapped accurately – both regarding the location and dominant failure mechanism. Only one of these sites which was surveyed was missed due to cloud cover. Some sites of earthquake induced liquefaction were correctly identified. This was primarily for sites where lateral spreading had caused movement of large areas of mangrove swamp, and where the failure of dykes caused emptying of the shrimp ponds. However, there was evidence of liquefaction induced damage over a much greater area than had been mapped. This had been anticipated by BGS prior to our mission. The damage in the areas that were not identified can be characterised by much smaller magnitudes of lateral displacements and of ground with little vegetation.

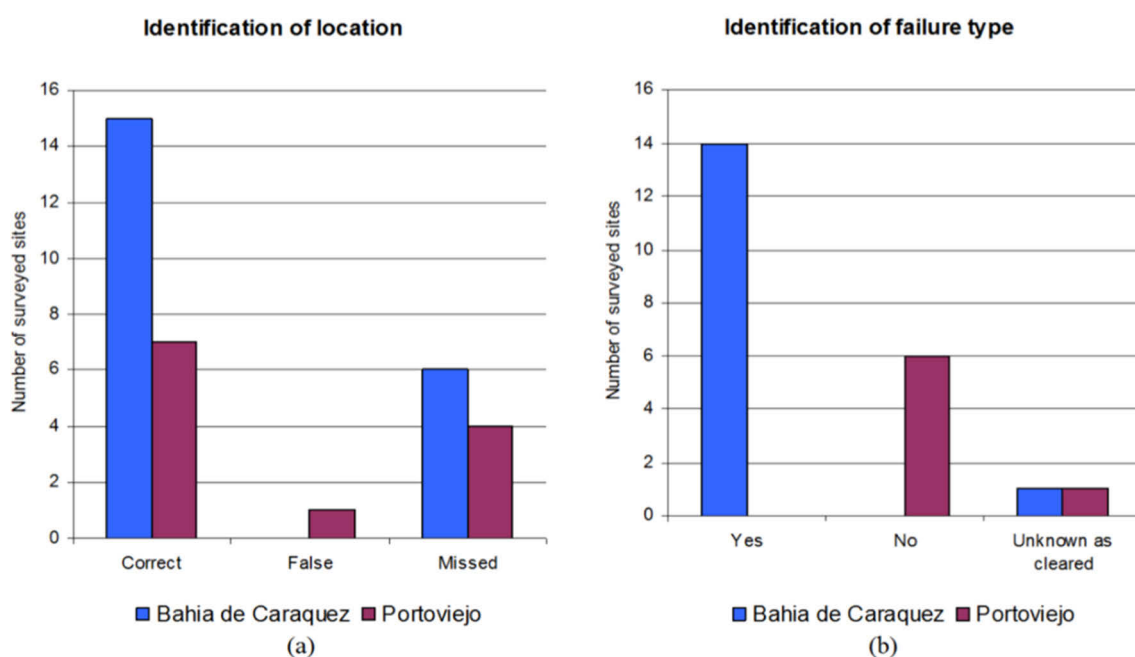


Figure 4-16 Graphs to show the accuracy of the preliminary co-seismic landslide inventory maps for the sites surveyed around Bahía de Caráquez and in Portoviejo; (a) location, (b) failure type.

Summary

The collaboration between EEFIT and BGS is ongoing at the time of writing. This small ground-truthing campaign and ongoing collaboration could further improve early satellite-based landslide assessments after an earthquake, in turn enhancing response operations, road clearing, and emergency route identification.

The findings and observations made by the EEFIT team following this ground-truthing exercise can be summarised as:

- a. The identification of the location and type of landslide was found to be highly successful for landslides which were not liquefaction induced.
- b. The identification of failure due to liquefaction induced lateral spreading was more problematic. In Portoviejo it was not identified as the dominant mechanism for any of the sites. Close to Bahía de Caráquez it was successfully identified where major failure of earthworks or significant movement of vegetation occurred. However, it was not identified in large areas.
- c. Cloud cover is a major limitation of this technique. Flooding also appears to make accurate identification of landslide sites difficult.

4.3.3. San Isidro

Two sites of extensive landslides and significant ground failure were visited close to the town of San Isidro, 150km SSW of the epicentre (Figure 4-17). The area is situated in a hilly, rural, less inhabited in-land region, with the vast extent of land difficult to access. The main activity there is agriculture rather than tourism as is mostly the case in the low-lying coastal plains where the rest of the mission was carried out. The area, like the others visited, had experienced notable rainfall preceding the earthquake.

The impressive scale of the failure of the San Isidro Site B described below made it to the news and hence pushed the team to travel to survey the site, specifically because of the question whether it could be linked to the rupture of the San Isidro segment of the Canaveral Fault. Site A described below was highlighted to the EEFIT team by local residents who had been affected by the damage and who guided the team throughout the day.

The EEFIT mission met with the military and civilians involved in local post-earthquake response in San Isidro and accessed information on the ongoing technical investigations of the mechanisms that led to the numerous landslides observed in the area by Sevilla (2016) and Echeverria (2016). This information was shown to the EEFIT team by the San Vicente Municipality. Some of the findings of these studies are presented for reference here below.

However, more work remains to be done to consolidate these findings, especially in determining to what extent the failures observed are associated to the type of superficial deposits, and to what extent it may have been associated to local tectonic features. These studies may be instrumental in better understanding and building revised seismotectonic hazard models for the region and the area.



Figure 4-17 Localisation of the landslide sites surveyed close to San Isidro, and the town of San Isidro on the right on which one of many co-seismic landslides is visible.

San Isidro Site A

The affected site was not inhabited. A dirt track used by local farmers crossed the edge of the site. The soil failed in an alignment and in the directions shown on Figure 4-18, of which an aerial drone image is shown in Figure 4-19. Primary and secondary scars of the landslides are shown in Figure 4-18 and some of the secondary features in the alignment of B are shown in Figure 4-20. A superficial clayey shale deposit was observed on the scars, as shown in Figure 4-21.

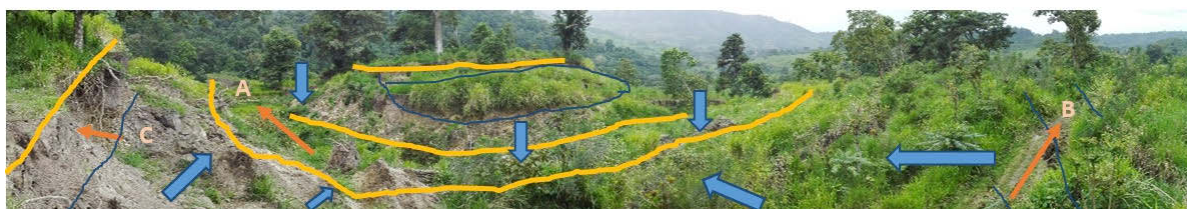


Figure 4-18 Panoramic view of the ground failure at Site A (yellow lines indicate primary scars, and blue ones the secondary ones; the blue arrows show the movement of the soil).



Figure 4-19 Isidro site A taken from a drone, looking along the ridge at location (A) on figure above.



Figure 4-20 San Isidro site A, rotation and translation of surficial blocks of soil close to the head of the slope. Photo taken of ground along the path defined as (B) on panoramic picture above.



Figure 4-21 Face of scar at location C shown on panoramic picture of Site A above.

San Isidro Site B

The affected site was located further away in the South-West direction from San Isidro as shown in Figure 4-17. It mainly affected one property comprising four structures associated to a cattle ranch. Eighty heads of cattle were lost in the earthquake, and three buildings collapsed. Luckily, the structure used for accommodation next to the collapsed cattle ranch stayed intact, and the three inhabitants in the house at the time of the earthquake survived (see Figure 4-22). A river runs below the site, along the toe of the slope.

The EEFIT team met the family affected on site. Reportedly, the mountain “rose” 12m during the mainshock then went down and is now settling. Before the mainshock occurred, two “explosion-like” noises could be heard as if coming from the valley below, around 12am. Shaking was felt for about 1 minute during the mainshock, and the soil felt “like jelly”. Replicas were also felt very strongly. On the day of the survey, there had been an aftershock felt at 5am. Dogs and monkeys in the hills were reported to make significant noise before the shocks, warning of replicas before they occurred.

Echeverria (2016) proposes an analysis of the landslide mechanism based on the analysis of drone imagery looking at the scars observed (Figure 4-23). Two potential faults that may have contributed to the damage observed were identified. Further analysis and work is likely to go into determining the causes of these dramatic landslides and those observed in the surrounding area to better understand the geodynamics and tectonics at play.



Figure 4-22 San Isidro site B, taken from a drone. A river runs through the trees at the bottom of the slope, to the right of the figure (the yellow circle shows the intact house next to the slope that failed).

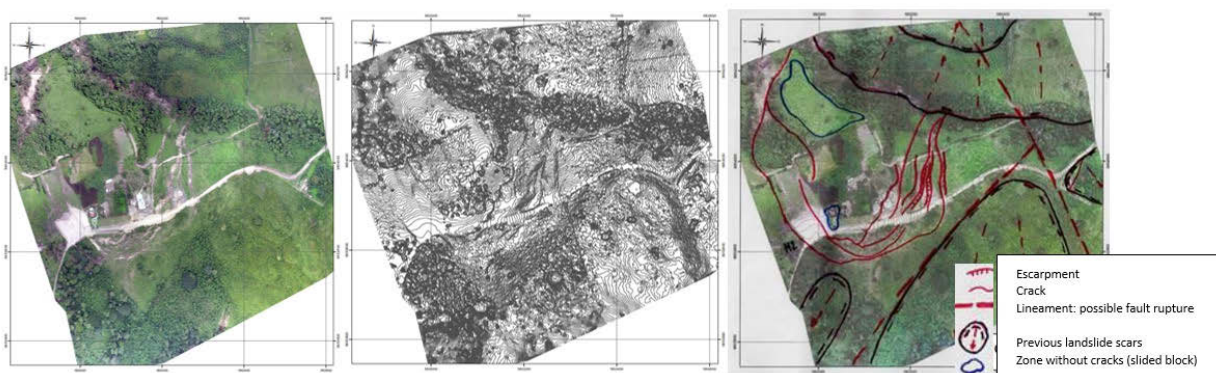


Figure 4-23 El Relleno San Isidro Site B Landslide analysis by Echeverria (2016).

Summary

Both sites were located at the crest of ridges, so are expected to have experienced topographic amplification of the earthquake induced ground accelerations (Brennan and Madabhushi, 2009). The inhabitants of site B felt they were thrown upwards into the air during the main shock, indicating a large vertical component of acceleration at the site. The combination of strong ground shaking and a high water table following the heavy rainfall is anticipated to have caused a reduction in soil strength due to an increase in pore water pressure.

Deforestation of the sites will have removed natural stabilisation provided by vegetation. This is in contrast to many of the hillsides surrounding these sites. The cattle at the ranch situated at Site B are also likely to have altered the biological and chemical composition of the ground and thus created an inconsistent and weak soil.

The map of Quaternary faults and folds of Ecuador and its offshore regions by Eguez *et al.* (2003) shows the Canaveral Fault segments c and d in close vicinity of the observed Site A and Site B landslides. The mapped location of the faults on Figure 4-24 is very coarse and may very well be closer or further away from the sites. However, it shows a fairly good correlation and justifies the recommendations to look into this further to better identify the risks associated to this fault.

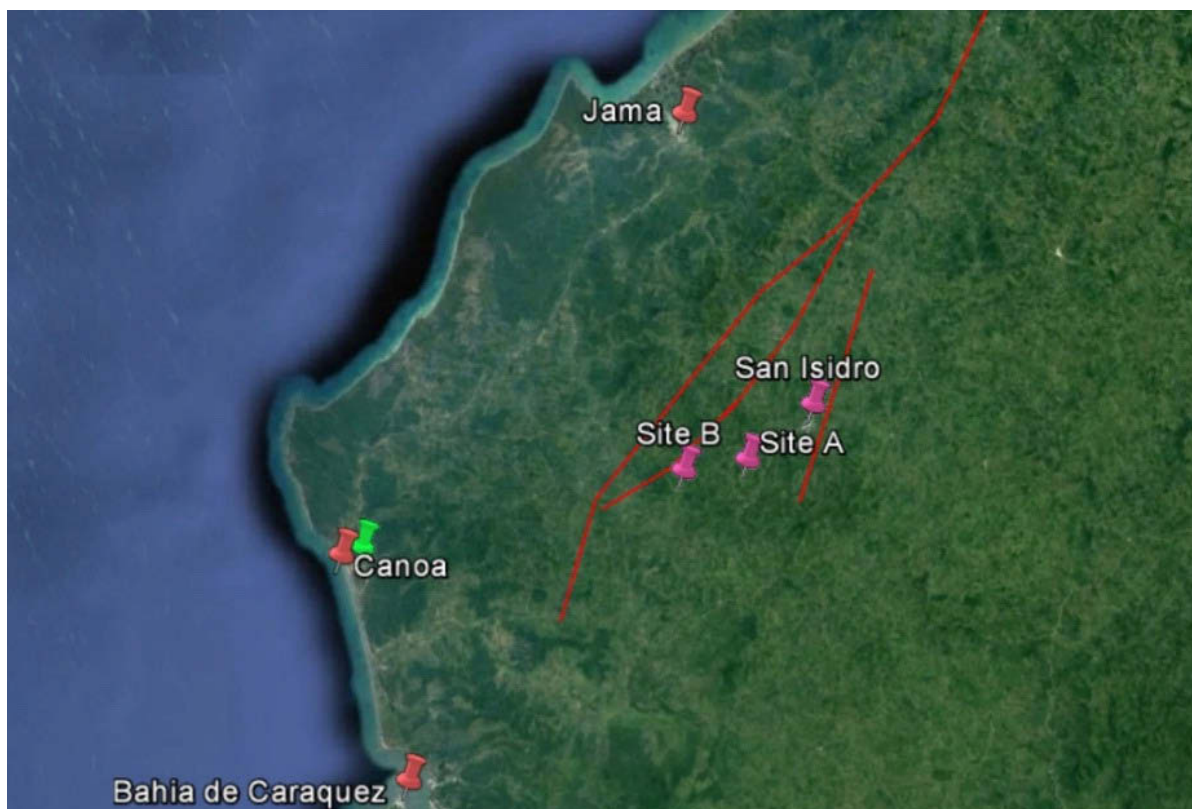


Figure 4-24 Site A and B relatively to the main surrounding cities and the potential active Canaveral fault segments mapped by Eguez (2003) shown as red lines.

4.3.4. Other Landslides

Numerous other landslides were observed along the road and in the different locations visited during the mission. Because of time constraints and other practicality reasons, a detailed surveying of all these landslides could not be carried out. However, a few general comments on the main trends noticed are provided below.

Coastal Landslides

Several landslides were observed along the coast, mostly when on the coastal road from San Vicente to Canoa (*e.g.*, see Figure 4-25). Landslides may have occurred at other places along the coast in the steep slopes and cliffs, but only this part of the coast was travelled on the road. The damage and impact was principally to the roads (see Section 7), creating difficulties of access to the north-most part of the region most affected by the main event. Some beach-side hotels on the other side of the roads, and other structures close to the slopes were also damaged.

Most of the landslides were associated to the mainshock but several were indicated by local residents to have occurred following the significant aftershock of the week preceding the mission. Road rehabilitation works were still being carried out in many locations (Figure 4-26).

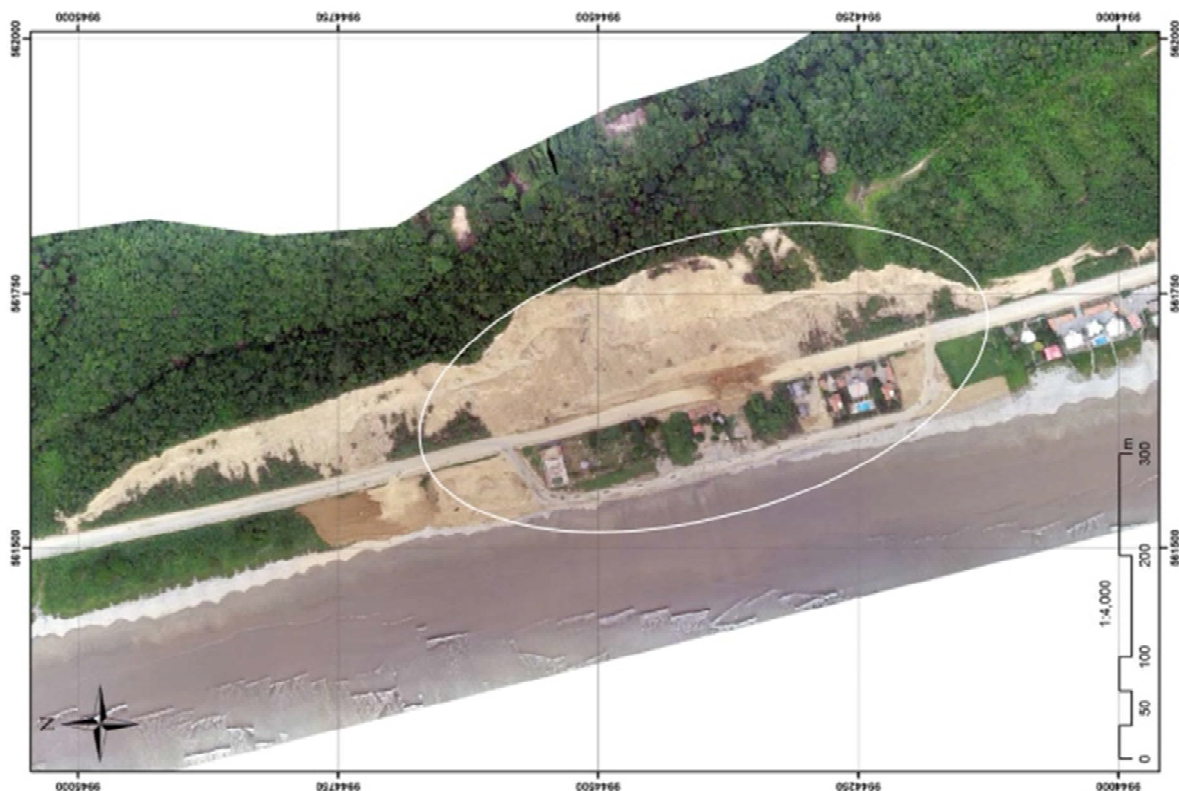


Figure 4-25 Example of a landslides on the coastal road between San Vicente and Canoa (Echeverria, 2016).



Figure 4-26 Road Rehabilitation Works carried out on the coastal road between San Vicente and Canoa.

Landslides in Pedernales

Some of the most damaging landslides on the coast were observed in Pedernales, where they were directly involved in many building destructions. At the south end of the coastal extent of the city, a slope failure destroyed and heavily damaged many huts located at its toe in an informal settlement (Figure 4-27). The lavish property at the top of the slope was completely destroyed. In the North, many hotels and luxurious houses were built on the slope overlooking the beach. Most of them were very heavily damaged if not collapsed. This may have been due

to a combination of topographic amplification of an already very high ground motion and slope instability (see Figure 4-28).



Figure 4-27 Informal settlement damage South of Pedernales due to slope failure (drone image of the head of the slope on the right).



Figure 4-28 Slope instability damage North of Pedernales.

Inland Landslides

On the road from Canoa to San Isidro, many landslides were observed along the road and in the surrounding areas (e.g. Figure 4-29, Figure 4-30).

It is worth noting that slope failures may have occurred in many other places, but very little information on damage to the rural areas inland in the coastal cordillera is available due to the low density of population as well as the difficulty to access these remote places. It would be beneficial to further investigate ground failures in these environments to inform the regional geological and tectonic models, and provide more evidence of the potential movements associated to the Canaveral Fault.



Figure 4-29 Major landslide observed on the road from Canoa to San Isidro



Figure 4-30 Map of landslide sightings in the San Isidro area (courtesy of Echeverria and Sevilla, 2016).

Other Observations and Comments

It is interesting to note that no significant landslide was observed or pointed out by local residents in Portoviejo's hilly surroundings. This may either show that there weren't indeed many landslides in the area or that they did not affect directly structures, infrastructure and/or people. The latter could be explained by the fact that the hills surrounding Portoviejo are classified as natural reserve for the dry forest and that building there above 60m is forbidden. In the houses below 60m, not much damage was noticed. The local residents and cars in hills reportedly "jumped" about 50cm into the air at the time of the mainshock, whilst the motion reported in the valley was much more horizontal.

4.3.5. Overall Conclusions

The damage caused by landslides indicates a lack of understanding and planning against the associated risks, even for major infrastructure works. It also points at other issues associated with informal construction in high risk areas. Thoughts to tackle some of the issues arising from the landslide observed include:

- Mapping the landslide risk in the region, including coupled effects associated to liquefaction potential and saturation of soils from heavy rain;
- Building structures and roads at a safe distance from unstable slopes, determined based on slope instability analyses;
- Avoiding or better controlling the quarrying of the materials for construction close to structures (planned or constructed);
- Reducing risk by removing material from the head of the slope
- Installing drainage systems to avoid build-up of pore pressure that increase the risk of instability;
- Implementing stabilization techniques using vegetation such as vetiver grass, rock-fill buttresses, shotcrete spraying or bolted anchors;
- Controlling and minimizing the impacts of the failure using catch ditches, gabions, retaining walls, wire nets, rock curtains, and slope debris-flow barriers;
- Monitoring the unstable slopes, especially after the rainy season, to capture the increase in vulnerability and regularly assess the need for reinforcement.

In addition, it was observed that practices for clearing landslide debris seemed to ignore the risk involved (Figure 4-31). It is important to note that the largest aftershocks in May triggered landslides and aggravated some triggered by the main shock. These occurred during the emergency response phase, at a time when road rehabilitation works were being carried out. Improvements should be undertaken to ensure the safety of workers.



Figure 4-31 Unsafe practice clearing landslide debris (Chone Estuary).

5. Perspective on Seismic Hazard Considerations in Local Building Code

This section investigates the evolution of the seismic hazard considerations and the main requirements specified in the Ecuadorian building code. This is followed by a review of the current seismic hazard provisions of the code against the recorded ground motions in the main shock event on 16 April 2016, providing a view on how the code performed. Code limitations that may have played a role in the damage observed are highlighted.

5.1. Seismic Code History in Ecuador

As with other country's seismic codes, Ecuador's first adoption of seismic design regulations, and subsequent updates, have often followed major earthquakes in the country or elsewhere. The first building code in Ecuador that included seismic design requirements was introduced in 1951 following the 1949 M_w 6.9 earthquake in Ambato that killed 6,000 people (The Telegraph, 1949). An update of this code was published in 1977, following damaging earthquakes in 1976 in Esmeraldas and Cotopaxi. Although there were earthquakes in the 1980's in Ecuador (*e.g.*, the 1987 M_w 7.2 earthquake in the northeast that killed 1,000 people – Albornoz and Anda, 2014; Farias *et al.*, 2015), the next seismic code update was not published until 2001, following the 1998 M_w 7.2 earthquake in Bahía de Caráquez (Chileh *et al.*, 2014). The most recent version of the Ecuador seismic code was published in 2011 and made official in 2015.

Table 5-1 summarises the history of seismic codes in Ecuador with notes about the developments on each update.

Table 5-1 Summary of seismic code history in Ecuador.

Year	Title	Notes
1951	Ecuadorian Construction Code CEC-51	Introduced in 1951 and deemed mandatory for the whole country in 1952, this code included seismic design requirement, amongst others; however, these were not applied by all contractors and government entities (INEN, 1976). No seismic hazard zonation was included in this code.
1977	Ecuadorian Construction Code CEC-77	This update (as well as previous version CEC-51) did not include a seismic hazard zonation. The seismic loads were defined as a function of the building's characteristics, local geology, and an importance factor. Despite the code not having a seismic hazard component, a practical design guide (GPE INEN 009-1976), published around the same time as a companion to the code, provided good practice seismic design and detailing for (mainly) reinforced concrete buildings. For instance, avoidance of plan and vertical irregularities was encouraged; closed 135°-bend shear links were specified; lap splices needed to be avoided at column ends; etc. Although this guide stated that it applied only to buildings up to 3 storeys, these good practice recommendations could have been extended to taller buildings.
2001	Ecuadorian Construction Code CPE INEN 5:2001 (also referred to as CEC-2000 in the literature)	A seismic hazard zonation was incorporated in this update, with values of bedrock PGA ranging from 0.15-0.40g (zones 1 to 4) for a 475-year return period. The highest seismicity (zone 4) corresponded to the coastal areas in the west and it decreased towards the east, with the exception of a central area that was also assigned to zone 4. Aguiar (2008) argued that based on a seismic hazard assessment (Aguiar, 1982), assigning the highest seismicity to this central area may not be appropriate. This update adopted many design guidelines from UBC-97 (ICC, 1997) and adapted them to the local practice.
2011 (official in 2015)	Ecuadorian Construction Norm NEC-11/NEC-11 (officially NEC-SE-DS)	The seismic hazard zonation was updated to include six zones, with values of bedrock PGA ranging from 0.15g to >0.50g for a 475-year return period. NEC-SE-DS includes the possibility of adopting the displacement-based design approach as an alternative of the typical force-based approach that most design codes in the world have adopted. There is a seismic risk, assessment, and retrofit section (NEC-SE-RE), that requires essential and special structures to go through a seismic performance check using a nonlinear analysis. It also sets forth procedures for seismic assessment and retrofit of buildings based on ASCE 41 (ASCE, 2014), seismic risk and loss assessments of buildings and at a regional scale, and recommends FEMA 154 (FEMA, 2002) for rapid assessments of buildings.

5.2. Current Seismic Design Code Hazard Provisions (NEC-15)

The current code provides a seismic hazard zonation map that divides the country into six seismic zones (see Figure 5-1). Table 5-2 shows the value of factor Z for each seismic zone, which represents the Peak Ground Acceleration (PGA) value with a 10% chance of exceedance in 50 years (475-year return period). The region mostly affected by the 16 April 2016 earthquake lies in Zone VI (the highest seismicity). Zone VI represents a saturated PGA value of 0.50g, which has been subject to discussion by recent seismic hazard assessments (Parra *et al.*, 2016) that argue that bedrock PGA values in the coast of Ecuador could be as high as around 0.70g. The code acknowledges that PGA values in this zone are $> 0.50g$ but allows the use of $Z = 0.50$.

The code's elastic response spectrum, (S_a) (see Figure 5-2) is defined based on the factor Z and other factors that depend on the site conditions and location. The site conditions are assessed based on soil parameters and characteristics of the upper 30m of the deposit. The site is classified using Table 5-3. The factors F_a , F_d , and F_s (see Table 5-4) are based upon the soil type and the seismic zone of the site.

Other factors used in the construction of the elastic response spectrum are η and r . The former is based upon the site's location, although it is not explicitly stated which provinces are located in the Coast, the Mountains, or the East:

- $\eta = 1.80$: Provinces on the Coast (excluding the province of Esmeraldas);
- $\eta = 2.48$: Province of Esmeraldas

The factor r depends upon the soil type:

- $r = 1$: All soil types but soil type E; and
- $r = 1.5$: Soil type E.

The code's design base shear V is then defined using the following equation:

$$V = \frac{I \cdot S_a(T)}{R \cdot \phi_P \cdot \phi_E} W$$

Where:

- I : Importance factor (see Table 5-5);
- $S_a(T)$: Spectral acceleration from elastic response spectrum, for a period of vibration T (see Figure 5-2);
- R : Strength reduction factor (see Table 5-6)
- ϕ_P & ϕ_E : Coefficients for correction for irregularity in plan and elevation, respectively. ϕ_P & ϕ_E can adopt values of 1.0 (regular), 0.9 (one irregularity), or 0.81 (several irregularities); and
- W : Seismic weight of the building.

Table 5-2 Seismic zone factor Z from NEC-SE-DS (NEC-15).

Seismic Zone	I	II	III	IV	V	VI
Z	0.15	0.25	0.30	0.35	0.40	> 0.50

Table 5-3 Soil type for seismic design from NEC-SE-DS (NEC-15).

Soil Type	Description
A	Competent rock; $V_s \geq 1500\text{m/s}$
B	Medium stiffness rock; $1500\text{m/s} > V_s \geq 760\text{m/s}$
C	Very dense soil or soft rock that meets: (1) $760\text{m/s} > V_s \geq 360\text{m/s}$; or (2) either $N \geq 50$ or $S_u \geq 100\text{kPa}$
D	Stiff soil profile that meets: (1) $360\text{m/s} > V_s \geq 180\text{m/s}$; or (2) either $50 > N \geq 15$ or $100\text{kPa} > S_u \geq 50\text{kPa}$
E	Soil profile that meets: (1) $V_s < 180\text{m/s}$; or (2) soil profile with total thickness H greater than 3m of soft clays that meets : $PI > 20$, $w \geq 40\%$, or $S_u < 50\text{kPa}$
F	Soil Type F profiles require an explicit assessment on site done by a geotechnical engineer. Soil profiles include: F1 – soils susceptible to failure or collapse caused by seismic excitation such as liquefiable soils, sensitive clays, <i>etc.</i> ; F2 – peat and organic clays ($H > 3\text{m}$); F3 – high plasticity clays ($H > 7.5\text{m}$ with $PI > 75$); F4 – thick layers of clays with medium-to-low stiffness ($H > 30\text{m}$); F5 – soil profiles with contrast in impedance factor α within the top 30m, including contact between soft soil and rock, with abrupt changes in V_s ; F6 – non-engineered landfill

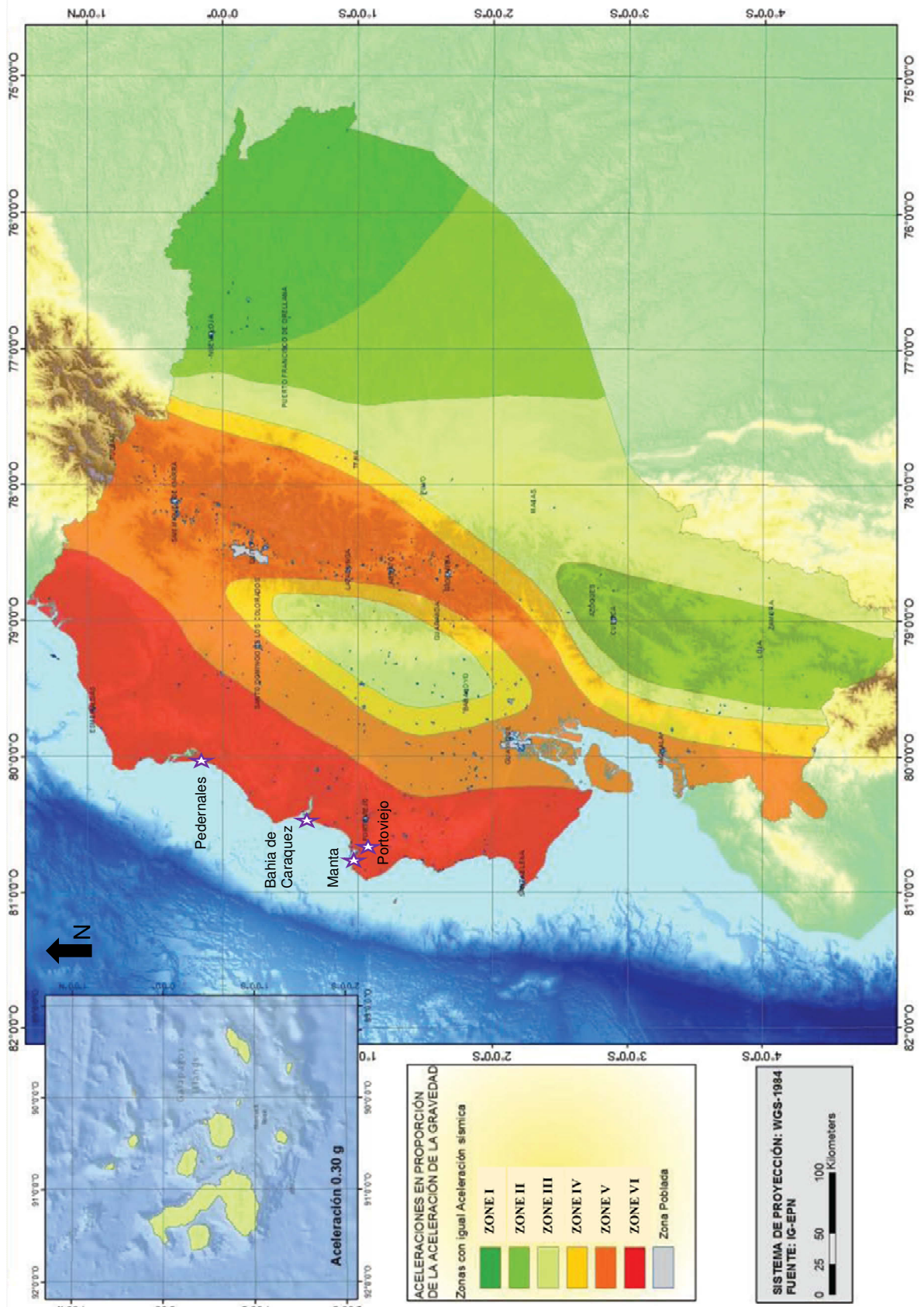


Figure 5-1 Ecuador seismic hazard zonation from NEC-SE-DS (NEC-15).

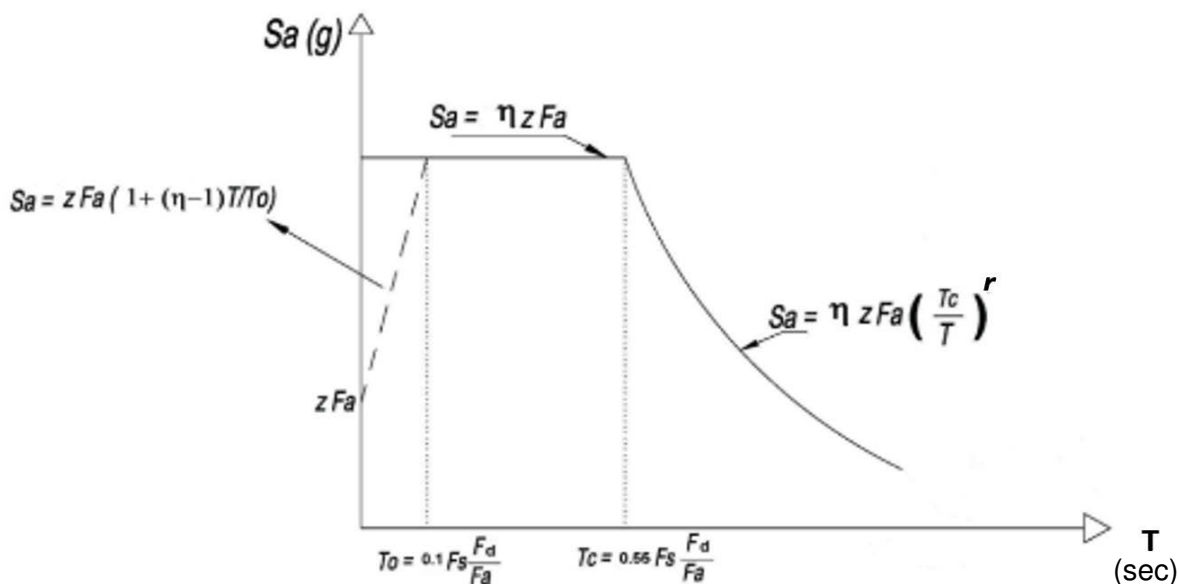


Figure 5-2 Ecuador seismic code's elastic response spectrum for 5% damping, from NEC-SE-DS (NEC-15). NB: dashed line for periods $T < T_0$ is only allowed for modes of vibration other than the fundamental mode of vibration when performing modal response spectrum analysis.

Table 5-4 F_a , F_d , and F_s factors for construction of elastic response spectrum S_a (see Figure 5-2), from NEC-SE-DS (NEC-15).

Soil Type	Seismic Zone																	
	I			II			III			IV			V			VI		
	F_a	F_d	F_s	F_a	F_d	F_s	F_a	F_d	F_s	F_a	F_d	F_s	F_a	F_d	F_s	F_a	F_d	F_s
A	0.90	0.90	0.75	0.90	0.90	0.75	0.90	0.90	0.75	0.90	0.90	0.75	0.90	0.90	0.75	0.90	0.90	0.75
B	1.00	1.00	0.75	1.00	1.00	0.75	1.00	1.00	0.75	1.00	1.00	0.75	1.00	1.00	0.75	1.00	1.00	0.75
C	1.40	1.36	0.85	1.30	1.28	0.94	1.25	1.19	1.02	1.23	1.15	1.06	1.20	1.11	1.11	1.18	1.06	1.23
D	1.60	1.62	1.02	1.40	1.45	1.06	1.30	1.36	1.11	1.25	1.28	1.19	1.20	1.19	1.28	1.12	1.11	1.40
E	1.80	2.10	1.50	1.40	1.75	1.60	1.25	1.70	1.70	1.10	1.65	1.80	1.00	1.60	1.90	0.85	1.50	2.00

Table 5-5 Building importance classification and importance factor I , from NEC-SE-DS (NEC-15).

Category	Type of use and importance	Importance Factor - I
Essential Buildings	Hospitals, health centers, and emergency units. Military facilities, police and fire stations, and civil defence facilities. Car parks or garages for emergency response vehicles and aircrafts. Air control towers. Telecommunication and other emergency response centers. Structures housing power units. Tanks and other structures storing water or other firefighting substances. Structures storing explosives, chemical, toxic, and other hazardous materials.	1.5
Special Occupation Structures	Museums, churches, schools, and education or sports centers housing 300 people or more. All structures housing 5,000 people or more. Public buildings that require continuous operation.	1.3
Other Structures	All building structures and others not classified in aforementioned categories.	1.0

Table 5-6 Strength reduction factor R for ductile and limited ductility structural systems, from NEC-SE-DS (NEC-15).

Ductile Structural System		R
Dual Systems		
Reinforced Concrete (RC) special moment-resisting frames, with RC shear walls or steel braces		8
Steel special moment-resisting frames, with RC shear walls or steel concentrically/eccentrically braced frames		8
Frames with RC columns and steel beams, with steel concentrically/eccentrically braced frames		8
RC special moment-resisting frames with flat slabs, with RC shear walls or steel braces		7
Moment-Resisting Frames		
RC special moment-resisting frames		8
Steel special moment-resisting frames		8
Frames with RC columns and steel beams		8
Other Structural Systems for Buildings		
RC ductile shear walls		5
RC special moment-resisting frames with flat slabs		5
Limited Ductility Structural Systems		R
Moment-Resisting Frames		
RC frames with cross section dimensions smaller than specified in NEC-SE-HM (code for structural design in RC), limited to 2 storeys and 5m spans		3
RC frames with cross section dimensions smaller than specified in NEC-SE-HM, with welded wire mesh reinforcement		2.5
Cold-formed steel, aluminium, timber, limited to 2 storeys		2.5
Shear Walls		
Unreinforced masonry, limited to 1 storey		1
Reinforced masonry, limited to 2 storeys		3
Confined masonry, limited to 2 storeys		3
RC shear walls, limited to 4 storeys		3

5.3. Seismic Hazard Code Provision Performance in the 2016 Muisne event.

The response spectra corresponding to the recorded motions at the seismometer stations in the region affected are shown in Figure 5-3, in comparison to the NEC-15 design spectra shown for Site Class B to E conditions. The ground motion records were provided by IG (personal communication, 2016). This comparison shows that:

- The highest ground motion recorded in Pedernales well exceeded the seismic hazard design level recommended in NEC-15, for structural periods ranging from 0 to 2s;
- In Manta and Portoviejo, peaks of spectral acceleration around structural periods between 0.2-0.5s exceeded the design provisions in NEC-15;

In Chone, the peak that exceeded the NEC-15 design hazard provisions corresponded to greater structural periods between 1 and 1.8s. Table 5-7 also shows a comparison of the NEC-15 recommendations for the region ($Z=0.5$), the recorded PGAs and the PGA assessed in several probabilistic seismic hazard assessments (PSHAs) for Manta, Portoviejo, and Pedernales for return periods of 475 and 2475 years corresponding to standard design levels. These PSHA results are given for Site Class B conditions, whilst the site classes corresponding to the seismometer locations where the ground motion was recorded vary between C and D.

Using the NEC-15 approach, the bedrock PGA corresponding to the recorded level of ground motion was back-calculated based on $PGA_{bed} = PGA_{rec}/Fa_{Site\ Class}$. This allowed the derivation of amended design spectra following the shape of the NEC-15 design recommendations, but using site specific bedrock PGAs instead of Z. Figure 5-4 shows the comparison with the response spectra of the recorded motions.

There is a much better match between the new amended design spectrum for Pedernales and the ground motion record. The scaling of the code spectrum to the measured PGA also provides a better match to the response spectrum of the recorded motion at Manta, although

the plateau of the design spectrum is larger than the shape of the record and therefore conservative for structural periods from 0.4 to 1.4s. For Portoviejo, the complex ground motion amplification/attenuation effects due to the potential basin effect identified in Section 3 may justify the apparent mismatch between the recorded ground motion spectrum and the code spectrum. This highlights the importance of more detailed site specific hazard studies for design rather than the sole use of simplified code spectra when there are complex site effects to be considered.

Although further investigation and analysis should be carried out to understand how to best amend the code for it to be adequately representative of the seismic hazard of the coast of Ecuador, this quick analysis identifies that the designation of the factor $Z_{max}=0.5$ for the whole coastal region is a significant limitation of the code.

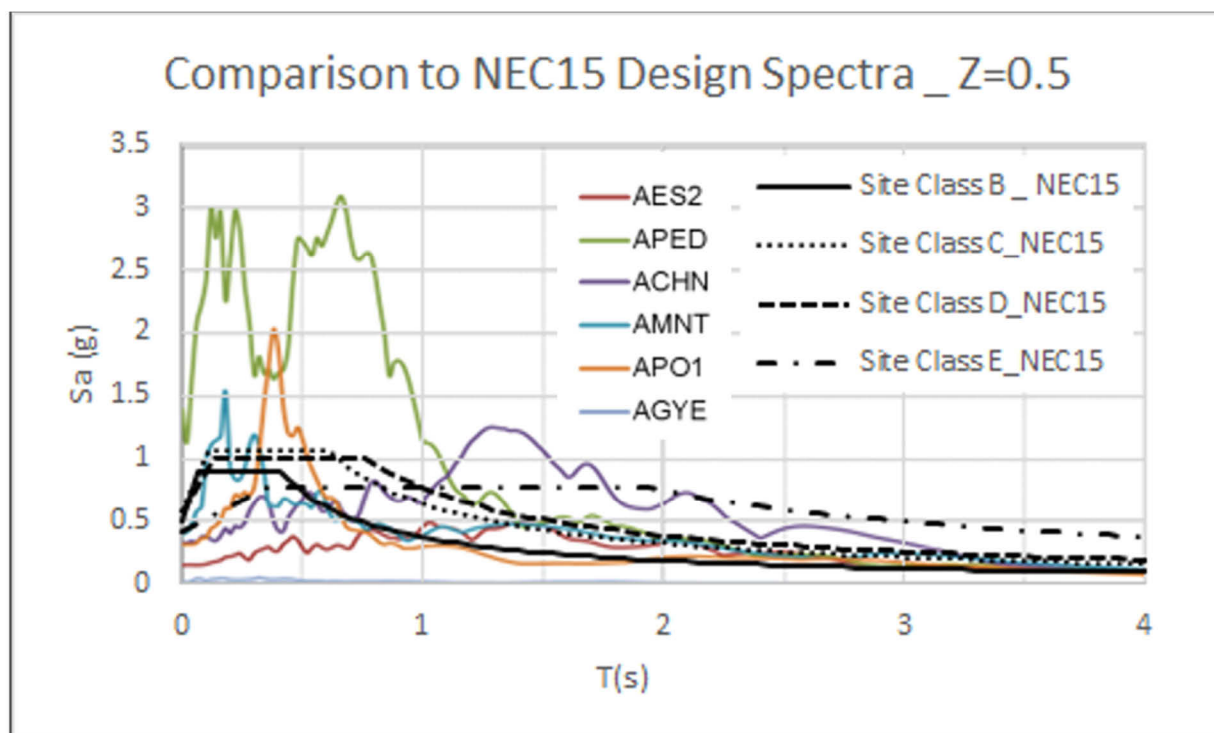


Figure 5-3 Comparison of recorded motions at the seismometer locations listed and the NEC15 design spectra for $Z=0.5$ and site conditions ranging from Class B to E. Ground motion records locations: AES2 – Esmeraldas record; APED – Perdernalas record; ACHN - Chone Estuary record; AMNT – Manta record; APO1 – Portoviejo record; AGYE: Guayaquil record.

Table 5-7 Comparison between Seismic Hazard PGA Level Recommendations from literature review and recorded PGAs for Manta, Portoviejo and Pedernales.

PGA values in (g)	YRP	Manta	Portoviejo	Pedernales
Recorded: 16 of April (IG, 2016)	-	0.68	0.51	1.41
(Site Class)		(Site Class C)	(Site Class D)	(Site Class C-D)
$PGA_{bed} = PGA_{rec}/F_a_{Site\ Class}$	-	0.58	0.46	1.26
PSHA studies (results on rock sites)				
Wong <i>et al.</i> (2012)	475	0.35	-	-
	2475	0.65	-	-
Parra <i>et al.</i> (2016)	475	0.7	0.6	0.65-0.7
	2475	1.15	1	1.15
SARA (GEM, 2015)	475	0.37-0.47		
	2475	0.7-0.9		
Code (NEC-15)	475	0.5		

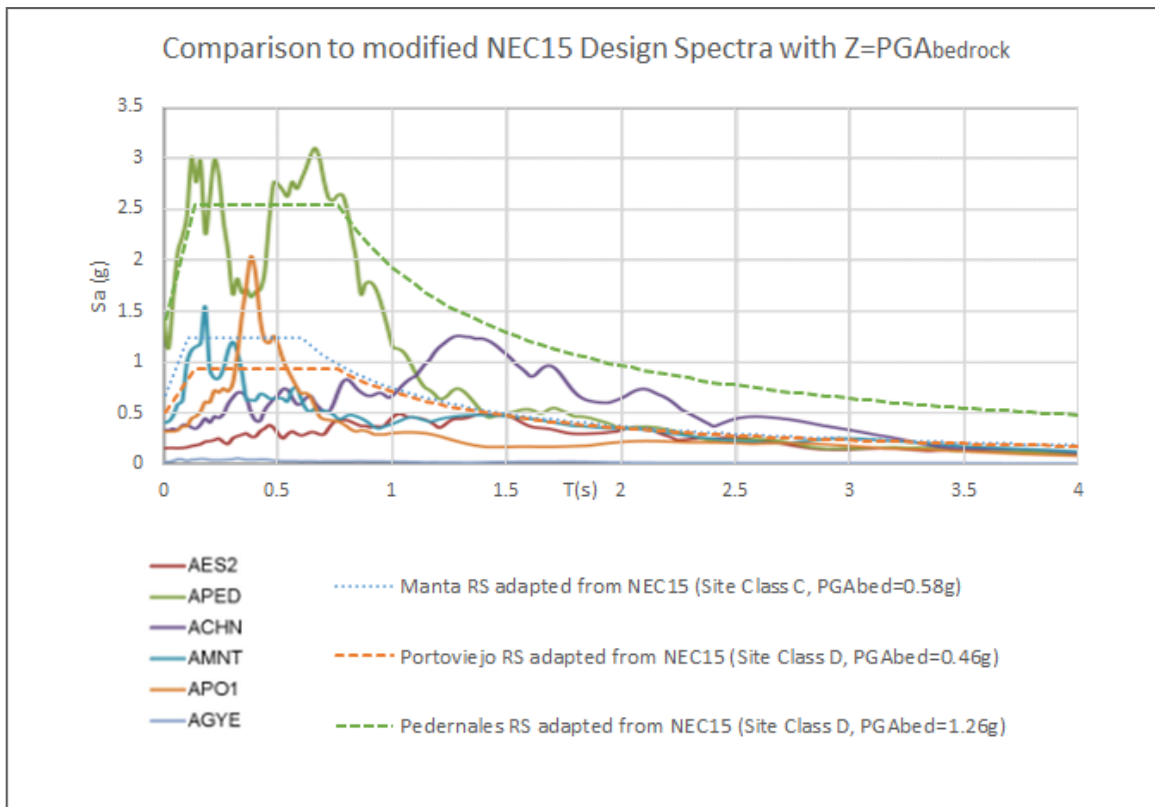


Figure 5-4 Comparison of the recorded motions to the adapted NEC-15 for Manta, Portoviejo and Pedernales with appropriate Site Conditions from V_s measured by (GEER, 2016) and back calculated $Z=PGA_{bed}$ from recorded ground motion.

6. Building Performance Observations

6.1. Introduction

The structural team from the EEFIT mission visited seven urban areas: Manta, Portoviejo, Bahía de Caráquez, Canoa, Jama, Pedernales, and Chamanga. The team aimed to gather information on the primary reasons for earthquake damage, in addition to surveying the levels of damage to different building typologies throughout the affected area.

This section of the report presents: the methodologies used to collect data, the typical building typologies in the affected area, observed building damage, the damage data from the surveys, a number of case studies of buildings of interest, and observations on tagging conducted immediately after the earthquake.

It is important to note that the surveys were conducted over a month after the earthquake, and therefore many of the buildings had already been demolished and the extent and cause of damage was not observed.

6.2. Survey Methodology

The team used a number of surveying methods to fit with different objectives for different survey areas. These are explained briefly here.

6.2.1. Rapid Surveys (see also Section 6.5)

The simplest method used to gather data was a rapid visual survey which the team completed at a slow walking pace. This collected data on the following:

Table 6-1 Rapid visual survey data collected.

	Data collected	Additional data collected, where possible
1	Photograph of façade	Photographs of specific damage
2	GPS location	Identifying features (e.g. name of property)
3	Main structural material	Roof type, floor type, lateral load resisting system
4	Maximum number of storeys	
5	EMS-98 damage grade	Specific notes on damage

The EMS-98 (Grünthal *et al.*, 1998) damage descriptions were used throughout when describing damage. Where structural and non-structural damage descriptions did not match, preference was given to the structural descriptors.

If a building appeared to have been demolished, a photo of the site was taken and the GPS location was noted. In some cases, locals were able to offer information on the buildings that previously stood on the sites. This information was recorded and, where possible, checked for accuracy with existing imagery such as Google street view, Google earth, or photos from other sources.

6.2.2. Detailed Surveys

Detailed visual surveys were also used to collect more information on structural characteristics and sustained damage to a number of structures of specific interest. Photos and GPS locations were taken for each structure. These detailed surveys were carried out on a number of key buildings, such as churches, public facilities, hospitals, and high-rise (8+ storeys) apartment blocks. Internal and external inspections were carried out, and where possible,

questions were asked to someone knowledgeable about the building, *i.e.* the owner, or security guard.

The team also performed detailed surveys using Arup's REDI system (Almufti and Willford, 2013), and an extended version of Global Earthquake Model's inventory capture tool (Brzev *et al.*, 2013). Both of these survey methods are still in the development phase.

6.3. Observed Building Stock

There are a number of different building typologies in the earthquake affected region, with varying levels of engineering input, quality, and durability. The types described in this section are those observed on the fieldwork mission – others may also exist that were not seen.

6.3.1. Reinforced concrete frame with masonry infill walls

This was the most common building typology observed in the affected region and consists of reinforced concrete (RC) columns, beams and slabs with masonry infill walls. Two sub-types of this typology exist:

1. Non-engineered, typically low-rise (<6 storeys): Figure 6-1.
2. Engineered, typically high-rise (≥ 6 storeys): Figure 6-2.

The non-engineered type of this system tended to have a slender RC frame, with thin columns and either a shallow or in some cases no beam at all, and a conventional RC slab (flat or ribbed) (Figure 6-1). Slender clay brick masonry walls (single skin, sometimes with bricks orientated on their short side, making the aspect ratio of the wall even more slender) formed the façade and internal partition walls of most buildings, which were in some cases connected back to the frame with light reinforcement. The masonry walls were relatively dense, however at ground floor there was often a shop front and/or a sheltered corridor, so the walls generally were less dense here. These buildings are often built in stages, with the first floor or two constructed first and then additional floors added when money becomes available – they did not generally exceed around six storeys in height. The buildings appeared to be largely non-engineered, likely built by a local builder (known as *maestros de obra*) possibly with some input from an architect and limited, if any, input from engineers. In reality, the lateral load-resisting system of these buildings is likely to be the RC frames braced by the masonry infill walls – by inspection the RC frames, without infill walls, are too slender to attract significant load when compared to the stiff masonry wall panels.

The system is not too distant from confined masonry, at least visually, however: the construction sequence (frame then masonry instead of vice versa) means the panels are not fully confined, the panels are too slender, the panels are generally not positively connected to the frame, and the detailing of the columns and tie beams appeared insufficient – the combination of these means the masonry and frame do not purposefully act together under lateral load as shear walls. Therefore, these buildings tended to be hybrids, a cross between a moment frame and a confined masonry building, but lacking the correct design and detailing for either.

The engineered type of this system tends to have a significantly stockier RC frame, with large columns supporting downstand beams and a conventional RC slab (flat or ribbed) (Figure 6-2). Clay or other brick masonry walls form the façade and internal partition walls, which are in some cases connected back to the frame with reinforcement. These walls vary in width as in some cases thicker bricks appeared to be used. The masonry walls vary in density depending on building use. These buildings appeared to be built in one go, and were typically six to fifteen storeys in height. The buildings were clearly engineered due to the sensible aspect ratio of the frame, however, the masonry (usually hollow concrete block) infill walls

EEFIT

were likely considered as non-structural elements and not included in the analysis as providing lateral stiffness. In reality, the lateral load-resisting system of these buildings is likely to be predominantly the RC frame acting as a moment frame (as it would be designed presumably) – the masonry infill will likely inadvertently attract some of the load since no soft movement joint between the masonry and the frame was observed on any of these buildings. No RC shear wall lateral load resisting systems were observed, but these were recorded by others (Lanning *et al.*, 2016).



Figure 6-1 Reinforced concrete frame with masonry infill walls – non-engineered low-rise.



Figure 6-2 Reinforced concrete frame with masonry infill walls – engineered high-rise.

6.3.2. Quincha/bahareque

Quincha also known as *bahareque* is a derivative of wattle-and-daub popular in Latin America (Figure 6-3) (López *et al.*, 2004; Carazas-Aedo & Rivero-Olmos, 2013, Kaminski, 2013). *Quincha* was observed in many of the areas surveyed, and in this region typically consists of a timber frame, clad in a matrix of bamboo strips, plastered in manure, soil and/or lime, sometimes with straw or horse hair added for strength. This structural system is primarily used for one or two storey structures, with the floor and roofing frame constructed from timber and a roof using clay tiles or corrugated metal sheets.

It is very common to see the ground floor used for retail with an overhang, while the upper floor may be residential or used for storage. Properly constructed and maintained *quincha* has been shown to possess good structural unity and some ductility, and thus can behave well in earthquake shaking (López *et al.*, 2004; Gutiérrez, 2000). In addition, since it is relatively light, it attracts less seismic load. However, it requires a reasonable standard of construction, detailing and maintenance to avoid deterioration through rot or insect attack. The *quincha* structures observed tended to be relatively old (>40 years), often showing serious signs of rot and insect (especially termite) attack.



Figure 6-3 Quincha structure.

6.3.3. Timber frame with and without masonry infill

Timber framed structures were observed in all of the areas surveyed, usually only one and two storeys. The timber used for the frame was likely to be a naturally-durable hardwood. The frame was often braced, and either contained masonry infill (clay brick or concrete block) or had a timber or corrugated metal sheet façade (Figure 6-4). In some cases, this system was combined with *quincha* or RC frame with masonry infill, with the heavier system on the ground floor and the lighter system on the first floor. Maintenance of these buildings is also essential, and many of these structures showed signs of insect attack and rot.



Figure 6-4 Timber frame with masonry infill.

6.3.4. Informal rural housing

Informal housing in rural areas generally used either timber and/or bamboo for the frame (Figure 6-5) or RC frames with masonry infill. These systems are completely non-engineered and vary significantly in their ad-hoc stability.



Figure 6-5 Informal rural housing.

6.3.5. Others

Small numbers of steel framed, unreinforced masonry, and completely bamboo framed housing were observed, but as these typologies did not make up a significant proportion of the buildings, they have not been presented in detail in this report. It is noted that the team did not see any adobe buildings during the mission.

6.4. Overview of Observed Building Damage

This section provides an overview of the different forms of building damage seen. Note that many of the reasons for failure are intrinsically linked.

6.4.1. Reinforced concrete frame with masonry infill walls

Very high levels of structural damage were seen in the non-engineered low-rise types of these buildings. However the engineered high-rise type experienced low levels of structural damage and mainly non-structural issues.

a) Inadequate design and detailing of RC moment frames

RC moment frames in seismic areas require several key considerations to ensure they behave safely in an earthquake:

- Sufficient overall moment and shear capacity.
- Columns' flexural strength should exceed that in the beams, such that flexural failure occurs first in the beams.
- Columns and beams should be stronger in shear than in flexure, such that a ductile flexural failure mode occurs before a brittle shear failure mode.
- Adequate detailing of the reinforcement in all elements.

Damaged RC structures observed generally failed some or all of these requirements (Figure 6-6). In addition, they could not truly be considered to be confined masonry structures because the detailing was still inadequate and the masonry inadequately confined.



Figure 6-6 Collapsed building, showing failure of façade and frame.

b) Inadequate masonry infill design and construction

The masonry used to infill RC frames to provide facades and partition walls was inadequate in a number of areas (Figure 6-7):

- The connections between the columns and the masonry were often insufficient – in many buildings no reinforcement bars existed connecting the two. This lack of a proper connection at the column interface can lead to the walls failing out-of-plane.

EEFIT

- Where reinforcement bars did exist connecting the columns to the masonry, the masonry was often too thin and the mortar too poor quality to enable the bars to properly bond to the masonry.
- The aspect ratio of the panels was in nearly all cases too large for the thickness of the masonry, which means that the masonry is unable to arch under out-of-plane load, nor able to be stable under in-plane load, and can fail/buckle out-of-plane. This was due to RC beams and columns placed far apart, and since the wall was single skin with the bricks often placed on their short side.
- Where the designated lateral load-resisting system is a moment frame, the masonry should be decoupled from the frame through the introduction of a 'soft' joint on three sides of the masonry panel (typically 10-40mm thick), filled with a compressible material. This 'best-practice' was not observed in any building.

Inadequate masonry design and detailing was observed in nearly all buildings that had infill masonry walls.



Figure 6-7 Inadequate masonry infill wall design and construction.

c) Inadequate shear design and detailing

In seismic areas, the shear links within RC elements need special detailing. In particular, shear links need to be closely spaced, the two ends of the loop need to return into the column by an angle greater than 135 degrees, and the length of the returns need to be sufficient. This detailing ensures that the shear capacity of the concrete is as designed, helps to reduce buckling of the longitudinal bars and helps to confine the concrete in the core. In many RC buildings surveyed some or all of these detailing requirements were not present (Figure 6-8).

d) Weak and soft storeys

Upper floor soft/weak storey failures occur when a floor is weaker in strength or less stiff than the adjacent storeys, resulting in load concentration at this floor level, which can exceed the capacity and result in damage to or collapse of that floor (Figure 6-9). This form of collapse was seen in a number of buildings, interestingly many of which were at an upper floor instead of a ground floor (which is generally more typical). Some of the soft/weak storey failures are likely due to a discontinuity in frame and/or masonry strength between floors, while it is suspected that others are due to inadequate lapping of primary column reinforcement (see item e) *Inadequate laps*).



Figure 6-8 Inadequate design and detailing for shear – insufficient link spacing, poor link detailing and plain links used.

e) Inadequate laps

A number of buildings experienced upper floor weak/soft storeys without a clear change in stiffness or strength. It is known that the reinforcement bars come in set lengths, and when placed for construction the top of the bars were often observed to rise just above the second floor. It is common to build just two storeys initially and leave extra reinforcement exposed, ready for an additional floor in the future (Figure 6-10).

In many cases, the amount of reinforcement sticking out waiting for future construction may not be sufficient for a proper reinforcement lap, which would lead to a weak and brittle connection between old and new. In addition, the reinforcement bars are often left out for many years and so can experience surface corrosion, which can weaken their bond to the new concrete once poured. Finally, all of the rebar is often lapped at one height, causing potentially weak spots in the same location in all columns, causing in turn specific floors which are relatively weaker than those above or below.



Figure 6-9 Weak and soft storey failures.



Figure 6-10 Exposed reinforcement with possible inadequate lap lengths for future construction, and an upper storey soft/weak storey failure.

f) Short columns

This failure occurs when partial height stiff walls are constructed against columns. This construction promotes a brittle shear failure mode prior to a ductile flexural mode (Figure 6-11 and Figure 6-12). This failure mode was seen in a number of buildings, with a reoccurring detail of high level windows for the full length of the frame bays.



Figure 6-11 Short columns at a school in Pedernales.



Figure 6-12 Short columns at a shop front – note the local crushing of the masonry lining up with an imaginary compression strut and local shear failure of the column.

g) Insufficient cover to steel reinforcement

Sufficient cover to reinforcement is required to protect the reinforcement against corrosion. In coastal areas, the environment is more aggressive and the requirements for cover increase. In many columns, the cover was very low (0-20mm), which caused corrosion to the steel (Figure 6-13). For comparison, for this region UK codes generally require around 50mm cover in good quality concrete to provide adequate protection in a coastal environment.



Figure 6-13 Insufficient cover to rebar – note 100% section loss to some of the links.

h) Pounding

Pounding occurs when buildings move out of sync in an earthquake and impact on each other. In very few locations seismic gaps were seen in-between buildings and floor slabs were often out of alignment, leading to localised pounding (Figure 6-14).



Figure 6-14 Pounding of a column head by a slab of an adjacent building.

i) Inadequate design of plastic hinges

Designated plastic hinges in RC elements require special detailing to ensure they yield in a controllable and ductile manner, as opposed to a brittle manner. Where plastic hinges were seen, damage was often seen to be brittle, with failure mechanisms involving local concrete crushing and bursting, and buckling of longitudinal reinforcement, instead of pure tensile yielding of bars (Figure 6-15).



Figure 6-15 Inadequate design of plastic hinges.

j) Inadequate securing of non-structural elements

Non-structural elements require securing back to the structure in order to minimise injury and damage, allow occupants to safely escape and allow the building to continue to function after the seismic event. Adequate securing of non-structural elements was rarely seen, with significant damage of facades, furniture, fittings and ceilings (Figure 6-16).



Figure 6-16 Inadequate securing of non-structural elements – the image on the right depicts a hospital corridor.

k) Poor quality concrete

The concrete used in RC frames was observed to be of low quality in some areas (Figure 6-17), likely for a number of reasons:

- Inadequate mix design – some concrete clearly had too much or too little coarse aggregate.
- Excess water – with informal construction, it is common to add excess water to the mix to improve workability, which weakens the concrete.
- Poor compaction – some concrete clearly had not been properly compacted and voids were evident at the bottom of pours.



Figure 6-17 Poor quality concrete.

l) Use of sea sand and/or sea water for construction

It was mentioned by a number of local engineers and the national media that some of the damage could be attributed to the use of sea sand and/or sea water for construction. It is important to note that using unwashed sea sand and/or salty sea water in concrete (provided organic material has been removed in both) is not proven to result in a significant long-term reduction in strength, nor is there any further chemical reaction which breaks down the concrete – this is described in what is widely regarded as the bible of concrete: Neville (1995). However, the salt that this places in the concrete does have two effects:

1. It speeds up the rate of carbonation of the concrete.
2. It speeds up corrosion once carbonation reaches the steel.

Therefore, the use of sea sand and/or sea water may have increased the rates of corrosion of the steel reinforcement within the concrete (see point *g*: *Insufficient cover to steel*). However, it will not have a significant direct impact on the concrete itself. It is possible however that the concrete did contain organic material, which would increase the permeability of water and air into the concrete, effectively further reducing the cover to the steel, hence speeding up corrosion.

6.4.2. Buildings using timber or bamboo

a) Rot and damage due to insects

The majority of the damaged timber or bamboo buildings showed evidence of mild to severe damage due to rot, termites or beetles, or a combination (Figure 6-18) (van Drunen et al., 2016). This was due to:

1. A lack of appropriate prior treatment of the materials.
2. Inadequate selection of durable timbers.
3. Inadequate design leading to large areas of the walls fully exposed to the elements.
4. A general lack of maintenance, including replacing damaged elements and painting.
5. The encasing of timber or bamboo within concrete as a connection to the foundation.



Figure 6-18 Examples of rot and insect damage.

b) Inadequate connections between primary structural elements

In some buildings, it was evident that the traditional connections used to connect timber elements together were not robust enough to resist lateral loads, or in some cases may even have been missing (Figure 6-19).



Figure 6-19 Lack of positive connection between frame and masonry upstand, leading to sliding of column laterally.

c) Debris from adjacent buildings

Some buildings appeared to have damage to their sides facing other buildings that had collapsed, while the remainder was undamaged. This suggests that debris from adjacent buildings while they collapsed (or in some cases were crudely knocked down) may have damaged the facades of timber/bamboo buildings (Figure 6-20). While this may be applicable to all building types, it may be more significant for timber or bamboo buildings, which are inherently less resistant against heavy debris impact compared to concrete framed buildings.



Figure 6-20 Possible damage due to debris from adjacent buildings.

6.5. Damage Data from Rapid Surveys

6.5.1. Motivation

The team collected damage data using rapid surveys from urban areas throughout the affected region. Damage data can be used to:

- Better understand the scale and spread of damage;
- Better understand patterns of damage by typology, height, location, *etc.*;
- Produce empirical fragility and vulnerability functions (Rossetto *et al.* 2014);
- Validate analytical fragility and vulnerability functions (D'Ayala *et al.* 2013).

The data presented in this section highlights the data collected using rapid surveys. In one city, the rapid surveys were supplemented by a video survey taken from a car and analysed upon return to the UK. The survey routes are highlighted for each urban area surveyed.

6.5.2. Limitations

With data collected in the field, limitations are inevitable, and these are presented below:

- By the dates of the EEFIT mission to Ecuador, many buildings had already been demolished, with no record of the damage levels or information about the building. In these instances, the surveys were unable to capture the damage grades and building typologies. The demolished building sites were recorded with unknown building typologies assigned. In some instances, locals were able to help with information (number of storeys or construction types) about the demolished buildings.
- In some cases, particularly with lesser-damaged buildings, the surveyors were unable to observe the primary structural system due to cladding. In these cases the best judgement of the surveyor was used.
- The rapid surveys were only conducted from outside the buildings, with no internal inspections. This may have led to misclassification of building typology and/or damage grade.
- With limited time in the field, the areas surveyed were small compared to the size of the urban areas affected. The survey routes are highlighted to enable readers to judge biases in the data.
- The accuracy of the surveyor may impact the results. Four experts covered different survey areas, with the results unable to be corroborated between experts, hence errors and biases (although hopefully minimised through practice exercises in assigning damage grades) may exist.

6.5.3. Damage Data

The damage data are presented in tabular format, for each urban area surveyed. Maps of the survey routes are also included to provide readers some context to the data. In any instances where information was unknown or missing, it is classified as unknown (denoted as 'Unk'). Building classes are grouped into the broad groups of reinforced concrete (with masonry infill), timber, and other (including steel, unreinforced masonry, etc.).

a) Manta

Figure 6-21 and Figure 6-22 show the survey routes for the restricted area of Tarqui and near the seismometer station, respectively. Table 6-2 and Table 6-3 present the damage data for the Tarqui surveys, and the Manta station surveys, respectively.



Figure 6-21 Survey routes (blue lines) in the restricted zone (yellow shaded area) in Tarqui, Manta. Centre of image: (-0.9535, -80.7149).

Table 6-2 Damage data from Tarqui, Manta.

Building type	No. storeys	EMS-98 damage grade (D denotes demolished)							Total
		0	1	2	3	4	5	D	
Reinforced concrete	1	15	5	1	4	0	1	0	26
	2	9	5	6	3	1	0	5	29
	3	7	14	5	8	1	1	0	36
	4	1	9	16	4	2	0	3	35
	5	1	2	7	4	0	0	1	15
	6	0	2	2	1	0	1	1	7
	7	0	1	0	1	0	0	0	2
	Unk	0	0	1	0	0	0	0	1
Total	33	38	38	25	4	3	10	151	
Timber	1	1	1	0	2	0	1	0	5
	2	0	4	3	4	7	1	1	20
	3	0	0	1	0	1	0	1	3
	Total	1	5	4	6	8	2	2	28
Other	1	3	2	1	2	0	0	3	11
	2	3	1	1	1	0	0	0	6
	3	0	0	0	1	1	0	0	2
	Total	6	3	2	4	1	0	3	19
Un known	Unk	0	0	0	0	0	0	1	1
	Total	0	0	0	0	0	0	1	1
Grand total									199

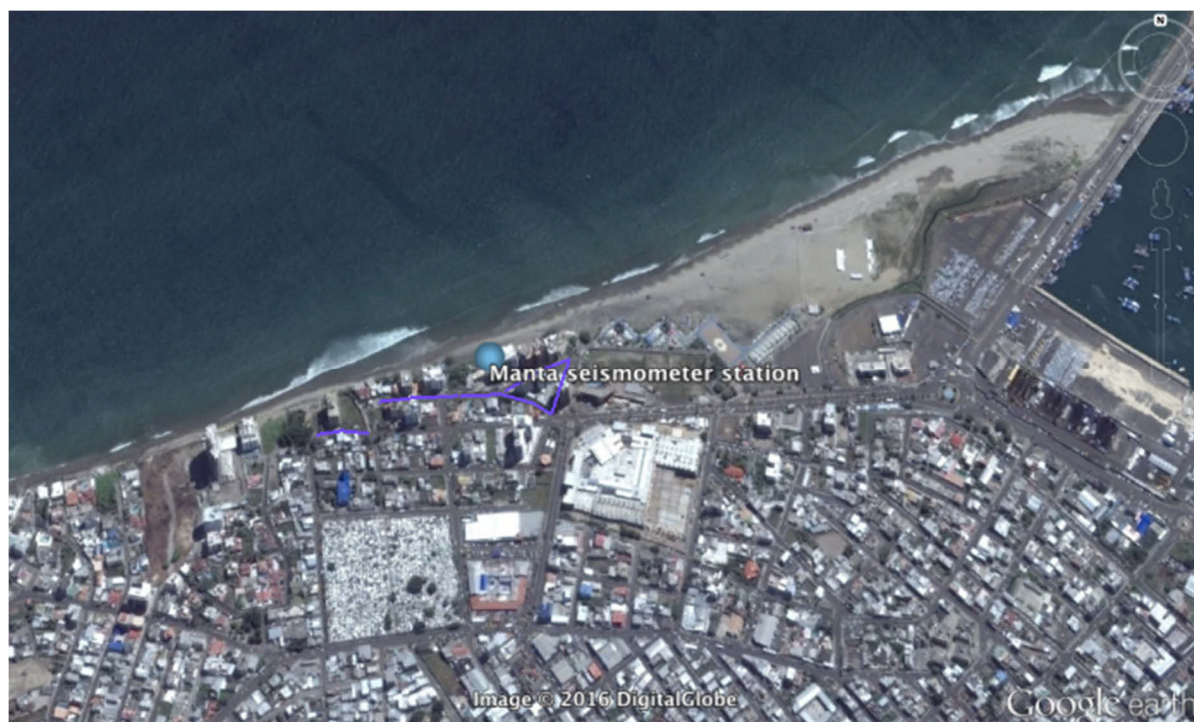


Figure 6-22 Survey routes (purple lines) near Manta seismometer station. Centre of image: (-0.9415, -80.7332).

Table 6-3 Damage data from Manta seismometer station survey.

Building type	No. storeys	EMS-98 damage grade (D denotes demolished)							Total
		0	1	2	3	4	5	D	
Reinforced concrete	1	1	0	0	0	0	0	0	1
	2	4	2	0	0	0	0	0	6
	3	0	1	0	0	0	0	0	1
	4	1	1	1	0	0	0	0	3
	5	0	1	0	0	0	0	0	1
	6	0	0	0	0	0	0	0	0
	7	0	1	0	0	0	0	0	1
	8	0	0	0	0	0	0	0	0
	9	0	0	2	0	0	0	0	2
	10	0	1	2	0	0	0	0	3
	11	0	0	2	0	0	0	0	2
	12	0	0	0	0	0	0	0	0
	13	0	0	2	0	0	0	0	2
	14	0	0	1	0	0	0	0	1
	15	0	0	1	0	0	0	0	1
	Total	6	7	11	0	0	0	0	24
Timber	1	0	0	1	0	0	0	0	1
	Total	0	0	1	0	0	0	0	1
Grand total									25

b) Portoviejo

Figure 6-23 shows the map urban area of Portoviejo and gives the location of the seismometer station, the shelter camp and the key army base. It also highlights the extent of video surveying undertaken in the city, which was used to supplement the walking surveys. Figure 6-24 focuses in on the restricted 'ground zero' region, and indicates the survey routes near the seismometer station. The data is presented separately for the rapid surveys in 'ground zero' (Table 6-4), near the seismometer station (Table 6-5) and for the video survey (Table 6-6).

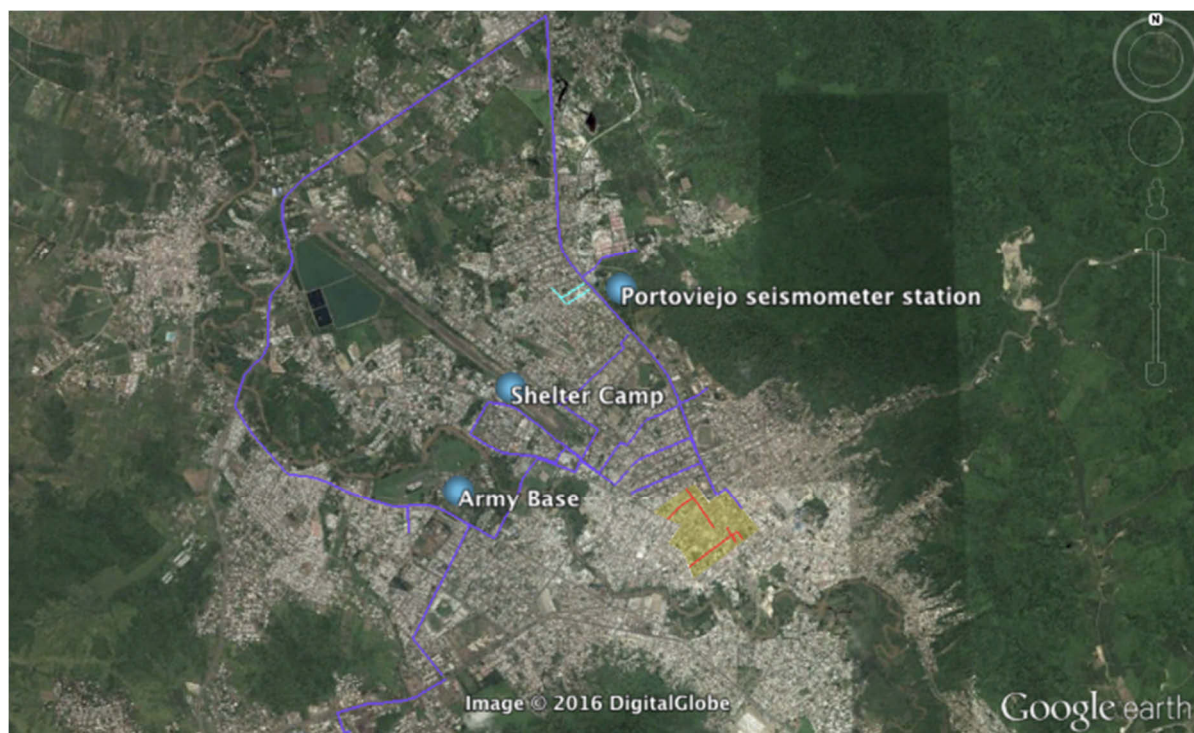


Figure 6-23 Overview of Portoviejo with key locations (blue dots), video survey routes (purple lines), ground zero (yellow shaded area), ground zero survey routes (red lines), and survey routes near the seismometer station (light blue lines). Centre of image: (-1.0432, -80.4569).

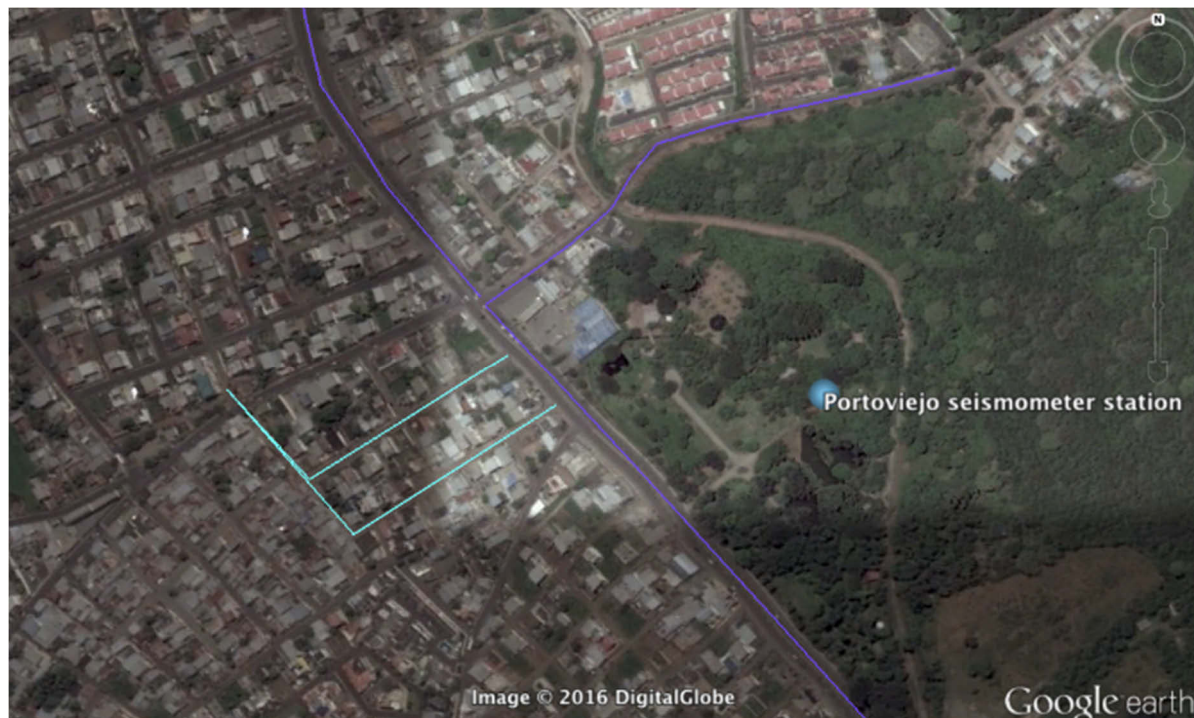


Figure 6-24 Survey routes (light blue lines) near Portoviejo seismometer station. Centre of image: (-1.0373, -80.4622).

Table 6-4 Damage data for ground zero, Portoviejo.

Building type	No. storeys	EMS-98 damage grade (D denotes demolished)							Total
		0	1	2	3	4	5	D	
Reinforced concrete	1	6	1	2	1	0	0	2	12
	2	7	2	2	0	0	0	1	12
	3	8	4	2	2	0	0	1	17
	4	2	2	1	0	0	0	2	7
	5	0	0	2	4	1	1	0	8
	6	0	0	1	0	1	0	0	2
	Total	23	9	10	7	2	1	6	58
Timber	1	1	0	1	0	1	0	2	5
	2	4	3	4	1	1	0	1	14
	3	1	0	1	0	0	0	0	2
	Total	6	3	6	1	2	0	3	21
Other	1	3	0	0	0	0	0	1	4
	2	0	1	0	0	0	0	0	1
	3	0	0	1	0	0	0	0	1
	Total	3	1	1	0	0	0	1	6
Grand total									85

Table 6-5 Damage data from surveys near to the Portoviejo seismometer station.

Building type	No. storeys	EMS-98 damage grade (D denotes demolished)							Total
		0	1	2	3	4	5	D	
Reinforced concrete	1	22	1	0	0	0	0	0	23
	2	24	2	1	0	0	0	0	27
	3	10	2	1	0	0	0	0	13
	4	1	0	0	0	0	0	0	1
	Total	57	5	2	0	0	0	0	64
Timber	1	3	0	0	0	0	0	0	3
	Total	3	0	0	0	0	0	0	3
Other	1	1	0	0	0	0	0	0	1
	Total	1	0	0	0	0	0	0	1
Grand total									68

Table 6-6 Damage data from the Portoviejo video survey.

Building type	No. storeys	EMS-98 damage grade (D denotes demolished)							Total
		0	1	2	3	4	5	D	
Reinforced concrete	1	10	0	0	0	0	0	0	10
	2	61	6	2	2	0	0	0	71
	3	38	7	0	1	0	1	0	47
	4	10	2	2	1	3	3	0	21
	5	1	6	0	0	0	1	0	8
	6	0	1	0	0	0	0	0	1
	7	0	1	0	0	0	0	0	1
	Total	120	23	4	4	3	5	0	159
Timber	1	6	0	0	0	0	0	0	6
	2	1	1	0	0	3	1	0	6
	Total	7	1	0	0	3	1	0	12
Other	1	8	0	0	0	0	0	0	8
	2	2	0	0	0	0	0	0	2
	3	1	0	0	0	0	0	0	1
	4	0	0	0	0	2	0	0	2
	Total	11	0	0	0	2	0	0	13
Unknown	1	135	0	0	0	0	1	0	136
	2	172	2	0	0	0	1	0	175
	3	72	4	0	0	0	2	0	78
	4	4	0	0	0	0	0	0	4
	5	2	0	0	0	0	0	0	2
	Total	385	6	0	0	0	4	0	395
Grand total									579

6.6. Jama

Figure 6-28 shows a map of the urban area of the small town of Jama. The rapid survey route is depicted using purple lines. The data is presented in Table 6-7.



Figure 6-25 Map of survey routes (purple lines) in Jama. Centre of image: (-0.2017, -80.2639).

Table 6-7 Damage data from Jama.

Building type	No. storeys	EMS-98 damage grade (D denotes demolished)							Total
		0	1	2	3	4	5	D	
Reinforced concrete	1	4	5	4	1	1	0	0	15
	2	4	2	2	3	3	1	1	16
	Unk	0	1	0	0	0	0	1	2
	Total	8	8	6	4	4	1	2	33
Timber	1	5	5	1	0	0	0	0	11
	2	2	7	1	6	6	3	0	25
	Unk	0	0	0	0	3	0	3	6
	Total	0	12	2	6	9	3	3	35
Other	1	1	0	0	0	0	0	0	1
	2	0	0	1	0	0	0	0	1
	Total	1	0	1	0	0	0	0	2
Unknown	4	0	0	0	0	0	0	1	1
	Unk	0	0	0	0	0	0	31	31
	Total	0	0	0	0	0	0	32	32
Grand total									102

6.7. Pedernales

Figure 6-26 shows a map of the urban area of Pedernales and gives the location of the seismometer station, the temporary army posts, the primary shelter camp, and some key buildings. The survey routes are shown as purple lines, and the resulting data are presented in Table 6-8.

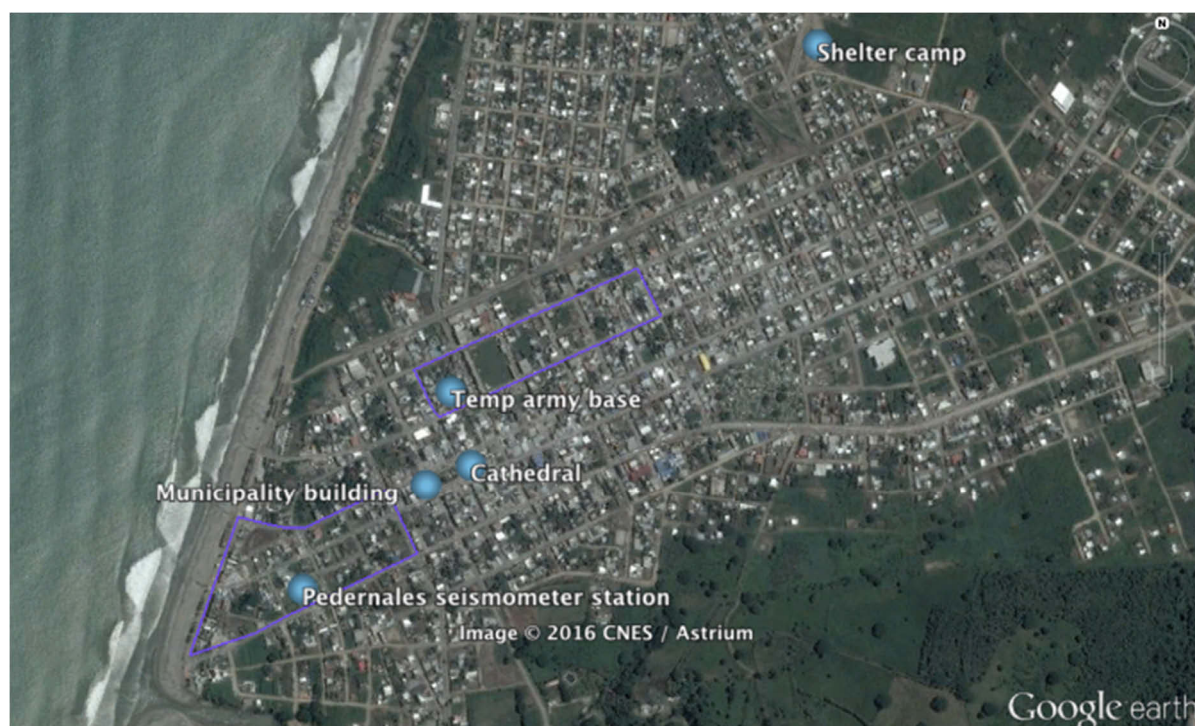


Figure 6-26 Map of Pedernales showing key sites (blue dots), and survey routes (purple lines). Centre of photo: (0.0721, -80.0520).

Table 6-8 Damage data for Pedernales.

Building type	No. storeys	EMS-98 damage grade (D denotes demolished)							Total
		0	1	2	3	4	5	D	
Reinforced concrete	1	21	15	10	2	0	0	2	50
	2	4	6	8	14	2	1	5	40
	3	0	0	1	1	0	0	2	4
	4	0	0	1	0	0	0	0	1
	5	0	0	1	0	0	0	0	1
	6	0	0	0	1	0	0	0	1
	Unk	0	0	0	1	0	0	21	22
Total		25	21	21	19	2	1	30	119
Timber	1	11	7	4	1	1	3	2	29
	2	2	5	8	8	2	0	0	25
	Unk	0	0	0	0	0	0	4	4
	Total		13	12	12	9	3	3	6
Other	2	0	0	1	0	0	0	0	1
	Total		0	0	1	0	0	0	1
Unknown	Unk	0	0	0	0	0	0	27	27
	Total		0	0	0	0	0	0	27
Grand total									147

6.8. Case Study Observations

This section describes a number of buildings which the team conducted detailed visual inspections on, both externally and internally.

6.8.1. Technical University of Manabi (Universidad Tecnica de Manabi – UTM)

The structural team spent several hours surveying a number of large university teaching blocks across the campus. The buildings generally consisted of regular multi-storey (three to five storey) heavy reinforced concrete framed buildings with masonry facades and partitions

and large windows. Damage varied considerably, with some showing structural damage and others only non-structural. Typical failure modes observed included:

- Short columns, generally in line with long window openings along the length of the building (Figure 6-27).
- Out-of-plane masonry infill failures (Figure 6-28).
- In-plane masonry infill shear failure (Figure 6-29).
- Pounding (Figure 6-30).

Movement joints were seen between some of the buildings, but in many cases, they were very small in size or filled in with rubble, thus ineffective (Figure 6-31). Two buildings were seen to have permanent lateral drift in the order of around 50mm (Figure 6-32).



Figure 6-27 Shear cracking due to short column effect.



Figure 6-28 Complete out-of-plane failure of masonry perimeter infill walls.



Figure 6-29 In-plane shear cracking of masonry infill walls.



Figure 6-30 Pounding at movement joint.



Figure 6-31 Movement joint filled with rubble (prior to event).



Figure 6-32 Permanent lateral drift of buildings relative to one another of approximately 50mm (follow movement joint below “DE”).

6.8.2. Portoviejo Airport Building

The structural team briefly reviewed one of the two storey buildings of the disused Portoviejo Airport (the site of a major temporary shelter camp). The team observed retrofitting of existing reinforced concrete columns which commenced prior to the earthquake (Figure 6-33). The retrofit consisted of steel angles fitted to the corners of the columns, with side plates site welded to the angles. The retrofit was presumably designed to either confine the concrete, or provide additional shear capacity. The design was considered questionable, since the site weld quality was poor (Figure 6-34) and the steel plates were not fixed tight up against the rough concrete surface.



Figure 6-33 Steel plate retrofit to reinforced concrete column.



Figure 6-34 Site welded steel plate.

6.8.3. Hospital Miguel Hilario Alcivar De Bahía De Caraquez

This four-storey long building consisted of a reinforced concrete frame with masonry infill (Figure 6-35). The building experienced heavy non-structural damage to many internal and external masonry walls, some which fell completely out-of-plane (Figure 6-35 and Figure 6-36). Significant damage was also seen to the services and false ceilings (Figure 6-36 and Figure 6-37). The structure appeared to experience only minor structural damage. The building had been retrofitted after the 1998 earthquake through the addition of RC shear walls in each elevation coupled to the columns, which were also retrofitted by concrete jacking. Minor damage was seen at the connection between the coupled columns and the new RC shear walls (Figure 6-38) – the detail connecting the two did not appear optimal.



Figure 6-35 Hospital Miguel Hilario Alcivar De Bahía De Caraquez.



Figure 6-36 In-plane shear cracks.



Figure 6-37 Significant damage to false ceiling and fittings.



Figure 6-38 Damage at interface between coupled column and shear wall.

6.8.4. Pedernales Cathedral

This building was a tall single storey reinforced concrete framed building with a steel upper roof (Figure 6-39). Clay bricks were used for the unreinforced perimeter walls. Non-structural damage was heavy, with some significant masonry wall damage, and many dislodged heavy ceiling tiles (Figure 6-40). Roof cladding panels had also fallen during the earthquake. Observed structural damage was light and appeared to be generally caused by connections to the masonry infill walls.



Figure 6-39 Pedernales Cathedral, with damage to the roof and masonry façade.



Figure 6-40 Internal damage to ceiling tiles and masonry walls.

6.8.5. Main Municipality Office, Pedernales

This is a five-storey building in Pedernales, with an RC frame and clay brick masonry infill (Figure 6-41). The building is one of the main government offices in Pedernales. The frame had a reasonable beam and column size aspect ratio, and the reinforcement detailing appeared reasonable (where exposed). Structural damage was light to moderate, with some cracking and spalling at the beam-column connections (Figure 6-42), and moderate damage to the RC staircase (Figure 6-43). Non-structural damage was heavy, with complete failure of many internal and external masonry wall panels (Figure 6-43 and Figure 6-44).



Figure 6-41 Main municipality building in Pedernales.



Figure 6-42 Local damage to head of RC column.



Figure 6-43 Moderate damage to RC staircase.



Figure 6-44 Heavy non-structural damage to internal and external masonry wall panels.

6.9. Observations on the Immediate Structural Inspection of Buildings

Carlos Molina-Hutt of University College London deployed to Ecuador with the European Union Civil Protection Team (EUCPT), to assist with immediate structural inspections of buildings: here their work in Portoviejo is reported, followed by some observations from the EEFIT team.

6.9.1. Immediate Structural Inspection of Buildings

Civil protection assistance consists of governmental aid delivered in the immediate aftermath of a disaster. It can take the form of in-kind assistance, deployment of specially-equipped teams, or assessment and coordination by experts sent to the field. Following the 16 April 2016 earthquake in Ecuador, the EU Civil Protection Mechanism deployed a team to the field to enable coordinated assistance from the participating states to victims of the earthquake, working alongside the United Nations Disaster Assessment and Coordination (UNDAC) team. There were three Structural Engineering Experts in the EUCPT: Agostino Goretti (Italy), Lida Hedelund (Sweden) and Carlos Molina Hutt (UK).

The goal of the structural engineers on the team was to support the Ecuadorian authorities in assessing the situation, notably on structural damage assessments and facilitating the coordination of incoming assistance from participating states who deployed teams to the field. Overall, the European teams assessed over one thousand buildings while on the ground.

Upon arrival in Portoviejo on 24 April, the EUCPT held a meeting at the On-Site Operation Coordination Centre (OSOCC) with UNDAC and representatives from Ministerio de Desarrollo Urbano y Vivenda (MIDUVI, Ministry of Urban Development and Social Housing), as seen in Figure 6-45. MIDUVI were responsible, within the Ecuadorian Emergency Management Organisation, for building and infrastructure damage assessment. MIDUVI defined Portoviejo, the capital of the Province of Manabí, as site of operations for all EU structural assessment teams. After further communications with Portoviejo Municipality, the structural assessment efforts were focused in the city centre, which due to the extent of damage, was cordoned off by local authorities within 48 hours of the earthquake. Figure 6-46 is a map of the city centre of Portoviejo, which illustrates the extents of the cordoned off area, referred to as Zone Zero (delimited by the dashed red line).



Figure 6-45 Coordination meeting at the OSOCC upon arrival in Portoviejo.

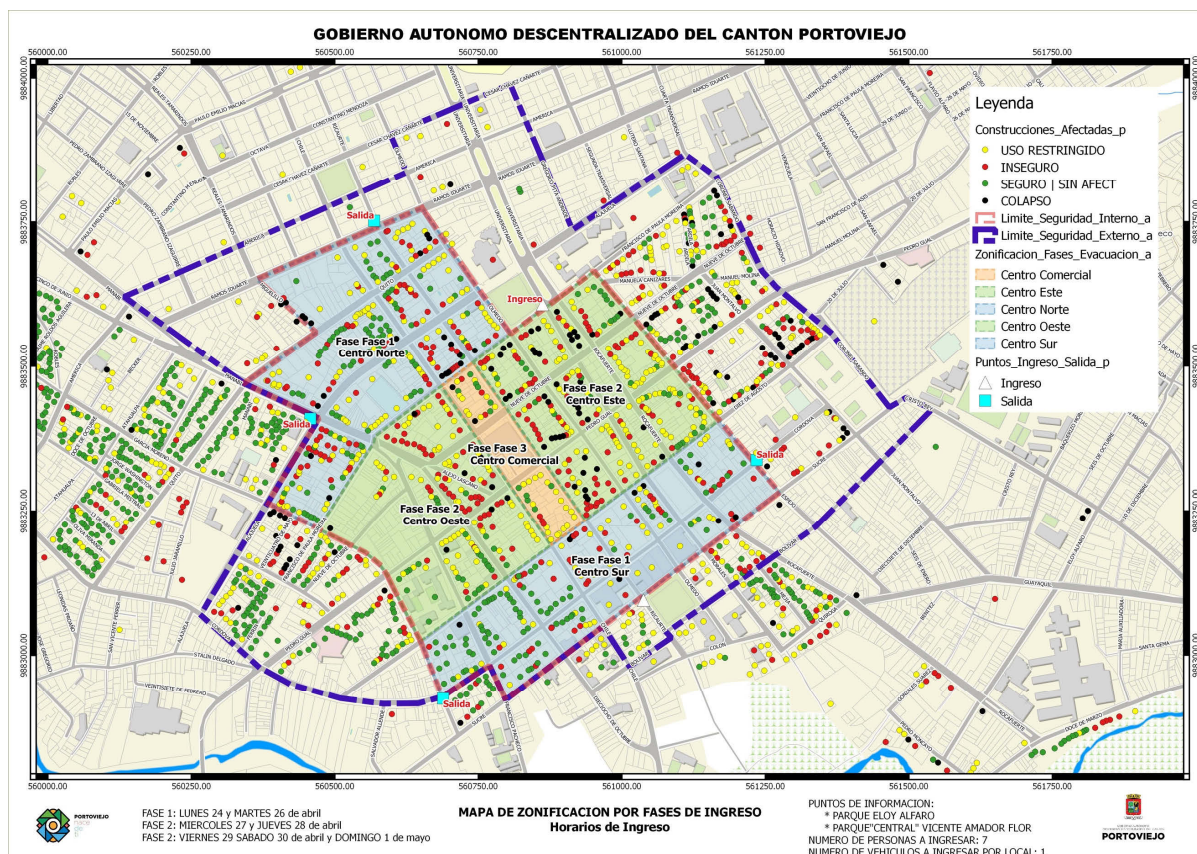


Figure 6-46 Map of Portoviejo illustrating the extents of Zone Zero (delimited by faded red dashed line).

Structural assessments were carried out by the three structural experts of the EUCPT, as well as teams of experts from Italy, France, and the UK. The Italian team was composed of eight firefighters. They operated in three sub-teams from 25 April to 4 May. The French team was composed by six firefighters. They operated in two sub-teams from 26 April to 7 May. Both contributed to assessment work in Portoviejo. The UK team, deployed on bilateral agreements, was composed of three structural engineering experts and conducted similar work, from 27 April to 5 May, in Pedernales.

The teams conducted several types of assessment, based on needs and priorities established by Ecuadorian authorities. All teams were accompanied by local experts, both to facilitate entrance into buildings and knowledge transfer. The following field assessments were performed:

- Rapid Post-Earthquake Safety Assessment of Buildings:

A rapid assessment is a quick but thorough evaluation of the risks that the damage caused to a building may impose on occupants and the surrounding area. Buildings were tagged as green, yellow or red, as shown in Figure 6-47. The methodology and the procedures were already in place when the teams arrived there in the field. A later study revealed that they existing tags were the result of a disaster risk-reduction pilot project which was underway at the time of the earthquake (Goretti et al., 2017). The inspection procedures were mainly based on ATC-20 (1989) documentation arranged to fit local building types. The implications of each tag, which are shown in Figure 6-47, are as follows:

- Green: A green tag indicates that no damage observed during the inspection poses a safety risk for entry or occupancy of the building.

- Yellow: A yellow placard indicates that there are restrictions on the building usage. The restrictions are based on the inspection team’s judgment. A yellow tag might allow occupants to enter for a short time to remove contents when the building is not safe for longer occupancy.
- Red: A red placard indicates that the building is unsafe for occupancy. However, it does not mean that the building must be demolished. In certain occasions, a building may be tagged as red due to non-structural damage only or due to hazards from surrounding buildings.



Figure 6-47 The tagging system.

- Demolition Verification:

Due to the immediate availability of vehicles for demolitions provided by Ecuadorian government, many buildings had already been demolished before the arrival of the EUCPT. These had been selected for demolition without a structured procedure. Demolitions were often performed with inadequate vehicles and there were some concerns for public safety. As a result, the municipality requested an assessment prior to proceeding with further demolition work in order to ensure that no buildings that could be salvaged would be demolished. The evaluation was performed only on the red tagged buildings in Zone Zero and surrounding areas. For this purpose, a specific form was drafted by EUCPT experts in order to report back the result of the assessment. Figure 6-48 illustrates the placard that was used to identify red-tagged buildings that required demolition. This placard was generally added to those shown in Figure 6-47.



Figure 6-48 Placard for demolition.

- Safe Road Access through Zone Zero:

Portoviejo Zone Zero was an area devoted to commercial activities and the closure of this area due to widespread damage had an important economic and social impact on the

population. This assessment was intended to open up the arteries of Zone Zero to allow for a prompt reactivation of economic activity in the city centre. A unique form was drafted by EUCPT experts containing the elements to be removed or propped, or fencing to be erected on buildings alongside roads in order to enable safe access through the roads.

- Detailed Post-Earthquake Safety Assessment of Buildings:

Detailed evaluations follow the same tagging procedure as that noted in the rapid assessment. However, they entail a more thorough review of the building. These were conducted for certain buildings (hospitals, schools, public buildings, etc.) under the direct request of Ecuadorian authorities. A detailed evaluation form was drafted by EUCPT structural experts. The building structural system description benefitted from the experience gathered during the rapid assessments. The form contains both the damage grade and the damage extent to all building components.

Table 6-9 and Table 6-10 summarise the tasks completed between 25 April and 7 May in Portoviejo.

Table 6-9 Number of assessed buildings for rapid and detailed assessment in Portoviejo.

Assessment Type	Building Count	Green	Yellow	Red
Rapid	510	34%	35%	31%
Detailed	159	58%	16%	26%
Total	669	39%	31%	30%

Table 6-10 Number of assessed buildings for safe route access and demolition verification in Portoviejo.

Assessment Type	Building Count
Safe route access	192
Demolition verification	153
Total	345

After performing demolition verification, about 8% of all buildings assessed required demolition. In Pedernales, more than 140 buildings were assessed. The results are shown in Table 6-11.

Table 6-11 Number of assessed buildings in Pedernales.

	Building Count	Green	Yellow	Red
Assessments	144	39%	28%	33%

The contributions of the structural engineers in the EUCPT were mainly i) to facilitate the activities of the Italian, French and UK teams, ii) support local authorities in planning and drafting proper methodologies and tools, and iii) perform direct assessments. The high number of inspected buildings is a proof of the efforts that all teams put in their activities.

6.9.2. EEFIT Mission's Observations on Immediate Structural Inspection of Buildings

The EEFIT team observed many of the stickers placed by the EUCPT and many other organisations, including architects, municipality departments, and even reports in one town of undergraduate engineering students.

It was observed that the traffic light tagging system used in the affected areas varied in interpretation in the different cities and towns. For instance, 'red' in one area was understood by some to signify demolition needed; whereas in other areas it meant 'do not enter' as it was deemed a life safety hazard. Additionally, it was observed that within individual towns, assessors and those responsible for demolition did not appear to have agreed a consensus on the meaning of red tags. With such rapidly moving demolition post-event, it was widely reported that buildings that could have been repaired and retrofitted were demolished unnecessarily (as also reported by the EUCPT).

It was also observed that in some cases people may have inadvertently assumed that a green tag meant that the structure was safe against future earthquakes, as opposed to just being 'safe due to not having experienced significant damage during the previous earthquake'. This is an important distinction that needs to be communicated.

In general, buildings with red and yellow tags were being demolished. In smaller towns like Canoa and Chamanga the demolition process appeared to have almost finished at the time of the EEFIT visit. The team found that in some of the smaller and lower-income areas such as Chamanga and Rio Canoa, the building owners are carrying out their own demolition and reconstruction process. There was a time-limited free demolition service provided by the authorities available in the major urban areas and this may have encouraged hasty decisions by property owners based solely on tag colours and prior to expert structural engineering advice. It was reported that some property owners removed their buildings from the demolition lists after no additional damage occurred to their buildings following the large 18 May aftershocks.

We found in Chamanga that people were demolishing concrete slabs and beams, and leaving the existing reinforcement mesh for pouring new concrete to be able keep using their buildings. It is likely that these works are being carried out without any engineering advice. In rural Rio Canoa people are adding vertical timber posts to supposedly improve or enhance the seismic performance of their buildings; the lateral resistance was not being considered.

In general, the combination of lacking communication of the purpose and meaning behind different tags, and the time-limited free demolition provided may have led to instances of unnecessary demolition, and in some cases over-confidence in a building's seismic capabilities.

7. Infrastructure Performance Observations

Major disruption of infrastructure networks (electricity, communications, transportation, etc.) were reported following the main event and the major aftershocks of the sequence. The EEFIT mission focused on transportation infrastructure damage including roads and bridges due to practical reasons and time available, but also because of the impacts this type of damage has directly on essential emergency response activities.

7.1. Roads

Earthquake damage to roads can be disastrous for two main reasons. First, it can result in casualties and fatalities. Second, it can severely disrupt the initial emergency response by making it difficult to access affected areas.

At the time of the EEFIT mission, all major roads were passable. However, it was evident that a notable number had been impassable for some time after the earthquake due to landslides. This was particularly evident along the coastal road past the towns of Canoa and Jama, and in the mountainous region around San Isidro. Highway 15, near Canoa and Jama, runs along the bottom of steep sided coastal cliffs of friable ground. Shallow landslides had deposited debris across the road (Figure 7-1a). There was no evidence of any slope reinforcement or nets or walls to stop any debris from falling onto and across the road.

In the rural, mountainous region near San Isidro, a number of landslides had extended across, and caused damage to, rural roads (Figure 7-1b). Substantial cracking was also seen on roads (Figure 7-2), particularly near the crest of slopes. Crest amplification of earthquake shaking, and the sloping ground close to the road are likely to have caused this.

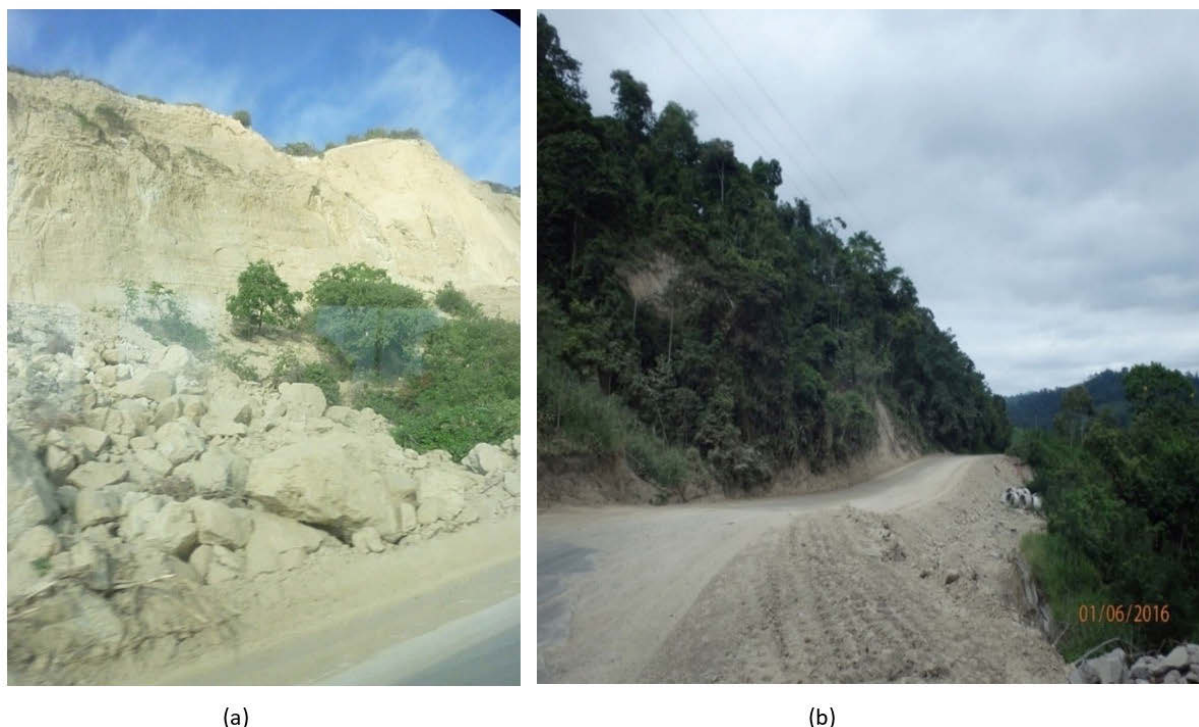


Figure 7-1 Landslide damage to roads (a) on the Highway 15, near Canoa (b) on rural road near San Isidro.



Figure 7-2 Examples of cracking on roads near San Isidro.

Along Highway 383A, east of San Vicente, cracks in the road parallel to the river were observed in a number of locations (Figure 7-3a). These cracks are likely to have been caused by liquefaction induced lateral spreading of the soil below and surrounding the road towards the river. This is consistent with other observations of liquefaction induced damage in the area. The cracks in this section of road were particularly found at the edges and midway of the asphalt. Crack widths of 500mm stretched for more than 10m long in places and settlements of up to 300mm were measured. Damage of a similar nature was also observed in Portoviejo close to the river. Some cracks had been filled in to ensure that the road was passable (Figure 7-3b).



Figure 7-3 Damage to roads due to liquefaction induced lateral spreading (a) Chone river estuary near San Vicente, (b) Portoviejo, close to the Rio Portoviejo.

Along the seafrent in Pedernales, vertical settlements of 100mm were observed for rectangular cross sections parallel to the road (Figure 7-4). This damage is believed to have been caused by liquefaction of poorly compacted fill material. The protrusion of manholes nearby demonstrates the high possibility of liquefaction of the fill material.



(a)



(b)

Figure 7-4 Road damage in Pedernales due to settlement of trench fill (a) and settlement of sand underneath (b).

7.2. Bridges

7.2.1. Mejía Bridge – Highway 39A Portoviejo – Rocafuerte

On the second day of the mission, the team headed to Portoviejo from Manta. Along the highway 39A, the team stopped at the location of the Mejía bridge (-0.9899N; -80.4697E), which crosses the River Portoviejo, to make observations on the bridge's seismic performance after heavy damage was initially reported (see Figure 7-5).

The bridge consists of two separate sections (two lanes and shoulders each side) with a single simply supported span composed of steel girders (see Figure 7-5). The deck is made of composite concrete and metal decking construction. The bridge is supported by reinforced concrete abutments at both ends with monolithic return wingwalls. Gabion walls were provided for retention of ground on one side of the bridge only, at both ends next to the abutments.



Figure 7-5 Mejía bridge – Highway 39A Portoviejo – Rocafuerte (-0.9899N; -80.4697E). Gabion walls provided on this side of the bridge only. Left – from EEFIT mission; Right - from EERI (2016), posted on twitter just after the main shock (<http://www.eqclearinghouse.org/>).

No damage was observed to the bridge structure itself, however, it could be observed that the south approach of the bridge had suffered significant settlements, causing the drivers to pass slowly over the bridge ends. Furthermore, differential settlements of over 1m in the N-S lanes with respect to the S-N lanes were observed (see Figure 7-6 right).



Figure 7-6 Mejía bridge, differential settlement between the two separate sections as seen from the bridge's approach.

The settlements were caused due to the failure of one side of the embankment (see Figure 7-7 left). On the same side of the embankment, the gabion wall at one side of the bridge's abutment had also failed (see Figure 7-7 right).



Figure 7-7 Mejía bridge, embankment (left) and gabion wall (right) failure.

The settlements on the bridges approach had also caused some damage to the bridge's concrete abutment that would possibly need inspection and repair (Figure 7-8).



Figure 7-8 Mejía bridge, damage in abutment.

7.2.2. Los Caras Bridge – Highway 15 between Bahía de Caraquez and San Vicente

The Los Caras bridge (Figure 7-9) opened in 2010 and is one of the biggest infrastructure projects built in Ecuador in recent years. The bridge spans almost 2km across the River Chone between Bahía de Caraquez and San Vicente. It was designed and built by Ecuador's Army Corps of Engineers, with the design led by Prof. Marcelo Romo from Escuela Politécnica del Ejército – ESPE (Polytechnic School of the Army).



Figure 7-9 Los Caras bridge (-0.6094N; -80.4162E), viewed from Bahía de Caraquez. The piles can be seen at low tide.

The bridge consists of a ~2,000m central section and approach sections of ~200m and ~600m on the Bahía de Caraquez and San Vicente sides, respectively. The bridge's central section is supported by 48 piers, each pier consisting of four columns distributed on a square shape. The bridge's deck consists of multiple prestressed precast concrete beams spanning 45m between piers, with cast-in-situ concrete slabs (Figure 7-10). The deck is made continuous by means of cast-in-situ slabs in 180m-long sections, with a movement joint in between continuous sections (see Figure 7-11).



Figure 7-10 Los Caras bridge, 45m-long decks supported by 4-column piers (left) and deck's prestressed concrete beams showing also seismic isolators (right).

One of the key features of the bridge is that it used seismic isolators in between the bridge decks and the piers; the first example of the use of this technology in Ecuador. Triple friction pendulum isolators were used, designed to accommodate around 50-60cm of lateral displacement in any direction. Each pier had four seismic isolators; one on top of each pier column (see Figure 7-12).

The foundations under each pier consisted of 8 or 9 piles. The piles are open-ended steel pipe piles, 1.21 m in diameter with 20 mm wall thickness (Morales, 2016). They vary in length from 32 m to 65 m. The site of the Los Caras bridge is characterised by alluvial deposits consisting of a layer of silty sand down to a depth of 5m to 35m which overlays soft clay (Morales, 2016). Ground investigation data utilised in the analysis for Bahía de Caraquez and its surroundings are shown in Appendix A.



Figure 7-11 Los Caras bridge, continuous connection between main spans (left) and movement joint between main spans (right).



Figure 7-12 Los Caras bridge, location of seismic isolators (left) and close-up view of seismic isolator (right).

The bridge performed well during the seismic shaking, and remained operable immediately after the earthquake. A team from Ecuador's Army Corps of Engineers, including Prof. Marcelo Romo, inspected the bridge after the main shock and found no evidence that required the closure of the bridge. The EEFIT team surveyed the bridge on a boat, accompanied by the bridge design engineer. The observations corroborated that the superstructure of the main section did not suffer any major structural damage. The seismic isolators performed within their deformation capacities in all but one of the bridge's piers, Pier 12 (with piers numbered from 1 to 48, starting at the west side of the bridge).

Prof. Marcelo Romo informed us that a liquefaction assessment was performed during the design stage and highlighted liquefaction potential on the site, which was considered in the design of the foundations. The bridge design engineer believes the high displacements at Pier 12 may be due to liquefaction having occurred at a greater depth than anticipated at that location, causing a greater reduction in lateral capacity than had been designed for. The designer stated that some soil densification remedial works are planned to improve the ground surrounding the foundations of Pier 12. There are no plans to improve the ground around any of the other piers.

A small check of crude liquefaction susceptibility was carried out in order to see how the available geotechnical information could compare with the observed damage of the seismic isolator at Pier 12. The liquefaction susceptibility analysis was conducted for the silty sand layer at the Los Caras bridge using the liquefaction assessment method detailed by Boulanger and Idriss (2014). Based on the information provided by Morales (2016), the N_{60} values at Pier 37 and Pier 40, where ground investigation information was available down to 22m depth, were used (see Table 7-1). The following assumptions were made in the analysis:

- The PGA at the site of the bridge was assumed the same as that measured at the nearest measuring station, located 30km to the southeast of the bridge in Chone.
- The fines content of the silty sand layer was assumed to be 15%.
- The saturated unit weight of the silty sand was assumed to be 19kN/m^3 .

The results of the calculations are presented in Table 7-1 and Figure 7-13. A factor of safety less than 1 indicates that liquefaction is expected to have occurred in the silty sand layer at both piers 37 and 40 of the Los Caras bridge where ground investigation information was available down to 22m depth. The high earthquake induced cyclic stress ratio (CSR) value at a depth of 2m below the ground surface is due to a high ratio of total vertical stress to effective vertical stress at this depth because the water table is well above the ground surface. The appropriateness of the procedure at this depth is questionable.

Table 7-1 Los Caras liquefaction susceptibility analysis. N60 values provided by Morales 2016. Water table 8 m above ground surface (river bed).

Depth (m)	CSR	N60		CRR		Factor of safety against liquefaction	
		Pier 37	Pier 40	Pier 37	Pier 40	Pier 37	Pier 40
2	1.513	25	11	13.314	0.154	8.798	0.102
12	0.596	8	15	0.121	0.126	0.203	0.211
22	0.452	15	10	0.132	0.0927	0.293	0.205

Based on the relatively consistent geological profile from P36 to P42 according to the information provided by the Army’s Corps of Engineers (see Appendix A), liquefaction is likely to have occurred at similar depths along the bridge alignment at least for this segment of the bridge. It is therefore likely that liquefaction occurred in the ground surrounding Pier 12 and may have contributed to the seismic isolator exceeding its maximum design displacement. The specificity of the situation at Pier 12 that has caused higher displacements would need to be looked at in the light of detailed ground investigation information along the entire bridge, including at Pier 12. Lateral stratigraphic variations along the bridge alignment may have induced higher relative displacements on the piles than designed for, and more ground data would allow accurate conclusions to be drawn. The information relative to the liquefaction criteria for which the bridge was designed was not provided, nor the detailed ground investigation report on which the simplified geological model was based. More detailed information and analyses would be required to assess how appropriate the design may be considering the liquefaction risk, and what remediation works may be needed.



Figure 7-13 Los Caras Bridge liquefaction susceptibility analysis.

7.2.3. Footbridges

In the beachside town of Canoa, damage to a relatively recent footbridge was observed. The footbridge crosses the river Canoa on the beach at the northeast end of the town. The footbridge was a suspension bridge with the suspension cables anchored on the southern end to concrete blocks that were built on an abutment, and on the northern end to a concrete anchor block that was built on the ground. Figure 7-14 shows the footbridge that collapsed due to the earthquake.

The footbridge's deck collapsed due to the suspension cables losing their anchorage at the northern end (see Figure 7-15). Evidence found suggests that the southern end anchor blocks experienced uplift during the earthquake (see Figure 7-16). The concrete towers did not appear to suffer significant damage.



Figure 7-14 Collapsed footbridge in Canoa.



Figure 7-15 Footbridge in Canoa, right end anchorage block (left) and suspension cable end that failed at anchorage (right).



Figure 7-16 Footbridge in Canoa, left end anchor points experienced uplift.

In Pedernales, liquefaction-induced lateral spreading caused the pile foundations of Puente Chile, a pedestrian bridge across the river, to rotate towards the river (see Figure 7-17). The foundations had also displaced relative to the bridge deck in the direction parallel to the river. The bridge was still in frequent use by locals at the time of the reconnaissance mission, despite this notable damage to the bridge foundations.



Figure 7-17 Structural damage due to lateral spreading along Rio Portoviejo observed on the rotation and lateral displacement of foundations of the Puente Chile in Pedernales.

7.2.4. Other Bridges

The performance of a number of bridges were effected by liquefaction, particularly due to lateral spreading. This was observed along the Rio Portoviejo at several locations, including but not limited to the Meija Bridge and the Puente Chile.

For example, the movement of soil due to lateral spreading has exposed an increased proportion of the Velasco Ibarra bridge piled foundations (Figure 7-18). This will have reduced the capacity of the bridge abutment foundations, but it has not yet affected the serviceability of the bridge.

The number of bridges observed to have been affected by liquefaction induced damage across the Manabi province highlights a lack of awareness of the risk and/or ground investigation data

to inform the design or a need to better utilise appropriate mitigation methods to avoid liquefaction induced damage.

Bridge damage was also reported in other places of the region hit by the 2016 sequence, including for example a major overpass bridge in Guayaquil (see Figure 7-19), the second most populated city in Ecuador.



Figure 7-18 Movement of soil from around the Velasco Ibarra bridge foundations.



Figure 7-19 Bridge collapse in Guyaquil after the 2016 Ecuador Main Shock (<http://abcnews.go.com/International/drone-video-captures-deadly-earthquake-aftermath-ecuador/story?id=38473672>).

7.3. Other Infrastructure

In addition to roads and bridges, other infrastructure assets were affected by the earthquake.

The port of Manta suffered heavily due to the 16 April earthquake. Although not visited by the EEFIT mission, the field reconnaissance mission by GEER (2016) visited the port days after the earthquake and observed evidence of liquefaction induced damage, including liquefaction-induced lateral spreading and settlement of fill material and natural sediments (see Figure 7-20). These caused shear failures at the heads of a significant number of pile foundations supporting the wharfs, damage to surfaces and walls (GEER, 2016). Lateral spreading of the breakwater also occurred.



Figure 7-20 Manta Port damage (left: aerial photograph showing extent of liquefaction damage at surface; right: port wall damage, showing for scale K. Rollins, at GPS 0o56'29.6"N, 80o43'27.4"E – from GEER, 2016).

The Airport of Manta was also heavily affected by the event, as the control tower collapsed (Figure 7-21). Nevertheless, the airport still operated at a restricted capacity at the time of the mission.



Figure 7-21 Airport control tower collapse.

Electricity and communication networks were also impacted, particularly in more remote areas such as Chamanga or San Isidro, where the loss of communication transmission meant that requests for initial emergency response teams were not able to be made, despite being much needed. Cellular phone companies were very prompt to mobilise teams across the territory and provide access to cellular networks whilst the main communication network underwent repairs.

Oral reports highlighted important issues with waste management in the aftermaths of the event which could potentially lead to significant longer-term issues such as ecological issues from the waste dumped without control in the sea or construction safety issues when the waste is compacted and used as fill for future construction sites.

The mission did not include any surveying of the power, communication services or waste management infrastructure systems because of the time constraints and difficulty to liaise with the critical infrastructure services providers/operators. It is, however, believed that it would be beneficial in future missions to integrate observations and investigations of the damage of such critical networks.

8. Socio-Economic and Community Vulnerability

8.1. Background

This section covers the socio-economic and community vulnerability aspects after the M_w 7.8 16 April 2016 Muisne earthquake in Ecuador. The primary aim of this section is focused on analysing the socio-economic impacts on affected communities, and to understand the post-disaster living conditions in the temporary shelters.

Addressing community vulnerability in disaster risk reduction (DRR) is an important aspect that is being neglected quite often (Wisner *et al.* 2004, Hewitt 1983). ‘No people, no disaster’ – this is the core concept of prioritising disaster-affected people and bringing the social issues to the forefront (Alexander 2000, O’Keefe *et al.* 1976). This section accounts for the risk perception of the people that suffered the catastrophic disaster. The case of the 16 April 2016 earthquake in Ecuador is analysed, covering three different earthquake refugee shelters in Manabí province. The plan was to analyse their living conditions before and after the earthquakes, as well as to understand their perception to recovery from the earthquake disaster.

8.2. Location of the Earthquake Shelters

The surveyed earthquake shelters were located in the Aeropuerto Reales Tamarindos, Portoviejo (1°2’45" South 80°28’5" West), Canoa (0°27’42" South 80°27’8" West) and Pedernales (0°4’43" North 80°2’52" West) cities (Figure 8-1). The camp in Canoa (Figure 8-1b) is administered by a local NGO named – “Deja Tu Huella por Manabí”, and the Ecuadorian Army operates the other two camps. All the families in the camps were provided with electricity, toilets and showers, water supply, medical support, playing grounds, social services, training facilities for adults, and educational facilities for the children, etc. The services were being provided for free. The Ecuador Army identified the locations of the shelters by considering the consequences of the aftershocks and other safety factors. Mostly the shelters were established in previously unoccupied or vacant open spaces where it was easy to get access to transportation and other emergency facilities. For example, in case of Portoviejo, the shelters were located on the runway of a closed airport (Figure 8-2). In Canoa, the shelters were found at an abandoned football field (Figure 8-3).

8.3. Getting Accommodation in the Shelters

Not all affected communities or people were allowed refuge in the shelters. Certain rules and priorities were imposed to get entry clearance into the camps to comply with acute shortages of temporary shelters. First, the authorities from the nearest shelters notified the affected people/victims who were genuinely unable to inhabit in their houses because of total or partial damage to their homes. After receiving notifications, the victims had to make an appointment with the camp inspectors for an assessment of suitability to continue living in their old/damaged houses. If the house was found permanently or temporarily inhabitable, the applicants were placed in a waiting list. Elderly, pregnant women, children and people with disabilities were given priorities in getting a secured accommodation in the shelters.

An alternative to staying in the camp was to apply for a rent subsidy for an apartment in a safe building. The tents were organised in groups or blocks. The shelter administrators maintained strict policy of cleaning and cooking routines.

(a)



(b)



(c)



Figure 8-1 The earthquake refugee shelters in (a) Portoviejo, (b) Canoa, and in (c) Pedernales, Ecuador. Source: Bayes Ahmed, field visit, May-June 2016.



Figure 8-2 The location of the shelters in Aeropuerto Reales Tamarindos, Portoviejo (1°2'45" South 80°28'5" West), Ecuador. Image (a) was acquired on 17 April 2016 and image (b) was captured on 24 April 2016. It depicts the increase of shelters in the airport. Source: The Google Earth Images.

8.4. Facilities in the Shelters

The shelters authorities provided both facilities and activities. Facilities generally consisted of entry clearance provision through an information counter, a kitchen and dining area, sanitation facilities with toilets and showers designated for men and women separately, recreation and education areas, and healthcare desks etc. The services available at the camps included healthcare, potable water, electricity, and laundry. The activities were often related to capacity building, recreation, and providing education. Refugees were liable for running the shelters mainly through food preparation, cleaning and arranging fun/leisure activities. Photographs of the different activities organised in the shelters are illustrated in Appendix D.



Figure 8-3 The location of the earthquake shelters in Canoa, Ecuador. (a) It was a football field back in 2013, and (b) later was converted to temporary shelters. Source: The Google Earth Images.

The camps were highly secured by the military, well organised and no outsiders were allowed to enter. It was possible to find the number of families living in the shelters, including numbers with disabilities and pregnant women, etc. Figure 8-4 shows a notice board summarising the necessary information in a shelter (as on 30 May 2016):

- Total families = 308, Total people = 1193
- Total disabled people: 84, of which 46 men and 38 women
- The age distribution of disabled people in the camp: 1-10 year's = 10, 11-20 years = 14, and 21-100 years = 60
- Pregnant women: 7
- Available sanitation facilities: toilets = 76 and showers = 16
- Total number of tents: 230, Number of tents in use: 217, Available tents: 13.

ALBERGUE EX AEROPUERTO	
Fecha:	30-MAY-2016
Total Familias:	308
Total Personas:	1193
Carpas Total:	230
Carpas Habitadas:	217
Carpas Disponibles:	13
Personas	
Ingresadas:	0
Salieron:	
DISCAPACID.	T.84
T. HOMBRES	46
T. MUJERES	38
T. EDAD 1-10A.	10
11-20A.	14
21-100	60
SAUARIOS	
BATERIAS:	76
Duchas:	16
EMBARAZADAS	
BURBOS C.	A9
Bermello C	C3
Rodriguez M	D2
MOLINAG	C47
Ibarrak	D28
DELGADO O	(5)
BERMELLO	C8

Figure 8-4 Information board of the Aeropuerto Reales Tamarindos camp in Portoviejo [30 May 2016].

8.5. Norms and Regulations

The formal shelters had basic rules and agreements that meant to keep a peaceful and liveable communal environment. Some principle norms were: respect each other, stick to the assigned schedules, keep activities in the designated areas, contribute by taking part in the workgroups, no drug consumption, keep the assigned tent and surrounding areas clean, and collaborate to maintain an exclusive environment for everyone in the shelter.

The informal camp in Canoa was administered by a foundation called “Deja tu huella” from Portoviejo. The foundation helped setting-up the informal camps by providing building materials. The occupants did the building of the camp on their own. They had no access to electricity for two weeks after the earthquake events. Water was being delivered in the camp by a tanker, which was loaded up at a collection centre. Refugees at this camp were threatened with the disruption of water and electricity services subject to refusal to move to the official camps. No serious health issues were reported other than some isolated cases of diarrhoea and/or vomiting. Medical brigades visit this camp regularly that was organised by the foundation.

The refugees prefer to stay in the informal camp rather than the official ones, as the informal camp was closer to their former houses and their local community and the camp restrictions and schedules were more relaxed compared to the other formal camps.

The Pedernales camp was known as “Divino niño”. At the time of visit, it accommodated 721 refugees from 172 families. Most of the camp residents were allowed to go outside during daytime to work or look after their belongings in their former houses. Around 200 refugees remained in the camp during the daytime. The camp was fully built and operational within 2 weeks after the earthquake. There were still 5 tents available at the time of interview. The camp had facilities to keep valuable objects in a safe storage. According to the camp policy, the refugees were constrained to return to their homes after their damaged houses are repaired and made safe to occupy. Homeless people were not provided accommodations in these camps.

8.6. Findings from the Questionnaire Surveying

A structured questionnaire (Appendix E) was prepared after piloting in the Manta earthquake shelter (Figure D1–a). The survey took place from 28 May to 5 June 2016. The survey team comprised of two members: Bayes Ahmed and Nicolás van Drunen. Everth Mera occasionally assisted the team (Figure 8-5). Several focus group discussions were conducted with the affected people and organisations in charge (*i.e.* the Army Corps of Ecuador and the local NGOs that were providing support) to understand the living environment in the camps and the process of recovery from the disaster. A total of 120 families living in those temporary shelters were surveyed using a random sampling method. Questions covered demographic information, economic status, change of occupation, damaged house (year of construction, material type, ownership pattern), damage and losses due to earthquakes, preparedness, problems in the shelters, and future housing and livelihood plans to recover from earthquakes. The findings from the questionnaire surveying are discussed in the following sub-sections. Ethical clearance and necessary permissions were obtained from the concerned officials, institutions, local people/community and the individual interviewee. The questionnaire was anonymous and only non-vulnerable adults willing to participate were surveyed. Each questionnaire interview took around 12-15 minutes to complete. A database was prepared using the SPSS software (version 25) that was used for further analysis.



Figure 8-5 The survey team members conducting questionnaire interview in the shelters in Ecuador.

8.6.1. Demographic Characteristics

Approximately 53% of the respondents were found within the range of 18-65 years; implying they are of working class. The second highest age group was between 6-17 years (30%), followed by 13% aged between 0-5 years, and 4% elderly people (Table 8-1). Average family size was 4. The respondents consisted of 49% male and 51% female (Table 8-2). 47% respondents completed primary education and 39% had secondary education. Only 6% were found illiterate and 5% completed undergraduate level education, see Table 8-3.

Table 8-1 Age group distribution.

Age Group	0-5 Years	6-17 Years	18-65 Years	>65 Years	Row Total
Member 1	1	10	102	7	120
Member 2	13	32	65	4	114
Member 3	19	38	36	2	95
Member 4	10	33	30	2	75
Member 5	8	21	22	2	53
Member 6	7	10	10	1	28
Member 7	3	9	5	1	18
Member 8	3	3	1	1	8
Column Total	64	156	271	20	511
Percentage (%)	12.52	30.53	53.03	3.91	100

Table 8-2 Gender distribution.

Gender	Male	Female	Row Total
Member 1	76	44	120
Member 2	56	58	114
Member 3	42	53	95
Member 4	32	43	75
Member 5	27	26	53
Member 6	10	18	28
Member 7	4	14	18
Member 8	1	7	8
Column Total	248	263	511
Percentage (%)	48.53	51.47	100

Table 8-3 Educational background.

Education Level	Initial	Primary (12 yr.)	Secondary (13-18 yr.)	Under-graduate	Post-graduate	Illiterate	Row Total
Member 1	0	49	51	10	0	9	119
Member 2	5	48	42	7	0	7	109
Member 3	4	45	28	3	0	2	82
Member 4	1	35	26	3	0	2	67
Member 5	3	19	22	0	0	3	47
Member 6	3	12	5	2	0	2	24
Member 7	1	9	5	0	0	1	16
Member 8	0	3	1	0	0	1	5
Column Total	17	220	180	25	0	27	469
Percent (%)	3.62	46.91	38.38	5.33	0	5.76	100

8.6.2. Economic Status

No significant disparity in monthly household income was found. On an average, around 24% of households earned US \$151-300 monthly, and 20% of the households' monthly income had been reported to US \$76-150 (Table 8-4).

Table 8-4 Current monthly household income.

Income Range (US \$)	Frequency	Valid Percent (%)
0-75	12	10
76-150	24	20
151-300	29	24
301-450	24	20
451-700	17	14
>700	13	11
Total	119	100

After the earthquake, a change in primary household occupation was observed. Approximately 55% of the respondents became unemployed, particularly those who were involved in retail business (17%), fishing/fish selling (7%), construction (4%), hotel business (4%), day labour (3%), and tourism (3%) sectors (Table 8-5).

Table 8-5 Changes in occupation pattern.

Before Earthquake			After Earthquake			Changes (%)
Occupation	Freq.	%	Occupation	Freq.	%	
Bartender	2	1.67				-1.67
Beauty Parlour	1	0.83	Beauty Parlour	1	0.83	0
Business	1	0.83				-0.83
Butcher	1	0.83				-0.83
Carpenter	1	0.83				-0.83
Coconut Sell	1	0.83	Coconut Sell	1	0.83	0
Construction	11	9.17	Construction	6	5.00	-4.17
Cook	2	1.67	Cook	1	0.83	-0.84
Day Labour	7	5.83	Day Labour	4	3.33	-2.5
Delivery	1	0.83	Delivery	1	0.83	0
Driver	6	5.00	Driver	4	3.33	-1.67
Engineer	1	0.83				-0.83
Fishermen/ Fish Business	15	12.50	Fishermen/ Fish Business	7	5.83	-6.67
Garments	1	0.83				-0.83
Hotel	5	4.17				-4.17
Housemaid	2	1.67	Housemaid	1	0.83	-0.84
Housewife	6	5.00	Housewife	3	2.50	-2.5
Job Others	2	1.67	Job Others	2	1.67	0
Laundry	1	0.83	Laundry	1	0.83	0
Magazine Sell	1	0.83				-0.83
Professor	1	0.83	Professor	1	0.83	0
Public Job	7	5.83	Public Job	6	5.00	-0.83
Retail	25	20.83	Retail	5	4.17	-16.66
Security Guard	3	2.50				-2.5
Singer	1	0.83	Singer	1	0.83	0
Teacher	2	1.67	Teacher	1	0.83	-0.84
Technician	4	3.33	Technician	2	1.67	-1.66
Tourism	3	2.50				-2.5
Unemployed	5	4.17	Unemployed	71	59.17	+55
Waste Collect	1	0.83	Waste Collect	1	0.83	0
Total	120	100	Total	120	100	0

8.6.3. Information on Damaged Buildings

The victims mainly came from houses built in the 2010s (47%). About 13% of the damaged houses were constructed during the 2000s, and 9% houses were built in the 1980s (Table 8-6). The damaged houses (Table 8-7) were mostly one (46%) and two storeys (45%). Most of the buildings where the surveyed families came from were made of either reinforced concrete (RC) or RC-timber/bamboo (31% and 45%, respectively, Table 8-8). Approximately, 58% of the respondents owned a house, and the remaining used to rent houses (Table 8-9). The refugees in the camps primarily (93%) originated from the city centres/ urban areas (Table 8-10), and most of their houses (65%) were completely destroyed (Table 8-11).

Table 8-6 Construction year of the damaged buildings.

Construction Year		Frequency	Percent	Valid Percent
Valid	<1960s	3	2.5	2.6
	1960s	3	2.5	2.6
	1970s	3	2.5	2.6
	1980s	10	8.3	8.8
	1990s	27	22.5	23.7
	2000s	15	12.5	13.2
	2010s	53	44.2	46.5
Total	114	95.0	100.0	
No Answer		6	5.0	
Total Surveyed		120	100.0	

Table 8-7 Number of floors in the building (before earthquake scenario).

Building Height		Frequency	Percent	Valid Percent	Cumulative Percent
Valid	1	54	45.0	46.2	46.2
	2	53	44.2	45.3	91.5
	3	4	3.3	3.4	94.9
	4	4	3.3	3.4	98.3
	5	2	1.7	1.7	100.0
Total		117	97.5	100.0	
No Answer		3	2.5		
Total Surveyed		120	100.0		

Table 8-8 Building materials (before scenario).

Building Material		Freq.	Percent	Valid Percent	Cumulative Percent
Valid	RC	36	30.0	31.3	31.3
	Timber/Bamboo	27	22.5	23.5	54.8
	RC-Timber/Bamboo	52	43.3	45.2	100.0
	Total	115	95.8	100.0	
Missing	System	5	4.2		
Total		120	100.0		

Table 8-9 Ownership of the house.

Type		Frequency	Percent	Valid Percent	Cumulative Percent
Valid	Owned	69	57.5	57.5	57.5
	Rented	51	42.5	42.5	100.0
	Total	120	100.0	100.0	

Table 8-10 Settlement location (before scenario).

Type		Frequency	Percent	Valid Percent	Cumulative Percent
Valid	Urban	112	93.3	93.3	93.3
	Rural	8	6.7	6.7	100.0
	Total	120	100.0	100.0	

Table 8-11 Household destruction pattern.

Class		Freq.	Percent	Valid Percent	Cumulative Percent
Valid	Completely destroyed	78	65.0	65.0	65.0
	Partially destroyed	42	35.0	35.0	100.0
	Total	120	100.0	100.0	

8.6.4. Existing Problems

The survey participants were asked about earthquake preparedness. Most of them were not prepared (98%) for the earthquake disaster (Table 8-12). Next, they were asked to select top two problems they were facing while living in the shelters. As a first choice, they identified shortage in food (26%) and water (18%) supply as major problems, and 23% reported having no problem (Table 8-13). In the second preference category, 45% said they were not facing further problems, and hot weather (26%) and lack of proper sanitation (15%) were identified as problems from the remaining options (Table 8-14).

Table 8-12 Earthquake preparedness.

Category		Frequency	Percent	Valid Percent	Cumulative Percent
Valid	No	118	98.3	98.3	98.3
	Yes	2	1.7	1.7	100.0
	Total	120	100.0	100.0	

Table 8-13 Problems living in the shelters (first priority).

Category		Frequency	Percent	Valid Percent	Cumulative Percent
Valid	Food	31	25.8	25.8	25.8
	Tent size	7	5.8	5.8	31.7
	Medicine	2	1.7	1.7	33.3
	Water	21	17.5	17.5	50.8
	Toilets & showers	9	7.5	7.5	58.3
	Security	8	6.7	6.7	65.0
	Hot weather	14	11.7	11.7	76.7
	No problem	27	22.5	22.5	99.2
	Others	1	0.8	0.8	100.0
	Total	120	100.0	100.0	

Table 8-14 Problems living in the shelters (second priority).

Category		Frequency	Percent	Valid Percent	Cumulative Percent
Valid	No Problem	54	45.0	45.0	45.0
	Tent size	1	0.8	0.8	45.8
	Medicine	2	1.7	1.7	47.5
	Water	7	5.8	5.8	53.3
	Toilets & showers	18	15.0	15.0	68.3
	Security	2	1.7	1.7	70.0
	Hot weather	31	25.8	25.8	95.8
	Others	5	4.2	4.2	100
	Total	120	100	100	

8.6.5. Future Direction

The respondents were asked to select their top two priorities. They desired to regain employment (59%) and housing facilities (34%) in order to get back to their normal life-style (Table 8-15). Some desired to get loans (25%) and relocate to other places (17%) as a second preference (Table 8-16). Mostly the victims and affected families wanted to live in one-storey buildings (88%, Table 8-17) that are made of timber (52%) and bamboo (17%, Table 8-18). Note that traditional Ecuadorian housing – *Quincha/Bahareque* – in most cases uses a combination of both timber and bamboo (formal housing that just uses timber is very uncommon). Homeowners may not be aware of this mix of materials, and therefore while the results appear to show a preference for timber over bamboo, both preferences may actually be for the same traditional form of house which uses both. Here, ‘timber’ type stands for the housing material is dominated by timber. About 38% of them wanted to stay in the city centre or in urban areas, 31% aspired to relocate to a safer place, and 13% wanted to live in the same place (Table 8-19).

Table 8-15 Recovery plan from the disaster (first priority).

Recovery Plan	Freq.	Percent	Valid Percent	Cumulative Percent
Employment	70	58.3	58.3	58.3
Housing	41	34.2	34.2	92.5
Education	2	1.7	1.7	94.2
Loans	4	3.3	3.3	97.5
Medical-treatment	3	2.5	2.5	100
Total	120	100	100	

Table 8-16 Recovery plan from the disaster (second priority).

Category	Freq.	Percent	Valid Percent	Cumulative Percent
Valid	No Answer	12	10.0	10.0
	Housing	40	33.3	43.3
	Education	10	8.3	51.7
	Loans	30	25.0	76.7
	Relocation	20	16.7	93.3
	Psychological help	7	5.8	99.2
	Other	1	0.8	100.0
	Total	120	100.0	

Table 8-17 Number of floors in the building (after scenario).

Category	Frequency	Percent	Valid Percent	Cumulative Percent
Valid	1	105	87.5	88.2
	2	14	11.7	100.0
	Total	119	99.2	
No Answer	1	0.8		
Total Surveyed	120	100.0		

Table 8-18 Building materials (after scenario).

Category	Frequency	Percent	Valid Percent	Cumulative Percent
No answer	1	0.8	0.8	0.8
Concrete	26	21.7	21.7	22.5
Timber	62	51.7	51.7	74.2
Bamboo	20	16.7	16.7	90.8
RC-timber/brick	6	5.0	5.0	95.8
Steel structure	5	4.2	4.2	100.0
Total	120	100.0	100.0	

Table 8-19 Settlement location (after scenario).

Location	Freq.	%
City/ urban areas	45	37.50
Far from sea	11	9.17
No choice	6	5.00
Out of risk zone	14	11.67
Relocation	23	19.17
Rural	5	4.17
Same place	16	13.33
Total	120	100

8.6.6. Contingency Tabular Analysis

Crosstabulation or contingency tabular analysis was applied to understand the relationship between two or more categorical (nominal or ordinal) variables. An attempt was undertaken to understand the relationships among the building materials, floor height, construction year, and destruction pattern (more results are attached in Appendix F). Strong correlations were found between building material and number of floors ($\chi^2 = 0.000$), and year of construction and number of floors ($\chi^2 = 0.002$). 32% of affected families came from buildings of two storeys made of RC-timber/bamboo (Figure 8-6). Most of the buildings were constructed in the 2010s (47%) followed by 24% in the 1990s (Figure 8-7).

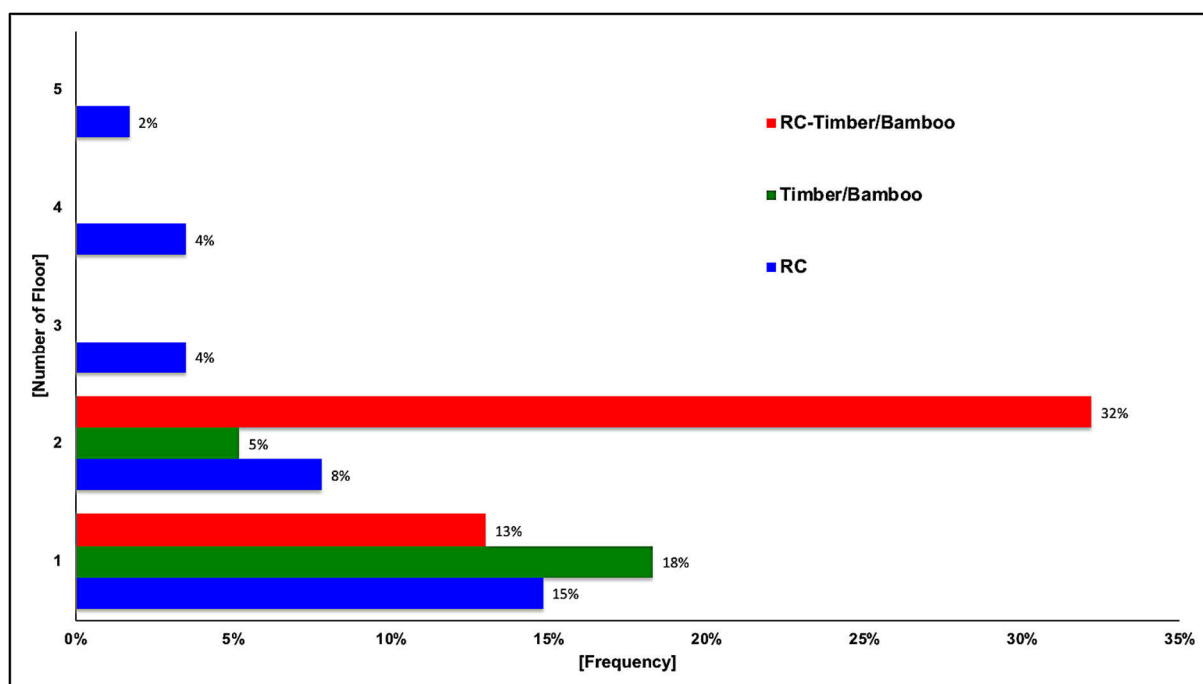


Figure 8-6 Relationship ($\chi^2 = 0.000$) between building material and number of floors (before scenario).

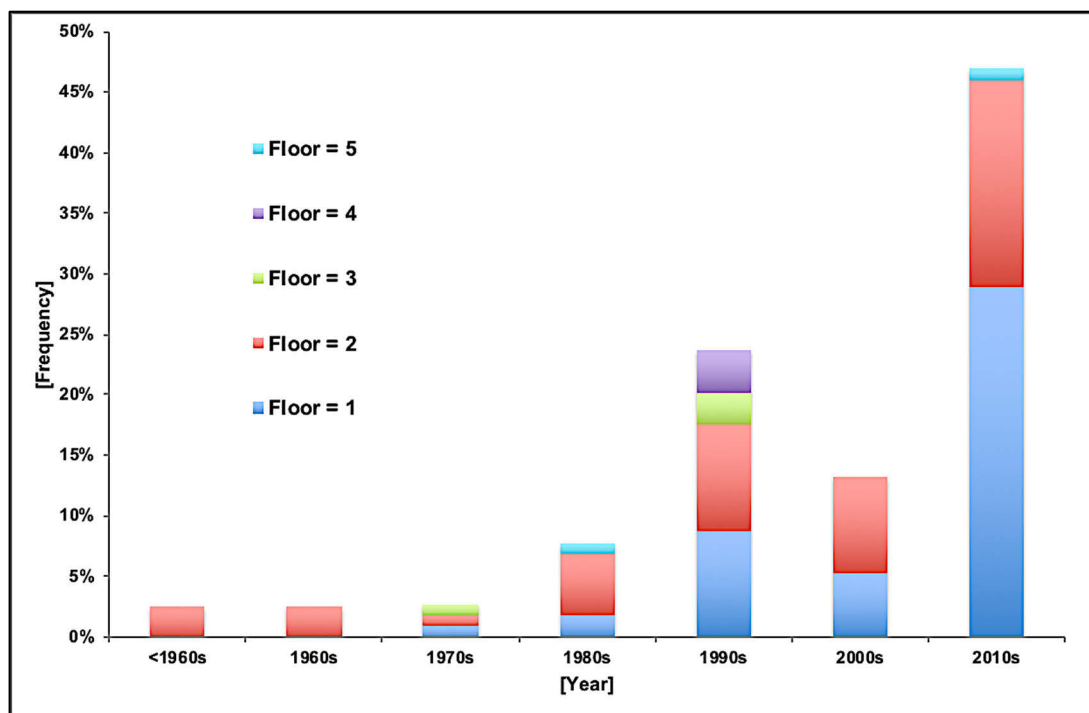


Figure 8-7 Relationship ($\chi^2 = 0.002$) between year of construction and number of floors (before scenario).

A significant percentage of buildings constructed in the 1990s (21%) and 2010s (26%) were destroyed completely (Figure 8-8) and a strong correlation ($\chi^2 = 0.028$) was calculated. Buildings made of RC and RC-timber/bamboo were completely destroyed by 23% and 25% respectively (Figure 8-9), though it shows a weak correlation. Another weak correlation ($\chi^2 = 0.167$) was observed between year of construction and building materials (Figure 8-10). It proves – no relationship exists for construction of buildings with different materials and the year of construction.

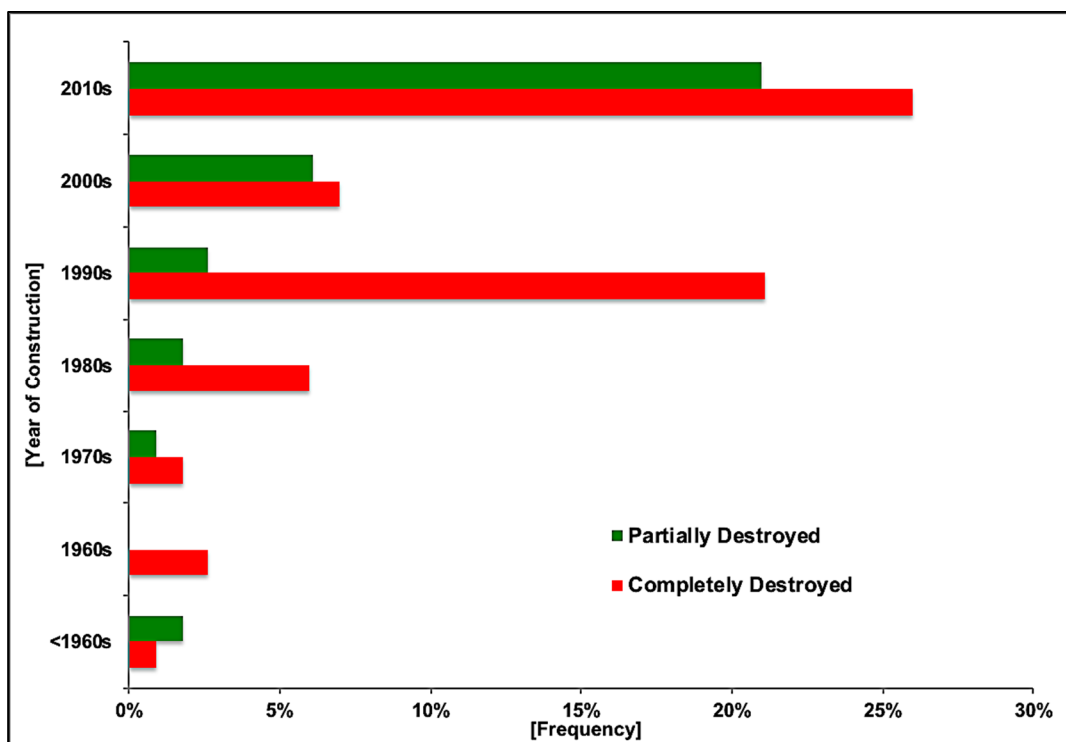


Figure 8-8 Relationship ($\chi^2 = 0.028$) between year of construction and destruction pattern (before scenario).

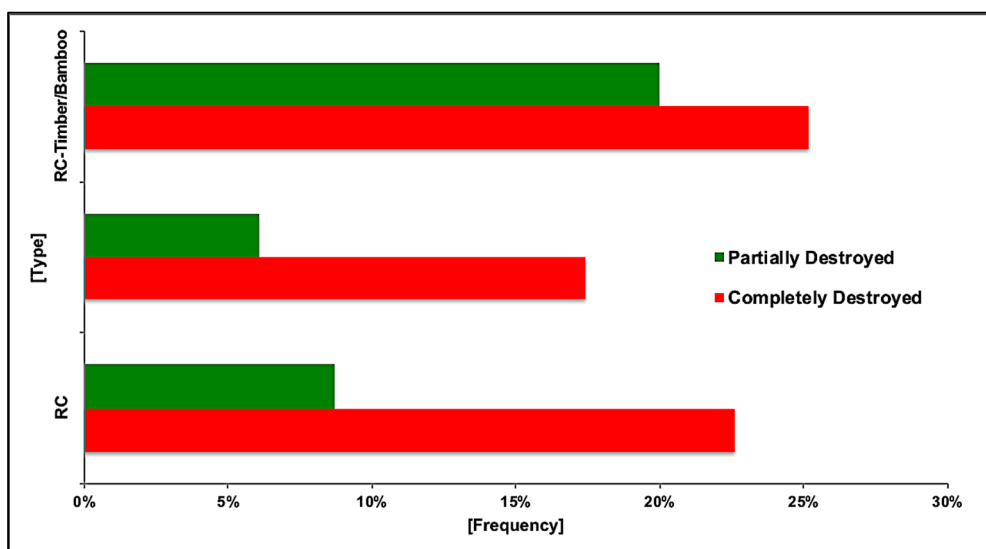


Figure 8-9 Relationship ($\chi^2 = 0.254$) between building material and destruction pattern (before scenario).

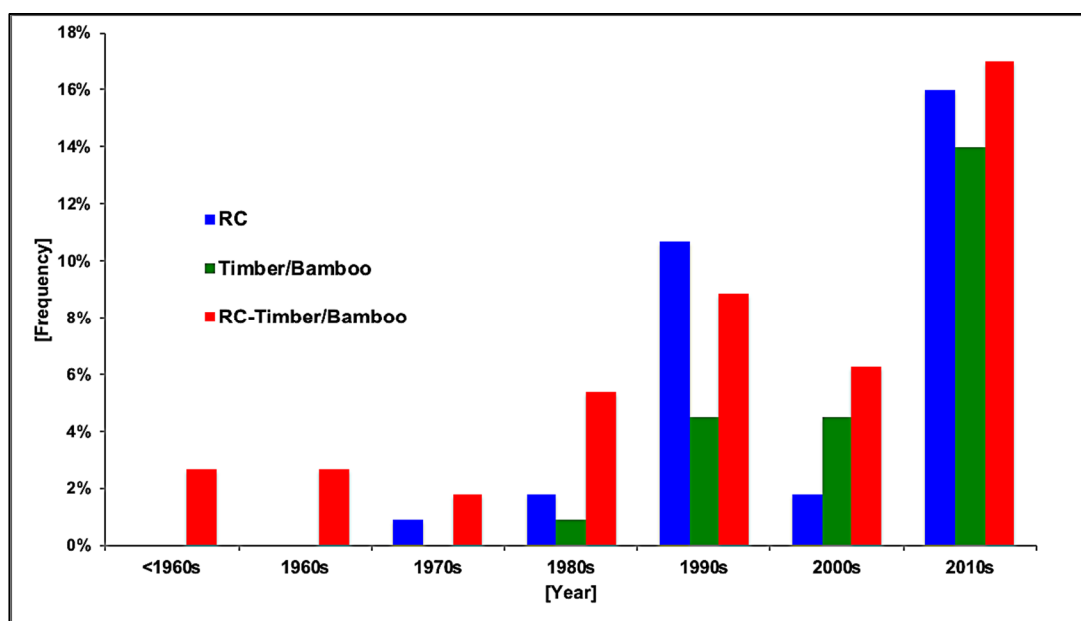


Figure 8-10 Relationship ($\chi^2 = 0.167$) between year of construction and building materials (before scenario).

A strong correlation ($\chi^2 = 0.006$) was calculated for building materials before and after the earthquakes (Table 8-20). Some of the victims from the RC-timber/bamboo houses wanted to relocate in houses predominantly made of timber (21%) or bamboo (13%).

Table 8-20 Building material before and after scenario.

Building Material (Before)	Building Material (After)					Total
	Concrete	Timber	Bamboo	Timber & Brick Mix	Steel Structure	
RC	8.7%	19.1%	0.9%	2.6%		31.3%
Timber/ Bamboo	7.0%	13.0%	2.6%	0.9%		23.5%
RC-Timber/ Bamboo	5.2%	20.9%	13.0%	1.7%	4.3%	45.2%
Total	20.9%	53.0%	16.5%	5.2%	4.3%	100.0%

	Value	df	Asymp. Sig. (2-sided)
Pearson Chi-Square	21.333 ^a	8	0.006
Likelihood Ratio	24.769	8	0.002
N of Valid Cases	115		

a. 7 cells (46.7%) have expected count less than 5. The minimum expected count is 1.17.

At large, the respondents urged to be relocated in one-storey buildings (88%). Approximately 37% of the 88% came from two-storey buildings. It shows a strong relationship with a Pearson Chi-Square (χ^2) value of 0.045 (Table 8-21).

Table 8-21 Floor height before and after scenario.

Number of floors (before)	Number of floors (after)		Total
	1	2	
1	44.0%	2.6%	46.6%
2	37.1%	7.8%	44.8%
3	1.7%	1.7%	3.4%
4	3.4%		3.4%
5	1.7%		1.7%
Total	87.9%	12.1%	100.0%

	Value	df	Asymp. Sig. (2-sided)
Pearson Chi-Square	9.750 ^a	4	0.045
Likelihood Ratio	8.811	4	0.066
Linear-by-Linear Association	1.293	1	0.255
N of Valid Cases	116		

a. 6 cells (60.0%) have expected count less than 5. The minimum expected count is 0.24.

The respondents' decision on relocating to a new house made of a particular building material (in this case timber and/or bamboo mixed) was found highly dependent (P -value = 0.002) on their past experiences related to their monthly household income, house destruction pattern; and ownership, number of floors, building materials and year of construction of their previous houses. In all the cases, the null hypothesis was found true (i.e. the categorical variables are independent; P -value > 0.05) after applying the Chi-square statistical tests (see the tables below; under Table 8-22).

Table 8-22 Results from the linear regression modelling.

Model Summary ^b								
Model	R	R Square	Adjusted R Square	Std. Error of the Estimate	Change Statistics			
					R Square Change	F Change	df1	df2
1	0.425 ^a	0.181	0.134	1.036	0.181	3.855	6	105

Model Summary ^b	
Model	Change Statistics
	Sig. F Change
1	0.002

a. Predictors: (Constant), Monthly household income (US\$), House destroyed, Ownership of the house, Building materials (Old), Year of building construction, Number of floors in the building

b. Dependent Variable: Building materials (New)

ANOVA ^a						
Model		Sum of Squares	df	Mean Square	F	Sig.
1	Regression	24.806	6	4.134	3.855	0.002^b
	Residual	112.613	105	1.073		
	Total	137.420	111			

a. Dependent Variable: Building materials (New)

b. Predictors: (Constant), Monthly household income (US\$), House destroyed, Ownership of the house, Building materials (Old), Year of building construction, Number of floors in the building

Coefficients ^a							
Model		Unstandardised Coefficients		Standardised Coefficients	t	Sig.	95.0% Confidence Interval for B
		B	Std. Error	Beta			Lower Bound
1	(Constant)	2.542	0.656		3.874	0.000	1.241
	Building materials (old)	0.280	0.073	0.354	3.823	0.000	0.135
	Ownership of the house	-0.367	0.217	-0.162	-1.692	0.094	-0.797
	Year of building construction	0.002	0.063	0.003	0.032	0.974	-0.122
	Number of floors in the building	-0.092	0.137	-0.070	-0.668	0.506	-0.364
	House destroyed	-0.347	0.215	-0.148	-1.611	0.110	-0.774
	Monthly household income (US\$)	0.000	0.000	0.037	00.404	0.687	0.000

Coefficients ^a		
Model		95.0% Confidence Interval for B
		Upper Bound
1	(Constant)	3.843
	Building materials (old)	0.424
	Ownership of the house	0.063
	Year of building construction	0.126
	Number of floors in the building	0.180
	House destroyed	0.080
	Monthly household income (US\$)	0.001

a. Dependent Variable: Building materials

8.7. Summary of the Social Survey Findings

The major findings are as follows:

- The average family size was 4, with persisting gender balance.
- The respondents were adult working-class (18-65 years) and without higher educational background (mostly completing primary level).
- The average household income was US \$75-300/month.
- They were involved in retail business, fishing, construction works, and day-laboured jobs. Most of them became unemployed after the disaster and their first priority was to continue their livelihood activities.
- The affected people were mostly house-owners from one-storey buildings made of RC-timber/bamboo.
- Most buildings were constructed in the 1990s and 2010s, and had one and two floors.
- The residents were found to be happy with the facilities and services provided in the shelters/camps.

- Those surveyed were not prepared for this earthquake disaster at all. They suggested one-storey buildings made of timber/bamboo as their preferred future building, and to continue their livelihood in urban areas.
- The majority of the victims from multi-storey buildings expressed their desire to relocate in single-storey buildings made of primarily timber and/or bamboo.
- The decision to relocate in a safer house combining with a particular building material (mixed-timber/bamboo) was found to be related to their past experiences.

The findings of this research only represent the risk perception of the affected people who were residing temporarily in the three earthquake-surviving shelters in Manabí province, Ecuador. It should be noted that all the victims or affected family members were not accommodated or did not want to take refuge in the shelters. Many did not take refuge in the shelters for various reasons – e.g. the location of the camp being far away from their damaged houses. Other factors include staying close to their local community, protect their belongings from looting or continue caring for their cattle/pets and family members with limited mobility. It is also worthwhile noting that the wealthiest amongst the affected community generally had other options, for example temporarily living at friends or neighbours whilst their house was being repaired. The views and opinions as discussed in this chapter do not necessarily represent the affected community as a whole. This was a pilot study based on a reconnaissance type questionnaire surveying under a limited time period and funding restriction. Expanding this survey effort to a participatory survey incorporating all possible vulnerable community groups and vulnerability dimensions would be beneficial to gain a broader and more comprehensive understanding of how the community was affected (as discussed in Ahmed and Kelman, 2018) by the catastrophic earthquake event.

It is equally important to note that the survey was conducted just six weeks after the earthquake disaster. It was difficult to interview a good number of families as they were mentally traumatised or some were physically injured. The survey team had to deal with other regulatory, emotional and ethical restrictions to question the refugees. Considering all the limitations, the questionnaire was designed to be as flexible as possible and the sample size was also limited to only 120 victim families in some of the pre-selected temporary camps. The survey would have benefited from allowing more time and interactions with the affected people to apply a more diverse and comprehensive set of participatory surveying tools to achieve further representative results.

References

- Adger, W.N. (2006). Vulnerability. *Glob. Environ. Chang.* 16, 268–281.
- Aguiar (1982). Cuantificación de la amenaza sísmica del Ecuador en términos probabilísticos y mapa de zonificación. Tesis de grado para obtener el título de Master en Ciencias. Universidad Central de Venezuela, 187 p., Caracas.
- Aguiar (2008). *Análisis Sísmico de Edificios*, 1st Ed. Escuela Politécnica del Ejército, Quito, Ecuador.
- Ahmed, B., Kelman, I. (2018). Measuring Community Vulnerability to Environmental Hazards: A Method for Combining Quantitative and Qualitative Data. *Natural Hazards Review*, 19(3), 04018008.
- Alexander D., Magni M. (2013). Mortality in the L'Aquila (Central Italy) Earthquake of 6 April 2009: A Study in Victimisation. *PLOS Currents Disasters*. doi: 10.1371/50585b8e6efd1.
- Alexander, D. (2000). *Confronting catastrophe: New perspectives on natural disasters*. Terra Publishing, Harpenden, England, 282 pp.
- Alexander, D.E. (2014) Communicating earthquake risk to the public: the trial of the “L'Aquila Seven”. *Nat Hazards* 72: 1159. doi:10.1007/s11069-014-1062-2

- Alexander, D.E. (2013). Resilience and disaster risk reduction: An etymological journey. *Nat. Hazards Earth Syst. Sci.* 13, 2707–2716.
- Almufti, I., Willford, M. (2013). REDi Rating System. London: Ove Arup and Partners.
- ATC-20 (1989). Procedures for Postearthquake Safety Evaluation of Buildings. Applied Technology Council, California, USA.
- Bachmann, R. (2001). The Caribbean plate and the question of its formation. Institute of Geology, University of Mining and Technology Freiberg Department of Tectonophysics
- Baldock, J.W. (1982). *Geologica del Ecuador: Boletín de la explicación del mapa Geológico de la república del Ecuador* esc 1:100000. 70p.
- Bard, P (1999). Microtremor measurements: A tool for site effect estimation? In: IRIKURA, KUDO, OKADA SASATANI, (Eds.) *The Effects of Surface Geology on Seismic Motion*. Netherlands: Balkema. 1251-1279.
- Benford, B., DeMets, C., Calais, E. (2012). GPS estimates of microplate motions, northern Caribbean: evidence for a Hispaniola microplate and implications for earthquake hazard: *Geophysical Journal International*, v. 191, p. 481-490
- Benítez, S.B. (1995). Evolution géodynamique de la province côtière sud-équatorienne au Crétacé supérieur-Tertiaire. *Géol. Alp*, 71: 3–163.
- BGS (2016a): Preliminary Co-Seismic Landslide Inventory Map for Portoviejo, Ecuador. BGS, Keyworth, UK.
- BGS (2016b). Preliminary Co-seismic Landslide Inventory Map for Bahía de Caráquez, Ecuador. BGS, Keyworth, UK.
- Bird, P. (2003). An updated digital model of plate boundaries. *Geochemistry, Geophysics, Geosystems*, 4(3).
- Bommer, J., Bird, C., Crowley, H. (2006). Earthquake losses due to ground failure (liquefaction and landslides). First European Conference on Earthquake Engineering and Seismology. Geneva, Switzerland, 3-8 Sept. 2006.
- Boulanger, R.W., Idriss, I.M. (2014). CPT and SPT Based Liquefaction Triggering Procedures. Report No. UCD/CGM-14/01 University of California, Davis, California.
- Boulanger, R.W., Idriss, I.M. (2006). Liquefaction susceptibility criteria for silts and clays. *Journal of Geotechnical and Geoenvironmental Engineering*, 132(11), pp. 1413-1426.
- Bourgeois, J (2013). A Review on Tectonic Record of Strain Buildup and Stress Release across the Andean Forearc along the Gulf of Guayaquil-Tumbes Basin (GGTB) near Ecuador-Peru Border. *International Journal of Geosciences*, 4, 618-635.
- Brennan, A.J., Madabhushi, S.P.G. (2009). Amplification of seismic accelerations at slope crests. *Canadian Geotechnical Journal*, 46. pp. 585-594. ISSN 0008-3674
- Brzev, S., Scawthorn, C., Charleson, A., Allen, L., Greene, M., Jaiswal, K., Silva, V. (2013). GEM Building Taxonomy Version 2.0. Pavia: GEM.
- BSSC (2004). NEHRP recommended provisions for seismic regulations for new buildings and other structures (FEMA 450). Part 1: provisions.
- Carazas-Aedo, W., Rivero-Olmos, A. (2013). A Wattle and Daub Anti-seismic Construction Handbook. [Online]. Available at: www.misereor.org/fileadmin/redaktion/Wattledaub%20handbook%20anti-seismic%20construction.pdf (Accessed: May 2013)
- Cardona, A., Valencia, V. A., Bayona, G., Duque, J. (2011). Early-subduction-related orogeny in the northern Andes: Turonian to Eocene magmatic and provenance record in the Santa Marta Massif and Rancheria Basin, Northern Columbia. *Terra Nova*, 23, 26-34.

Cediel, F., Shaw R. P., Cañales C. (2003). Tectonic assembly of the Northern Andean Block. The Circum-Gulf of Mexico and the Caribbean: Hydrocarbon habitats, basin formation, and plate tectonics: AAPG Memoir 79, 815–848.

Chian, S.C., Tokimatsu, K., Madabhushi, S.P.G. (2014). Soil liquefaction-induced uplift of underground structures: physical and numerical modelling. *Journal of Geotechnical and Geoenvironmental Engineering*, Vol. 140, No. 10, 04014057.

Chlieh, M., Mothes, P.A., Nocquet, J.-M., Jarrin, P., Charvis, P., Cisneros, D., Font, Y., Collot, J.-Y., Villegas-Lanza, J.-C., Rolandone, F., Vallée, M., Regnier, M., Segovia, M, Martin, X., Yepes, H. (2014). Distribution of discrete seismic asperities and aseismic slip along the Ecuadorian megathrust. *Earth and Planetary Science Letters* 400, 292–301

Collot, J. Y., Agudelo, W., Ribodetti, A., Marcaillou, B. (2008). Origin of a crustal splay fault and its relation to the seismogenic zone and underplating at the erosional north Ecuador–south Colombia oceanic margin. *Journal of Geophysical Research: Solid Earth* (1978–2012), 113(B12).

Collot, J.-Y., Charvis, P., Gutscher, M.A., Operto, S. (2002). Exploring the Ecuador-Colombia active margin and interplate seismogenic zone: Eos (Transactions, American Geophysical Union), v. 83, p. 189–190.

Colmenares, L., Zobak, M.D. (2003). Stress field and seismotectonics of northern South America. *Geology*. v. 31; no. 8; p. 721–724.

David Alexander. "A Tale of Three Cities and Three Earthquake Disasters" (2012). URL: http://works.bepress.com/david_alexander/2/

D'Ayala, D. (2013). *Guidelines for Analytical Vulnerability Assessment*, Pavia: GEM Foundation.

DeMets, C., Wiggins-Grandison, M. (2006). Deformation of Jamaica and motion of the Gonâve microplate from GPS and seismic data. *Geophysics Journal International*, v. 168, p. 362-378

Deniaud, L., Baby, P., Basile, C., Ordonez, M., Mascle, G., Montenegro, G. (1999). Neogene evolution of the main Ecuadorian fore-arc sedimentary basins and sediment mass-balance inferences. Fourth ISAG. Goettingen, Germany, 04-06/10/1999.

Echeverria, M. (2016). Reporte de visita tecnica a san vicente – Manabi. Part 2. Interpretacion fotogeologica. 5 May 2016, Presentation.

Eguez, A., Alvarado, A., Yepes, H. (2003). *Map of Quaternary Faults and Folds of Ecuador and Its Offshore Regions*. USGS, Reston, USA.

Evan, C.D.R, Whittaker, J.E. (1982). The geology of the western part of the BorbonBasin, North-West Ecuador. In: publ. Geol. Soc. London. Spec., trench-forearc Geology, 10, p.191-200.

Farias A, Nasser A, Turel M, Ghosh J, Lai T, Yin YY (2015). The Application of a Uniform Framework of Seismic Vulnerability Assessment to South American Countries. SECED 2015 Conference: Earthquake Risk and Engineering towards a Resilient World. 9-10 July 2015, Cambridge, UK.

Faucher, B., Savoyat, E. (1973). Esquisse geologique des Andes de l'Equateur. *Revue de physique et de geologie dynamique*, Paris (2), vol. XV, fasc. 1-2, pp 115-142.

Font, Y., Segovia, M. Vaca, S., Theunissen, T. (2013). Seismicity patterns along the Ecuadorian subduction zone: new constraints from earthquake location in a 3-D a priori velocity model. *Geophysics Journal Int.*, 193, 263–286.

Franco, G., Stone, H., Ahmed, B., Chian S.C., Hughes, F., Jirouskova N., Kaminski, S., Lopez, J., van Druenen, N.G., Querembás, M. (2017). The April 16 2016 Mw7.8 Muisne Earthquake in Ecuador – Preliminary Observations from the EEFIT Reconnaissance Mission of May 24 - June 7. 16th WCEE, 2017, Santiago, Chile.

Gailler, A., Charvis, P., and Flueh, E. R. (2007). Segmentation of the Nazca and South American plates along the Ecuador subduction zone from wide angle seismic profiles. *Earth and Planetary Science Letters*, 260(3), 444-464.

- GEER (2016). GEER-ATC Earthquake Reconnaissance, April 16th 2016, Muisne, Ecuador V1. Available at http://www.geerassociation.org/component/geer_reports/?view=geerreports&id=77&layout=default (Accessed 28/10/2016)
- GEM Secretariat (2015). South America Risk Assessment (SARA) Final Report 2015, Version 1.0., December 2015. SARA Project.
- Geoestudios, SA, (2016). Measurement of shear wave velocity in strong motion stations from Ecuador, Data collected for GEER, Geoestudios, SA.
- Geoestudios, SA, 2016. Post-earthquake borings compilation.
- Goretti, A., Molina Hutt, C. and Hedelung, L. (2017). "Post-Earthquake Safety Evaluation of Buildings in Portoviejo, Manabí following the M7.8 Coastal Ecuador Earthquake of 16 April 2016." *International Journal of Disaster Risk Reduction*.
- Grunthal, G., Musson, R., Schwarz, J., Stucchi, M. (1998). European Macroseismic Scale 1998 (pp. 1–101). Luxembourg: European Seismological Commission.
- Guillier, B., Chatelain, J., Jaillard, E., Yepes, H., Poupinet, G., Fels, J. (2001). Seismological evidence on the geometry of the Orogenic System in central-northern Ecuador (South America). *Geophysics Research Letters*, 28 (19), 3749–3752.
- Gutiérrez, J. (2000). Technical Report 19: Structural adequacy of traditional bamboo housing in Latin America. Beijing: INBAR
- Gutscher, M.-A., Malavieille, J., Lallemand, S., Collot, J.-Y (1999). Tectonic segmentation of the North Andean margin: impact of the Carnegie Ridge collision. *Earth and Planetary Science Letters* 168 (1999) 255–270
- Gutscher, M.-A. (2002). Andean subduction styles and their effect on thermal structure and interplate coupling. *Journal of South American Earth Sciences*, 15(1), 3-10.
- Hayes, G., Wald, D., Johnson, R. (2012). Slab1. 0: a three-dimensional model of global subduction zone geometries. *Journal of Geophysics Research*, 117 (B1), 1-15.
- Hewitt, K. (2013). *Interpretations of Calamity from the Viewpoint of Human Ecology*, 1st ed.; Allen & Unwin: London, UK,.
- Hidroplan (2016). Estudio de geotecnia, mecanica de suelos, prediseño estructural del sistema de cimentacion y sistema de contencion. Proyecto: "estudios complementarios de implantacion, estudios de geotecnia, mecanica de suelos y obtencion de la licencia ambiental para el centro de atencion ciudadana "cac" de la ciudad.
- Hughes, R. A., Pilatasig, L. F. (2002). Cretaceous and Tertiary terrane accretion in the Cordillera Occidental of the Ecuadorian Andes. *Tectonophysics*, v. 345, p. 29 - 48.
- IG (2016). <http://www.igeqn.edu.ec/eq20160416-informes-noticias>
- IGM (2016). Set of aerial and satellite-based imagery rapid damage assessments for main cities in Manabi following the 2016 April 16th Main Shock.
- INEN (1976). Guia popular de construccion sismo resistente. Instituto Ecuatoriano de Normalización, Quito, Ecuador.
- Ishihara, K. (1993). Liquefaction and flow failure during earthquakes, *Géotechnique*, 43(3), pp. 351-451
- Kaminski, S. (2013). Engineered bamboo houses for low-income communities in Latin America. *The Structural Engineer* 91(10): 14–23.
- Kanamori, H., Cipar, J. J. (1974). Focal process of the Great Chilean earthquake May 22, 1960. *Physics of the Earth and Planetary Interiors*, 9(2), 128-136.

- Koseki, J., Matsuo, O., Koga, Y. (1997). Uplift behaviour of underground structures caused by liquefaction of surrounding soil during earthquake. *Soils and Foundations*, 37(1), pp. 97-108.
- Krinitzky, E. L., Hynes, M. E. (2002). The Bhuk, India, earthquake: Lessons learned for earthquake safety of dams on alluvium. *Engineering Geology*, 66(3-4), pp. 163-196.
- Lewis J. (2012). The Good, The Bad and The Ugly: Disaster Risk Reduction (DRR) Versus Disaster Risk Creation (DRC). *PLOS Currents Disasters*. doi: 10.1371/4f8d4eaec6af8.
- Lewis, J. (1999). *Development in Disaster-Prone Places: Studies of Vulnerability; Intermediate Technology*: London, UK.
- Litherland, M., Aspden, J., Jemielita, R.A. (1994). The metamorphic belts of Ecuador. Nottingham, British Geological Survey, Overseas Memoir, No. 11, 147 p.
- Lonsdale, P. (2005). Creation of the Cocos and Nazca plates by fission of the Farallon plate. *Tectonophysics*, 404(3-4), 237-264.
- López M., Bommer J., Méndez P. (2004). The seismic performance of bahareque dwellings in El Salvador, 13th World Conference on Earthquake Engineering. Vancouver, Canada, 1-6 August 2004
- LUP (2016). Draft ground Investigation results at sites Bahia, Jama and Canoa. Personal Communication.
- Luzieux, L.D., Heller, F., Spikings, R., Vallejo, C., and Winkler, W. (2005). Origin and Cretaceous tectonic history of the coastal Ecuadorian forearc between 1°N and 3°S: Paleomagnetic, radiometric and fossil evidence. *Earth and Planetary Science Letters*, 249: 400–414. Lonsdale, P. (1988). Structural Pattern of the Galapagos Microplate and Evolution of the Galapagos Triple Junctions, *Journal of Geophysical Research*, 93(B11), 13551-13574.
- Madabhushi, S.P.G., Saito, K., Booth, E.D. (2013). EEFIT mission to Haiti following the 12th January 2010 earthquake. *Bulletin of Earthquake Engineering*, 11(1), pp. 35-68.
- Michaud, F., Pazmino, N., Collot, J. (2009). El karst submarino de mega depresiones circulares de la Cordillera de Carnegie (Ecuador): posible origen por disolución submarina. In: Collot J, Sallares V, Pazmino N(eds) *Geología y Geofísica Marina y Terrestre del Ecuador*, 1st edn. Argudo & Asociados, Guayaquil. Ecuador.
- MICROMED (2013a). Grilla ver 6.4. spectral and HVSR analysis-user's manual. Treviso, Italy: Micromed.
- MICROMED (2013b). Tromino. [Online] Available from: www.tromino.eu [Accessed 16/10/14].
- Morales, E. (2016). GEER-rapid report, Musine Earthquake, Personal communication.
- Nakamura, Y. (1989). Method for dynamic characteristics estimation of subsurface using microtremor on the ground surface. *Quarterly Report of RTRI (Railway Technical Research Institute) (Japan)*, 30(1), 25-33.
- Nelson, C. E. (2011). The metallogenic evolution of the Greater Antilles. *Geologica Acta*, 9.3, 229-264.
- Neville A (1995). *Properties of Concrete*, Fourth Edition, Longman, Harlow, UK
- Norabuena, E. O., Dixon, T. H., Stein, S., Harrison, C. G. A. (1999). Decelerating Nazca-South America and Nazca-Pacific plate motions. *Geophysical Research Letters*, 26(22), 3405-3408.
- O'Keefe, P., Westgate, K., Wisner, B. (1976). Taking the naturalness out of natural disasters. *Nature*, 260, 566-567.
- Parra (2016). Desarrollos metodológicos y aplicaciones hacia el cálculo de la peligrosidad sísmica en el Ecuador continental y estudio de riesgo sísmico en la ciudad de Quito.
- Parra, H., Benito, M.B., Gaspar-Escribano, J.M. (2016): Seismic hazard assessment in continental Ecuador. *Bulletin of Earthquake Engineering*, 1-31.
- Ramos, V.A. (1999). Plate tectonic setting of the Andean Cordillera. *Episodes*, 22(3), 183-190.

- Ray, J. S., Mahoney, J. J., Duncan, R. A., Ray, J., Wessel, P., Naar, D. F. (2012). Chronology and geochemistry of lavas from the Nazca ridge and Easter seamount chain; an approximately 30 myr hotspot record. *Journal of Petrology*, 53(7), 1417-1448.
- Reyes (2008). Quantification relative du soulèvement de la cordillere cotiere (equateur) a partir de la geomorphologie sur MNT. Thesis Report.
- Reyes, P. and Michaud, F. (2012). Mapa Geologico de la Margen Costera Ecuatoriana. Escuela Politécnica Nacional, Quito, Ecuador.
- Ripalda, O. (2007). Boring logs for Port of Manta Expansion.
- Romo, M. (2016). Personal Communication.
- Rossetto, T. (2014). Guidelines for Empirical Vulnerability Assessment, Pavia: GEM Foundation
- Sanclémente, E. (2014). Seismic imaging of the structure of the central Ecuador convergent margin: relationship with the inter-seismic coupling variations. PhD Thesis. Université de Nice-Sophia Antipolis - UFR sciences. École Doctorale de Sciences Fondamentales et Appliquées
- Searle, R. C., Francheteau, J. (1985). Morphology and Tectonics of the Galapagos Triple Junction, *Marine Geophysical Researches*, 8, 95-129.
- Searle, R. C., Francheteau, J. (1985). Morphology and Tectonics of the Galapagos Triple Junction, *Marine Geophysical Researches*, 8, 95-129.
- Sevilla, J. (2016). Reporte de visita tecnica a san vicente – Manabi. Part 1. Aspectos geologicos, sismologicos y Cartograficos. 5 May 2016, Presentation.
- Smith, D. K., Schouten, H., Cann, J. R., Zhu, W., Montesi, L. G., Mitchell, G. A. (2009). The Galapagos Microplate Revealed, American Geophysical Union Fall Meeting 2009.
- Sobolev, S. V., & Babeyko, A. Y. (2005). What drives orogeny in the Andes? *Geology (Boulder)*, 33(8), 617-620.
- Tallet-Williams, S., Gosh, B., Wilkinson, S., Fenton, C., Burton, P., Whitworth, M., Datla, Franco, G., Trieu, A., Dejong, M., Novellis, V., White, T., Lloyd, T. (2016). Site amplification in the Kathmandu Valley during the 2015 M7.6 Gorkha, Nepal earthquake. *Bull Earthquake Eng.* 14:3301–3315.
- Tallett-Williams, S., Fenton, A., Booth, D., Clark, R.A., Raines, M.G, Ward, D. (2015). The Value of Alternative Geophysical Methods in Determining Shear Wave Profiles for Critical Infrastructure. 6th International Conference on Earthquake Geotechnical Engineering 1-4 November 2015 Christchurch, New Zealand.
- Tao, C., Li, H., Wu, G., Su, X., Zhang, G. (2011). First Hydrothermal Active Vent Discovered on the Galapagos Microplate, American Geophysical Union Fall Meeting 2011.
- Trenkamp, R., Kellogg, J., Freymuller, J., Mora, H. (2002). Wide plate margin deformation, South Central America and Northwestern South America, CASA GPS observations. *Journal of South American Earth Sciences*, (2), 157–17.
- Tschopp, H.J. (1953). Oil exploration in the Oriente, Ecuador, 1938–1950. *AAPG Bulletin*, No. 37, p. 2303 - 2347.
- UNITAR-UNOSAT (2016). Preliminary Satellite Based Damage Assessment Report 29 April 2016. UNITAR, Geneva, Switzerland.
- USGS (2014). Seismic Hazard Sumamry report on South America
- USGS (2016). General Summary of the M7.8 Muisne Event. USGS, Reston, USA.
- USGS (2016). Largest Earthquakes in the World Since 1900. https://earthquake.usgs.gov/earthquakes/world/10_largest_world.php
- van Drunen, N., Cangas, A., Rojas, S., Kaminski, S. (2016) Reporte postsismo sobre estructuras de bambú, y recomendaciones para la reconstrucción con bambú en la costa Ecuatoriana. INBAR, Quito.

Vera-Grunauer, X. (2014). Seismic Response of a Soft, High Plasticity, Diatomaceous Naturally Cemented Clay Deposit, Doctoral Dissertation, University of California, Berkeley. GEER (2016). Field Investigation Report.

Vera, R. (2016). Geology of Ecuador, geologyofecuador.com/, last accessed 7/17/16.

Wair, B.R., DeJong, J.T., Shantz, T. (2012). Guidelines for Estimation of Shear Wave Velocity Profiles. PEER Report 2012/08. December.

Wisner, B.; Blaikie, P., Cannon, T., Davis, I. (2004). At Risk: Natural Hazards, People's Vulnerability and Disasters, 2nd ed.; Routledge: London, UK.

Wong, I., Dober, M., Hemphill-Haley, M., Terra, F. (2012). Seismic Hazard along the coast of Ecuador. 15WCEE. Lisbon.

Yasuda, S., and Kiku, H. (2006). Uplift of sewage manholes and pipes during the 2004 Niigataken-Chuetsu Earthquake. *Soils and Foundations*, 45(6), pp. 885-894.

Ye, L, Kanamori, H., Avouac, J-P, Li, L, Cheung, K.F., Lay, T (2016). The 16 April 2016, M W 7.8 (M S 7.5) Ecuador earthquake: A quasi-repeat of the 1942 M S 7.5 earthquake and partial re-rupture of the 1906 M S 8.6 Colombia–Ecuador earthquake. *Earth Planet Sc. Letter*. Under print

Youd, T.L., Idriss, I.M., Andrus, R.D., Arango, I., Castro, G., Christian, J.T., Dobry, R., Finn, W.L., Harder Jr, L.F., Hynes, M.E. Ishihara, K. (2001). Liquefaction resistance of soils: summary report from the 1996 NCEER and 1998 NCEER/NSF workshops on evaluation of liquefaction resistance of soils. *Journal of Geotechnical and Geoenvironmental Engineering*, 127(10), pp. 817-833.

Appendix A: External geotechnical investigation data available

Manta

Table A - 1 Summary of external available ground investigation data available for Manta

Source	GI ID	GI Type	Date of GI completion	Location Description	Lat	Lon
GEER (2016)	HV1	HVSR	Apr-16	Tarqui	0°57'17.68"S	80°42'38.00"W
	HV2	HVSR	Apr-16	Tarqui	0°57'30.34"S	80°42'33.88"W
	HV3	HVSR	Apr-16	Tarqui	0°57'30.03"S	80°42'27.46"W
	HV4	HVSR	Apr-16	Tarqui	0°57'30.34"S	80°42'33.88"W
	HV5	HVSR	Apr-16	Tarqui	0°57'8.94"S	80°42'42.07"W
	HV6	HVSR	Apr-16	Tarqui	0°57'7.58"S	80°42'55.66"W
	HV7	HVSR	Apr-16	Tarqui	0°57'21.91"S	80°42'54.64"W
	VS_AMNT	MAM/MASW + HVSR	Apr-16	AMNT Seismometer Station	0°56'27.60"S	80°44'6"W
	VS_MPWD	MAM/MASW	Apr-16	Port Wharf Deck	0°56'14.90"S	80°43'29"W
	VS_MPPA	MAM/MASW + HVSR	Apr-16	Port Parking Area	0°56'25.78"S	80°43'31"W
VS_IESS	MAM/MASW + HVSR	Apr-16	IESS Manta Hospital	0°57'15.5"S	80°43'25.8"W	
BH_Mobil	Log	Apr-16	Manta coastline	0°56'52.80"S	80°43'15.60"W	
Ripalda (2007)	B116	DH + log	Jun-07	Offshore Manta Port Deck	0°55'50.00"S	80°43'11.00"W
	B123	DH + log	Jun-07	Offshore Manta Port Deck	0°55'40.00"S	80°43'9.00"W
	B138	DH + log	Jun-07	Offshore Manta Port Deck	0°56'6.00"S	80°43'23.00"W
EEFIT	T1	HVSR	May-16	Shelter	0°57'26.45"S	80°41'43.14"W
	T2	HVSR	May-16	Shelter	0°57'25.79"S	80°41'39.83"W
	T13	HVSR	May-16	Tarqui	0°57'5.28"S	80°42'51.95"W

Source	GI ID	EI (m)	Depth of Investigation (m)	GW depth (m)
GEER (2016)	HV1	?	-	-
	HV2	?	-	-
	HV3	?	-	-
	HV4	?	-	-
	HV5	?	-	-
	HV6	?	-	-
	HV7	?	-	-
	VS_AMNT	33	60	-
	VS_MPWD	5	23	-
	VS_MPPA	5	60	-
VS_IESS	10	60	-	
BH_Mobil	?	5	2	
Ripalda (2007)	B116	0	60	0?
	B123	0	60	0?
	B138	0	45	0?
THIS MISSION	T1	19	-	-
	T2	17	-	-
	T13	10	-	-

EEFIT

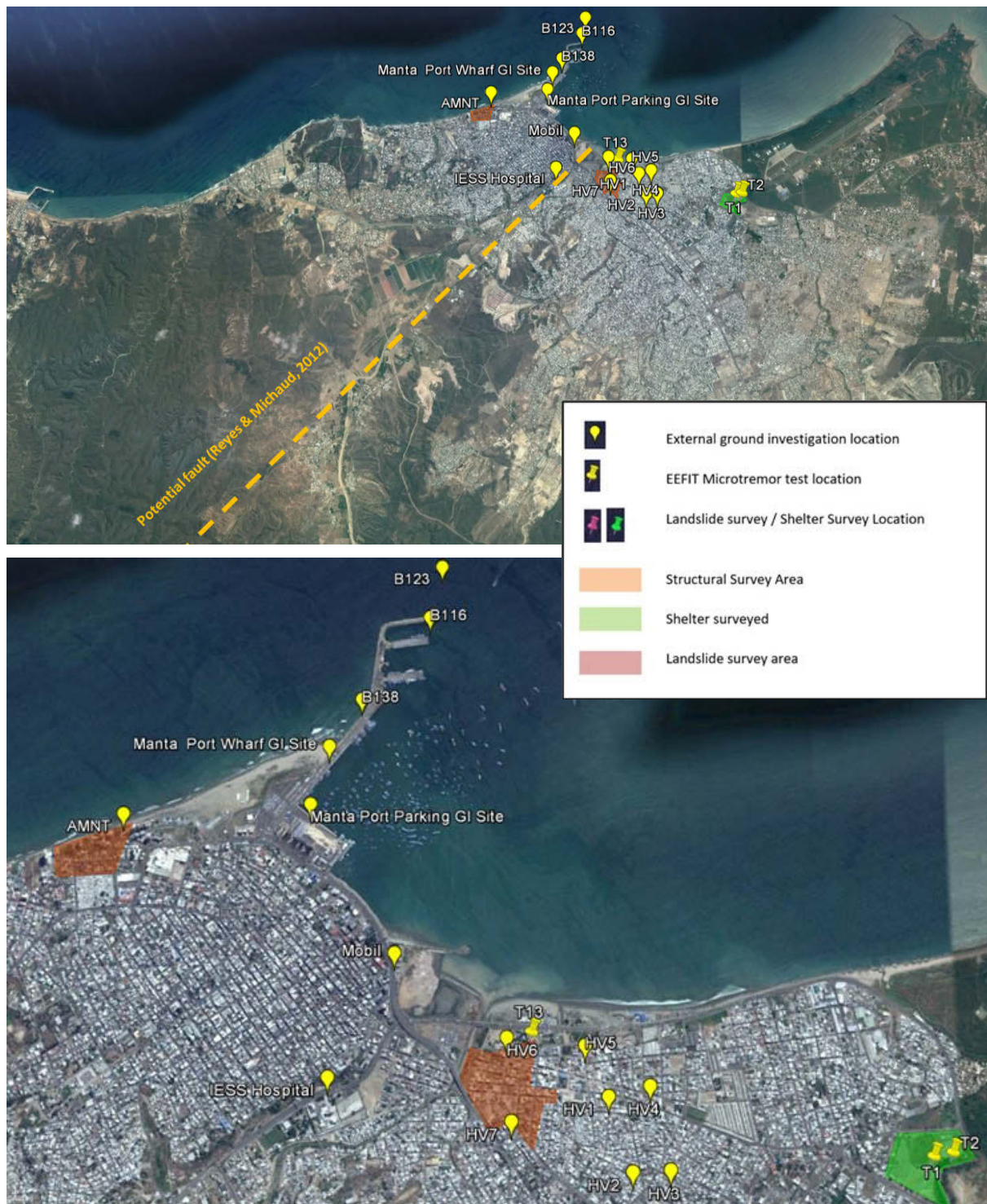


Figure A - 1 Location of external ground investigation locations for which information is available, EEFIT microtremor tests locations as well as areas of structural survey during the EEFIT mission (Manta)

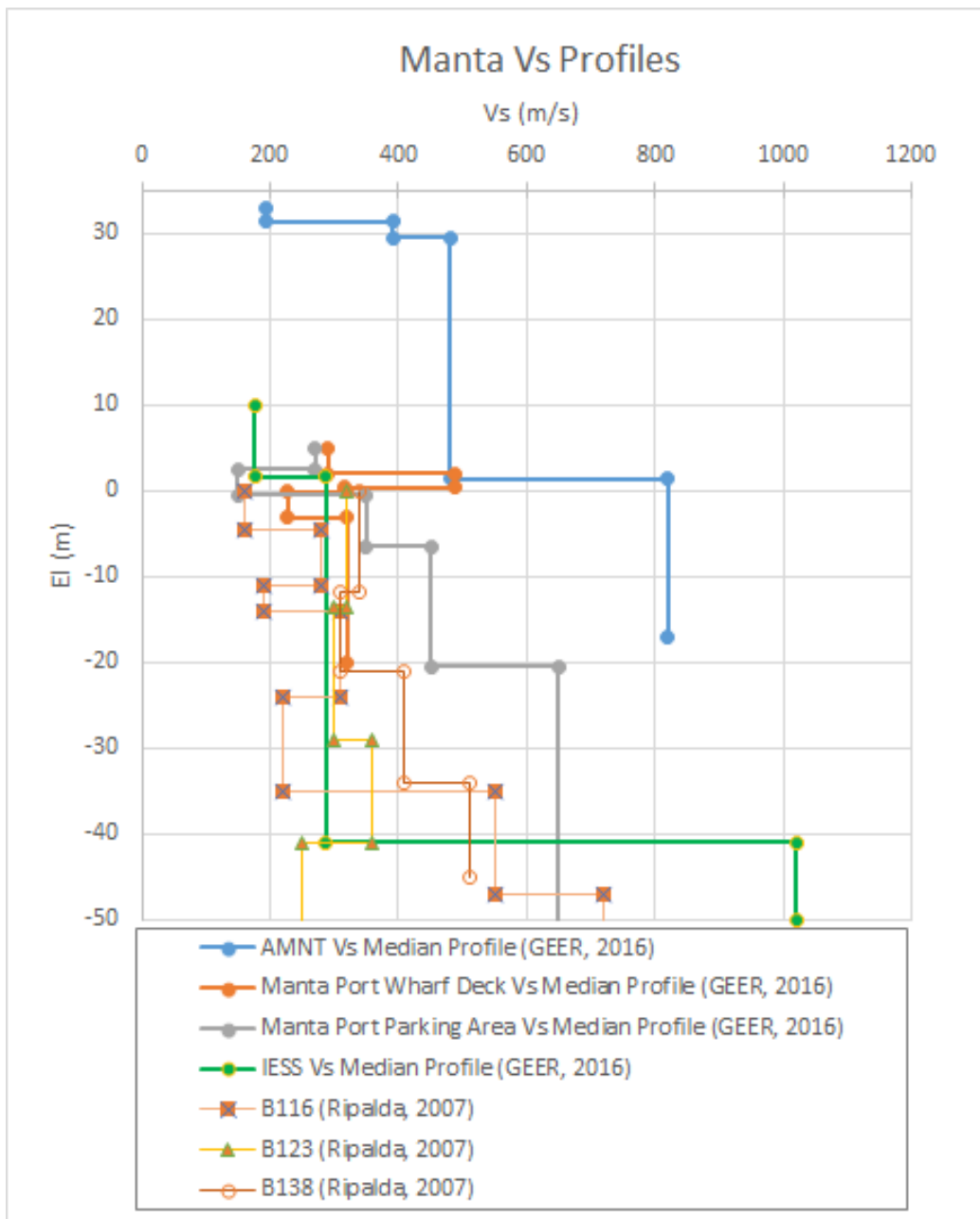


Figure A- 2 V_s profiles from external ground investigation information for Manta

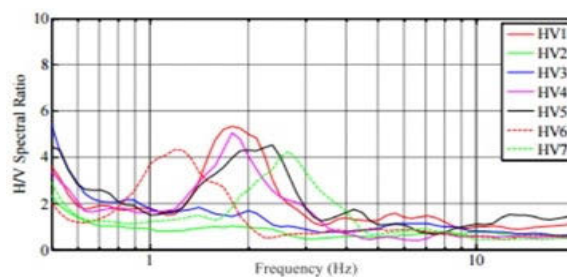


Figure A- 3 HVSR results for Manta from GEER (2016) mission

Portoviejo

Table A- 2 Summary of external available ground investigation data available for Manta

GI ID	GI Type	Date of GI completion	Location Description	Lat	Lon
APO1	SPT + MASW + MAM	Apr-16	Botanical Garden	1° 2'13.20"S	0°27'32.40"W
Los Tamarindos	SPT + Vs (?)	?	West Portoviejo	1° 3'41.50"S	80°28'9.35"W
P1	Log+ G + AL + SPT	< Jun-16	CAC_SE Portoviejo	1° 4'20.80"S	80°26'49.60"W
P2	Log+ G + AL + SPT	< Jun-16	CAC_SE Portoviejo	1° 4'20.80"S	80°26'49.60"W
P3	Log+ G + AL + SPT	< Jun-16	CAC_SE Portoviejo	1° 4'20.80"S	80°26'49.60"W
P4	Log+ G + AL + SPT	< Jun-16	CAC_SE Portoviejo	1° 4'20.80"S	80°26'49.60"W
P5	Log+ G + AL + SPT	< Jun-16	CAC_SE Portoviejo	1° 4'20.80"S	80°26'49.60"W
P6	Log+ G + AL + SPT	< Jun-16	CAC_SE Portoviejo	1° 4'20.80"S	80°26'49.60"W
P7	Log+ G + AL + SPT	< Jun-16	CAC_SE Portoviejo	1° 4'20.80"S	80°26'49.60"W
P8	Log+ G + AL + SPT	< Jun-16	CAC_SE Portoviejo	1° 4'20.80"S	80°26'49.60"W
P9	Log+ G + AL + SPT	< Jun-16	CAC_SE Portoviejo	1° 4'20.80"S	80°26'49.60"W
P10	Log+ G + AL + SPT	< Jun-16	CAC_SE Portoviejo	1° 4'20.80"S	80°26'49.60"W
T3	HVSR	May-16	Z0	1° 3'17.70"S	80°27'10.20"W
T4	HVSR	May-16	Z0	1° 3'25.02"S	80°27'6.24"W
T5	HVSR	May-16	River Bank	1° 3'43.36"S	80°27'3.16"W
T6	HVSR	May-16	Botanical Garden	1° 2'13.75"S	80°27'36.04"W
T7	HVSR	May-16	Botanical Garden	1° 2'13.93"S	80°27'35.94"W
T8	HVSR	May-16	Botanical Garden	1° 2'14.10"S	80°27'35.81"W
T9	HVSR	May-16	Botanical Garden	1° 2'15.42"S	80°27'34.34"W

Source	GI ID	Depth of investigation (m)	EI (m)	GW depth (m)
GEER (2016)	APO1	40	41	not detected
	Los Tamarindos	40	-	?
Hidroplan (2016)	P1	15	45	4
	P2	15	45	4.5
	P3	15	45	5.5
	P4	15	45	4
	P5	15	45	4
	P6	15	45	4.5
	P7	15	45	5
	P8	15	45	4.5
	P9	15	45	5
	P10	15	45	4
THIS MISSION	T3	-	45	-
	T4	-	45	-
	T5	-	36	-
	T6	-	42	-
	T7	-	42	-
	T8	-	43	-
	T9	-	44	-

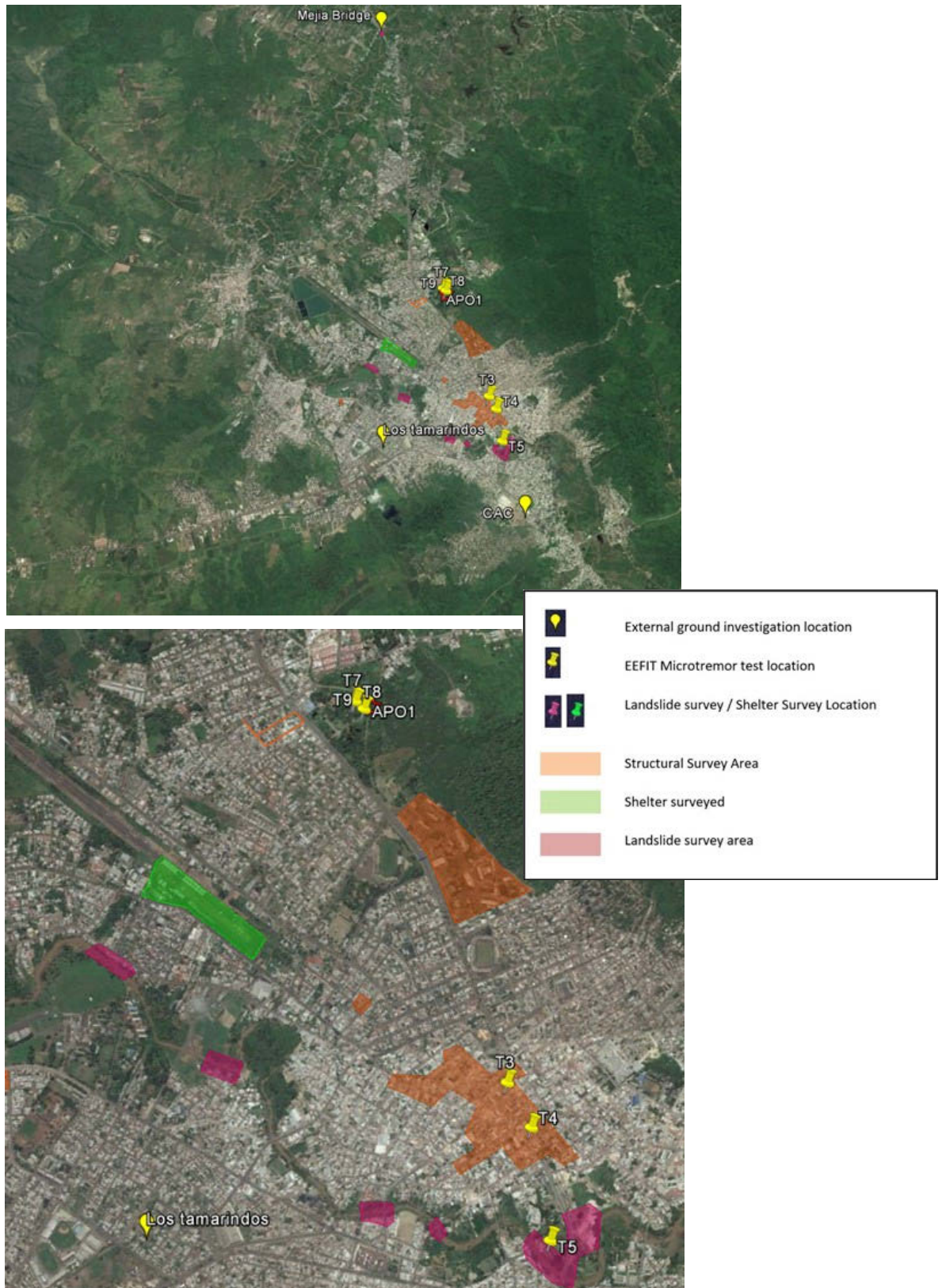


Figure A- 4 Location of external ground investigation locations for which information is available, EEFIT microtremor tests locations as well as areas of structural survey during the EEFIT mission (Portoviejo)

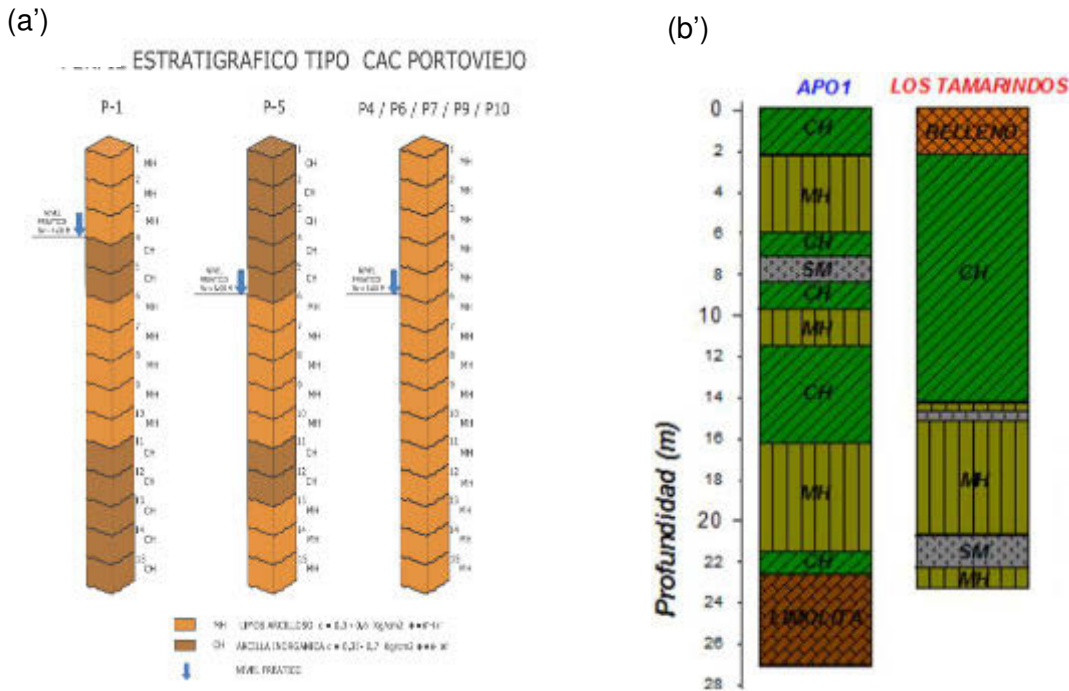
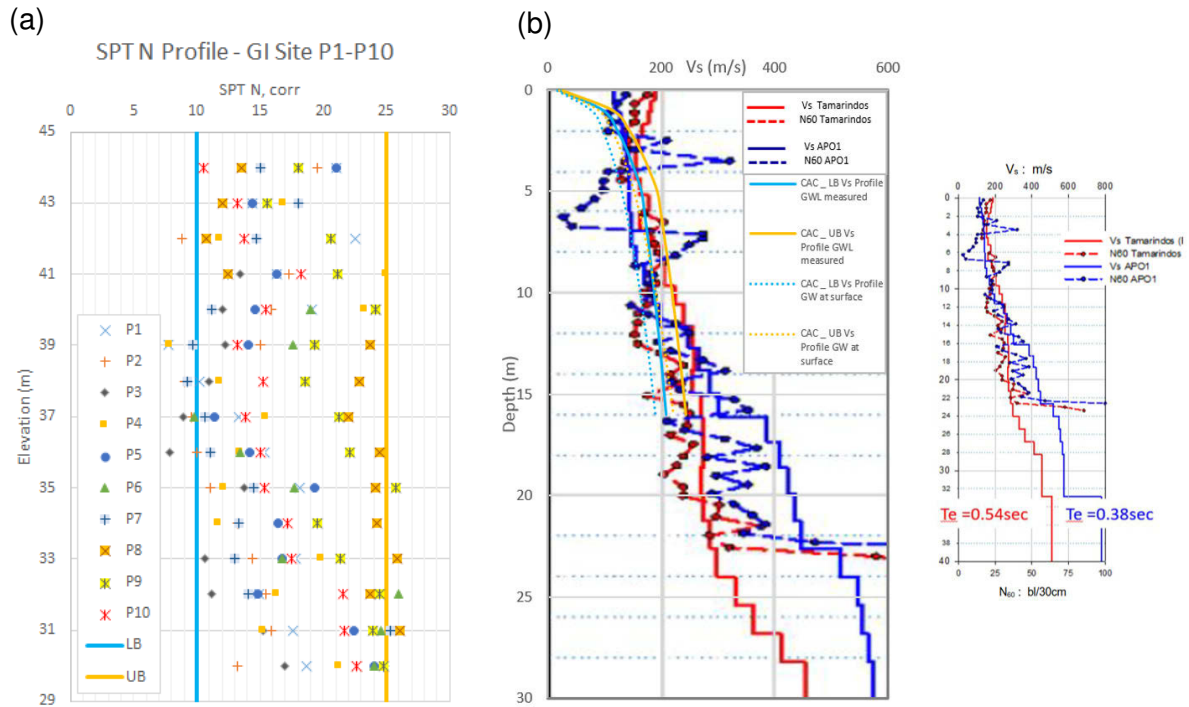


Figure A- 5 Summary of key ground investigation findings from external sources. (a) SPT data and (a') soil model for P1 to P10 (Hidroplan, 2016); (b) V_s Profiles and (b') soil model from boreholes from APO1 and Los Tamarindos ground investigation (GEER, 2016).

Bahía de Caráquez and surroundings

Table A- 3 Summary of external available ground investigation data available for Bahía de Caráquez

Source	GI ID	GI Type	Date of GI completion	Location Description	Lat	Lon
GEER (2016) *	GI_Bridge	SPT	?	Los Caras Bridge	0°36'33.58"S	80°24'58.68"W
LUP (2016)	B01	SPT	Jul-16	Central Bahía (CB)	0°36'12.2"S	80°25'25.1"W
	B02	SPT	Jul-16	Central Bahía (CB)	0°36'12.2"S	80°25'25.1"W
	B02	SPT	Jul-16	Central Bahía (CB)	0°36'12.2"S	80°25'25.1"W
	B04	SPT	Jul-16	Punta Lado De la Ria Bahía (PRB)	0°35'45.2"S	80°25'18.5"W
	B05	SPT	Jul-16	Punta Lado De la Ria Bahía (PRB)	0°35'45.2"S	80°25'18.5"W
	B06	SPT	Jul-16	Punta Lado De la Ria Bahía (PRB)	0°35'45.2"S	80°25'18.5"W
	B07	SPT	Jul-16	Lado de la Playa Malecon (PMB)	0°35'43.5"S	80°25'26.2"W
	B08	SPT	Jul-16	Lado de la Playa Malecon (PMB)	0°35'43.5"S	80°25'26.2"W
	B09	SPT	Jul-16	Lado de la Playa Malecon (PMB)	0°35'43.5"S	80°25'26.2"W
THIS MISSION	T10	HVSR	May-16	Bahía Hospital	0°37'19.00"S	80°25'39.50"W
	T12	HVSR	May-16	NW side of Bahía Los Caras Bridge	0°36'26.19"S	80°24'27.73"W

*Courtesy of the Ecuador's Army Corps of Engineers, Adolfo Caicedo

Source	GI ID	Depth of investigation (m)	El (m)	GW depth (m)
GEER (2016) *	GI_Bridge	75	~ -5m	0
LUP (2016)	B01	16	10	1.4
	B02	16	10	1.5
	B02	16	10	1.6
	B04	16	10	2.1
	B05	16	10	2
	B06	16	10	1.75
	B07	16	17	2.8
	B08	16	17	2.5
	B09	16	17	2.7
THIS MISSION	T10	-	19	-
	T12	-	0	-

EEFIT

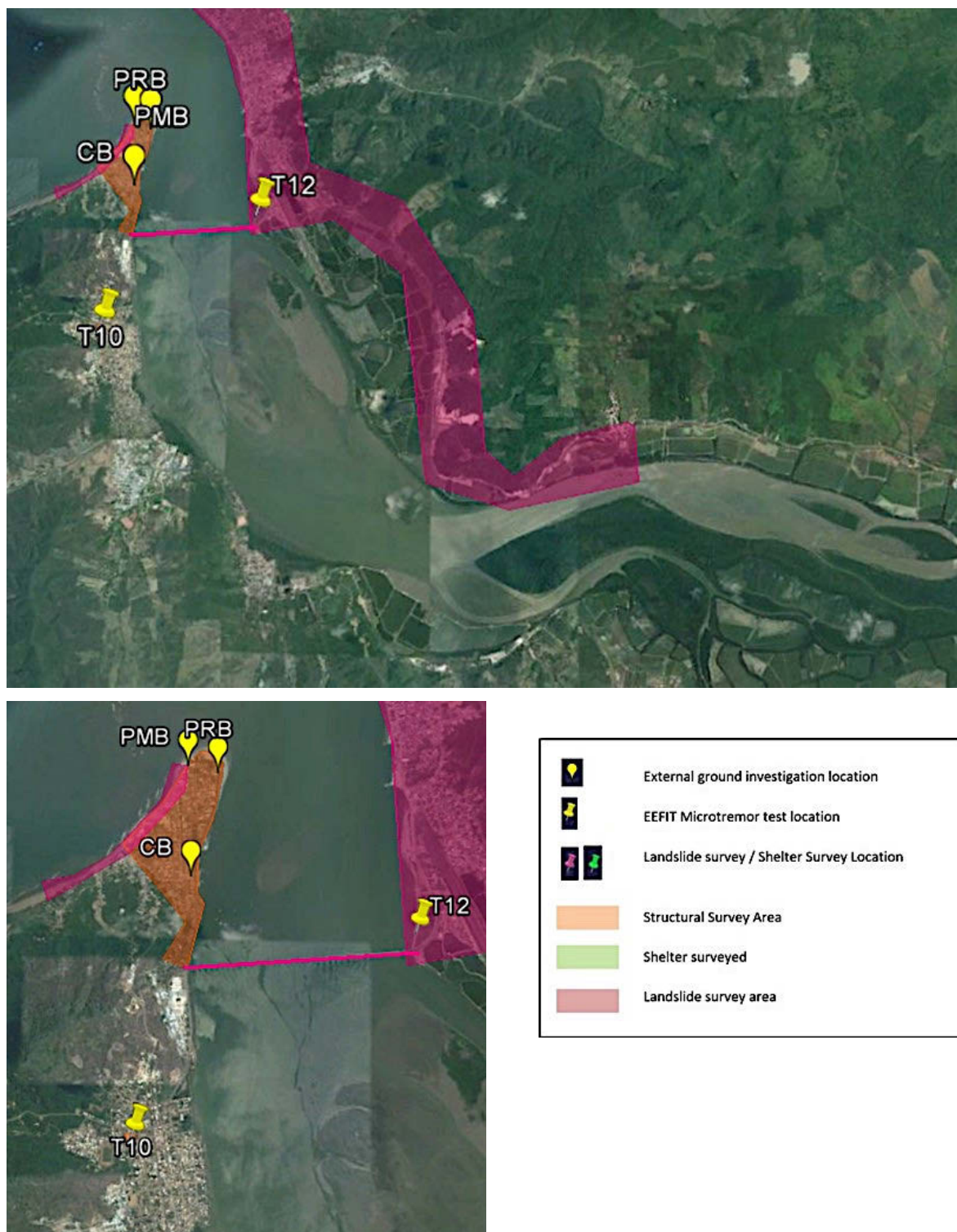


Figure A- 6 Location of external ground investigation locations for which information is available, EEFIT microtremor tests locations as well as areas of structural survey during the EEFIT mission

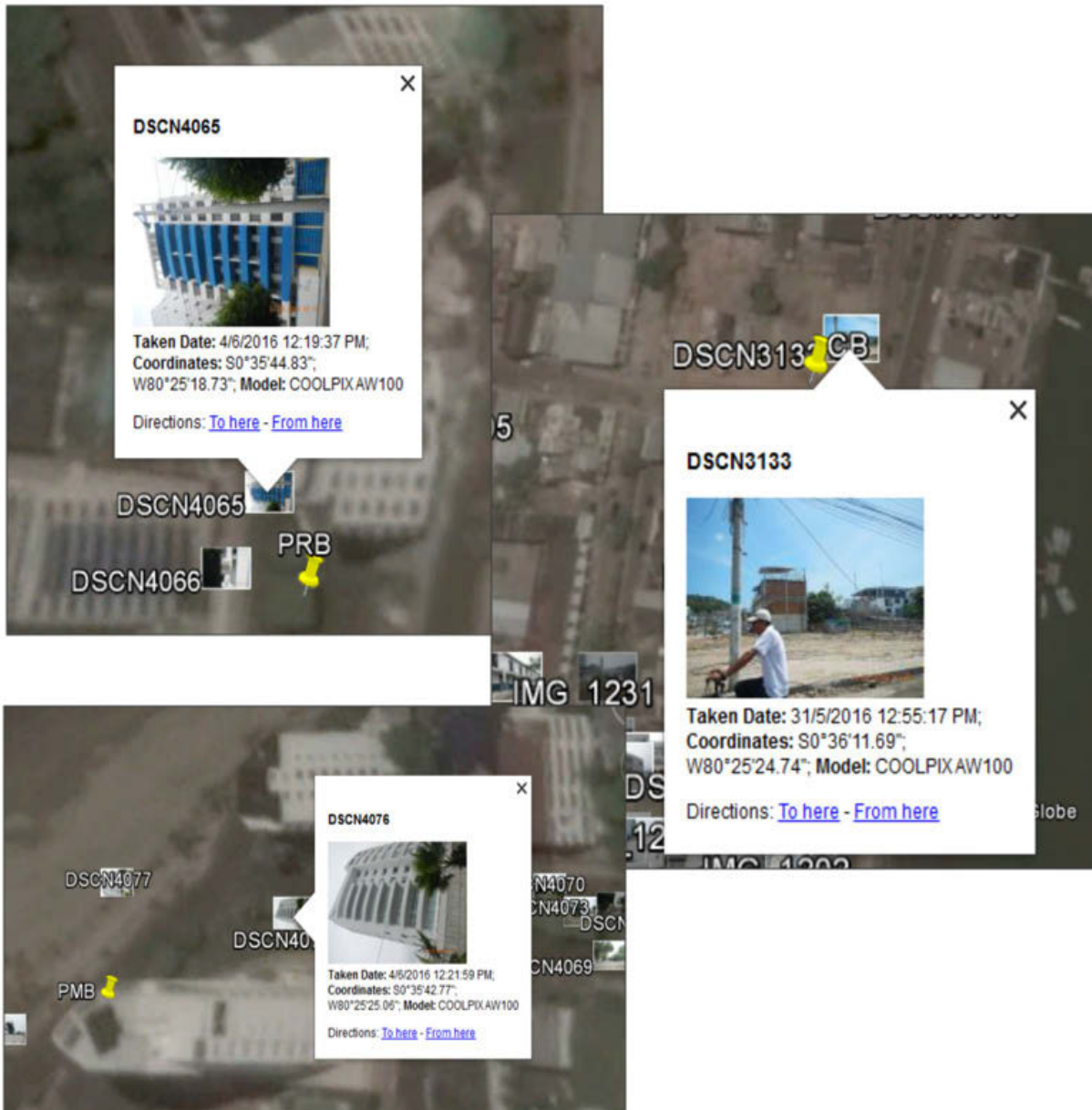


Figure A- 7 Closest observations to the ground investigation locations where information is available for Bahia de Caraquez

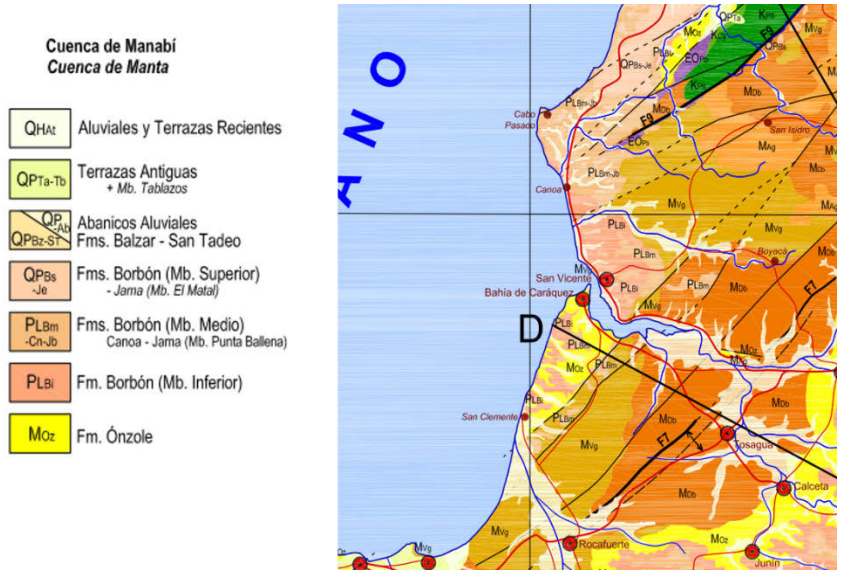


Figure A- 8 Close-up of Reyes and Michaud (2012) geological map for the Chone Estuary.

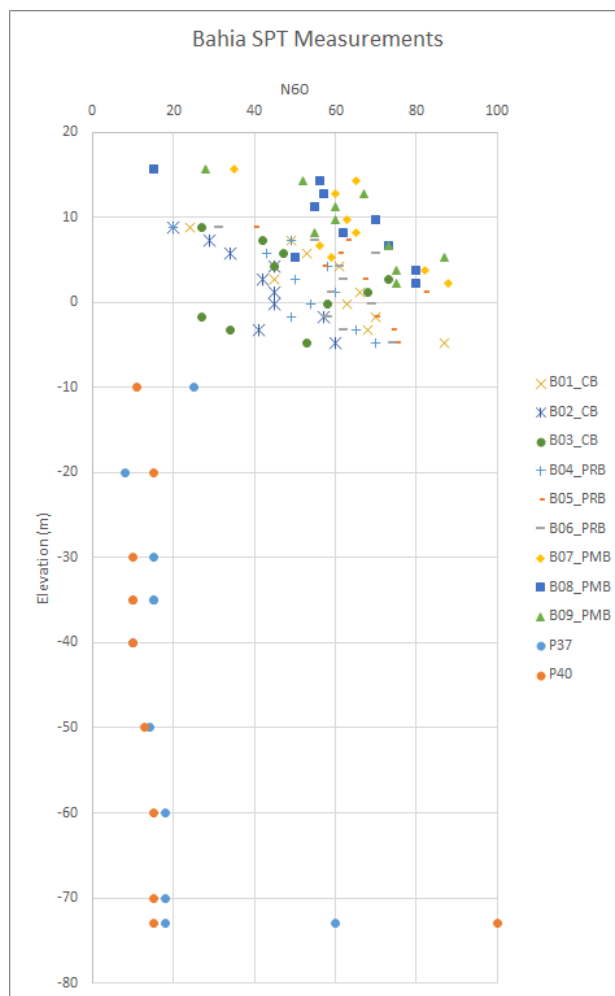


Figure A- 9 SPT measurements from ground investigation in the region of Bahia de Caraquez

Canoa

Table A- 4 Summary of external available ground investigation data available for Canoa

Source	GI ID	GI Type	Date of GI completion	Lat	Lon	Depth of investigation (m)	EI (m)	GW depth (m)
LUL 2016	C1	Log + G + AL + SPT	Jul-16	0°27'42.2"S	80°27'05.7"W	16	?	?
	C2							
	C3							



Figure A- 10 Locations surveyed in Canoa and location the site for which external ground investigation data is available

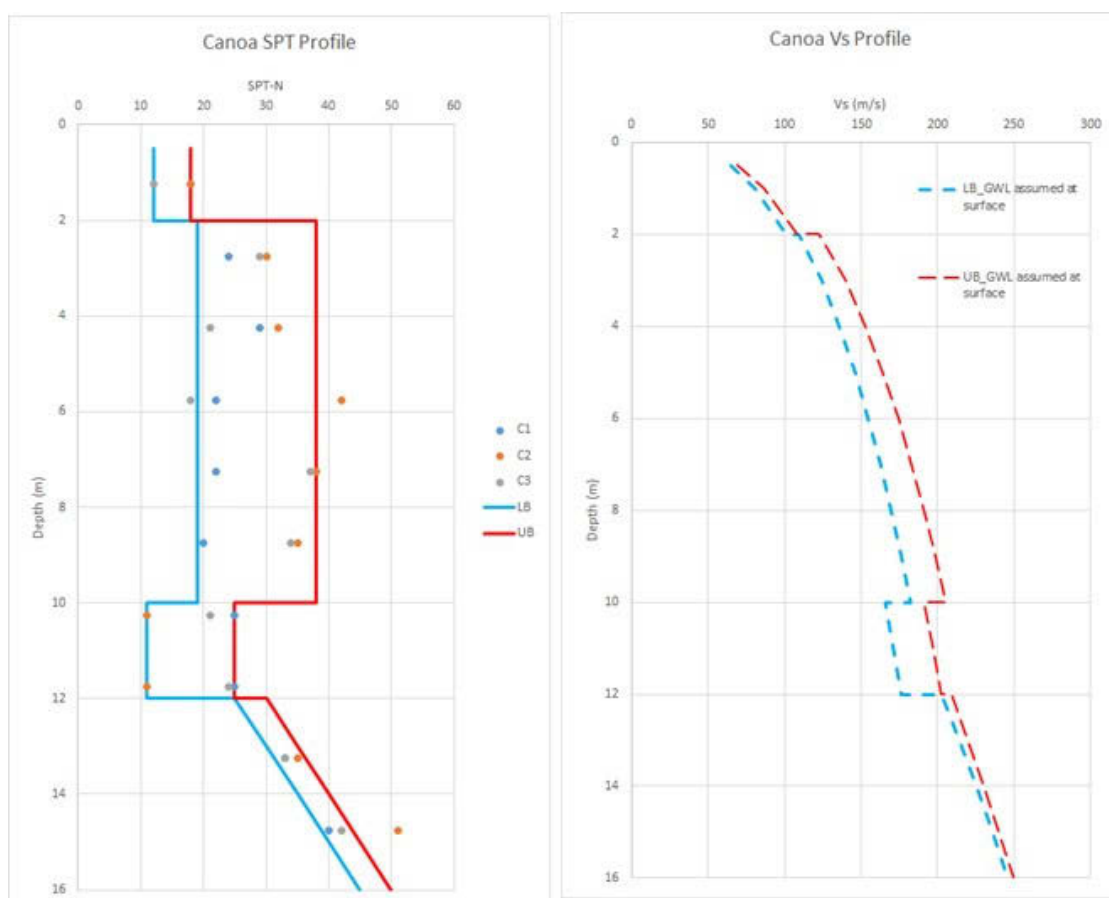


Figure A- 11 SPT and SPT-based V_s profiles for Canoa

Jama

Table A- 5 Summary of external available ground investigation data available for Jama

Source	GI ID	GI Type	Location Description	Lat	Lon	Depth of investigation (m)	EI (m)	GW depth (m)
LUP 2016	J1	Log + G + AL + SPT	NW Jama Coast	0°11'9.70" S	80°17'16.70" W	16	?	12.5
	J2					16	?	12.5
	J3					16	?	12

NB: Date of GI completion unknown

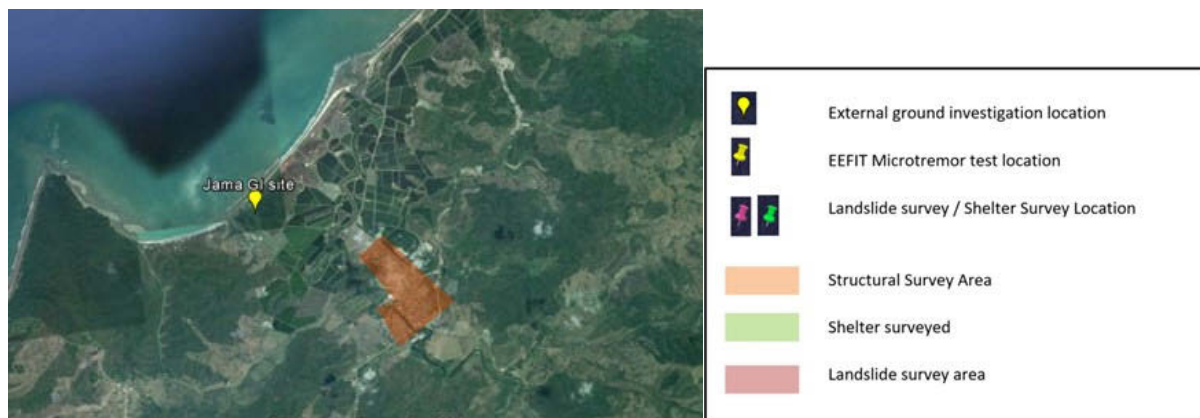


Figure A- 12 Locations surveyed in Jama and location of the site for which external ground investigation data is available

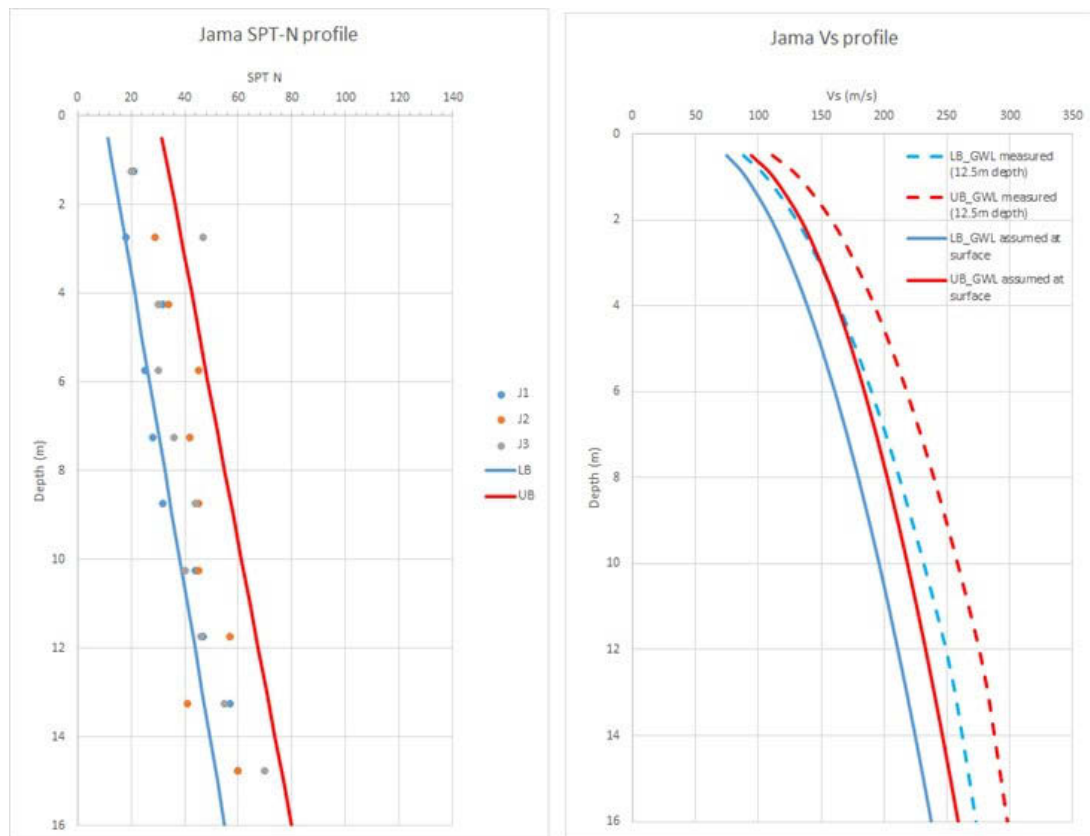


Figure A- 13 SPT and SPT-based V_s profiles for Jama

Pedernales

Table A- 6 Summary of external available ground investigation data available for Pedernales

Source	GI ID	GI Type	Date of GI completion	Lat	Lon	Depth of investigation (m)	EI (m)
GEER (2016)	APED	MASW + MAM	Apr-16	0°4'4.36"N	80°3'25.95"W	80	15
THIS MISSION	T11	HVSR	May-16			-	15



Figure A- 14 Locations surveyed in Pedernales and location of the site for which external ground investigation data is available

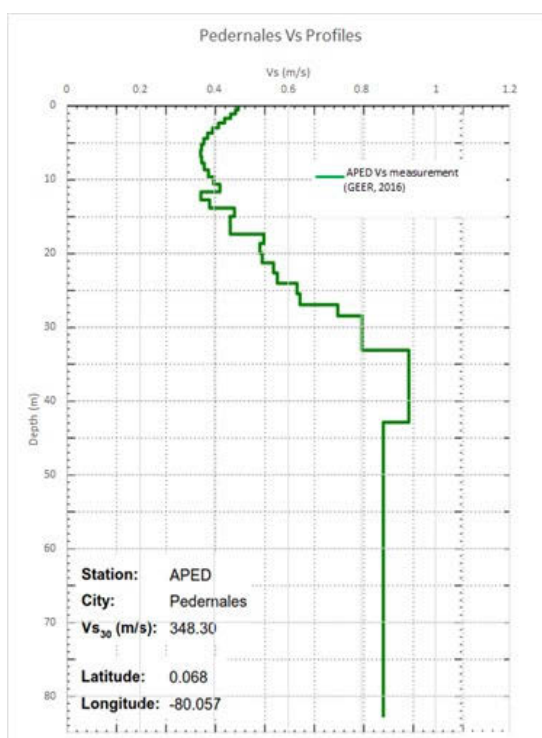


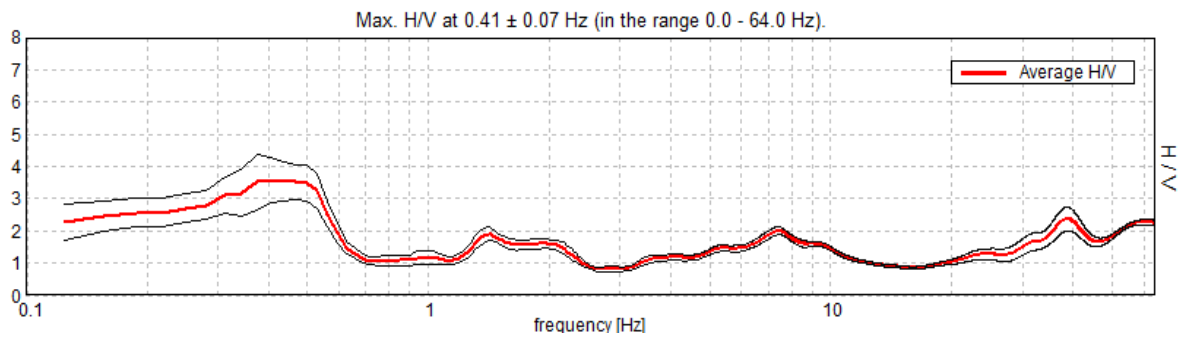
Figure A- 15 V_s Profile at APED in Pedernales (GEER, 2016)

Appendix B: Microtremor test readings

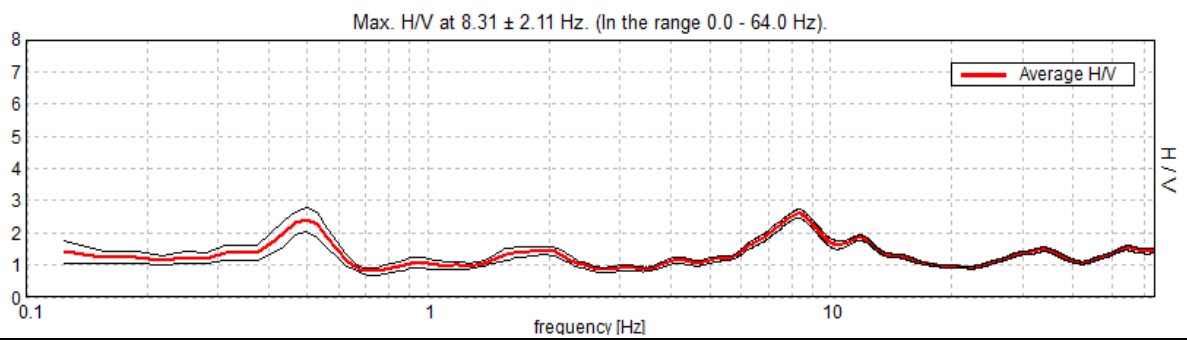
Manta

Shelter site

T1

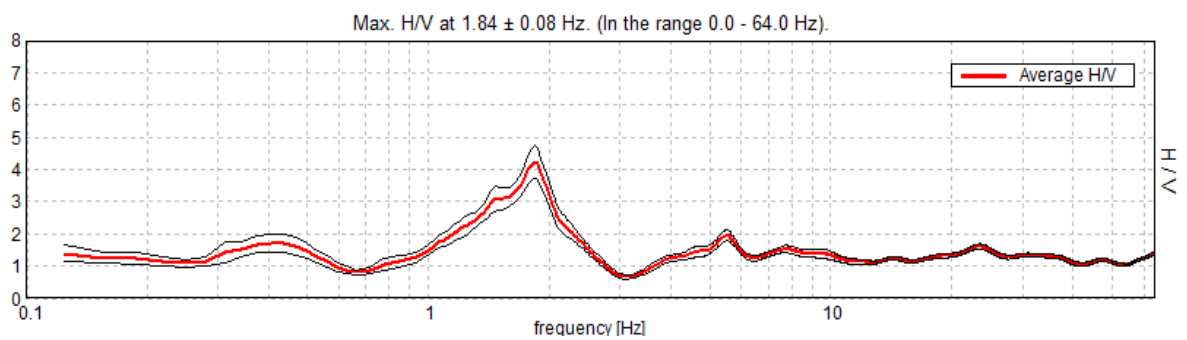


T2



Tarqui

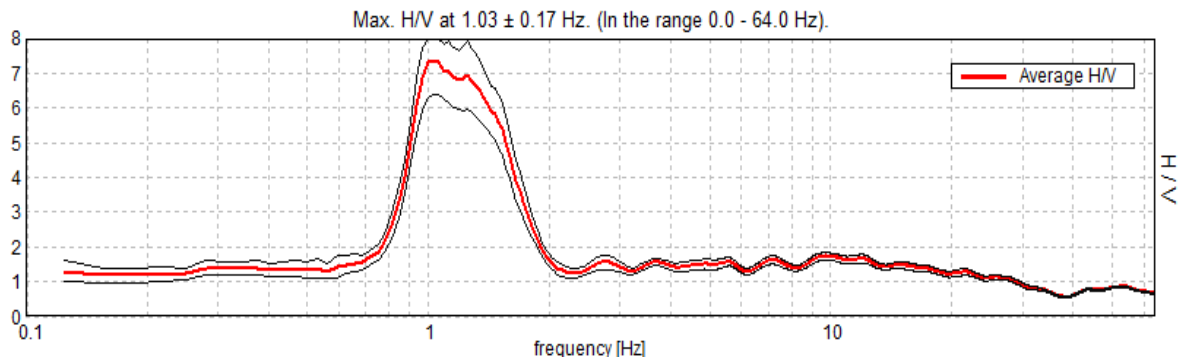
T3



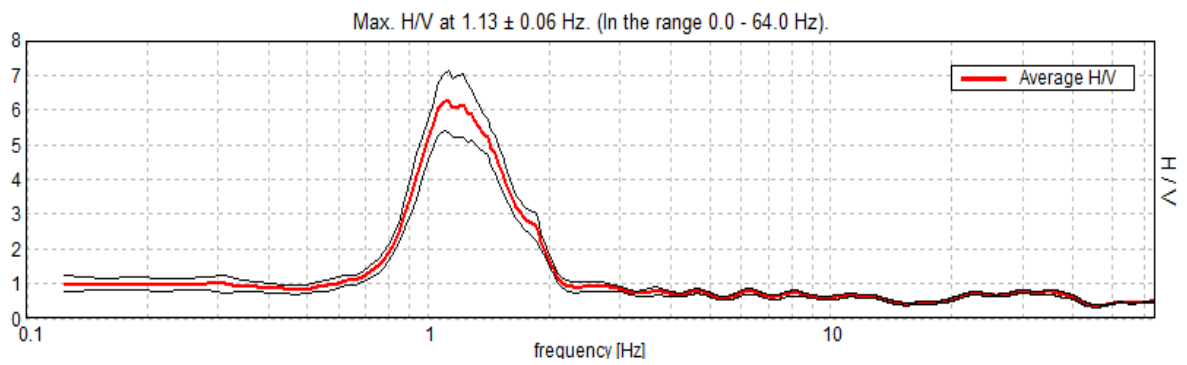
Portoviejo

GROUND ZERO

T3

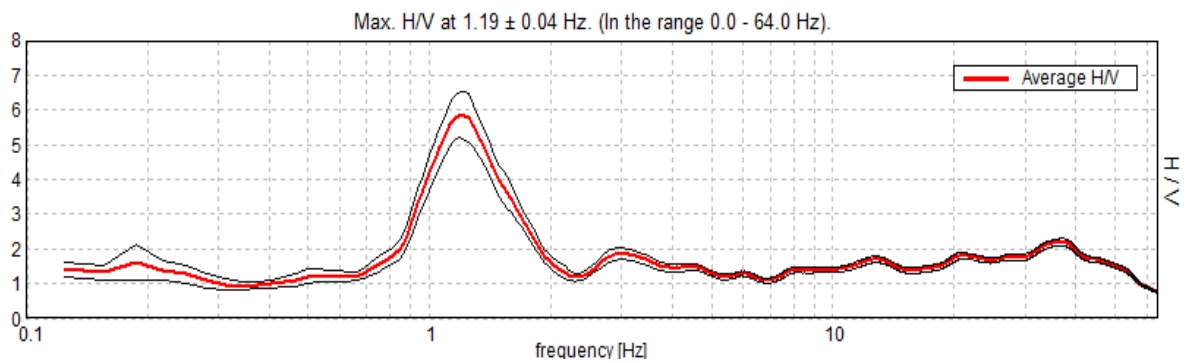


T4



RIVER SIDE

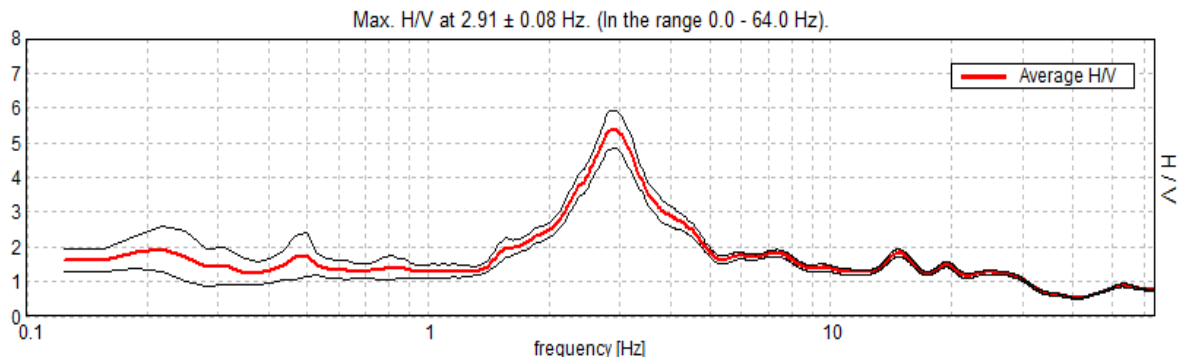
T5



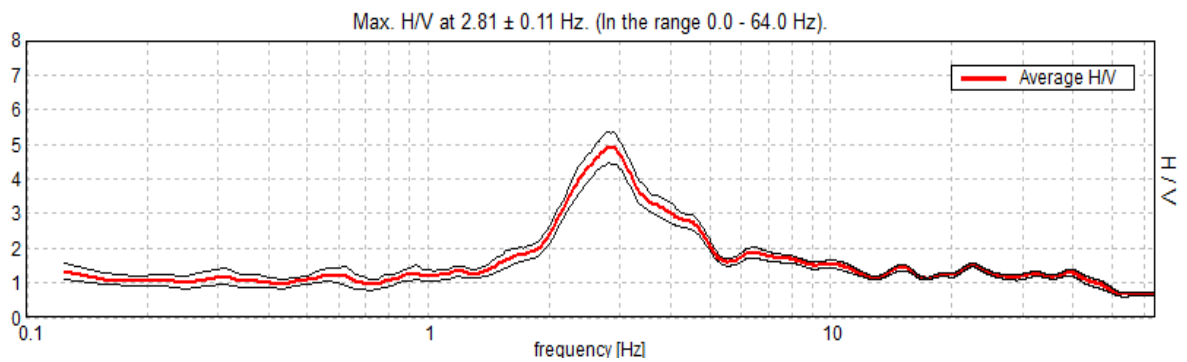
T4

Botanical Garden

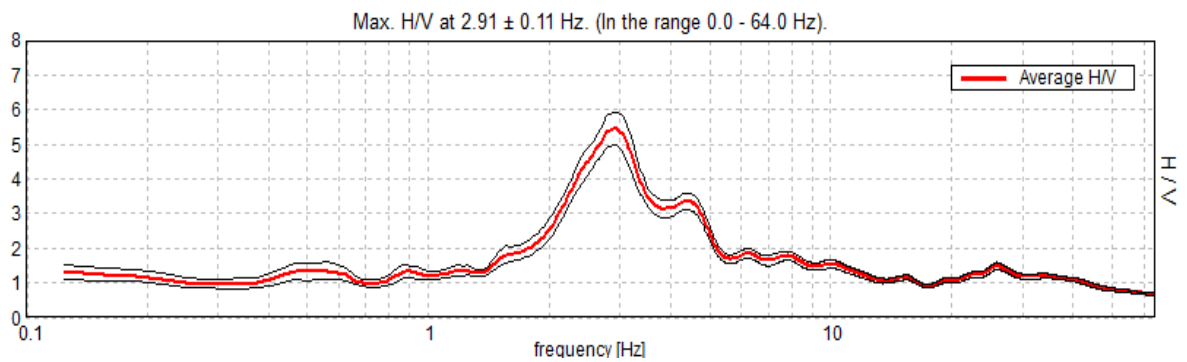
T6



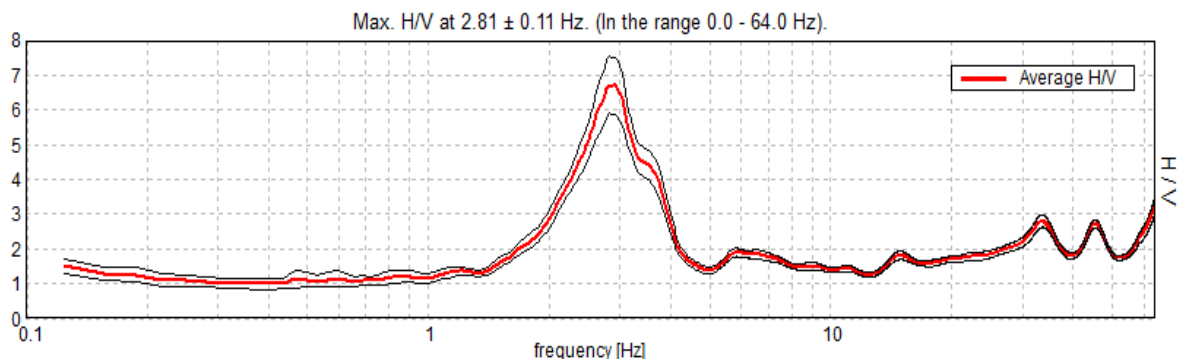
T7



T8

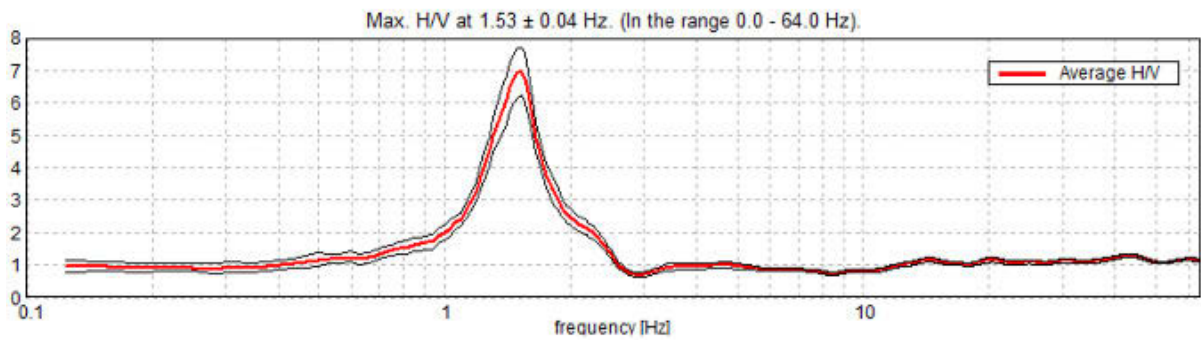


T9

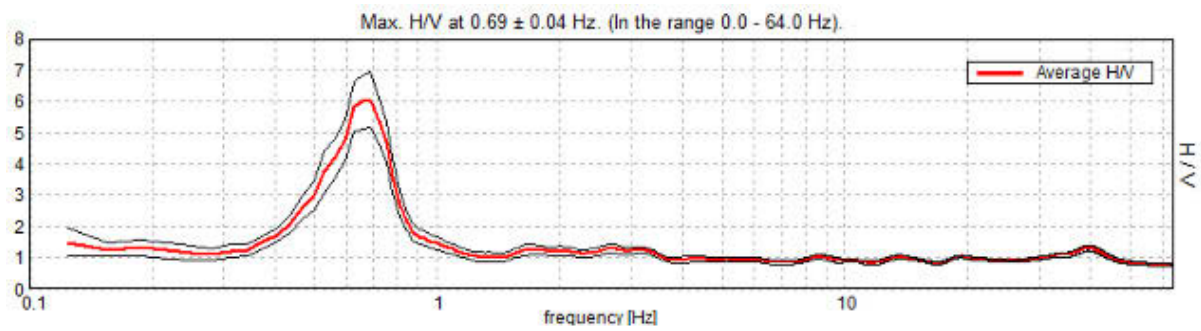


Bahía de Caráquez and surroundings

T10

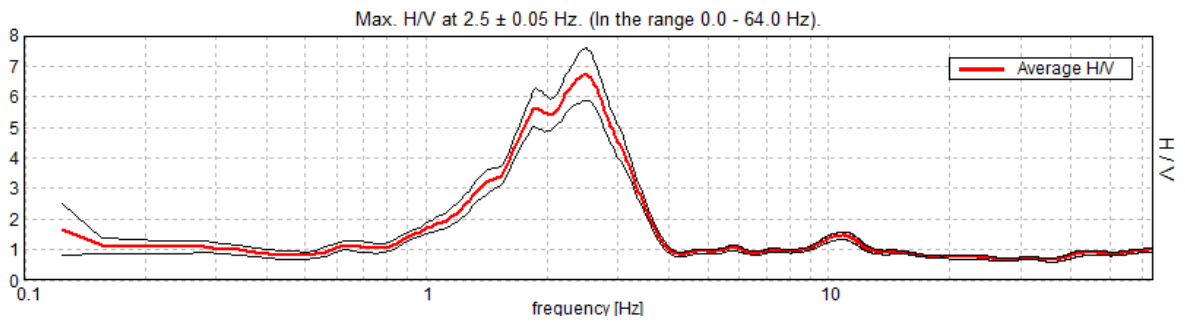


T12



Pedernales

T11



Appendix C: BGS Rapid satellite-based landslide assessment maps ground-proofing

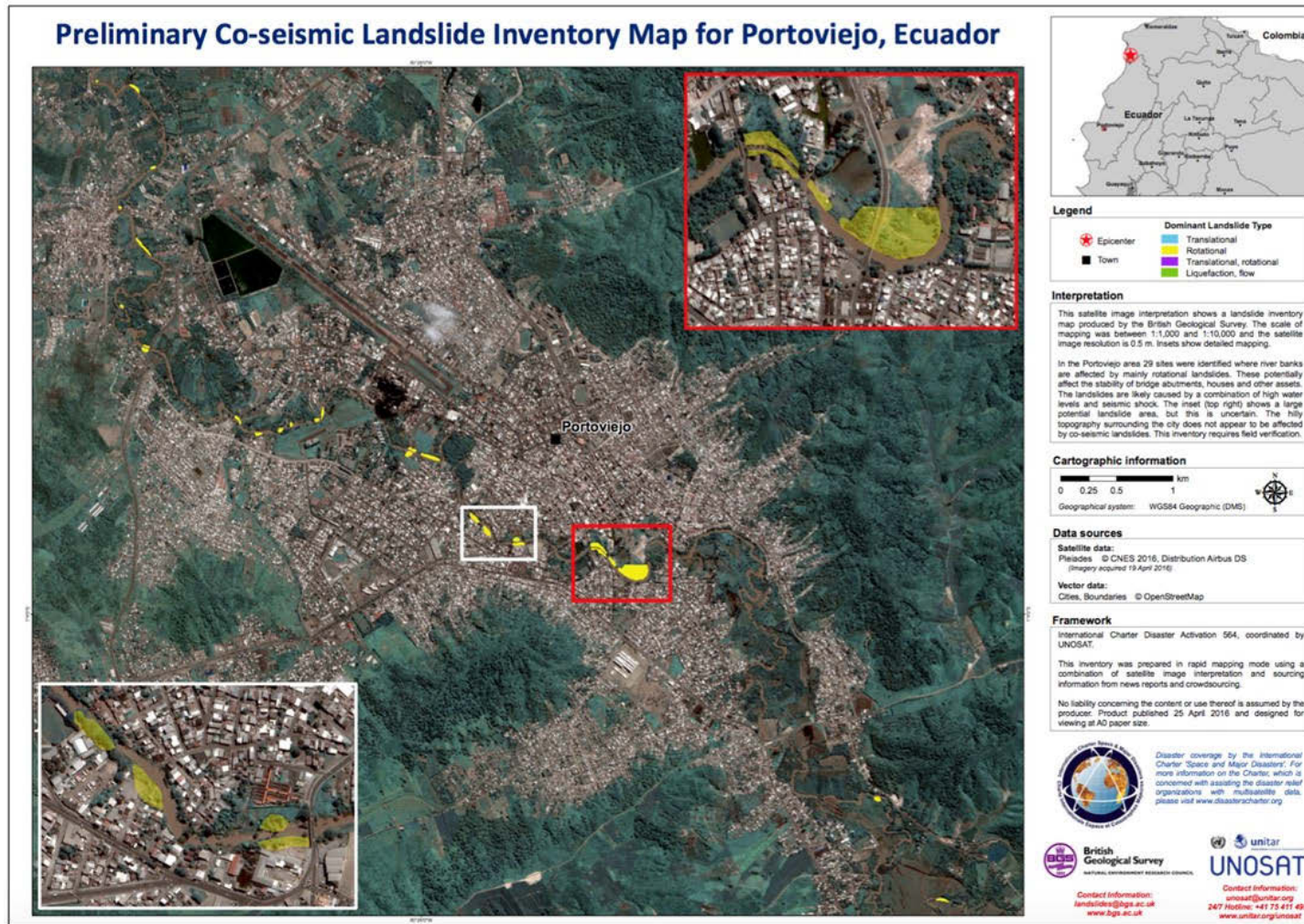


Figure C-1: BGS Preliminary co-seismic landslide inventory map for Portoviejo

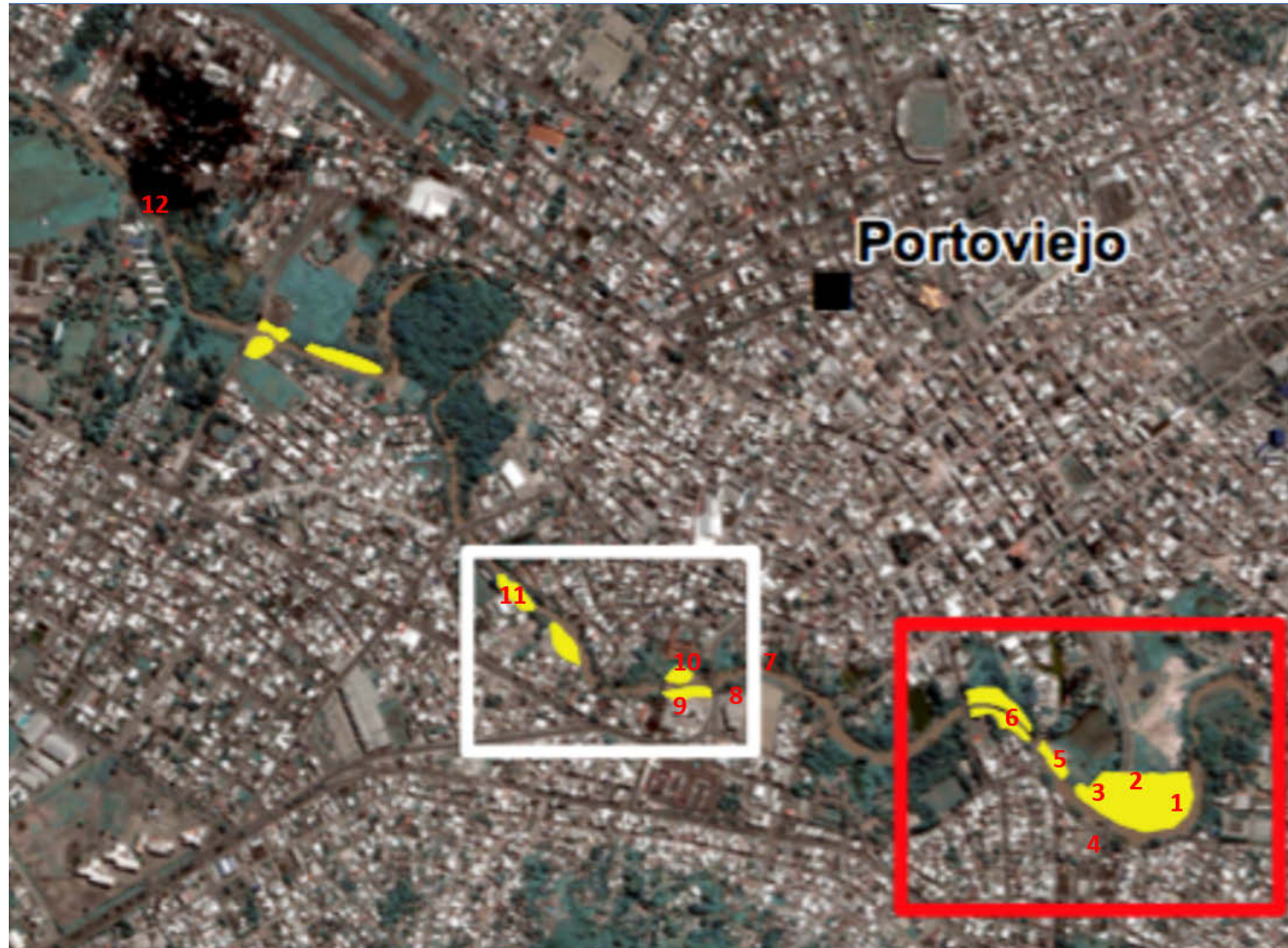


Figure C-2: Close up of landslide locations surveyed in Portoviejo

Table C-1: Details of landslide locations surveyed in Portoviejo

Map ID	Coordinates	Accuracy of BGS identification		Co-seismicity validation by locals	Visual Assessment Reliability Estimate		Observations	Discussion with locals	Photos
		Location	Type		Reliability Level	Comment			
1	-1.062656, -80.449346	X	NA	?	Adequate		<p>No major damage observed. Potentially some lateral spreading, but no signs of significant spreading.</p> <p>BGS mapping may correspond to flooded area rather than slope failure.</p>	<p>Flooding occurred around bridge in the days before the main shock.</p> <p>Local interviewed also mentioned that the municipality had changed the course of the river around this section to avoid too many meanders, thereby possibly aggravating the vulnerability of the river banks following floods due to increased speeds of the water.</p>	
2	-1.062988, -80.449746	✓	X	✓	Adequate		<p>Road approach to bridge on north side had cracks parallel and perpendicular to road. Cracks had been filled in, but looked like slight spread of road to sides.</p> <p>No landslide</p>	<p>Discussion with locals supporting evidence of co-seismicity of failure.</p>	

Map ID	Coordinates	Accuracy of BGS identification		Co-seismicity validation by locals	Visual Assessment Reliability Estimate		Observations	Discussion with locals	Photos
		Location	Type		Reliability Level	Comment			
3	-1.062683, -80.450329	✓	X	✓	Good		<p>Large crack formed, approximately 60 cm wide, running parallel to the river for over 30m, located in between house and river. Close to edge of river, looks to have been spreading of land into river.</p> <p>No landslide observed.</p>	<p>Neither houses close by suffered major damage – cracks to concrete flooring in one of them.</p>	
4	-1.063181, -80.450495	X	NA	✓	Good		<p>Significant amount of lateral spreading observed. Large cracks at top of slope. House further along slope had 1 m settlement of their patio, and lateral movement too (not measured). A retaining wall had rotated outwards.</p>	<p>Told that a bar under construction next door (roof and floors of bamboo) collapsed into the river. Building material has since been taken away by river or has been stolen.</p>	

Map ID	Coordinates	Accuracy of BGS identification		Co-seismicity validation by locals	Visual Assessment Reliability Estimate		Observations	Discussion with locals	Photos
		Location	Type		Reliability Level	Comment			
5	-1.061453, -80.451259	✓	X	✓	Good		Evidence of liquefaction-induced lateral spreading. Portal frame structure suffered significant settlement and rotation. Footing for football stand had settled approximately 2 m and moved laterally about 2 m.	Football pitch not commercially operable since earthquake with no prospect of how and when the owners may be able to carry out the necessary works and get back to being fully operable as a rented pitch for local football teams.	
6	-1.061275, -80.451510	✓	X	✓	Good		Significant rotation of bridge foundations into river. Evidence of liquefaction induced lateral spreading.	Told this house was flooded at time of earthquake. Told bridge had settled 60cm. Told trees moved 5m laterally into the river. Said river had been redirected around their house – used to run behind it, but now runs in front. Also river to the west of their house is protected due to native trees being present, so does not get dredged and does not have the river bank slope reengineered annually.	
7	-1.059800, -80.457436	X	NA	✓	Good		Significant lateral spreading into the river.	Flooded before earthquake, water knee height at houses. At time of earthquake water receding. Told that earthquake caused spreading of ground into river and rotation of trees.	

Map ID	Coordinates	Accuracy of BGS identification		Co-seismicity validation by locals	Visual Assessment Reliability Estimate		Observations	Discussion with locals	Photos
		Location	Type		Reliability Level	Comment			
8	-1.060450, -80.457982	X	NA	✓	Good		<p>Large slope failure damaged the car park of a supermarket to the extent that it was still closed at the time of the mission.</p> <p>Next to the car park, the bridge abutment suffered damage. Part of the bridge deck which was previously on fill was dangerously cracked and hanging without any support above the empty space left by the landslide below. No safety signs.</p>	<p>Told fill material had been used to extend the car park of new supermarket out into the edge of the river hence possibly aggravating the pre- earthquake flooding than before the works were carried out in previous years.</p> <p>The car park of the supermarket has not been operable since event.</p>	
9	-1.060591, -80.458651	✓	?	✓	Adequate	<p>Extent of contribution of liquefaction to landslide not clear.</p> <p>Clearing and rehabilitation works undergone</p>	<p>Large slope failure with soil movement away from garage into the river and in direction away from bridge.</p> <p>A couple of structures were completely damaged, as well as some car park area.</p> <p>However, some evidence of foundation failure (tilting of shallow raft foundation) could be observed. Evidence of pipe flotation was also observed, indicating liquefaction.</p>	<p>The earthquake was apparently followed by a large movement of land into river, engulfing 8 cars.</p> <p>The garage remained partially operable, with considerable rehabilitation works ongoing since the earthquake. The debris of the completely damaged structures had been already removed.</p>	

Map ID	Coordinates	Accuracy of BGS identification		Co-seismicity validation by locals	Visual Assessment Reliability Estimate		Observations	Discussion with locals	Photos
		Location	Type		Reliability Level	Comment			
10	-1.060063, -80.458596	✓	X	✓	Poor	Observation from afar	Potential scar and small slide noted from afar (on the bridge), as access was not possible. The visual assessment of the land movement appeared closer to the bridge than mapped by BGS.	Discussion with locals supporting evidence of co-seismicity of failure, rather than flood damage.	
11	-1.060013, -80.461145	✓	X	✓	Poor	Observation from car. No time to stop or get access	No direct observation	Told that was damage in this area due to liquefaction induced lateral spreading. Damage to buildings, including a school. Unfortunately, did not have time to stop and visit. Photos taken from the minibus	

Map ID	Coordinates	Accuracy of BGS identification		Co-seismicity validation by locals	Visual Assessment Reliability Estimate		Observations	Discussion with locals	Photos
		Location	Type		Reliability Level	Comment			
12	-1.048593, -80.471044	X	NA	✓	Adequate	Site already cleared.	<p>Under a cloud on BGS map.</p> <p>All collapsed houses had been cleared and the terrain remodelled. The less damaged adjacent structures and the observation of the ground on the banks of the river provided evidence of major slope failure, including concentric lines of failures in the damaged tiled patio of a historical house next to the river.</p> <p>Slope failure scar showed evidence that ground on which buildings are built is made of remodelled and re-compacted soil from the river.</p>	<p>Shown post earthquake photos from the municipality's report. 7 houses collapsed and 4 fatalities reported. Many of the adjacent houses considerably damaged.</p> <p>Very high water level of the river and saturated ground of the banks of the river at the foot of the damaged houses reported.</p> <p>Locals shared testimony of general practice in all Portoviejo of manually dredging and compacting the loose soil deposited in the river after the annual floods during the wet season to reshape the banks of the river. Once dry, it could be used as terrain to build structures upon such as in this case.</p>	

CHONE RIVER ESTUARY, CLOSE TO BAHIA DE CARAQUEZ

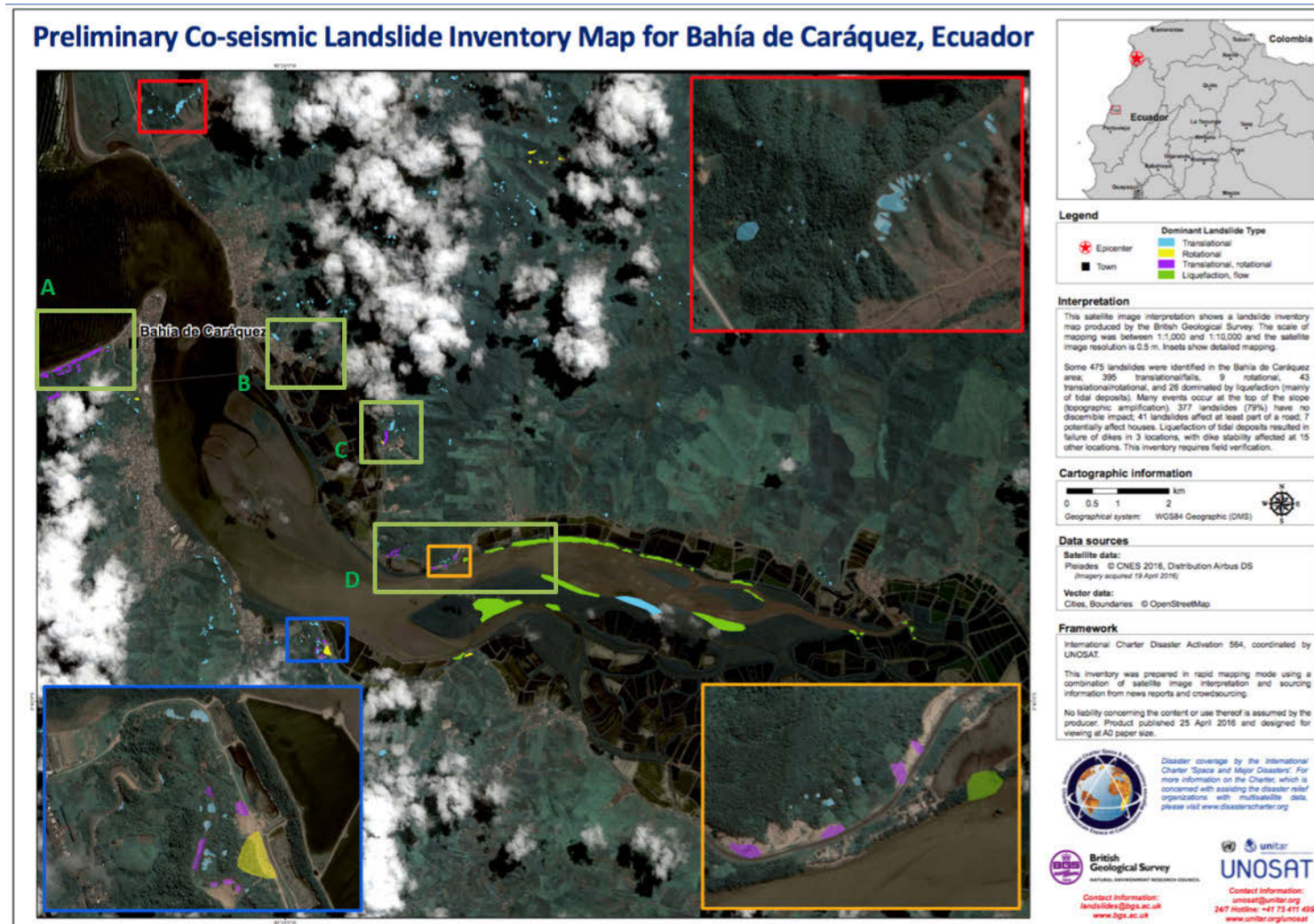


Figure C-3: BGS Preliminary co-seismic landslide inventory map for the Chone River estuary

The M_w 7.8 Muisne Ecuador Earthquake of 16 April 2016

EEFIT



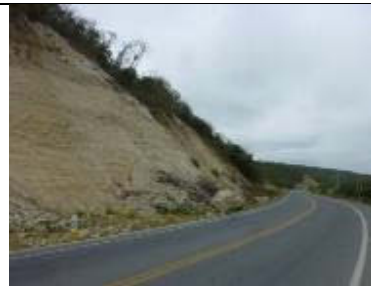
Figure C-4: Close up of landslide locations surveyed around the Chone River estuary

Table C-2: Details of landslide locations surveyed around the Chone River estuary

Map ID	Coordinates	Accuracy of BGS identification		Co-seismicity validation by locals	Visual Assessment Reliability Estimate		Observations	Discussion with locals	Photos
		Location	Type		Reliability Level	Comment			
1	-0.609010, -80.444420	✓	✓	?	Poor	Observation point far from scars and co-seismicity unsure	<p>Viewed from a distance, from the end of the peninsula in Bahía de Caráquez and from the coast opposite in San Vicente.</p> <p>Slopes looked to have little vegetation on them which may indicate recent landslides. The point of observation was too far from the scars to distinguish them individually and make a detailed assessment of the BGS mapping accuracy.</p>	<p>According to reports, these cliffs are prone to landslides over a long extent of the coast, especially in and after the wet season which was prior to the main shock.</p> <p>Some of the recent scars may have been co-seismic but which exactly was not clear in the oral accounts of the event.</p>	
2	-0.601983, -80.402002	✓	✓	✓	Adequate	Limited time spent at site.	See photo.	<p>Discussion with locals supporting evidence of co-seismicity of failure.</p>	

Map ID	Coordinates	Accuracy of BGS identification		Co-seismicity validation by locals	Visual Assessment Reliability Estimate		Observations	Discussion with locals	Photos
		Location	Type		Reliability Level	Comment			
3	-0.605204, -80.397303	X	NA	✓	Adequate	Limited time spent at site.	Two main scars could be observed, the upper one showing some vegetation having grown in the slope, whilst the bottom one does not. It would corroborate a recent reactivation of a previous slide at the toe of the slope.	The site was previously an informal quarry, one of many in the region. The slope was left without any stabilisation.	
4	-0.605986, -80.394861	X	NA	✓	Poor	Limited time spent at site. Observation point far from scar and angle not allowing to see extent fully.	Under cloud on map. Significant rock slide.	Discussion with locals supporting evidence of co-seismicity of failure.	
5	-0.606094, -80.398049	X	NA	✓	Good		Liquefaction induced lateral spreading and settlement of shrimp farm dykes. Crack widths approximately 50 cm wide. Settlements of approximately 1 m. Dykes running roughly N-S experienced more damage than those running E-W	According to the shrimp farm manager, damage to the dams significantly affected production.	

Map ID	Coordinates	Accuracy of BGS identification		Co-seismicity validation by locals	Visual Assessment Reliability Estimate		Observations	Discussion with locals	Photos
		Location	Type		Reliability Level	Comment			
6	-0.607813, -80.393328	X	NA	✓	Poor	Retrofit works already undergone	Next shrimp farm along from the one above. Considerable reconstruction work already taken place.	Similar damage to most shrimp farms within the estuary.	
7	-0.617601, -80.383835	✓	✓	✓	Good		Large scale circular slope failure scar. Drone footage taken from this location	Large amounts of dust generated in earthquake which covered the road.	
8	-0.620812, -80.382837	✓	✓	?	Poor	Rehabilitation works having already altered slope failure.	Face of the scar modified by ongoing works associated to the rehabilitation of the road, which seems to have been engulfed by the slide. Untouched top of slope shows large upper boundary of the scar. Unsafe clearing practice of removing soil from toe of slope without stabilisation or safety measures taken to avoid further slide from the top on workers.	Co-seismicity could not be validated with locals but ongoing rehabilitation works may provide evidence of recent failure likely to be associated to earthquake	

Map ID	Coordinates	Accuracy of BGS identification		Co-seismicity validation by locals	Visual Assessment Reliability Estimate		Observations	Discussion with locals	Photos
		Location	Type		Reliability Level	Comment			
9	-0.621530, -80.382699	X	NA	✓	Good		<p>Large scale circular scar of slope failure observed next to quarry behind the main road.</p> <p>Evidence of major rock fall in quarry also observed.</p>	<p>Discussion with locals supporting evidence of co-seismicity of failure.</p>	
10	-0.640501, -80.382973	✓	✓	✓	Good		<p>Fresh landslide scar and large boulders at toe slope.</p> <p>Evidence of major lateral spreading of road in direction of the lagoon. Substantial cracks 30-40 cm wide, 160 cm deep.</p>	<p>Discussion with locals supporting evidence of co-seismicity of failure.</p>	
11	-0.638964, -80.360506	✓	✓	✓	Good		<p>Significant cracking in dirt track, likely due to liquefaction.</p> <p>Mangrove trees into river.</p>	<p>Discussion with locals supporting evidence of co-seismicity of failure and displacement of the mangrove into the river from lateral spreading following main shock.</p>	

Map ID	Coordinates	Accuracy of BGS identification		Co-seismicity validation by locals	Visual Assessment Reliability Estimate		Observations	Discussion with locals	Photos
		Location	Type		Reliability Level	Comment			
12	-0.639077, -80.362471	✓	✓	✓	Good		Some masonry damage to small water pumping station used for shrimp farming. Damage to pipe and pipe supports from ground failure. Wooden props of the pipe and the structure's shallow foundation tilted in the direction of the river. Trees tops nearby tilted towards, if not in, the river.	Told that all trees were vertical before. Trees previously in same alignment on bank as pumping station, which would thereby provide some evidence of roughly 15 m lateral movement.	
13	-0.640087, -80.366996	✓	✓	✓	Good	-	Liquefaction and large dyke failure at a shrimp farm basin. Dyke already been reconstructed, but pool not filled yet. Large amounts of cracking and spreading observed in the empty pool.	During the main event, the dyke failed; all water flooded out of pool into the river, then wave of water refilled the pool, and then it all flooded out again. The entire culture of shrimps from this large basin was lost.	
14	-0.641688, -80.369571	X	NA	✓	Good	-	This site corresponded to the visitor entry point to the local natural reserve, focused on the wildlife and natural environment of the estuary. Two small wooden piers for exploration of the estuary by boat showed signs of damage. Piles at end were tilting into the river.	Jetty lost roof in main shock. Told lateral land movement at edge of river approximately 10 m (confirmed by observation 12).	

Map ID	Coordinates	Accuracy of BGS identification		Co-seismicity validation by locals	Visual Assessment Reliability Estimate		Observations	Discussion with locals	Photos
		Location	Type		Reliability Level	Comment			
15	-0.646017, -80.368035	✓	✓	✓	Poor	No direct observation possible from location.	Was not possible for us to see far enough to be able to determine the failure size and mechanism.	Discussion with locals however supported evidence of co-seismicity of similar failure of the banks to those opposite (see observations 11, 12, 14). Told mangroves on other side of river laterally spread into river as observed in 11.	No photo available
16	-0.640526, -80.369852	✓	✓	✓	Adequate	Limited time spent at site.	Major recent scars of landslides along roadside.	Discussion with locals supporting evidence of co-seismicity of failure.	
17	-0.642839, -80.373470	✓	✓	✓	Good		Landslide scar along road. A major crack in diagonal across the road causing localised partial closure of road surface was observed. The crack was approximately 10 cm wide.	Discussion with locals supporting evidence of co-seismicity of failure.	

Appendix D: Examples of activities and services provided in the temporary earthquake refugee shelters in Ecuador

EEFIT



Figure D-1 (a) Temporary shelter in Manta, (b) Mr. Bayes Ahmed in Canoa, (c) Plan International NGO office in Canoa, (d) toilet facilities, (e) water supply, (f) a kitchen in the shelter, (g) watering the ground to keep it dust-free, and (h) a dining facility. Source: Bayes Ahmed, fieldwork, May-June, 2016 in Manta, Ecuador.

EEFIT



Figure D-2 (a) The inside view of a room in the camp, (b) a concert arranged by the Navy officials for the children in Canoa, (c) basketball facility for the school-going pupil, (d) drawing competition for the children, (e) handball playing facility, (f) a child with a gift, (g) a local NGO booth, and (h) professional training provided for the camp people in Pedernales. Source: Bayes Ahmed, fieldwork, May-June, 2016 in Manta, Ecuador.

Appendix E: Questionnaire for assessing community vulnerability to earthquake disasters in the refugee shelters: the Ecuador 16 April 2016 earthquake

1. Family information:

Gender (M/F)	Age (Years)	Education	Monthly Income (US \$)

2. Occupation of household heads or adult:

Before Earthquake	After Earthquake

3. Information on the house you used to live before the earthquake:

Year of Construction:

Building Height:

Building Materials:

Ownership: **Owned** **Rented**

Area: **Urban** **Rural**

4. Damage and losses due to the earthquake:

Building: **Totally Destroyed** **Partially Destroyed**

Casualty (number):

Injury (number):

Other Loss:

5. Were you prepared for the earthquake? **Yes** **No**

6. What problems are you facing in the earthquake shelters? [Prioritize 2]

- Food
- Size of the tent
- Medicine
- Water
- Sanitation and showers
- Safety
- Hot weather
- Others (please define)

7. What is your future plan to recover from the disaster? [Prioritize 2]

- Employment
- Housing
- Education
- Loans
- Medical treatment
- Relocation
- Psychological help
- Other

8. What type of house do you feel is safer to live in the future?

Floor Height:

Construction Material(s):

Location:

Appendix F: Contingency tables from the questionnaire

Table F - 1. Relationship between building material and number of floors (before scenario).

Building Material (Before)		Number of floors in the building (before)					Total
		1	2	3	4	5	
RC	Count	17	9	4	4	2	36
	% of Total	14.8%	7.8%	3.5%	3.5%	1.7%	31.3%
Timber/ Bamboo	Count	21	6	0	0	0	27
	% of Total	18.3%	5.2%	0.0%	0.0%	0.0%	23.5%
RC-Timber/ Bamboo	Count	15	37	0	0	0	52
	% of Total	13.0%	32.2%	0.0%	0.0%	0.0%	45.2%
Total	Count	53	52	4	4	2	115
	% of Total	46.1%	45.2%	3.5%	3.5%	1.7%	100.0%

Chi-Square Tests (Table F1)

	Value	df	Asymp. Sig.* (2-sided)
Pearson Chi-Square	45.340 ^a	8	0.000
Likelihood Ratio	46.336	8	0.000
Linear-by-Linear Association	2.049	1	0.152
N of Valid Cases	115		

a. 9 cells (60.0%) have expected count less than 5. The minimum expected count is 0.47.

* Typically, a significance value < 0.05 is considered "significant".

Table F - 2. Relationship between year of construction and number of floors (before scenario).

Year of building construction		Number of floors in the building (before)					Total
		1	2	3	4	5	
<1960s	Count	0	3	0	0	0	3
	% of Total	0.0%	2.6%	0.0%	0.0%	0.0%	2.6%
1960s	Count	0	3	0	0	0	3
	% of Total	0.0%	2.6%	0.0%	0.0%	0.0%	2.6%
1970s	Count	1	1	1	0	0	3
	% of Total	0.9%	0.9%	0.9%	0.0%	0.0%	2.6%
1980s	Count	2	7	0	0	1	10
	% of Total	1.8%	6.1%	0.0%	0.0%	0.9%	8.8%
1990s	Count	10	10	3	4	0	27
	% of Total	8.8%	8.8%	2.6%	3.5%	0.0%	23.7%
2000s	Count	6	9	0	0	0	15
	% of Total	5.3%	7.9%	0.0%	0.0%	0.0%	13.2%
2010s	Count	33	19	0	0	1	53
	% of Total	28.9%	16.7%	0.0%	0.0%	0.9%	46.5%
Total	Count	52	52	52	4	4	2
	% of Total	45.6%	45.6%	45.6%	3.5%	3.5%	1.8%

Chi-Square Tests (Table F2)

	Value	df	Asymp. Sig. (2-sided)
Pearson Chi-Square	48.217 ^a	24	0.002
Likelihood Ratio	43.840	24	0.008
Linear-by-Linear Association	9.499	1	0.002
N of Valid Cases	114		

a. 29 cells (82.9%) have expected count less than 5. The minimum expected count is 0.05.

Table F - 3. Relationship between year of construction and destruction pattern (before scenario).

Year of building construction	House destroyed		Total
	Completely destroyed	Partially destroyed	
<1960s	0.9%	1.8%	2.6%
1960s	2.6%	0%	2.6%
1970s	1.8%	0.9%	2.6%
1980s	7.0%	1.8%	8.8%
1990s	21.1%	2.6%	23.7%
2000s	7.0%	6.1%	13.2%
2010s	25.4%	21.1%	46.5%
Total	65.8%	34.2%	100.0%

Chi-Square Tests (Table F3)

	Value	df	Asymp. Sig. (2-sided)
Pearson Chi-Square	14.184 ^a	6	0.028
Likelihood Ratio	16.260	6	0.012
Linear-by-Linear Association	3.418	1	0.064
N of Valid Cases	114		

a. 7 cells (50.0%) have expected count less than 5. The minimum expected count is 1.03.

Table F - 4. Relationship between building material and destruction pattern (before scenario).

Building Material (before)	Destruction pattern		Total
	Completely destroyed	Partially destroyed	
RC	22.6%	8.7%	31.3%
Timber/ Bamboo	17.4%	6.1%	23.5%
RC-Timber/ Bamboo	25.2%	20.0%	45.2%
Total	65.2%	34.8%	100.0%

Chi-Square Tests (Table F4)

	Value	df	Asymp. Sig. (2-sided)
Pearson Chi-Square	3.759 ^a	2	0.153
Likelihood Ratio	3.764	2	0.152
N of Valid Cases	115		

a. 0 cells (0.0%) have expected count less than 5. The minimum expected count is 9.39.

Table F - 5. Relationship between year of construction and building material (before scenario).

Year of building construction	Building Material (before)			Total
	RC	Timber/ Bamboo	RC-Timber/ Bamboo	
<1960s			2.7%	2.7%
1960s			2.7%	2.7%
1970s	0.9%		1.8%	2.7%
1980s	1.8%	0.9%	5.4%	8.0%
1990s	10.7%	4.5%	8.9%	24.1%
2000s	1.8%	4.5%	6.3%	12.5%
2010s	16.1%	14.3%	17.0%	47.3%
Total	31.3%	24.1%	44.6%	100.0%

Chi-Square Tests (Table F5)

	Value	df	Asymp. Sig. (2-sided)
Pearson Chi-Square	16.558 ^a	12	0.167
Likelihood Ratio	19.635	12	0.074
Linear-by-Linear Association	5.043	1	0.025
N of Valid Cases	112		

a. 14 cells (66.7%) have expected count less than 5. The minimum expected count is 0.72.

Table F - 6. Relationship between monthly household income and ownership pattern (before scenario).

Monthly Income (US\$)	Ownership of the house		Total
	Owned	Rented	
0-75	5.9%	4.2%	10.1%
76-150	10.9%	9.2%	20.2%
151-300	13.4%	10.9%	24.4%
301-450	11.8%	8.4%	20.2%
451-700	9.2%	5.0%	14.3%
>700	6.7%	4.2%	10.9%
Total	58.0%	42.0%	100.0%

Chi-Square Tests (Table F6)

	Value	df	Asymp. Sig. (2-sided)
Pearson Chi-Square	.622 ^a	5	0.987
Likelihood Ratio	.627	5	0.987
N of Valid Cases	119		

a. 0 cells (0.0%) have expected count less than 5. The minimum expected count is 5.04.

Table F -7. Relationship between monthly household income and building materials (before scenario).

Monthly Income (US\$)	Building Material (before)			Total
	RC	Timber/ Bamboo	RC-Timber/ Bamboo	
0-75	2.6%	1.8%	5.3%	9.6%
76-150	5.3%	7.9%	7.0%	20.2%
151-300	7.9%	4.4%	12.3%	24.6%
301-450	6.1%	6.1%	7.9%	20.2%
451-700	4.4%	2.6%	7.9%	14.9%
>700	5.3%	0.9%	4.4%	10.5%
Total	31.6%	23.7%	44.7%	100.0%

Chi-Square Tests (Table F7)

	Value	df	Asymp. Sig. (2-sided)
Pearson Chi-Square	7.730 ^a	10	0.655
Likelihood Ratio	7.622	10	0.666
Linear-by-Linear Association	.289	1	0.591
N of Valid Cases	114		

a. 6 cells (33.3%) have expected count less than 5. The minimum expected count is 2.61.

Table F -8. Relationship between monthly household income and number of floors (before scenario).

Monthly Income (US\$)	Number of floors in the building (before)					Total
	1	2	3	4	5	
0-75	6.9%	2.6%				9.5%
76-150	12.1%	6.9%	0.9%			19.8%
151-300	8.6%	13.8%	0.9%	0.9%		24.1%
301-450	10.3%	8.6%	0.9%	0.9%		20.7%
451-700	3.4%	8.6%	0.9%	0.9%	0.9%	14.7%
>700	4.3%	5.2%		0.9%	0.9%	11.2%
Total	45.7%	45.7%	3.4%	3.4%	1.7%	100.0%

Chi-Square Tests (Table F8)

	Value	df	Asymp. Sig. (2-sided)
Pearson Chi-Square	17.815 ^a	20	0.600
Likelihood Ratio	19.252	20	0.505
Linear-by-Linear Association	8.912	1	0.003
N of Valid Cases	116		

a. 18 cells (60.0%) have expected count less than 5. The minimum expected count is 0.19.

EEFIT

Earthquake Engineering Field Investigation Team

EEFIT is a UK based group of earthquake engineers, architects and scientists who seek to collaborate with colleagues in earthquake prone countries in the task of improving the seismic resistance of both traditional and engineered structures. It was formed in 1982 as a joint venture between universities and industry, it has the support of the Institution of Structural Engineers and of the Institution of Civil Engineers through its associated society SECED (the British national section of the International Association for Earthquake Engineering).

EEFIT exists to facilitate the formation of investigation teams which are able to undertake, at short notice, field studies following major damaging earthquakes. The main objectives are to collect data and make observations leading to improvements in design methods and techniques for strengthening and retrofit, and where appropriate to initiate longer term studies. EEFIT also provides an opportunity for field training for engineers who are involved with earthquake-resistant design in practice and research.

EEFIT is an unincorporated association with a constitution and an elected management committee that is responsible for running its activities. EEFIT is financed solely by membership subscriptions from its individual members and corporate members. Its secretariat is generously provided by the Institution of Structural Engineers and this long-standing relationship means that EEFIT is now considered part of the Institution.

© All material is copyright of the Earthquake Engineering Field Investigation Team (EEFIT) and any use of the material must be referenced to EEFIT, UK. No material is to be reproduced for resale.

This report can be downloaded from www.eefit.org.uk

EEFIT
c/o The Institution of Structural Engineers,
47 – 58 Bastwick St, London EC1V 3PS
Tel: +44 (0)20 7235 4535
Fax: +44 (0)20 7235 4294
Email: mail@eefit.org.uk
Website: <http://www.eefit.org.uk>